

1984

Soil-structure Interaction Under Dynamic Loads

Laila Mahmaud El-hifnawy

Follow this and additional works at: <https://ir.lib.uwo.ca/digitizedtheses>

Recommended Citation

El-hifnawy, Laila Mahmaud, "Soil-structure Interaction Under Dynamic Loads" (1984). *Digitized Theses*. 1326.
<https://ir.lib.uwo.ca/digitizedtheses/1326>

This Dissertation is brought to you for free and open access by the Digitized Special Collections at Scholarship@Western. It has been accepted for inclusion in Digitized Theses by an authorized administrator of Scholarship@Western. For more information, please contact tadam@uwo.ca, wlsadmin@uwo.ca.

The author of this thesis has granted The University of Western Ontario a non-exclusive license to reproduce and distribute copies of this thesis to users of Western Libraries. Copyright remains with the author.

Electronic theses and dissertations available in The University of Western Ontario's institutional repository (Scholarship@Western) are solely for the purpose of private study and research. They may not be copied or reproduced, except as permitted by copyright laws, without written authority of the copyright owner. Any commercial use or publication is strictly prohibited.

The original copyright license attesting to these terms and signed by the author of this thesis may be found in the original print version of the thesis, held by Western Libraries.

The thesis approval page signed by the examining committee may also be found in the original print version of the thesis held in Western Libraries.

Please contact Western Libraries for further information:

E-mail: libadmin@uwo.ca

Telephone: (519) 661-2111 Ext. 84796

Web site: <http://www.lib.uwo.ca/>

CANADIAN THESES ON MICROFICHE

I.S.B.N.

THESES CANADIENNES SUR MICROFICHE



National Library of Canada
Collections Development Branch

Canadian Theses on
Microfiche Service

Ottawa, Canada
K1A 0N4

Bibliothèque nationale du Canada
Direction du développement des collections

Service des thèses canadiennes
sur microfiche

NOTICE

The quality of this microfiche is heavily dependent upon the quality of the original thesis submitted for microfilming. Every effort has been made to ensure the highest quality of reproduction possible.

If pages are missing, contact the university which granted the degree.

Some pages may have indistinct print especially if the original pages were typed with a poor typewriter ribbon or if the university sent us a poor photocopy.

Previously copyrighted materials (journal articles, published tests, etc.) are not filmed.

Reproduction in full or in part of this film is governed by the Canadian Copyright Act, R.S.C. 1970, c. C-30. Please read the authorization forms which accompany this thesis.

THIS DISSERTATION
HAS BEEN MICROFILMED
EXACTLY AS RECEIVED

AVIS

La qualité de cette microfiche dépend grandement de la qualité de la thèse soumise au microfilmage. Nous avons tout fait pour assurer une qualité supérieure de reproduction.

S'il manque des pages, veuillez communiquer avec l'université qui a conféré le grade.

La qualité d'impression de certaines pages peut laisser à désirer, surtout si les pages originales ont été dactylographiées à l'aide d'un ruban usé ou si l'université nous a fait parvenir une photocopie de mauvaise qualité.

Les documents qui font déjà l'objet d'un droit d'auteur (articles de revue, examens publiés, etc.) ne sont pas microfilmés.

La reproduction, même partielle, de ce microfilm est soumise à la Loi canadienne sur le droit d'auteur, SRC 1970, c. C-30. Veuillez prendre connaissance des formules d'autorisation qui accompagnent cette thèse.

LA THÈSE A ÉTÉ
MICROFILMÉE TELLE QUE
NOUS L'AVONS REÇUE

SOIL-STRUCTURE INTERACTION UNDER
DYNAMIC LOADS

by

Laila Mahmaud El-Hifnawy

Faculty of Engineering Science

Submitted in partial fulfillment
of the requirements for the degree of
Doctor of Philosophy

Faculty of Graduate Studies
The University of Western Ontario

London, Ontario

March, 1984

© Laila Mahmaud El-Hifnawy 1984

ABSTRACT

A theoretical study of the soil-structure interaction effects on the dynamic behaviour of structures is presented. The substructure approach is employed for which foundation impedance functions are derived from static and dynamic continuum theories. Both rigid and flexible structures supported by various types of foundations are investigated. The free vibration analysis of the soil-structure interaction system indicates that the damped natural frequencies of structures on flexible foundation may be lower or higher than the undamped natural frequencies. It also shows that the foundation flexibility provides damping to the structure due to energy dissipation in soil and modifies the original structural damping. The effect of the foundation on the damping of structures is calculated using an energy consideration and by means of the complex eigenvalue analysis. Both methods give almost the same results for the first mode but may give considerably different results for the higher vibration modes.

The dynamic response of the soil-structure interaction system excited by shock, earthquake and wind loading is investigated. The analysis of hammer foundations, the most typical of the shock experiencing structures, proves

that the complex eigenvalue method is an efficient and accurate method of response prediction. Using this approach, the response of hammer foundations to either initial velocity of the anvil or pulse loading can be treated for any number of degrees of freedom.

Seismic loading and response of buildings depend on the flexibility of the foundation and its type. Shallow flexible foundations may increase the response and decrease the seismic forces of the structure, as compared to the response of the same structure on a rigid base. For pile foundations, the number and type of piles, their arrangement and the pile connection with the cap come into play. The study shows that, for small buildings and/or low intensity of earthquakes, the rigid connection of piles with the cap may not be necessary. The response of rigid structures to seismic loading is dealt with efficiently using the direct random vibration analysis.

Finally, the effect of foundation flexibility on structural response to gusting wind is explored using the gust factor approach. The parametric study indicates that while the gust effect factor may or may not be sensitive to soil flexibility, the resultant vibration may be substantially modified.

ACKNOWLEDGEMENTS

The author wishes to express her deep gratitude to Professor M. Novak for his never ending encouragement, interest and invaluable advice during the process of this work.

Thanks are also due to Ms. Joanne Lemon for the careful typing of this thesis.

Finally, the author wishes to express her sincere thanks to her husband without whom this work would not have been attempted.

TABLE OF CONTENTS

	Page
CERTIFICATE OF EXAMINATION.....	ii
ABSTRACT.....	iii
ACKNOWLEDGEMENTS.....	v
TABLE OF CONTENTS.....	vi
LIST OF TABLES.....	ix
LIST OF FIGURES.....	x
NOMENCLATURE.....	xviii
CHAPTER 1 - INTRODUCTION.....	1
1.1 Statement of the Soil-Structure Interaction Problem.....	1
1.2 Objective of the Study.....	4
1.3 Organization of the Study.....	4
CHAPTER 2 - IMPEDANCE FUNCTIONS OF FOUNDATIONS..	6
2.1 Introduction.....	6
2.2 Impedance Functions for Shallow Foundations.....	7
2.3 Adjustments of the Halfspace Theory.	11
2.3.1 Correction for Geometric Damping...	12
2.3.2 Embedment Effects.....	13
2.3.3 Soil Material Damping.....	13
2.3.4 Shallow Layers.....	15
2.4 Pile Foundations.....	19
2.4.1 Stiffness and Damping of Single Piles.....	21
2.4.2 Stiffness and Damping Constants of the Pile Group.....	23
2.5 Force-Displacement Relationship of Foundation.....	25
2.6 Soil-Structure Interaction System...	26
2.7 Conclusions.....	29
CHAPTER 3 - FREE VIBRATION OF SOIL-STRUCTURE INTERACTION SYSTEM.....	42
3.1 Introduction.....	42
3.2 Evaluation of Damping Using Energy Consideration.....	45
3.3 Evaluation of Damping Using Complex Eigenvalues Approach.....	50
3.4 Examples of Modal Properties.....	58
3.5 Conclusions.....	71

	Page
CHAPTER 4 - METHODS OF RESPONSE ANALYSIS.....	88
4.1 Introduction.....	88
4.2 Classical Modal Analysis.....	89
4.3 Nonclassical Modal Analysis.....	93
4.4 Complex Response Analysis.....	95
4.5 Direct Spectral Analysis.....	98
4.6 Direct Integration Methods.....	104
4.7 Concluding Remarks.....	109
CHAPTER 5 - STRUCTURAL RESPONSE TO SHOCK LOADING	112
5.1 Introduction.....	112
5.2 Hammer Foundation Systems.....	114
5.3 Stiffness and Damping Constants of The System.....	116
5.4 Equations of Motion.....	118
5.5 Initial Velocity Approach.....	122
5.6 Response to Pulse Loading.....	123
5.7 Examples.....	127
5.8 Conclusions.....	131
CHAPTER 6 - SOIL-STRUCTURE INTERACTION UNDER SEISMIC LOADING.....	153
6.1 Introduction.....	153
6.2 Modeling the Building and Its Foundation.....	155
6.3 Governing Equations and Their Solution.....	158
6.4 Example Problems.....	160
6.5 Conclusions.....	168
CHAPTER 7 - SOIL-STRUCTURE INTERACTION UNDER WIND LOADING.....	190
7.1 Introduction.....	190
7.2 Types of Aerodynamic Excitation.....	191
7.3 Basic Wind Characteristics.....	194
7.4 Aerodynamic Forces Due to Turbulence	198
7.5 Direct Solution.....	200
7.5.1 Formulation.....	200
7.5.2 Spectral Relationship.....	204
7.6 Prediction of Fluctuating Response Using Modal Analysis.....	207
7.6.1 Response of a Single Degree of Freedom System.....	208
7.6.2 Response of Multi Degree of Freedom System.....	209

	Page
7.7. Gust Factor Approach.....	214
7.7.1 Design Wind Pressure.....	217
7.7.2 Wind Induced Building Motion.....	218
7.8 Soil-Structure Interaction Under Gusting Wind.....	220
7.8.1 Design Wind Loads and Maximum Response.....	221
7.8.2 Numerical Examples.....	222
7.9 Conclusions.....	228
CHAPTER 8 - SUMMARY AND CONCLUSIONS.....	246
REFERENCES.....	251
VITA.....	262

LIST OF TABLES

Table	Description	Page
2.1	Stiffness and Damping Parameters (D=0) (Ref. 30).....	31
2.2	Stiffness and Damping Parameters of Horizontal Response for Piles With $l/R > 25$ for Homogeneous Soil Profile (Ref. 56).....	32
3.1	Building Properties.....	74
5.1	Functions $\bar{q}_j(t)$ for Main Types of Pulses..	134
6.1	Comparison of Peak Responses of a Silo Obtained by Time History Analysis and Random Vibration Approach.....	168
7.1	Comparison Between Exposures A and C Results for a Fixed-Base and Flexible Foundation 10-Storey Building.....	230
7.2	Comparison Between Exposures A and C Results for a Fixed-Base and Flexible Foundation 20-Storey Building.....	320

LIST OF FIGURES

Figure	Description	Page
2.1	System Considered.....	33
2.2	Notation for Calculation of Equivalent Radii of Rectangular Basis.....	34
2.3	Schematic of Embedded Foundation.....	34
2.4a	Examples of Stiffness Parameters c_1 and s_1 . (Poisson's ratio given in brackets, material damping $D=0$).....	35
2.4b	Examples of Damping Parameters \bar{c}_2 and \bar{s}_2 (Poisson's ratio given in brackets, material damping $D=0$).....	35
2.5	Stiffness and Damping Parameters for Vertical Vibration of Footings on Half-space and Strata of Limited Depth ($r_0=R$) (Ref. 35).....	36
2.6	Stiffness Functions for Embedded Foundations (after Elsabee) ($\nu=1/3$, $\beta = 0.05$) a - Embedded Foundation-Finite Layer b - Surface Foundation-Finite Layer c - Surface Foundation-Halfspace.....	37
2.7	Generation of Pile Stiffness in Individual Directions.....	38
2.8	Stiffness Parameters f_{v1} and Damping Parameters f_{v2} of Vertical Response for Endbearing Piles (Ref. 56).....	39
2.9	Stiffness Parameters f_{v2} and Damping Parameters f_{v2} of Vertical Response for Floating Piles (Ref. 56).....	39
2.10	Pile Displacements for Determination of Group Stiffness and Damping Related to Rotation $\psi=1$	40
2.11	Typical Shallow and Deep Foundations....	40
2.12	Model of Building-Foundation System.....	41

Figure	Description	Page
3.1	Vibrating Shear Building.....	75
3.2	Basic Types of Models for Structural Damping.....	76
3.3	Silo Supported by (a) Mat Foundation and (b) Pile Foundation (1 m = 3.281 ft)....	77
3.4	First Mode Damping Ratio of Mat Supported Silo for Various Silo Loadings.....	78
3.5	First Mode Damping Ratio of Mat Supported Silo For Varying Silo Loading.	78
3.6	Modal Damping Ratios of Pile Supported Silo For Varying Silo Loading.....	79
3.7	Modal Damping Ratios of Hammer Foundation For Variable Constant of Soil Damping.....	79
3.8	Modal Damping of Five-Storey Shear Building With Separate Foundations Derived From Soil of Varying Stiffness (1 ft/s = 0.3048 m/s).....	80
3.9	Modal Damping of Five-Storey Shear Building With Large Mat Foundation Derived From Soil of Varying Stiffness (1 ft/s = 0.3048 m/s).....	80
3.10	Damping of Five-Storey Shear Building With Mat Foundation Derived From Soil of Varying Stiffness and Foundation Damping Equal to One-Fifth of That Used in Figure 3.9 for Halfspace (1 ft = 0.3048 m).....	81
3.11	Modal Damping of Ten-Storey Shear Building With Large Mat Foundation Derived From Soil of Varying Stiffness (1 ft = 0.3048 m).....	81
3.12	Modal Damping of Ten-Storey Shear Building Due to Reduced Damping in the Foundation.....	82

Figure	Description	Page
3.13	Undamped Natural Frequencies and Frequencies $\omega_j = \mu_j $ of Five-Storey Shear Building for Varying Soil Stiffness (1 ft = 0.3048 m).....	82
3.14	Undamped and Damped Natural Frequencies of Five-Storey Shear Building With Damping Matrix Reduced to One-Fifth of the Value for Halfspace.....	83
3.15	Undamped and Damped Vibration Modes of Five-Storey Building With Mat Foundation ($ \phi $ -Absolute Displacement, $\phi\Pi$ -Phase Shift, $ \phi _u$ -Absolute Displacement of Undamped Mode; $V_s=660$ ft/s = 201 m/s)...	84
3.16	Comparison of Undamped Vibration in Classical Mode With Damped Vibration in Nonclassical Mode for Five-Storey Building With Mat Foundation. (Third mode with damping due to energy dissipation in soil; displacement shown at times ranging from $t = 0$ to half of natural period $T_3/2$).....	85
3.17	Structural Damping of Five-Storey Shear Building on Mat Foundation for Varying Soil Stiffness (1 ft = 0.3048 m; Both Methods Give Almost the Same Results)....	85
3.18	Structural Damping of Ten-Storey Shear Building on Mat Foundation for Varying Soil Stiffness (1 ft = 0.3048 m; Both Methods Give Almost the Same Results)....	86
3.19	First Natural Frequency and Damping Ratio for Ten-Storey Building (1 ft = 0.3048 m)	86
3.20	First Vibration Mode of Building on Different Foundations (a) - $V_s = 300$ ft/sec, (b) - $V_s = 600$ ft/sec.....	87
3.21	Types of Foundations.....	87
4.1	Intensity Envelope Functions: (a) Boxcar; (b) Trapezoidal; (c) Exponential.....	111

Figure	Description	Page
4.2	Linear Acceleration; Normal and Extended Time Steps for Wilson- θ Method.....	111
5.1	Examples of Structures Exposed to Pulse Loading.....	135
5.2	Basic Mathematical Models for Hammer Foundations.....	136
5.3	Schematic of Hammer Foundation.....	137
5.4	Notations for Asymmetrical Hammer Foundation With Six Degrees of Freedom.....	138
5.5	Basic Types of Pulses.....	139
5.6	Replacement of Pulse History by Simple Shape.....	140
5.7	Undamped and Damped Response of Two Mass Hammer Foundation to Sine Pulse of Varying Duration and Constant Power; Embedded Footing, Anvil Pad 6 in (0.15 m) Thick ($D_1 = 51\%$, $D_2 = 7.4\%$, Displacements in in., 1 in = 2.54 cm, Time in Milliseconds): (a) Anvil; (b) Foundation Block.....	141
5.8	Undamped and Damped Response of Two Mass Hammer Foundation to Sine Pulse of Varying Duration and Constant Power; Embedded Footing, Anvil Pad 1.5 in (0.04 m) Thick, Damping of Soil Reduced to 1/4 ($D_1 = 12.9\%$, $D_2 = 5.3\%$, Displacements in in., 1 in = 2.54 cm): (a) Anvil; (b) Foundation Block.....	143
5.9	Peak Values of Damped Vertical Response of Two Mass Hammer Foundation to Sine Pulse of Varying Duration and Constant Power for Full Value of Damping As in Figure 5.7.....	145
5.10	Peak Values of Damped Vertical Response of Two Mass Hammer Foundation to Sine Pulse of Varying Duration and Constant Power for Damping Reduced to 1/4 as in Figure 5.8.....	146

Figure	Description	Page
5.11	Vertical, Horizontal and Rocking Response of the Asymmetrical Hammer Foundation Shown in Figure 5.3 for Sine Pulse Loading of Different Duration and Constant Power ($e=0$, $e_1=2.0$ ft = 0.61 m; Response in in. and Radians, 1 in = 2.54 cm; $D_1 = 30.6\%$, $D_2 = 44.6\%$, $D_3 = 47.3\%$, $D_4 = 3.2\%$, $D_5 = 4.4\%$, $D_6 = 5.0\%$: (a) Anvil; (b) Foundation.....	147
5.12	Variation in Normalized Peak Values of Vertical Response of the Asymmetrical Foundation From Figure 5.3 With Duration of Sine Pulse Loading (Six Degrees of Freedom).....	149
5.13	Undamped and Damped Vibration Modes of Hammer Foundation From Figure 5.3.....	150
5.14a	Undamped and Damped Vertical Response of Two Mass Hammer Foundation for (a) Rectangular Pulse and (b) Sine Pulse ($e=e_1=0$, $t_p/T_1=0.5$) - Anvil.....	151
5.14b	Undamped and Damped Vertical Response of Two Mass Hammer Foundation for (a) Rectangular Pulse and (b) Sine Pulse ($e=e_1=0$, $t_p/T_1=0.5$) - Foundation.....	152
6.1	Pile Restoring Force k_v and Damping Coefficient c vs. Vertical Displacement v ..	171
6.2	Pile Vertical Displacement v as a Result of Cap Rocking in the Vertical Plane ψ ...	172
6.3	Maximum Storey Displacements, Drifts and Shears for Ten-Storey Building on Different Foundations, for Two Soil Shear Wave Velocities and Soil Material Damping $\beta = .025$ (1 in = 2.54 cm, 1 kip = 4.45kN)	173
6.4	Maximum Storey Displacements, Drifts and Shears for Ten-Storey Building on Different Foundations, for Two Soil Shear Wave Velocities and Soil Material Damping $\beta=.05$ (1 in=2.54 cm, 1 kip=4.45 kN).....	174
6.5	San Fernando Earthquake Record.....	175

Figure	Description	Page
6.6	Pile Forces (kips) and Storey Drift (in) for Ten-Storey Building Supported by 15, 21 and 27 Piles for Different Earthquake Intensity: (a) Pinned Endbearing Piles; (b) Pinned Floating Piles.....	176
6.7a	Base Shear of Ten-Storey Building vs. Number and Type of Piles and Intensity of Ground Shaking (1 kip = 4.45 kN).....	178
6.7b	Overturning Moment of 10-storey Building vs. Number and Type of Piles and Intensity of Ground Shaking (1 kip.ft = 1.36 kN.m).....	179
6.8	Maximum Storey Displacement of Ten-Storey Building Supported by 15 Piles for Different Tip Conditions and Intensity of Ground Shaking (1 in = 2.54 cm).....	180
6.9	Pile Forces (kips) and Storey Drift (in) for Five-Storey Building Supported by 15, 21 and 27 Piles for Different Earthquake Intensity: (a) Pinned Endbearing Piles; (b) Pinned Floating Piles.....	181
6.10a	Base Shear of 5-Storey Building vs. Number and Type of Piles and Intensity of Ground Shaking (1 kip = 4.45 kN).....	183
6.10b	Overturning Moment of 5-Storey Building vs. Number and Type of Piles and Intensity of Ground Shaking (1 kip.ft = 1.36 kN.m).....	184
6.11a	Pile Forces (kips) and Storey Drift (in) for Ten-Storey Building Supported by 27 Piles Arranged in Three or Five Rows ($\hat{a} = 0.11g$).....	185
6.11b	Pile forces (kips) and Storey Drift (in) for Ten-Storey Building Supported by 21 Piles Arranged in Three or Five Rows ($\hat{a} = 0.11g$).....	186
6.12	Pile Configurations.....	187

Figure	Description	Page
6.13	Power Spectrum for San Fernando Earthquake Acceleration.....	188
6.14	Response of Mat Supported Full Silo to Seismic Excitation: (a) Sliding in Horizontal Direction, u ; (b) Rocking in the Vertical Plane, ψ	189
7.1	Main Types of Wind-Induced Oscillations: (a) Vibration Due to Turbulence, (b) Vibration Due to Vortex Shedding, and (c) Aerodynamic Instability.....	231
7.2	Vertical Profiles of Mean Wind Velocity for Three Typical Terrains.....	231
7.3	Universal Spectrum of Horizontal Gustiness in Strong Winds.....	232
7.4	Relationship of Distribution of Largest Peak Value to Distribution of All Values (For a Stationary Random Process).....	232
7.5	Structural Model: (a) N-Story Building; (b) Story Unit; Forces on jth Story Unit.	233
7.6	Transition From Gust Spectrum to Response Spectrum (Ref. 106).....	234
7.7	Spectrum of Structural Response With Indication of Resonance Effect and Background Turbulence Effect.....	234
7.8	Peak Factor as a Function of Average Fluctuation Rate (Ref. 108).....	235
7.9	Exposure Factor as a Function of Terrain Roughness and Height Above Ground (Ref. 108).....	235
7.10	Background Turbulence Factor as a Function of Width and Height of Structure (Ref. 108).....	236
7.11	Size Reduction Factor as a Function of Width, Height and Reduced Frequency of Structure (Ref. 108).....	236

Figure	Description	Page
7.12	Gust Energy Ratio as a Function of Wave Number (Ref. 108).....	237
7.13	Flat Roof Buildings of Height Greater Than Twice the Width (Ref. 108).....	237
7.14	Windward and Leeward Forces Due to Wind Pressure.....	238
7.15	First Mode Damping Ratios of 10-Storey Building On Mat Foundation Computed With Various Shear Wave Velocities of Soil....	239
7.16	Variation of Gust Effect Factor, Maximum Top Total and Mean Displacements of 10-Storey Building on Mat Foundation With Wave Velocity of Soil (Exposure A; ∞ Indicates Fixed Base).....	240
7.17	Natural Frequency and Along and Across Wind Acceleration of 10-Storey Building on Mat Foundation Computed With Various Shear Wave Velocities of Soil (Exposure A; ∞ Indicates Fixed Base).....	241
7.18	First Mode Damping Ratios of 20-Storey Building on Mat Foundation Computed With Various Shear Wave Velocities of Soil....	242
7.19	Variation of Gust Effect Factor, Maximum Top Total and Mean Displacements of 20-Storey Building on Mat Foundation With Wave Velocity of Soil (Exposure A; ∞ Indicates Fixed Base).....	243
7.20	Natural Frequency and Along and Across Wind Acceleration of 20-Storey Building on Mat Foundation Computed With Various Shear Wave Velocity of Soil (Exposure A; ∞ Indicates Fixed Base).....	244
7.21	Natural Frequencies and Modal Damping Ratios of Chimney Computed With Various Shear Wave Velocities of Soil (Ref. 30)..	245
7.22	Variations of Gust Effect Factor for Chimney With Shear Wave Velocity of Soil (Three Exposures) (Ref. 30).....	245

NOMENCLATURE

A	=	face area of the structure, pile cross-sectional area
A_j	=	scalar
A_p	=	area of anvil or foundation pad
a_o	=	dimensionless frequency
a_D, a_W	=	along-wind and across-wind accelerations respectively
a, b	=	dimensions of rectangular base
B	=	background turbulence factor
B_j	=	scalar
b	=	depth of building
c_D	=	drag coefficient
C_e	=	exposure factor
c_o	=	impact velocity of hammer head
C_p	=	pressure coefficient
C_h	=	damping constant including material damping
c_{ij}	=	constant of equivalent viscous damping of structure or foundation
\bar{c}_{ij}	=	constant of equivalent viscous damping of foundation embedded in a homogeneous soil layer
D^a	=	aerodynamic damping
D_j	=	damping ratio of structure derived from soil
D_j^s	=	damping ratio of structure due to internal damping
D_j^t	=	total damping ratio of mode j
\bar{D}_j^s	=	structural damping ratio in case of rigid foundation

- E = complex constant
 E_p = Young's modulus of the pile, Young's modulus of the pad
 e = eccentricity of the hammer blow
 F = force, gust energy ratio
 \bar{F} = mean drag force
 F_i = external dynamic force pertinent to mass m_i
 f = frequency
 f_j = generalized force
 $f_{1,2}$ = dimensionless stiffness and damping parameters of pile, respectively
 $F_p(\omega), F_u(\omega)$ = Fourier transform of input forces and output displacement respectively
 G = soil shear modulus, gust effect factor
 G^* = complex shear modulus of soil
 G_s = shear modulus of the side layer
 g, g_α = peak factor
 g_0 = gravity acceleration
 H = thickness of soil layer including embedment
 $|H(\omega)|$ = transfer function
 h = depth of soil stratum, thickness of anvil or foundation pad
 h_i = height of i th floor
 I = pile moment of inertia, total mass moment of inertia
 K_j = scalar related to stiffness
 k_{ij} = stiffness constants of structure or foundation
 \bar{k}_{ij} = stiffness constants of foundation embedded in a homogeneous soil layer

- K_h = stiffness constant including material damping
- k_r = coefficient of restitution
- \hat{k} = effective stiffness matrix
- l = embedment depth
- l_i = tributary height of floor i
- M_b = base moment
- M_j = scalar related to mass; generalized mass
- m_i = ith mass of system
- m_b = mass of base
- N = number of floors, number of degrees of freedom
- n = number of piles, number of waveforms
- P_j = generalized force
- P_x = foundation force in the horizontal direction
- P_o = force amplitude (pulse)
- $p(v)$ = probability density function of velocity fluctuation
- Q_b = base shear
- q = reference mean-velocity pressure
- q_j = generalized coordinates of mode j
- R = radius or equivalent radius of foundation base for vertical and horizontal translation
- R_ψ = equivalent radius of foundation for rocking
- S = size reduction factor
- $S_F(f)$ = drag spectrum
- $S_p(\omega)$ = spectra of driving force
- $S_{p_{ij}}(f)$ = cross-spectral densities of the excitation forces

$S_u(\omega)$ = spectra of response
 $S_{\ddot{u}_g}(\omega)$ = local spectrum of ground acceleration
 $S_{\ddot{u}_g}^n(\omega)$ = normalized spectrum of ground acceleration
 $S_{1,2}(f)$ = cross-spectrum of wind speed at stations 1 and 2
 $S_V(f)$ = spectral density of fluctuating wind velocity
 u = horizontal translation
 u_b = horizontal displacement of base
 t_p = pulse duration
 \bar{u} = mean displacement
 \hat{u} = peak displacement
 \ddot{u}_g = ground acceleration
 \bar{V} = mean wind velocity
 V_s = shear wave velocity of soil
 v = vertical displacement
 $v(t)$ = fluctuating component of wind velocity
 W = width of building
 $|X_{aero}|^2$ = aerodynamic admittance function
 $|X_{mech}|^2$ = mechanical admittance function
 Y_c = vertical distance of the reference point from the base
 Z = complex modal coordinates
 z = variable
 α = exponent of velocity
 β = material damping ratio, constant of damping proportionality
 γ_{12}^2 = coherence function

Δ	=	peak displacement
Δ_i	=	storey drift of floor i
Δ_{st}	=	static displacement
ΔP	=	effective load vector
Δt	=	time interval
δ	=	embedment ratio, loss angle
η_j	=	generalized displacement of mode j
$\overline{\eta_i \eta_j}$	=	covariance of generalized coordinates
θ	=	dimensionless parameter
κ	=	surface drag coefficient
μ	=	complex eigenvalue, apparent frequency
ν	=	Poisson's ratio of the soil, average fluctuation rate
ϵ_g	=	ground damping ratio
ϵ_j	=	coefficient of structural damping modification in mode j caused by foundation flexibility
ρ	=	mass density of the halfspace, air density
ρ_b	=	equivalent density of building
ρ_s	=	mass density of the side layer
σ_i	=	the root mean square of function i
τ	=	variable (dummy time), extended time period
ϕ	=	complex modal displacement, undamped vibration mode
ϕ	=	phase shift
ψ	=	rotation in the vertical plane
ω_j	=	circular frequency of mode j
ω_g	=	ground predominant frequency

$\omega_u, \omega_v =$ first natural frequencies of the soil layer in the horizontal and vertical directions respectively

$\bar{\omega}_j =$ frequency close or equal to ω_j and equal to $|\mu|$

$\omega'_j =$ damped natural frequency

CHAPTER 1

INTRODUCTION

1.1 STATEMENT OF THE SOIL-STRUCTURE INTERACTION PROBLEM

A soil-structure interaction problem arises when the motion of the structure footing differs from that of the ground. Thus, effects of soil-structure interaction can be attributed to soil flexibility or compliance and associated energy dissipation in the form of wave propagation in the soil. Because soil flexibility is a relative notion, it is especially important to consider soil-structure interaction effects in the analysis and design of massive stiff structures.

The effect of soil flexibility on the dynamic response of structures can be favorable or unfavorable and can, therefore, represent a significant consideration in design. For this reason, soil-structure interaction has been a subject of considerable research in the last fifteen years. Nowadays, two methods of analysis are most often used to study the dynamic response of structures on flexible soils, namely the finite element method and the impedance approach.

The finite element method was first used by Clough (1)

and quickly spread into many fields, see e.g., Desai and Abel (2). Among the many applications, finite elements have been used to model the soil in the soil-structure interaction problems (3,4,5). Usually, a large mass of the soil near the structure is discretized by two-dimensional plane strain elements or axisymmetric solid elements. Frequently, the number of degrees of freedom for the soil model far exceeds that for the structure which is the real subject of investigation. Thus the overall efficiency of this approach may be poor (Clough and Penzien (6)) and very costly. However, it is a powerful tool which can give detailed information about the response and other effects such as liquefaction of the soil under a building in the case of seismic analysis. Also, it permits a non-linear analysis if the constitutive relations for the soil are available.

The impedance approach is based on the idea of substructuring. First, the foundation of the structure is considered alone and usually assumed to be rigid with only a few degrees of freedom. The supporting soil is either a deep deposit modeled by a homogeneous or nonhomogeneous viscoelastic halfspace or a shallow layer modeled as a homogeneous viscoelastic stratum of limited thickness (7 to 14). For a rigid foundation, only six-by-six stiffness and damping (impedance) matrices have to be

established. The second step, required only in the case of a seismic excitation, determines the modification of the ground motion due to the presence of the foundation (kinematic interaction). The third step is the dynamic analysis of the structure supported on a flexible soil defined by the stiffness and damping matrices of the foundation, subjected either to a direct dynamic loading or to the soil motion defined in the second step (inertial interaction). The kinematic interaction effect vanishes, if the foundation rests on the surface and the seismic waves are assumed to have the form of vertically propagating shear waves.

The impedance or substructure approach is limited to linear systems since it is based on the principle of superposition. However, nonlinear soil behavior can be accounted for by equivalent linearization or by adjusting the soil properties to the level of strain.

Using the impedance approach, the dynamic response of the soil-structure interaction system can be analyzed much more easily. A frequency domain analysis or a time domain analysis can be performed (15 to 17). The impedance approach was incorporated into the well known document ATC (14).

1.2 OBJECTIVE OF THE STUDY

The main object of this investigation is to examine the effects of soil-structure interaction under various types of dynamic loads using the impedance approach. First, the ways in which foundation properties can be described and included in the evaluation of modal properties and response to dynamic loads are outlined. Then, the effect of soil-structure interaction on the free vibration is studied. Finally, the dynamic response of structures supported by various types of foundations and exposed to earthquake, wind and impact loading is investigated. A variety of superstructures are analyzed. Some attention is given to structures supported by pile foundations and subjected to seismic excitation and uplift.

1.3 ORGANIZATION OF THE STUDY

This thesis consists of eight chapters. The literature survey and evaluation of recent work are included in the introduction to each chapter.

Chapter 1 introduces the general topic of soil-structure interaction and the objectives of the study.

Chapter 2 investigates the impedance functions used to represent the soil and introduces the equations of

motion for soil-structure interaction systems.

Chapter 3 describes classical and nonclassical modes of free vibration, a study of the effect of soil flexibility on modal properties, and presents a parametric study.

Chapter 4 deals with the methods of solution. These include initial value problems and transient problems.

Chapter 5 presents applications of the initial value approach to problems of shock loading. This is applied specifically to the problem of hammer foundations.

Chapter 6 investigates the soil-structure systems under seismic loads. Structures supported by different types of shallow foundations and by pile foundations with the uplift of the pile cap prevented or allowed are examined.

Chapter 7 deals with the response of the soil-structure interaction system excited by wind loading.

Chapter 8 gives the summary and conclusions.

CHAPTER 2

IMPEDANCE FUNCTIONS OF FOUNDATION

2.1 INTRODUCTION

For most structures, a simple and realistic way to model soil compliance in dynamic analysis of a building is to assume that the foundation of the building is a rigid body resting on soil represented by a suitable mathematical model. This model may consist of a spring and a dashpot defined for each possible degree of freedom of the rigid foundation of a structure (18). There are two ways in which the soil compliances can be presented.

(a) Frequency dependent compliance functions (10, 19, 20, 21, 22). Complex stiffness functions are formulated for footing resting at or near the surface, using the theory of a viscoelastic halfspace or a viscoelastic layered system. The halfspace and layered medium theories may also be used to generate approximate functions for embedded structures (23, 24).

(b) Frequency independent foundation springs plus dashpots may be employed (23, 25, 26). Various methods may be used to estimate these approximate representations of the soil.

The theories available can also be used in conjunction with equivalent linear soil properties to approximate nonlinear soil behavior. Once a linear model of the soil-structure system is set up, the equations of motion can be stated.

This chapter presents a summary of approaches and formulae which can be used to evaluate the impedance functions of both shallow and deep foundations.

2.2 IMPEDANCE FUNCTIONS FOR SHALLOW FOUNDATION

The principal advantages of the halfspace theory are that it accounts for energy dissipation through elastic waves (geometric damping), provides for systematic analysis, and describes soil properties by basic constants such as shear modulus or shear wave velocity that can be established by independent experiments. The theory presumes that the impedance functions are obtained from the analytical study of the response of a harmonically excited rigid foundation usually assumed to be circular (Figure 2.1). The basic theory also presumes that the foundation rests on the surface of the ground and that the halfspace is linearly elastic or viscoelastic, homogeneous, and isotropic. These assumptions differ from real conditions and, therefore, some adjustment of the theoretical results

is necessary in order to account for the shape of the base, embedment of the foundation, soil nonhomogeneity, and limited thickness of the soil stratum.

The correction for the shape of the base is made by the introduction of the equivalent radius of the base. The radius of the equivalent circular base, the equivalent radius for brevity, is usually determined by equating the areas of the true base and the equivalent base for the vertical and horizontal translations and from the equality of moments of inertia (second moment of area) for the rotation in the vertical plane (rocking). From these conditions, the following equivalent radii are obtained for a rectangular base having dimensions a and b (Figure 2.2):

Equivalent radii for

$$\text{Translation} \quad R = \sqrt{ab/\pi} \quad (2.1a)$$

$$\text{Rocking} \quad R_{\psi} = \sqrt[4]{a^3 b/3\pi} \quad (2.1b)$$

The equivalent radius works very well for square areas and quite well for rectangular areas with ratios a/b of up to about 2 (27). With increasing ratio a/b , the accuracy of this approach deteriorates. Dominquez (28) provided a solution method to obtain the dynamic stiffness functions for square and rectangular foundations. For

very long foundations the assumption of an infinite strip foundation may also be used (Gazetas (29)).

The stiffness, k_{ij} , and damping, c_{ij} , of a foundation are defined as forces in direction i associated with a unit amplitude and a unit vibration velocity, respectively, in direction j . For surface foundations, these stiffness and damping functions were presented by Veletsos and Verbic (10) and a few others. Novak et al. (25, 31) developed an approximate practical method for taking into account realistic embedment conditions, which when combined with surface foundation impedances such as those of Veletsos results in the following stiffness and damping constants:

For vertical vibration v , the stiffness constant is

$$k_{vv} = GR(\bar{c}_{v1} + \frac{G_s}{G} \delta \bar{s}_{v1}) \quad (2.2a)$$

and the damping constant is

$$c_{vv} = R^2 \sqrt{\rho G} (\bar{c}_{v2} + \bar{s}_{v2} \delta \sqrt{\frac{\rho_s G_s}{\rho G}}) \quad (2.2b)$$

For coupled horizontal translation u and rocking ψ , the stiffness constants are

$$k_{uu} = GR(\bar{c}_{u1} + \frac{G_s}{G} \delta \bar{s}_{u1}) \quad (2.3a)$$

$$k_{\psi\psi} = GR^3 \left[\left(\frac{y_c}{R} \right)^2 \bar{c}_{u1} + \frac{G_s}{G} \delta \left(\frac{\delta^2}{3} + \frac{y_c^2}{R^2} - \delta \frac{y_c}{R} \right) \bar{s}_{u1} \right] \quad (2.3b)$$

$$+ GR^3 \left(\bar{c}_{\psi 1} + \frac{G_s}{G} \frac{l}{R_\psi} \bar{s}_{\psi 1} \right)$$

$$k_{u\psi} = -GR[y_c \bar{c}_{u1} + \frac{G_s}{G} \delta (y_c - \frac{1}{2}\ell) \bar{s}_{u1}] \quad (2.3c)$$

and the damping constants are

$$c_{uu} = \sqrt{\rho G} R^2 (\bar{c}_{u2} + \delta \sqrt{\frac{\rho_s}{\rho} \frac{G_s}{G}} \bar{s}_{u2}) \quad (2.4a)$$

$$c_{\psi\psi} = \sqrt{\rho G} R^4 \left[\left(\frac{y_c}{R}\right)^2 \bar{c}_{u2} + \delta \sqrt{\frac{\rho_s}{\rho} \frac{G_s}{G}} \left(\frac{\delta^2}{3} + \frac{y_c^2}{R^2} - \delta \frac{y_c}{R}\right) \bar{s}_{u2} \right] + \sqrt{\rho G} R^4 (\bar{c}_{\psi 2} + \frac{\ell}{R_\psi} \sqrt{\frac{\rho_s}{\rho} \frac{G_s}{G}} \bar{s}_{\psi 2}) \quad (2.4b)$$

$$c_{u\psi} = -\sqrt{\rho G} R^2 [y_c \bar{c}_{u2} + \delta \sqrt{\frac{\rho_s}{\rho} \frac{G_s}{G}} (y_c - \frac{1}{2}\ell) \bar{s}_{u2}] \quad (2.4c)$$

In these equations, the embedment ratio $\delta = \ell/R$, where ℓ is the embedment depth (Figure 2.3) and y_c = the vertical distance of the reference point, C.G., from the base. Parameters c, \bar{c} relate to the stiffness and damping, respectively, derived from the medium under the base (the elastic halfspace or a stratum); parameters s, \bar{s} relate respectively to the stiffness and damping derived from the reaction of the side layer; G = soil shear modulus; ρ = mass density of the halfspace; and G_s, ρ_s are the shear modulus and mass density of the side layer (backfill), respectively.

The parameters c and \bar{c} depend primarily on the depth of the stratum, h , Poisson's ratio, ν , and the dimensionless frequency

$$a_0 = R \omega / V_s \quad (2.5)$$

in which ω = circular frequency and $V_s = \sqrt{G/\rho}$ = shear wave velocity. The parameters s depend on the dimensionless frequency. Examples of the variation of c and s with a_0 and ν are shown in Figure 2.4 for halfspace.

The analysis can be simplified if the frequency dependent parameters are replaced by suitably chosen frequency independent parameters. Such constants are indicated in Table 2.1. The values are given for cohesive soils as well as for granular soils with Poisson's ratio presumed as 0.4 and 0.25 respectively. The values shown in Table 2.1 correspond to dimensionless frequencies between 0.5 and 1.5. For other dimensionless frequencies numerically more accurate values can be computed. If a large frequency range is of importance, parameters c and s should be considered as frequency dependent and calculated from the forming expressions.

2.3 ADJUSTMENTS OF THE HALFSPACE THEORY

Equations 2.2 to 2.4 give results that agree quite well with the finite element solution (32), but some

adjustments are desirable to bring the numerical results of the formulae closer to experimental observations. These include: discrepancies between theory and experiments in the calculation of geometric damping, embedment, imperfect elasticity of the soil, and shallow layer. These are covered in the next four sections.

2.3.1 Corrections for Geometric Damping

Experiments indicate (33) that the halfspace theory tends to considerably overestimate the geometric damping of the surface foundation in the vertical direction. The reason for this discrepancy seems to be that the soil usually features some layering that reflects elastic waves back to the foundation and reduces geometric damping. An empirical reduction of \bar{c}_{v2} shown in Table 2.1 to about one half the values valid for homogeneous halfspace appears advisable for practical applications.

On the other hand, the first resonant amplitudes of coupled response of surface footings to horizontal forces are often overestimated by several hundred percent if material damping is neglected. This discrepancy, caused by the low level of radiation damping in rocking, can be eliminated by the inclusion of material damping as will be outlined in section 2.3.3.

2.3.2 Embedment Effects

The theory indicates that embedment provides a significant source of geometric damping and contributes also to stiffness. These theoretical suggestions were, in general, confirmed by experiments (33). However, it was also observed that, with heavy vibration, the soil may separate from the footing sides and a gap may occur as indicated in Figure 2.3. This gap is likely to develop close to the surface where the confining pressure is not sufficient to maintain the bond between the soil and foundation. The separation may be accounted for by considering an effective embedment depth, ℓ , smaller than the actual embedment depth L . The effective depth, of course, depends on conditions. The best bond is obtained when the footing is cast directly into the excavation. Another way of accounting for footing separation is to assume a weakened zone around the footing (34). When the footing is cast in forms and then backfilled, the backfill shear modulus and density are usually lower than the original values. Unless established more accurately, the ratios $\rho_s/\rho = 0.75$ and $G_s/G = 0.5$ may be adequate.

2.3.3 Soil Material Damping

Foundation stiffness and damping are also affected by imperfect elasticity of soil which manifests itself as

material damping. The material damping of soil is hysteretic and independent of frequency. It is conveniently described using the complex shear modulus

$$G^* = G + iG' = G(1 + i \tan \delta) \quad (2.6)$$

in which $i = \sqrt{-1}$, $\tan \delta = G'/G$, $\delta =$ the loss angle, and G' = the imaginary part of the complex soil modulus.

Another measure of material damping is the damping ratio

$$\beta = \frac{1}{2} \tan \delta .$$

Material damping can be incorporated using the correspondance principle of viscoelasticity. In the sense of the principle, the shear modulus, G , can be replaced by the complex shear modulus, G^* , everywhere it occurs in equations 2.2 to 2.4, that is even in $a_0 = \omega R / \sqrt{G/\rho}$. Approximately and after some manipulation, the stiffness and damping constants including material damping may be calculated as:

$$K_h = k - 2\beta c\omega \quad (2.7a)$$

$$C_h = c + 2\beta k/\omega \quad (2.7b)$$

in which k and c are evaluated from equations 2.2 to 2.4 without regard to material damping. As equations 2.7 suggest, material damping reduces the stiffness but increases the total damping. The degree of these effects

depends on the magnitude of both material and geometric damping. For vertical vibration and a halfspace, i.e., a deep layer under the footing, these effects are small; for rocking they are very significant.

With layers, the incorporation of material damping is particularly important as will be explained in the next section.

2.3.4 Shallow Layers

Another correction of the halfspace theory may be required if the deposit is a shallow layer. In such a case, the stiffness increases and geometric damping decreases or even vanishes. These effects, recognized already in the early studies such as (35), can be seen from Figure 2.5 in which the stiffness and damping parameters are plotted in dashed lines for layers of different depths, h , with material damping neglected. The parameters for the halfspace and side layers are also shown for comparison. This behavior is further elucidated by more general solutions of layered media presented by Bycroft (36), Luco (37), and others.

It can be seen from Figure 2.5 that geometric damping of strata is quite small or even absent at low frequencies. Then material damping may be the principal source of energy

dissipation. It can be evaluated using equation 2.7b.

Studies of the behavior of strata suggest that geometric damping may completely vanish if the frequency of interest, e.g., the excitation frequency, is lower than the first natural frequency of the soil layer (27, 38). For a homogeneous layer with soil shear wave velocity V_s , the first natural frequencies are

$$\omega_v = \frac{\pi V_s}{2h} \sqrt{\frac{2(1-\nu)}{1-2\nu}} \quad (2.8a)$$

for the vertical direction and

$$\omega_u = \frac{\pi V_s}{2h} \quad (2.8b)$$

for the horizontal direction. At frequencies lower than ω_v or ω_u , only material damping remains because no progressive wave occurs to generate geometric damping in the absence of material damping and only a very weak progressive wave occurs in the presence of material damping. The correction for a shallow layer is most important for both the vertical and horizontal directions in which the geometric damping of the halfspace is highest.

Footings embedded in a layer of limited thickness were also studied by a few investigators using the finite element method. The static stiffness for the horizontal and rocking modes was derived by Elsabee (39) and for the vertical and torsional modes by Kausel and Ushijima (12).

These authors suggest the following empirical expressions for the impedance functions for foundations embedded in a homogeneous soil layer:

$$\bar{k}_{uu} = k_{uu}^0 (k_{uu} - 2\omega\beta c_{uu}) \quad (2.9a)$$

$$\bar{k}_{\psi\psi} = k_{\psi\psi}^0 (k_{\psi\psi} - 2\omega\beta c_{\psi\psi}) \quad (2.9b)$$

$$\bar{k}_{u\psi} = k_{u\psi}^0 (k_{uu} - 2\omega\beta c_{uu}) \quad (2.9c)$$

$$\bar{c}_{uu} = k_{uu}^0 (c_{uu} + 2\beta k_{uu}/\omega) \quad (2.10a)$$

$$\bar{c}_{\psi\psi} = k_{\psi\psi}^0 (c_{\psi\psi} + 2\beta k_{\psi\psi}/\omega) \quad (2.10b)$$

$$\bar{c}_{u\psi} = k_{u\psi}^0 (c_{uu} + 2\beta k_{uu}/\omega) \quad (2.10c)$$

where \bar{k} and \bar{c} are stiffness and damping constants for shallow layer; k_{uu} , $k_{\psi\psi}$ are those of halfspace given by equations 2.3a and b with embedment terms, $s = 0$; β is material damping ratio; correction factors are:

$$k_{uu}^0 = (1 + \frac{R}{2H}) (1 + \frac{2\ell}{3R}) (1 + \frac{5\ell}{H}) \quad (2.11a)$$

$$k_{u\psi}^0 = R (.4 \frac{\ell}{R} - .03) k_{uu}^0 \quad (2.11b)$$

$$k_{\psi\psi}^0 = (1 + \frac{R}{6H}) (1 + \frac{2\ell}{R}) (1 + .71 \frac{\ell}{H}) \quad (2.11c)$$

in which R , ℓ , H are defined earlier as footing radius, embedment depth and thickness of layer including embedment. These correction factors are actually the modified static

stiffness functions provided by Kausel (19) divided by the corresponding static stiffnesses for halfspace. Also in equations 2.8 and 2.9:

$$c_{uu} = \left(\frac{8GR}{2-\nu}\right) \left(\frac{R}{V_s}\right) \frac{.65\beta a_{o1}}{1-(1-2\beta)a_o} \quad \text{for } a_o \leq \frac{\pi R}{2h} = a_{o1} \quad (2.12a)$$

For $a_o > a_{o1}$, c_{uu} is the halfspace solution (equation 2.4a with embedment terms $s = 0$), and

$$c_{\psi\psi} = \left(\frac{8GR^3}{3(1-\nu)}\right) \left(\frac{R}{V_s}\right) \left(\frac{.5\beta a_{o2}}{1-(1-2\beta)a_o}\right) \quad \text{for } a_o \leq \frac{\pi R}{2h} \sqrt{\frac{2(1-\nu)}{1-2\nu}} = a_{o2} \quad (2.12b)$$

For $a_o > a_{o2}$, $c_{\psi\psi}$ is the halfspace solution (equation 2.4b with embedment terms $s = 0$), where a_{o1} and a_{o2} are the (non-dimensional) fundamental shear beam and dilatation frequencies of the stratum. These stiffnesses refer to the C.G. of the base and are valid for $\delta = l/R \leq 1.5$, $l/H \leq 0.75$ and $R/H \leq 0.5$. Figure 2.6 shows these stiffness functions. In the low frequency range, these stiffness functions of layers differ substantially from those of the halfspace, as the geometric damping vanishes below the first layer resonance, and also differ from those produced by Warburton (35) for vertical vibration (Figure 2.5).

2.4 PILE FOUNDATIONS

Stiffness and damping of piles are affected by their interaction with the surrounding soil. In the past, consideration of this interaction was limited to the determination of the length of the so-called equivalent cantilever which was a free standing, bare pile shorter than the embedded pile. Pile damping was estimated:

More recent approaches (38, 40 to 45) consider soil-pile interaction in terms of continuum mechanics and account for propagation of elastic waves. For single piles, such studies indicate that dynamic soil-pile interaction modifies pile stiffness making it, in general, frequency dependent and generates geometric damping through energy radiation as with shallow foundations.

In groups of closely spaced piles, the character of dynamic stiffness and damping is further complicated by interaction between individual piles known as pile-soil-pile interaction or the group effect. Only recently were the solutions extended to include dynamic interaction between the piles in the group (46 to 51). Dynamic behavior of closely spaced pile groups is very complicated because it is much more frequency dependent than the behavior of single piles and its analysis requires the use of an efficient computer program. Nevertheless, an

approximate evaluation of group stiffness and damping is possible at least in some situations, for example at low frequencies, smaller groups or relatively large spacing between the piles. In such cases, the group stiffness and damping can be predicted using the properties of a single pile and accounting for the group effects by means of the interaction factors. For static loading, these factors were presented in the form of charts by Poulos (52 to 55). and for dynamic loads by Kaynia and Kausel (46).

When the spacing between the piles is large, pile-soil-pile interaction effects become negligible and the group stiffness and damping can be calculated by summation of the properties of single piles.

Thus, the stiffness and damping of single piles are basic items of information. Novak et al. (56) provided tabulated data and charts which facilitate the evaluation of stiffness and damping of vertical single piles for the following conditions: Soil is homogeneous or its shear modulus diminishes upward according to a quadratic parabola; pile heads are fixed or pinned; the piles are end-bearing or floating; and finally, geometric damping may be absent and material hysteresis may be the only source of damping.

2.4.1 Stiffness and Damping of Single Piles

Theoretical studies done by Novak (42) have shown that the stiffness constants, k , and the constants of equivalent viscous damping, c , of single piles can be described for individual motions of the pile head (Figure 2.7) as follows:

Vertical translation, v :

$$k_v = \frac{E_p A}{R} f_{v1}, \quad c_v = \frac{E_p A}{V_s} f_{v2} \quad (2.13a)$$

Horizontal translation, u :

$$k_u = \frac{E_p I}{R^3} f_{u1}, \quad c_u = \frac{E_p I}{R^2 V_s} f_{u2} \quad (2.13b)$$

Rotation of the pile head in the vertical plane, ψ :

$$k_\psi = \frac{E_p I}{R} f_{\psi1}, \quad c_\psi = \frac{E_p I}{V_s} f_{\psi2} \quad (2.13c)$$

Coupling between horizontal translation and rotation:

$$k_c = \frac{E_p I}{R^2} f_{c1}, \quad c_c = \frac{E_p I}{R V_s} f_{c2} \quad (2.13d)$$

where $k_c = k_{u\psi} = k_{\psi u}$.

In these expressions, E_p is the Young's modulus of the pile, A and I its cross-sectional area and moment of inertia (second moment of area), respectively and R pile radius or equivalent radius; and $V_s = \sqrt{G/\rho}$ is the characteristic shear wave velocity of soil; G = shear modulus

of soil and ρ its mass density.

The symbol $f_{1,2}$ represents dimensionless stiffness and damping functions (parameters) whose subscript 1 refers to stiffness and 2 refers to damping. The most important factors controlling these functions are: the stiffness ratio relating soil stiffness to pile stiffness, E_p/G , the soil profile and for the vertical direction, the tip condition and the slenderness ratio ℓ/R . For these factors, the stiffness and damping parameters $f_{1,2}$ appearing in equation 2.13 are given in Table 2.2 and Figures 2.8 and 2.9. These functions were calculated with material damping $\tan\delta = 0.05$ for soil and 0.01 for piles, mass ratio $\rho/\rho_p = 1$ and, apart from the layer, $a_0 = 0.3$ (43, 58) but with some qualifications outlined in (56) they can be used for other conditions as well. Also, a uniform circular cross-section was assumed.

Table 2.2 gives the parameters $f_{1,2}$ associated with horizontal vibration and rocking of pile heads. The soil is presumed to be homogeneous with depth.

Also included in Table 2.2 are data denoted f_{u1}^P and f_{u2}^P . These correspond to pin-headed piles for which the moment stiffness, k_ψ , and thus f_ψ , as well as the coupling stiffness $k_c = k_{u\psi} = k_{\psi u}$ and damping $c_c = c_{u\psi} = c_{\psi u}$ all vanish. The stiffness and damping of pin-headed piles

Table 2.2 Stiffness and Damping Parameters of Horizontal Response for Piles
 With $\lambda/R > 25$ for Homogeneous Soil Profile and $\lambda/R > 30$ for
 Parabolic Soil Profile (Ref. 56)

ν	E_{pile}	Stiffness Parameters					Damping Parameters				
		G_{soil}	$f_{\psi 1}$	f_{c1}	f_{u1}	f_{u1}^p	$f_{\psi 2}$	f_{c2}	f_{u2}	f_{u2}^p	
0.25	10000	0.2135	-0.0217	0.0042	0.0021	0.1577	-0.0333,	0.0107	0.0054		
	2500	0.2998	-0.0429	0.0119	0.0061	0.2152	-0.0646	0.0297	0.0154		
	1000	0.3741	-0.0668	0.0236	0.0123	0.2598	-0.0985	0.0579	0.0306		
	500	0.4411	-0.0929	0.0395	0.0210	0.2953	-0.1337	0.0953	0.0154		
	250	0.5186	-0.1281	0.0659	0.0358	0.3299	-0.1786	0.1556	0.0864		
0.40	10000	0.2207	-0.0232	0.0047	0.0024	0.1634	-0.0358	0.0119	0.0060		
	2500	0.3097	-0.0459	0.0132	0.0068	0.2224	-0.0692	0.0329	0.0171		
	1000	0.3860	-0.0714	0.0261	0.0136	0.2677	-0.1052	0.0641	0.0339		
	500	0.4547	-0.0991	0.0436	0.0231	0.3034	-0.1425	0.1054	0.0570		
	250	0.5336	-0.1365	0.0726	0.0394	0.3377	-0.1896	0.1717	0.0957		

HOMOGENEOUS SOIL
 PROFILE

point. Then the stiffness and damping constants are defined as forces that must act at the centroid to produce a sole unit displacement or unit velocity at the reference point. From this definition and the notation of Figure 2.10, the stiffness and damping constants of the pile group for the individual directions are as follows:

Vertical translation:

$$k_{vv} = \sum_r k_v \quad (2.14a)$$

$$c_{vv} = \sum_r c_u \quad (2.14b)$$

Horizontal translation:

$$k_{uu} = \sum_r k_u \quad (2.15a)$$

$$c_{uu} = \sum_r c_u \quad (2.15b)$$

Rotation of the cap in the vertical plane:

$$k_{\psi\psi} = \sum_r (k_{\psi} + k_v x_r^2 + k_u y_c^2 - 2k_c y_c) \quad (2.16a)$$

$$c_{\psi\psi} = \sum_r (c_{\psi} + c_v x_r^2 + c_u y_c^2 - 2c_c y_c) \quad (2.16b)$$

Coupling between horizontal translation and rotation:

$$k_{u\psi} = k_{\psi u} = \sum_r (k_c - k_u y_c) \quad (2.17a)$$

$$c_{u\psi} = c_{\psi u} = \sum_r (c_c - c_u y_c) \quad (2.17b)$$

The summation extends over all the piles. The distances

x_r, y_c refer to the reference point as indicated in Figure 2.10.

For closely spaced piles, equations 2.14 to 2.17 should be corrected for the pile-soil-pile interaction effects as already mentioned.

Many more data on impedance functions are available. Only those used in this study later herein are presented in this chapter.

2.5 FORCE-DISPLACEMENT RELATIONSHIP OF FOUNDATION

The impedance functions, discussed in the previous two subsections for both shallow foundations and deep foundations (pile), relate the foundation forces, P_x and M_b , and the horizontal translation, u_b , and rotation in the vertical plane (rocking), ψ , as follows (Figure 2.11):

$$\begin{Bmatrix} P_x \\ M_b \end{Bmatrix} = \begin{bmatrix} k_{uu} & k_{u\psi} \\ k_{\psi u} & k_{\psi\psi} \end{bmatrix} \begin{Bmatrix} u_b \\ \psi \end{Bmatrix} + \begin{bmatrix} c_{uu} & c_{u\psi} \\ c_{\psi u} & c_{\psi\psi} \end{bmatrix} \begin{Bmatrix} \dot{u}_b \\ \dot{\psi} \end{Bmatrix} \quad (2.18)$$

in which $\dot{u} = du/dt$, $\dot{\psi} = d\psi/dt$ and t is time, k = stiffness constant and c = the constant of equivalent viscous damping. Equation 2.18 can also be written as:

$$\begin{Bmatrix} P_x \\ M_b \end{Bmatrix} = \begin{bmatrix} k_{uu}(\omega) & k_{u\psi}(\omega) \\ k_{\psi u}(\omega) & k_{\psi\psi}(\omega) \end{bmatrix} \begin{Bmatrix} u_b \\ \psi \end{Bmatrix} \quad (2.19)$$

where $k(\omega) = k + i\omega c$ is the complex stiffness. Its real (in-phase) part defines the true stiffness, k , while its imaginary (out-of-phase) part describes the constant of equivalent viscous damping, c .

Either of equations 2.18 or 2.19 can be used to represent the force displacement relationship of the foundation depending on the method of solution of the equations of motion.

2.6 SOIL-STRUCTURE INTERACTION SYSTEM

A simple structure-foundation system, representing a shear building, is shown in Figure 2.12b. This simple system is chosen for discussion purposes mainly to facilitate the description of the soil-structure interaction phenomenon. The structure will be subjected to horizontal loads, e.g. free-field ground motion or wind loading. The displacement of the N floors and two interaction displacements at the base, u_b and ψ , completely define the response of the system.

The equation expressing the horizontal dynamic equilibrium of the i th floor mass is

$$m_i (\ddot{u}_b + h_i \ddot{\psi} + \ddot{u}_i) + \sum_j c_{ij} \dot{u}_j + \sum_j k_{ij} u_j = F_i \quad (2.20a)$$

In addition, there are two equations expressing the equilibrium of the building as a whole in translation and rotation:

$$\begin{aligned} (\sum_i m_i + m_b) \ddot{u}_b + (\sum_i m_i h_i) \ddot{\psi} + \sum_i m_i \ddot{u}_i + c_{uu} \dot{u}_b + c_{u\psi} \dot{\psi} \\ + k_{uu} u_b + k_{u\psi} \psi = Q_b \end{aligned} \quad (2.20b)$$

$$\begin{aligned} (\sum_i m_i h_i^2) \ddot{u}_b + (\sum_i m_i h_i^2 + I_t) \ddot{\psi} + \sum_i m_i h_i \ddot{u}_i + c_{\psi u} \dot{u}_b + c_{\psi\psi} \dot{\psi} \\ + k_{\psi u} u_b + k_{\psi\psi} \psi = M_b \end{aligned} \quad (2.20c)$$

In these equations, c_{ij} and k_{ij} are evaluated using floor stiffness and damping constants c_j, k_j . For example, $c_{11} = c_1 + c_2$, $c_{12} = -c_2$, $c_{13} = 0$, etc., u_i denotes the displacement of the i th floor due to structural deformations relative to the base; F_i is the external dynamic force pertinent to mass m_i ; Q_b, M_b are the base shear and moment, respectively, caused by external excitation; h_i is the height of the i th node above the base; and m_b is the mass of the base. Also, in equation 2.20, the summations are taken from 1 to N except for the total mass moment of inertia which is

$$I_t = \sum_{i=1}^{N+1} I_i \quad (2.21)$$

and includes both the floors and the base.

Equations 2.20 can be combined into one matrix equation:

$$[m]\{\ddot{u}\} + [c]\{\dot{u}\} + [k]\{u\} = \{P\} \quad (2.22)$$

in which

$$\{u\} = \begin{Bmatrix} \{u_i\} \\ u_b \\ \psi \end{Bmatrix} \quad \{P\} = \begin{Bmatrix} \{F_i\} \\ Q_b \\ M_b \end{Bmatrix}$$

$$[m] = \begin{bmatrix} [m] & & \\ \hline & m_b + \sum_{i=1}^N & \sum_{i=1}^N m_i h_i \\ & & I_t + \sum_{i=1}^N m_i h_i^2 \end{bmatrix} \quad (2.23)$$

(symm)

$$[c] = \begin{bmatrix} [c] & \{0\} & \{0\} \\ \hline \{0\} & c_{uu} & c_{u\psi} \\ \{0\} & c_{\psi u} & c_{\psi\psi} \end{bmatrix}$$

$$[k] = \begin{bmatrix} [k] & \{0\} & \{0\} \\ \hline \{0\} & k_{uu} & k_{u\psi} \\ \{0\} & k_{\psi u} & k_{\psi\psi} \end{bmatrix}$$

The matrices $[c]$ and $[k]$ list all the stiffness and damping constants of the structure, $[m]$ is the diagonal mass matrix of the structure, and $\{0\}$ is the null vector. The total mass matrix $[m]$ is not diagonal, however.

The governing equation of free damped vibration of a lumped mass system can be obtained from equation 2.22 with the only difference being that the right side of equation 2.22 becomes the null vector, $\langle \{0\} \ 0 \ 0 \rangle^T$, which yields

$$[m]\{\ddot{u}\} + [c]\{\dot{u}\} + [k]\{u\} = \{0\} \quad (2.24)$$

2.7 CONCLUSIONS

In this chapter a brief review of the various foundation types and their impedance functions is presented. Of main concern here is the evaluation of the force-displacement relationship of the base shear and the base moment with respect to the base translation and rotation in the vertical plane. The structure is modeled with regular linear members. The values of the impedance functions depend on the material properties and on the geometric configuration of the buildings and the soil.

Once the input dynamic excitation and the base impedances are known, the last step is reduced to a dynamic analysis of a multidegree of freedom system.

Free vibration of the soil-structure interaction system and the effects of soil flexibility on modal properties are discussed in the next chapter.

The solution for dynamic excitations can be carried in the time domain or in the frequency domain. Both methods are discussed in Chapter 4.

Table 2.1 Stiffness and Damping Parameters (D=0) (Ref. 30)
 (Parameters \bar{s} , \bar{c} are those appearing in equations 2.2 to 2.4)

Motion	Soil	Side Layer		Halfspace	
Sliding	coh.	$s_{u1} = 4.1$	$\bar{s}_{u2} = 10.6$	$c_{u1} = 5.1$	$\bar{c}_{u2} = 3.2$
	gran.	$s_{u1} = 4.0$	$\bar{s}_{u2} = 9.1$	$c_{u1} = 4.7$	$\bar{c}_{u2} = 2.8$
Rocking	coh.	$s_{\psi1} = 2.5$	$\bar{s}_{\psi2} = 1.8$	$c_{\psi1} = 4.3$	$\bar{c}_{\psi2} = 0.7$
	gran.			$c_{\psi1} = 3.3$	$\bar{c}_{\psi2} = 0.5$
Vertical	coh.			$c_{v1} = 7.5$	$\bar{c}_{v2} = 6.8$
	gran.	$s_{v1} = 2.7$	$\bar{s}_{v2} = 6.7$	$c_{v1} = 5.2$	$\bar{c}_{v2} = 5.0$

Table 2.2 Stiffness and Damping Parameters of Horizontal Response for Piles
 With $\lambda/R > 25$ for Homogeneous Soil Profile and $\lambda/R > 30$ for
 Parabolic Soil Profile (Ref. 56)

ν	E_{pile}	Stiffness Parameters					Damping Parameters				
		G_{soil}	$f_{\psi 1}$	f_{c1}	f_{u1}	f_{u1}^P	$f_{\psi 2}$	f_{c2}	f_{u2}	f_{u2}^P	
0.25	10000	0.2135	-0.0217	0.0042	0.0021	0.1577	-0.0333,	0.0107	0.0054		
	2500	0.2998	-0.0429	0.0119	0.0061	0.2152	-0.0646	0.0297	0.0154		
	1000	0.3741	-0.0668	0.0236	0.0123	0.2598	-0.0985	0.0579	0.0306		
	500	0.4411	-0.0929	0.0395	0.0210	0.2953	-0.1337	0.0953	0.0154		
	250	0.5186	-0.1281	0.0659	0.0358	0.3299	-0.1786	0.1556	0.0864		
0.40	10000	0.2207	-0.0232	0.0047	0.0024	0.1634	-0.0358	0.0119	0.0060		
	2500	0.3097	-0.0459	0.0132	0.0068	0.2224	-0.0692	0.0329	0.0171		
	1000	0.3860	-0.0714	0.0261	0.0136	0.2677	-0.1052	0.0641	0.0339		
	500	0.4547	-0.0991	0.0436	0.0231	0.3034	-0.1425	0.1054	0.0570		
	250	0.5336	-0.1365	0.0726	0.0394	0.3377	-0.1896	0.1717	0.0957		

HOMOGENEOUS SOIL
 PROFILE

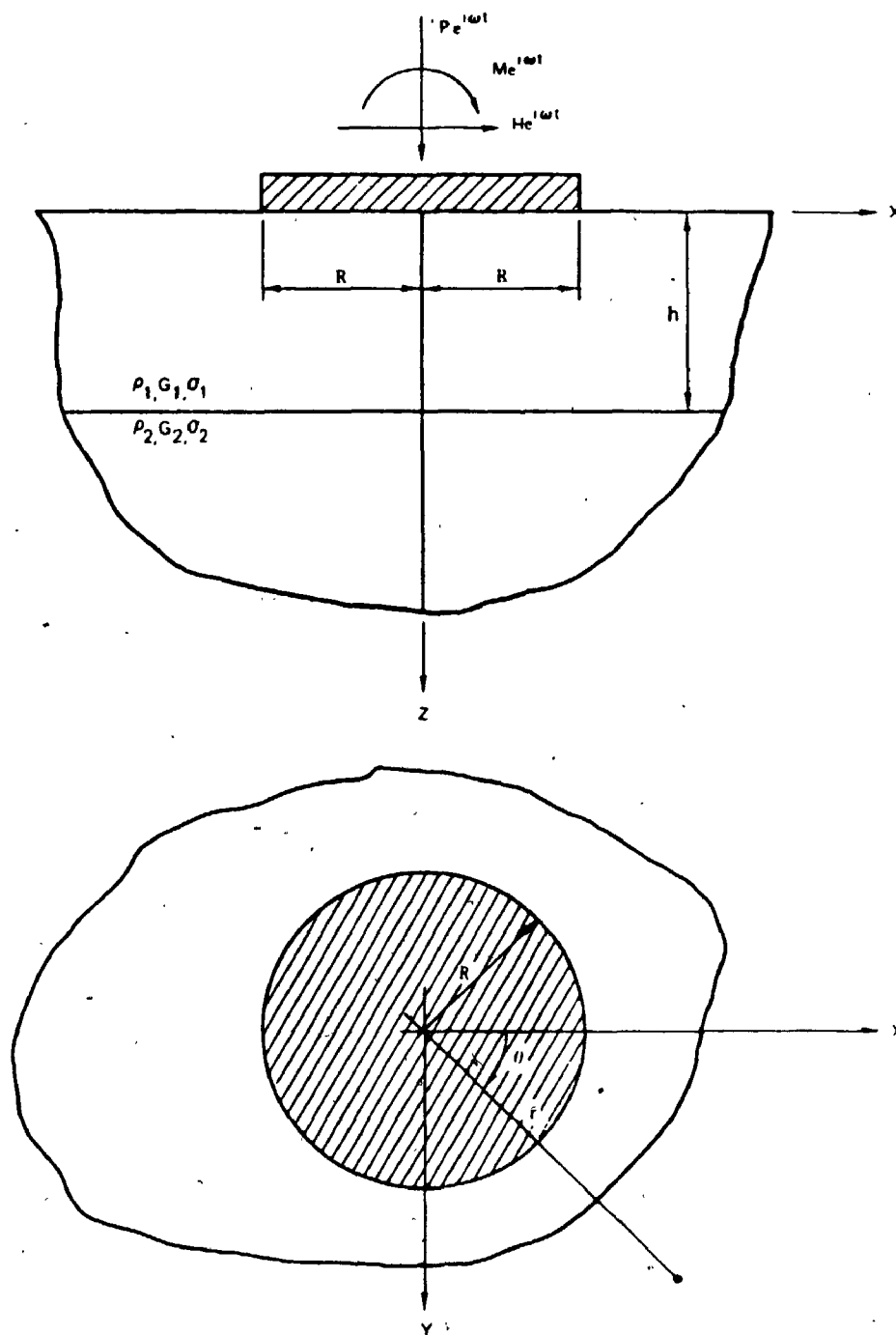


FIGURE 2.1 System Considered

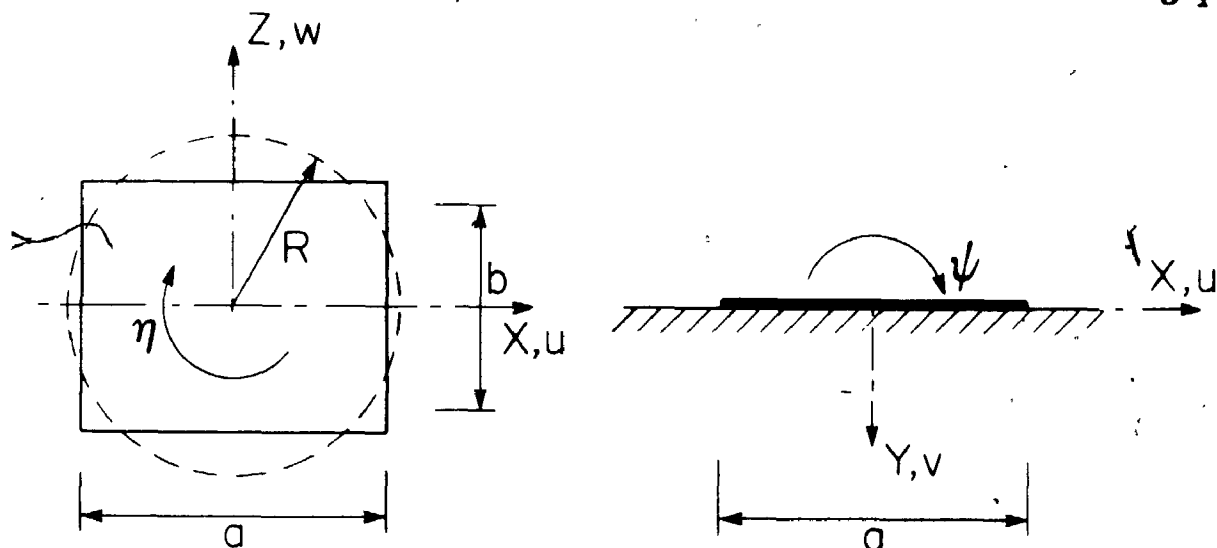


FIGURE 2.2 Notation for Calculation of Equivalent Radii of Rectangular Basis

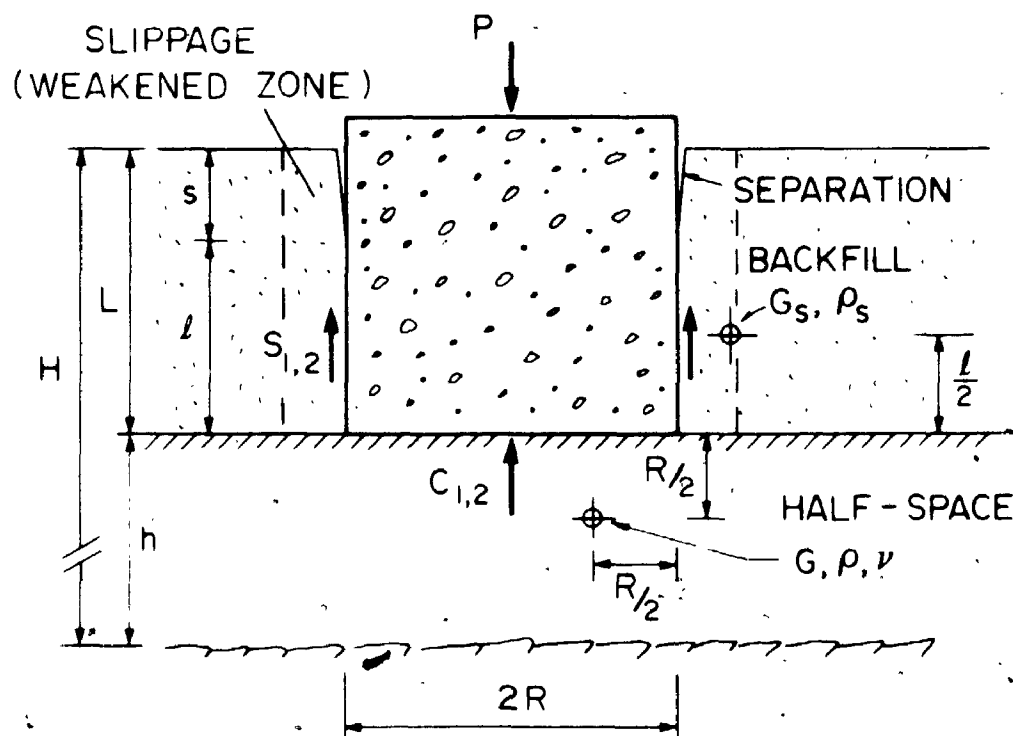


FIGURE 2.3 Schematic of Embedded Foundation

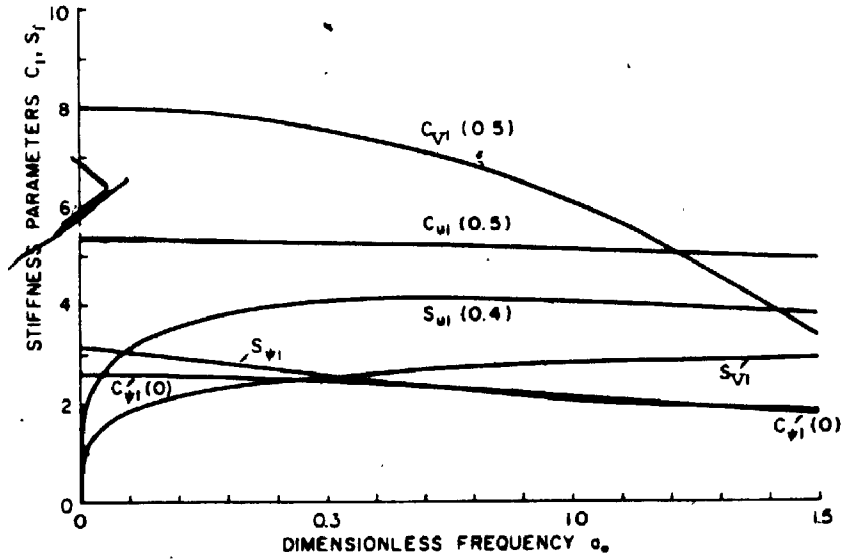


FIGURE 2.4a Examples of Stiffness Parameters C_1 and S_1 . (Poisson's ratio given in brackets, material damping $D=0$)

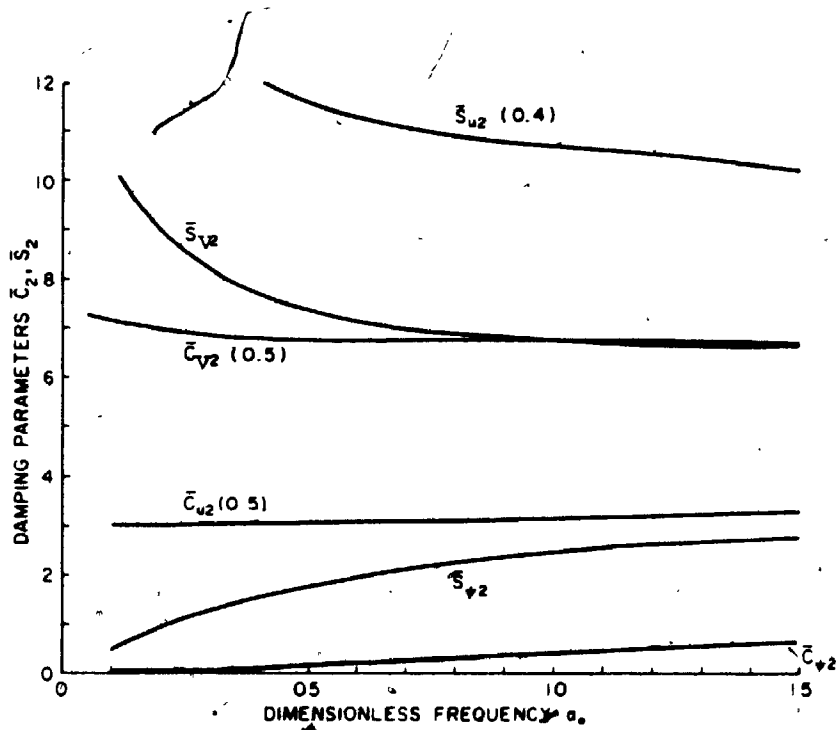


FIGURE 2.4b Examples of Damping Parameters \bar{C}_2 and \bar{S}_2 . (Poisson's ratio given in brackets, material damping $D=0$)

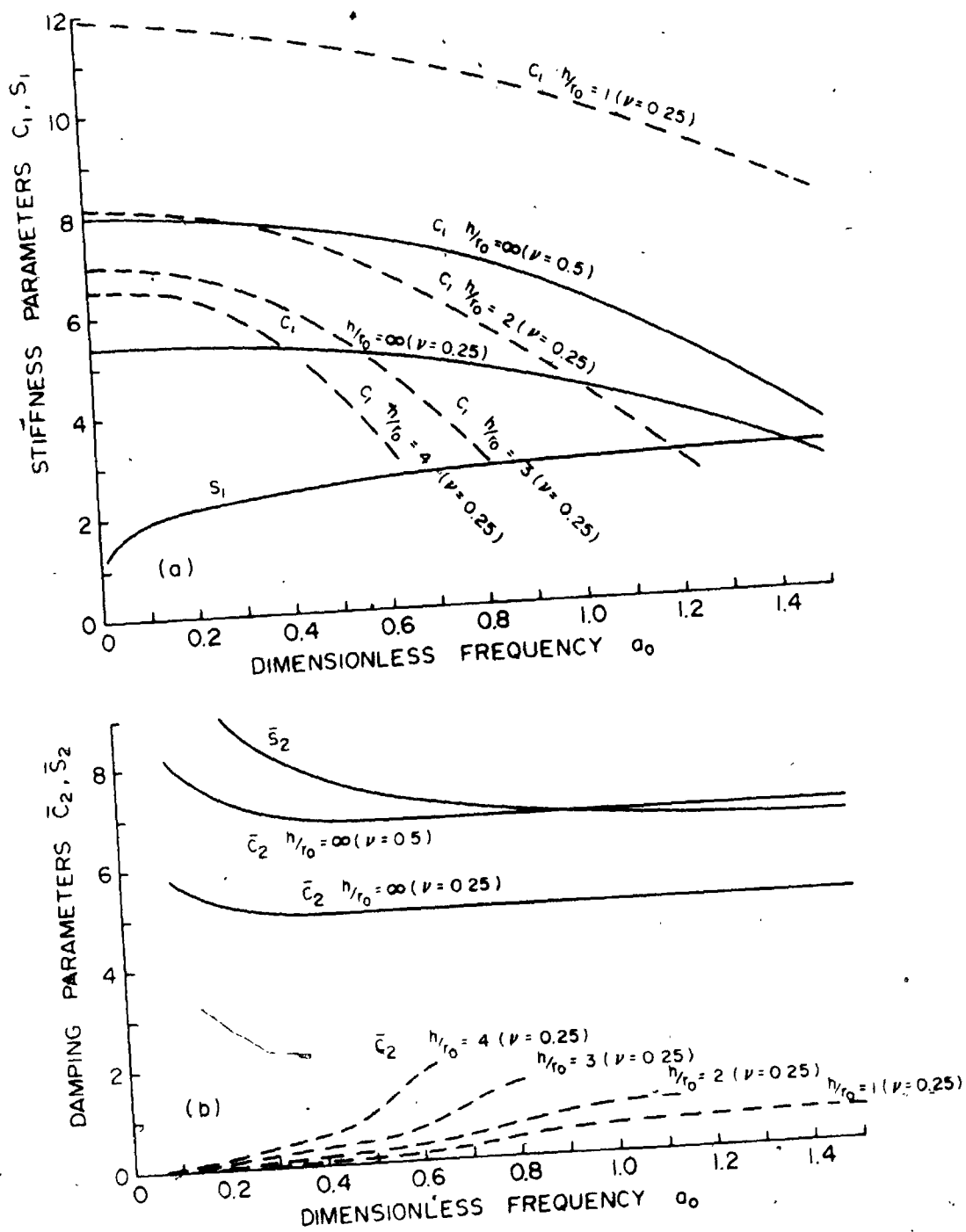


FIGURE 2.5 Stiffness and Damping Parameters for Vertical Vibration of Footings on Halfspace and Strata of Limited Depth ($r_0 = R$) (Ref. 35)

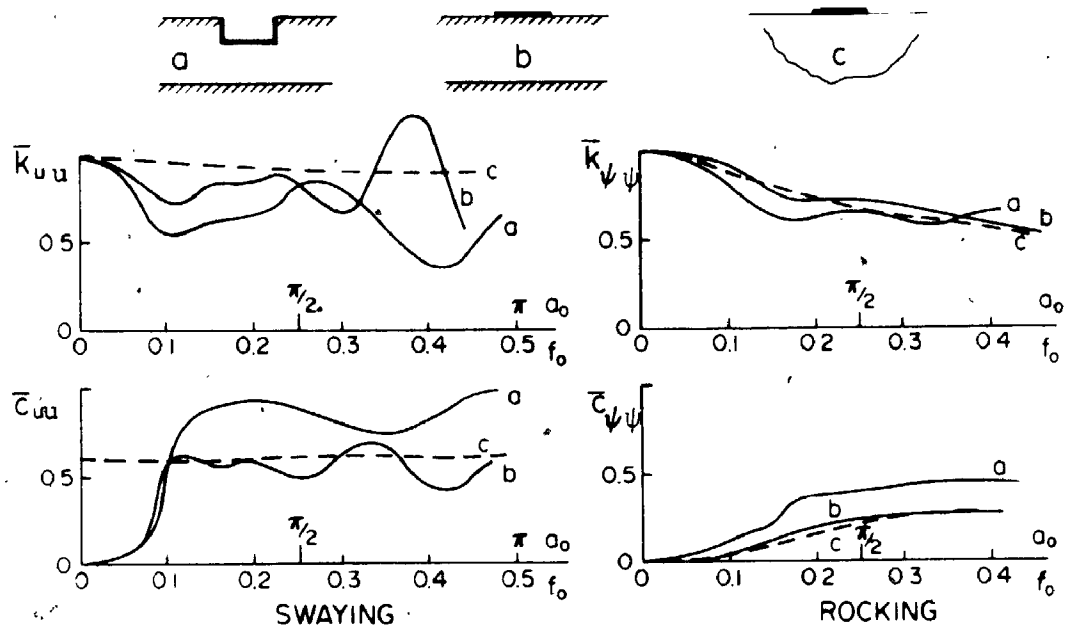


FIGURE 2.6 Stiffness Functions for Embedded Foundations (after Elsabee), $\nu = 1/3$, $\beta = 0.5$
 a - embedded foundation - finite layer
 b - surface foundation - finite layer
 c - surface foundation - halfspace

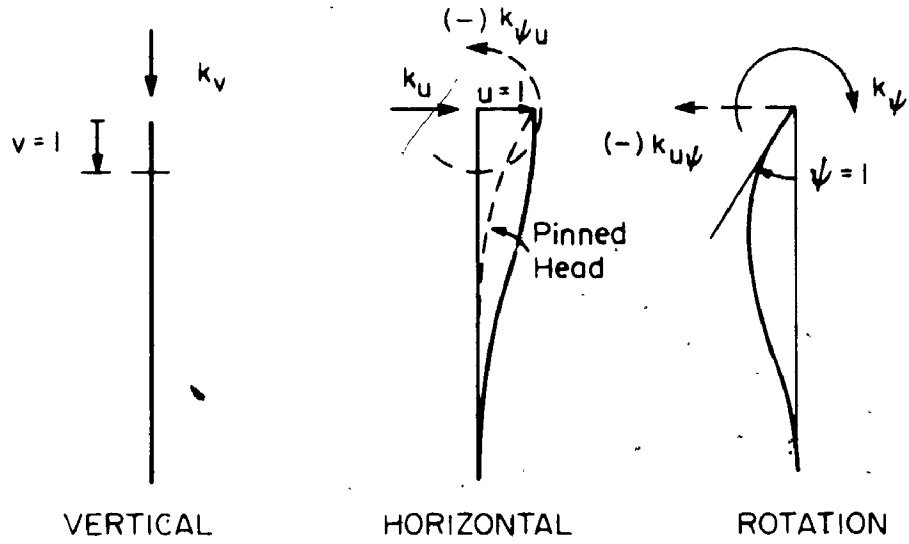


FIGURE 2.7 Generation of Pile Stiffness in Individual Directions

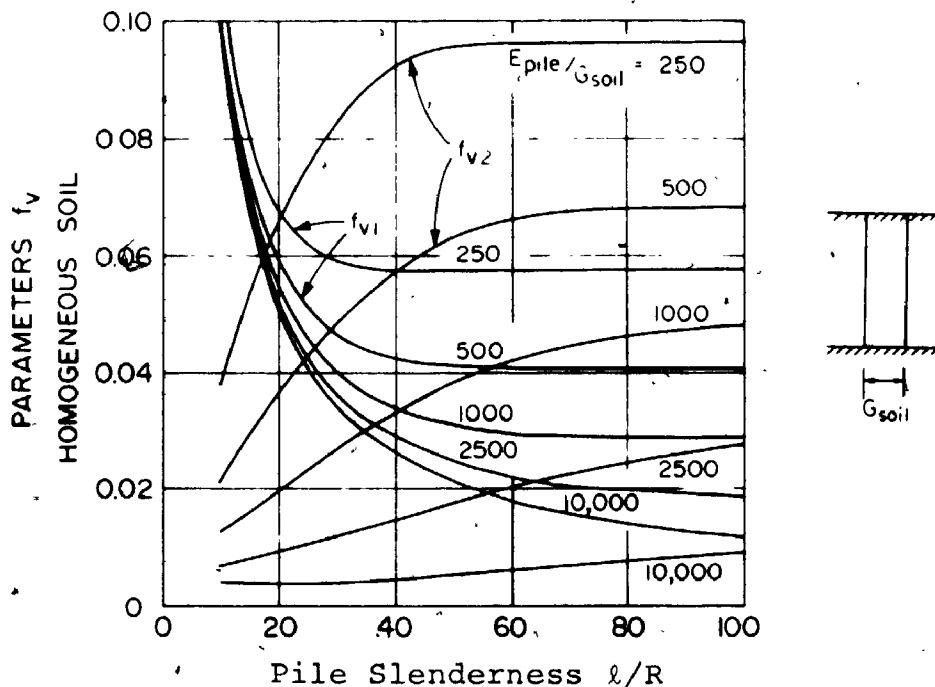


FIGURE 2.8 Stiffness Parameters f_{v1} and Damping Parameters f_{v2} of Vertical Response for Endbearing Piles (Ref. 56)

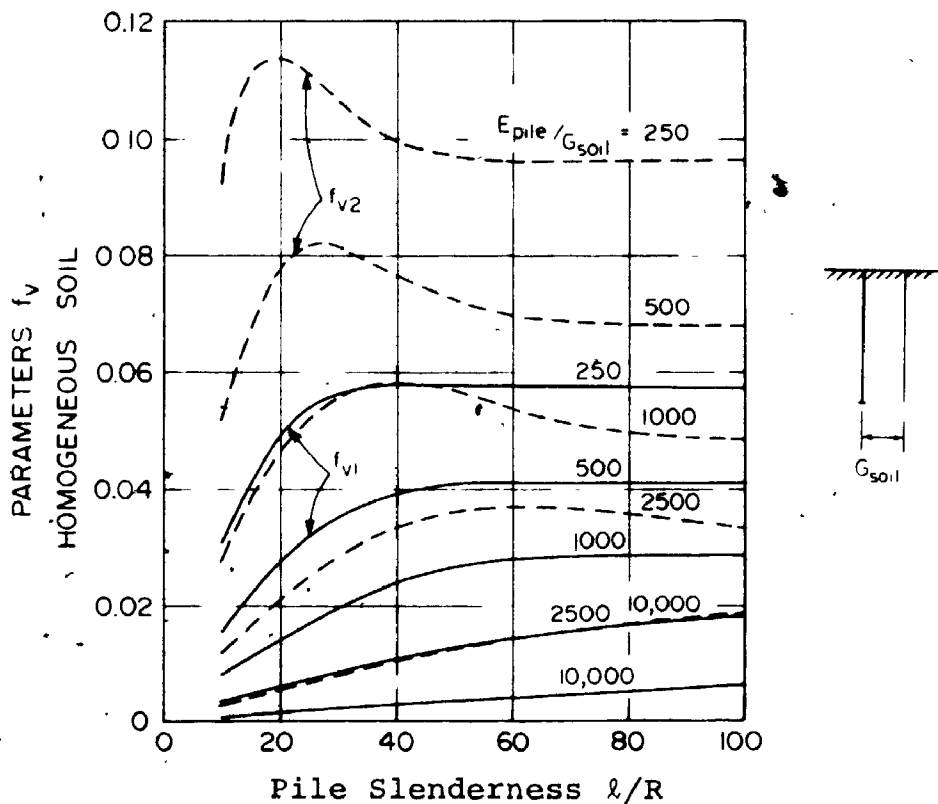


FIGURE 2.9 Stiffness Parameters f_{v1} and Damping Parameters f_{v2} of Vertical Response for Floating Piles (Ref. 56)

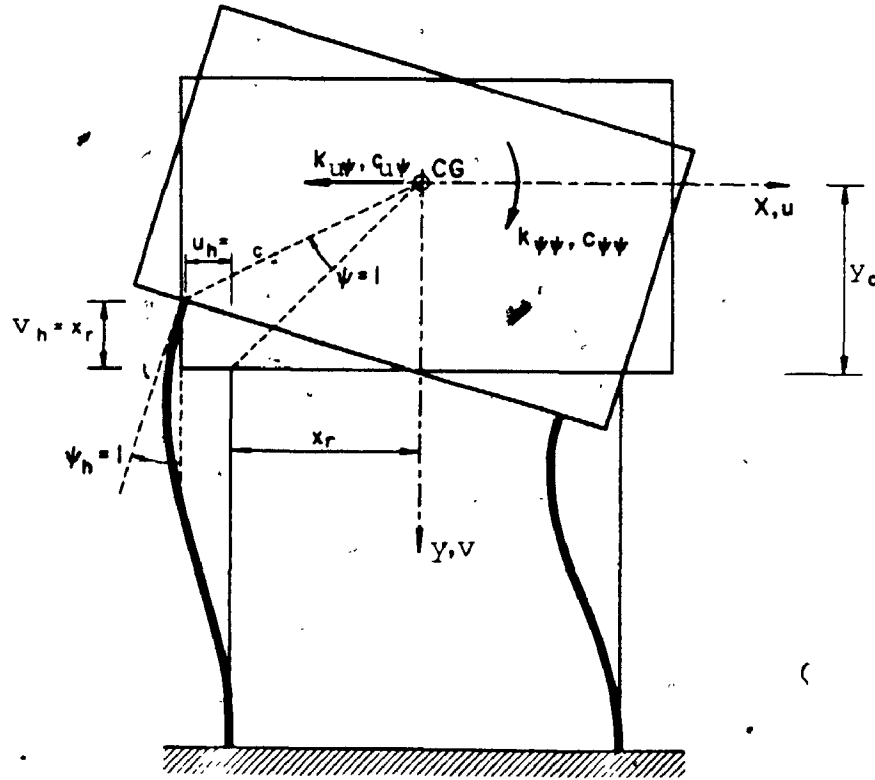


FIGURE 2.10 Pile Displacements for Determination of Group Stiffness and Damping Related to Rotation $\psi=1$

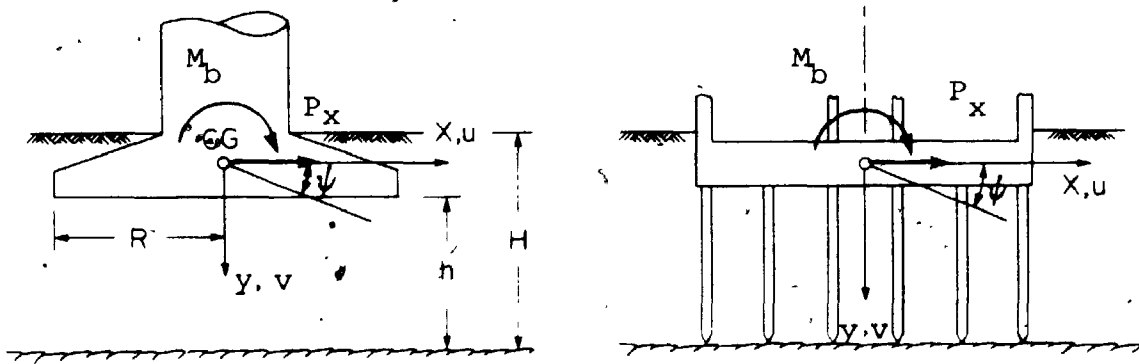
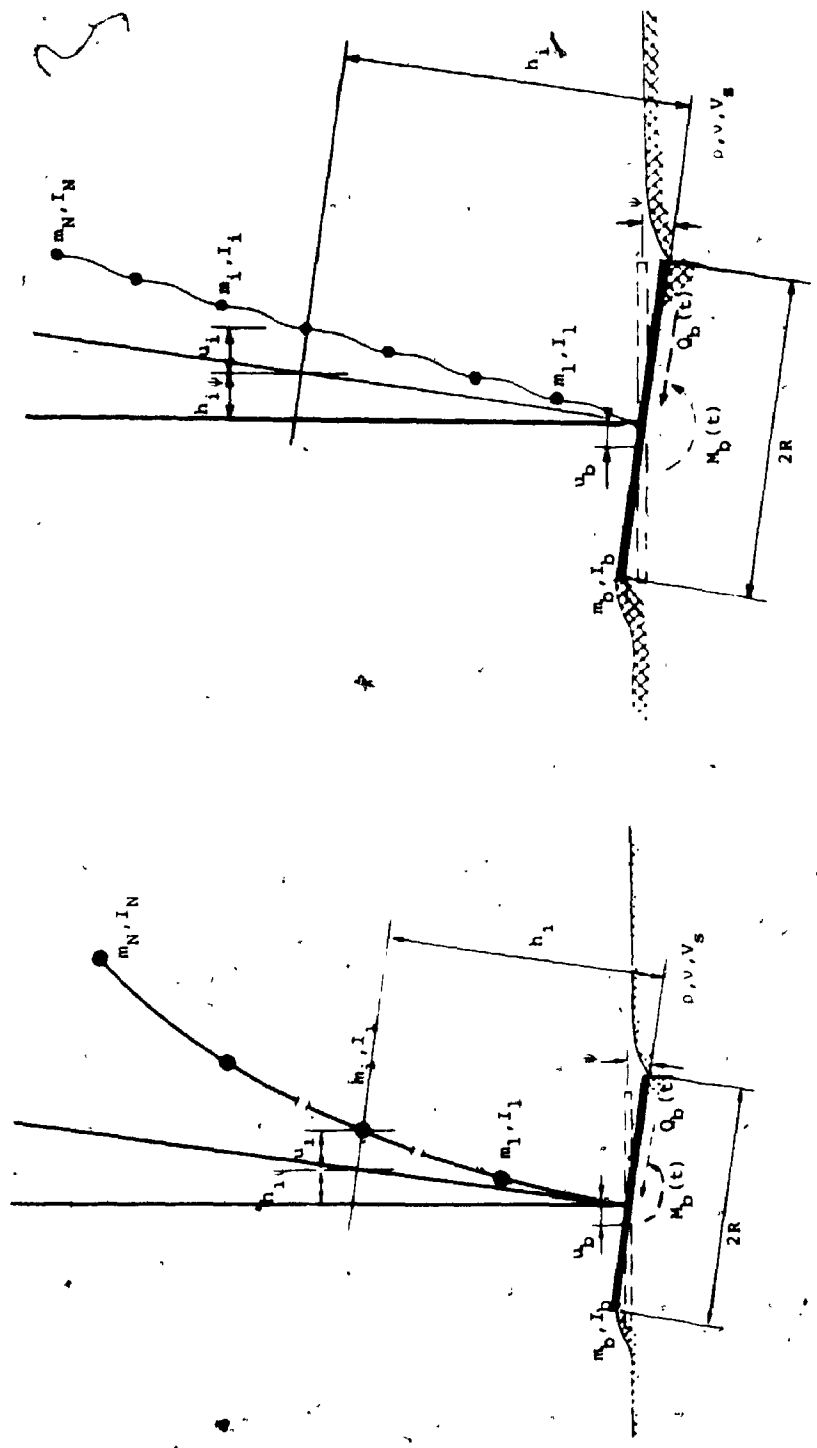


FIGURE 2.11 Typical Shallow and Deep Foundations



(a) General Model (Different Storey Rotations and Condensed Stiffness Matrix).
 (b) Shear Building (All Floor Rotations Equal)

FIGURE 2.12 Model of Building-Foundation System

CHAPTER 3

FREE VIBRATION OF SOIL-STRUCTURE INTERACTION SYSTEM

3.1 INTRODUCTION

It is well known that an undamped, linear, dynamic system possesses exactly the same number of normal modes as degrees of freedom. Each normal mode has associated with it a natural frequency and a characteristic shape. When properly released into a state of free vibration, the system can vibrate in any of its normal modes. A knowledge of normal mode shapes and frequencies is basic to an understanding and analysis of the dynamic response of a system under any kind of excitation. Two major advantages of the normal mode method result from the convenient properties of the normal modes. First, the complicated problem of a multi-degree-of-freedom system can readily be transformed into a set of simple problems of a single-degree-of-freedom system using the orthogonality relationships among mode shapes. Secondly, a good approximation for displacement can often be achieved by including only a few modes.

A system with proportional damping (i.e. damping proportional to stiffness or mass terms or a polynomial

combination of them) may be made to vibrate freely in a set of uncoupled modes which resemble, in shape, the normal modes of the undamped system, with amplitudes diminishing exponentially with time and uniformly over the system. These modes are distinguished by a definite spatial distribution of stationary nodal points. In contrast, a system with nonproportional damping may also be made to vibrate freely in a set of uncoupled "modes" in which all points in the system undergo exponentially damped motion at the same frequency, but at differing phase angles. In these modes, the nodes are not stationary. These modes are termed nonclassical modes in contrast with the classical modes associated with proportional damping or with undamped system.

The basic difficulty encountered in analyzing the type of soil-structure model, identified in Chapter 2, relates to the fact that the damping is nonclassical due to relatively large damping of the soil stemming from both material damping and geometric damping. In other words, the problem is a nonclassical damping problem.

The determination of nonclassical modes of a general viscously damped system requires a great deal of computational effort and the use of a computer. On the other hand, the classical normal modes can be obtained by means

of well established methods or even approximate or asymptotic procedures such as the Rayleigh-Ritz method or the Vianello-Stodola algorithm; also, frequency dependent damping can be readily accommodated.

The free vibration analysis is of interest because it elucidates the effect of foundation flexibility on modal properties of the structure-foundation system. This effect has three distinct components:

1. Reduction of the natural frequencies and modification of the modal shapes due to foundation flexibility;
2. Generation of damping in the structure through energy dissipation in the soil;
3. Modification of the original structural damping (calculated for clamped base) due to flexibility of the foundation.

Effects of soil-structure interaction on modal properties of the structures have received a great deal of attention in the literature. Some simplified analyses neglected coupling terms in the generalized damping matrix. Roesset, Whitman, and Dobry (59) used an undamped mode of a soil-structure system and calculated for it a weighted damping ratio. Similar analyses have been done by Rainer (60). Novak (25, 30) used an energy criterion for the evaluation

of an equivalent critical damping ratio in the soil-structure system. Another simplified method uses the shape of the fundamental mode of a structure on a fixed base and assigns to it an effective modal damping and frequency as well as a modified seismic input to reflect the effects of interaction (13, 61).

The results of the modal approach to soil-structure interaction have been adopted in the Tentative Provisions for the Development of Seismic Regulations for Building prepared by the Applied Technology Council (14). This approach is based on the studies due to Veletsos and Meek (62).

In this chapter, the effects of soil-structure interaction on modal damping are investigated using two approaches: the energy consideration which is a simple but approximate approach, and the complex eigenvalue analysis which is mathematically accurate but uses damped, non-classical vibration modes. These two methods are examined in detail and their results are compared; examples of modal damping, frequencies and mode shapes are given for typical rigid structures and flexible buildings.

3.2 EVALUATION OF DAMPING USING ENERGY CONSIDERATION

The damping a structure derives from energy dissipation

in the foundation when vibrating in a natural mode, as well as the modification of structural damping due to foundation flexibility, can be evaluated on the basis of an energy consideration. The basic assumption of this approach is that the damped vibration mode can be taken as equal to the undamped vibration mode.

The work done during a period of vibration $T = 2\pi\omega_j$, where ω_j is the frequency of the j th mode, by the damping forces $P(\dot{\delta})$ is, in general,

$$W = \int_0^T P(\dot{\delta}) d\delta(t) \quad (3.1)$$

in which δ is the effective path of the dashpot; for the foundation, δ is the absolute displacement, while for internal damping it is the relative displacement; e.g. for c_i in Figure 2.12 or Figure 3.1, $\delta_i = u_i - u_{i-1}$. The maximum strain energy of the whole structure can be calculated as maximum kinetic energy which is

$$L = \frac{1}{2} \omega_j^2 \{u_j\}^T [m] \{u_j\} \quad (3.2)$$

in which $\{u_j\}$ are modal displacements of floors including modal translation and rotation of the foundation u_{bj} , ψ_j . The damping ratio of the j th mode is defined as

$$D_j = W/(4\pi L) \quad (3.3)$$

Both soil damping and structural damping can be considered at the same time but it is more illustrative to consider them separately after W has been evaluated.

The damping ratio of the structure derived from the soil for mode j is obtained from equations 3.1 to 3.3 as

$$D_j = \frac{1}{2\omega_j M_j} (c_{uu} u_{1j}^2 + c_{\psi\psi} \psi_{1j}^2 + 2c_{u\psi} u_{1j} \psi_{1j}) \quad (3.4)$$

in which the magnitudes in the bracket refer only to the foundation and the generalized mass

$$M_j = \{u_j\}^T [m] \{u_j\} \quad (3.5)$$

includes the masses of the structure as well as the foundation. The foundation damping constants c_{uu} , $c_{\psi\psi}$ and $c_{u\psi}$ are defined by equation 2.18.

The modal damping due to soil described by equation 3.4 and derived using the energy consideration is actually equal to that obtained from the diagonal terms of the generalized damping matrix generated by means of the undamped vibration modes. If the matrix of the undamped modes listed as columns is $[u]$, the generalized damping matrix pertinent to equation 2.22

$$[C] = [u]^T [c] [u]$$

When considering the damping derived from the foundation,

only the foundation damping constants are non-zero and the j th diagonal element of $[C]$ reduces to

$$C_{jj} = \{u_j\}^T [c] \{u_j\} = c_{uu} u_{1j}^2 + c_{\psi\psi} \psi_{1j}^2 + 2c_{u\psi} u_{1j} \psi_{1j}$$

If the off diagonal elements of $[C]$, C_{ji} , are neglected, the generalized damping constant C_{jj} yields modal damping equal to that given by equation 3.4.

For a shear building, the damping ratio derived from internal damping of the structure follows from equations 3.1, 3.2 and 3.3 as

$$D_j^s = \frac{1}{2\omega_j M_j} \sum_{i=1}^n c_i [u_{ij} - u_{i-1,j} + (h_i - h_{i-1}) \psi_j]^2 \quad (3.6)$$

in which c_i is the damping constant of internal, inter-storey damping; and h_i is the height of the i th storey. Constants c_i are indicated by dashpots in Figure 3.1. The constants of internal damping c_i can be evaluated as being proportional to either the stiffness constant, k_i , or the mass m_i but other assumptions can also be made.

The damping constants proportional to stiffness can be established using the complex shear and Young's moduli as in equation 2.6. For frequency independent structural damping the constant of equivalent viscous damping follows from equation 2.7b as frequency dependent, i.e.

$$c_i = 2\beta k_i / \omega \quad (3.7a)$$

For viscous internal damping, β is replaced by $\beta'\omega$ and the equivalent damping constants become $c_i = 2\beta'k_i$, i.e. frequency independent.

For damping proportional to mass, the damping constants can be defined as

$$c_i = 2\alpha m_i \quad (3.7b)$$

where α is a constant. Damping proportional to stiffness or mass is known as proportional damping as stated earlier.

The modification of the structural damping due to foundation flexibility can be described as the ratio

$$\epsilon_j = D_j^S / \bar{D}_j^S \quad (3.8)$$

in which \bar{D}_j^S denotes the damping the structure would have on a rigid foundation, and D_j^S is the structural damping in the case of a flexible foundation. The ratio ϵ_j can be established by evaluating equation 3.6 twice: (1) with a rigid foundation; and (2) with a flexible foundation. This process eliminates the difficulty associated with the evaluation of the constants c_i because the constants of proportionality α , β cancel out in equation 3.8. Any other type of structural damping can be evaluated in the same way. The three basic types of models used to

represent structural damping are shown in Figure 3.2. They are absolute damping, relative damping and inter-storey damping. The latter model, used in the above discussion, appears most suitable to represent energy dissipation within the structure. The first model is suitable for aerodynamic damping and leads to a diagonal damping matrix.

The total modal damping of the structure is

$$D_j^t = D_j + \epsilon_j \bar{D}_j^s \quad (3.9)$$

The advantage of the energy approach, employed first in this form by Novak (25, 30), is that it uses undamped vibration modes which can be obtained by means of well established methods. The energy approach is, however, approximate. The degree of accuracy of the energy approach can be assessed by its comparison with the complex eigenvalue analysis which yields modal damping derived from damped vibration modes.

3.3 EVALUATION OF DAMPING USING COMPLEX EIGENVALUE APPROACH

In this approach, the modal damping is established from the complex eigenvalues obtained by the solution of the homogeneous governing equation of damped free vibration. The complex eigenvalue analysis is an extension of the

familiar approach to free undamped vibration and was given a comprehensive treatment already by Lord Rayleigh in 1877 (63). For an undamped system or for one in which damping is proportional, each component of any eigenvector is distinguished from other components by amplitude only, the phase being equal or 180° apart. In this case, the n equations of motion (for n -degrees-of-freedom system) provide a set of equations whose solution yields the set of n amplitude ratios for any given mode. For a system with nonproportional damping, each component of an eigenvector is distinguished not only by amplitude but also by phase. For the convenience of the mathematical solution of the eigenvalue problem in the case of nonproportional damping, the equations of motion are reduced to first order equations by adding n additional equations to the basic n equations of motion, equation 2.22. Frazer (64) and Foss (16) seem to be the first to supply the n additional equations in a most useful way. These equations are given by the following matrix identity

$$[m]\{\dot{u}\} - [m]\{\dot{u}\} = \{0\} \quad (3.10)$$

This equation added to equation 2.22,

$$[m]\{\ddot{u}\} + [c]\{\dot{u}\} + [k]\{u\} = \{P\}$$

gives the following matrix equation of order $2n$,

$$\begin{bmatrix} [0] & [m] \\ [m] & [c] \end{bmatrix} \begin{Bmatrix} \ddot{u} \\ \dot{u} \end{Bmatrix} + \begin{bmatrix} -[m] & [0] \\ [0] & [k] \end{bmatrix} \begin{Bmatrix} \dot{u} \\ u \end{Bmatrix} = \begin{Bmatrix} \{0\} \\ \{P\} \end{Bmatrix} \quad (3.11)$$

This equation can be written as the "reduced" equation, i.e.

$$[A]\{\dot{z}\} + [B]\{z\} = \{F\} \quad (3.12a)$$

where

$$\{z\} = \begin{Bmatrix} \dot{u} \\ u \end{Bmatrix}, \quad \{F\} = \begin{Bmatrix} \{0\} \\ \{P\} \end{Bmatrix} \quad (3.12b)$$

and

$$[A] = \begin{bmatrix} [0] & [m] \\ [m] & [c] \end{bmatrix}, \quad [B] = \begin{bmatrix} -[m] & [0] \\ [0] & [k] \end{bmatrix} \quad (3.12c)$$

The great advantage of this formulation lies in the fact that the matrices [A] and [B], both of order 2n, are real and symmetric. Therefore, to solve equation 3.12a techniques very similar to those used in the treatment of undamped systems may be employed.

The homogeneous equation of free damped vibration can be obtained by setting the right side of equation 3.12a equal to zero,

$$[A]\{\dot{z}\} + [B]\{z\} = \{0\} \quad (3.13)$$

The particular solution to this linear equation can be written as

$$\{z(t)\} = e^{\mu t} \{Z\} \quad (3.14)$$

If the solution for $\{u\}$ is assumed to have a similar form, $\{u\} = E e^{\mu t} \{\phi\}$, the complex vector $\{Z\}$ can be written as

$$\{Z\} = E \begin{Bmatrix} \mu\{\phi\} \\ \{\phi\} \end{Bmatrix}$$

in which E is a complex constant.

The substitution of equation 3.14 into equation 3.13 yields

$$(\mu[A] + [B]) \{Z\} = \{0\} \quad (3.15)$$

or

$$([U] - \frac{1}{\mu} [I]) \{Z\} = \{0\} \quad (3.16)$$

where

$$[U] = -[B]^{-1}[A] = \begin{bmatrix} [0] & [I] \\ -[k]^{-1}[m] & -[k]^{-1}[c] \end{bmatrix} \quad (3.16a)$$

In equation 3.16a, $[I]$ = the identity matrix of order n
 $[k]^{-1}[m]$ = the dynamical matrix of
 order n for the undamped system.

Equation 3.16 represents the eigenvalue problem of the matrix $[U]$ in a form resembling the familiar eigenvalue

problem of undamped systems. However, the dimension of the matrix $[U]$ is $2n \times 2n$ as opposed to the dimension $n \times n$ typical of undamped systems. A simple iterative method for the solution of equation 3.16 is given by Frazer et al. (64) and efficient subroutines are available. The solution of the eigenvalue problem yields $2n$ eigenvalues μ_i and $2n$ eigenvectors. For an overdamped system all values of μ_i are real and negative. For an underdamped, stable system, i.e. one in which decaying oscillation occurs, μ_i are complex with a negative real part and come in complex conjugate pairs with associated pairs of complex conjugate eigenvectors.

Thus, if the k th and l th eigenvalues are complex conjugates, they may be written as

$$\mu_{k,l} = \alpha_k \pm i\beta_k \quad (3.17)$$

Realizing that while μ is associated with $\{\phi\}$, the conjugate frequency μ^* is associated with the conjugate mode $\{\phi\}^*$ a solution for one mode is a sum of these two particular solutions featuring two complex integration constants, E . If these constants were independent, four initial conditions would be needed for their determination. Since only two initial conditions are available, i.e. initial displacements and velocities, the integration constants have to be conjugate. Then, the complete

solution for one vibration mode can be written as

$$\{u_j\} = E e^{\mu t} \{\phi\} + E^* e^{\mu^* t} \{\phi^*\} \quad (3.18)$$

in which E and E^* are complex conjugate constants given by initial conditions.

The eigenvectors of a damped system are orthogonal just as are those for an undamped system. The proof of orthogonality may be found in Ref. (65) and (66). The orthogonality conditions between j th and s th eigenvectors are:

$$\begin{aligned} \{z^j\}^T [A] \{z^s\} &= 0 && \text{for } s \neq j \\ &= A_j && \text{for } s = j \end{aligned} \quad (3.19a)$$

and

$$\begin{aligned} \{z^j\}^T [B] \{z^s\} &= 0 && \text{for } s \neq j \\ &= B_j && \text{for } s = j \end{aligned} \quad (3.19b)$$

Also

$$B_j = -\mu_j A_j \quad (3.19c)$$

In this study the EISPACK subroutine RGG was used to calculate the complex eigenvalues. It is efficient and has accuracy checks for ill-conditioned matrices. Other subroutines were also used for comparison.

Evaluation of Damping

Equations 3.14 and 3.17 indicate that the displacement in mode j is time dependent, i.e.,

$$e^{\mu_j t} = e^{\alpha_j} e^{i\beta_j t} \quad (3.20)$$

It can be seen that in the j th mode α_j will be negative for a damped system and β_j represents the frequency of damped free vibration. Consequently, equation 3.17 can be written more concisely in the form common with one-degree-of-freedom systems,

$$\mu_{1,2} = -D_j \bar{\omega}_j \pm i \bar{\omega}_j \sqrt{(1-D_j^2)} \quad (3.21a)$$

or

$$\mu_{1,2} = -D_j \bar{\omega}_j \pm i \omega_j^d \quad (3.21b)$$

where

$$\bar{\omega}_j = |\mu_j| \quad (3.22)$$

$$D_j = -\frac{\text{Re} \mu_j}{|\mu_j|} \quad (3.23)$$

and

$$\omega_j^d = \bar{\omega}_j \sqrt{(1-D_j^2)} = \text{Im} \mu_j \quad (3.24)$$

In equations 3.21 to 3.24, ω_j^d is the damped natural frequency and D_j the damping ratio of mode j related to

frequency $\bar{\omega}_j$. The frequency $\bar{\omega}_j$ depends on the damped vibration mode $\{\Phi\}$ and is close, but generally not equal, to the undamped frequency ω_j . Only for damping proportional to stiffness or mass $\bar{\omega}_j = \omega_j$. The damped natural frequency, ω_j^d , is always smaller than the undamped frequency, ω_j , if the damping is proportional to mass or stiffness. For nonproportional damping, i.e. nonclassical modes, ω_j^d may be smaller or greater than ω_j . In particular, the first damped frequency of the nonclassical mode may be greater than the first undamped frequency as was proved for weak damping by Caughey and O'Kelly (67) and is demonstrated for heavy damping later herein.

When the complex eigenvalues μ_j are available from the solution of the secular equation, equation 3.16, the damping ratio of mode j follows from equations 3.21 and 3.23 as

$$D_j = -\text{Re}\mu_j / \bar{\omega}_j = -\text{Re}\mu_j / |\mu_j| \quad (3.25)$$

Vibratory motion occurs as long as $D_j < 1$. Other details on the nonclassical mode analysis can be found, e.g. in References (16, 64, 66, 67 and 68). The complex eigenvalue approach is an efficient technique but its applications to structures have been scarce (69, 70).

The complex eigenvalue method is used most effectively

and with adequate rigor when the stiffness and damping matrices are frequency independent. If they depend on frequency, an iterative procedure can be used.

Equation 3.25 can be used to evaluate modal damping due to both the soil and the structure itself. The accuracy of this procedure is limited only by the accuracy with which the values of μ are established.

The modal damping ratios calculated from the complex eigenvalues can be compared with those obtained by means of the energy consideration. The results of such a comparison depend on the type of structure and its foundation and therefore, a few typical structures, both rigid and flexible, are examined below.

3.4 EXAMPLES OF MODAL PROPERTIES

Using the two approaches outlined, the effect of soil-structure interaction on modal damping and frequencies can be studied. While it is possible to evaluate both the soil damping and structural damping at the same time, it is more illustrative to consider them separately.

In the examples presented, soil material damping is neglected and foundation stiffness and radiation damping are taken as frequency independent. In any particular

situation the soil properties have to be chosen with regard to the frequency of interest, strain level and layering.

Rigid Structures

Rigid structures such as silos or machine foundations derive most of their damping from soil. Under horizontal loads such structures usually have just two degrees of freedom, i.e. horizontal translation u and rotation in the vertical plane (rocking) ψ . The governing equation is equation 2.24 with the diagonal mass matrix containing both the mass and mass moment of inertia of the whole structure and the stiffness and damping generated only by the foundation as described by equation 2.18. Such a system yields the first mode as rotation about a point lying below the foundation base and the second mode as rotation lying above the center of gravity.

A silo. A silo 22 m (72.18 ft) high with a base diameter of 10.5 m (34.45 ft) is analyzed for two types of foundation: a mat foundation (Figure 3.3(a)) and a pile foundation (Figure 3.3(b)). Coupled vibration consisting of horizontal translation and rocking is considered. The stiffness and damping of the mat foundation are calculated from the formulae (equations 2.3 and 2.4), assuming a very

deep soil layer (halfspace) with a shear wave velocity of soil V_s 152.4 m/s (500 ft/s), soil unit weight $\gamma = 1924$ kg/m³ (120 lb/ft³) and Poisson's ratio $\nu = 0.25$. The effects of embedment and soil material damping are neglected. The pile foundation comprises 72 endbearing wood piles. Their properties and the properties of soil are given in Reference (42, p. 588). The group effect is neglected for the sake of simplicity). The stiffness and damping of the pile foundation are evaluated using the procedure described in section 2.4.2.

The damping ratios of a silo depend on its loading and are, therefore, calculated for various levels of silo content ranging from an empty silo to a full silo. The unit weight is taken as 2330 kg/m³ (145 lb/ft³) for concrete and 820 kg/m³ (51.2 lb/ft³) for the content.

The damping derived from soil is calculated from equation 3.25 for the complex eigenvalue approach and from equation 3.4 for the energy approach. The damped ratio of the first mode is given for the mat supported silo in Figure 3.4. The damping ratio shown is related to $\bar{\omega}_1$ as suggested by equation 3.22 but is also evaluated with regard to the undamped frequency ω_1 used in the energy method. The difference between the two is quite small. The first mode damping ratio ranges from about

12 percent to 27 percent and in this range the energy method consistently overestimates the damping by about 15 to 22 percent. The modal damping of the second mode is not shown because it exceeds the critical damping ratio.

The frequencies of the first mode are shown in Figure 3.5. It can be seen that for lower levels of silo loading, for which the damping is highest, the damped natural frequency ω_1' is higher than the undamped frequency ω_1 . This is caused by the nonproportionality of the damping matrix. For the same reason, the frequency $\bar{\omega}_1$ is somewhat higher than both the damped and undamped frequencies. The surprising trend for the natural frequency to increase with silo loading is caused by the shifting of the center of gravity which may increase or decrease the interaction effects.

For the pile supported silo, the damping ratios of both modes D_1 and D_2 are shown in Figure 3.6. In this case, the damping ratios of both modes are considerably lower than for the mat foundation, and the energy approach and the complex eigenvalue approach give practically identical results. This is so because the damping matrix of the pile foundation is almost proportional to the stiffness matrix.

machines. Block foundations for these types of machine are analyzed in the same fashion as the rigid silo. A number of shallow foundations as well as foundations on piles were investigated. As with the silo, for the less damped pile supported foundations both methods of analysis give the same results while for the shallow foundations the energy method tends to overestimate the damping by about 10 to 20 percent depending on conditions.

Hammer foundations. Hammer foundations are most often modeled by two rigid bodies which vibrate in phase in the first mode and in antiphase in the second mode (Figure 3.7). The damping originates primarily from energy dissipation in soil for the first mode and from energy dissipation in the viscoelastic pad under the anvil, represented by the upper mass, for the second mode. In Figure 3.7, both modal damping ratios are presented for a foundation whose soil damping constant c_2 is supposed to vary from its full value, $c_2(\text{max})$, to zero. The maximum damping ratio of the first mode is about 50 percent. However, in the whole range of the damping ratios plotted in Figure 3.7, both methods of damping evaluation yield almost identical results. (The data on the foundation for which Figure 3.7 is represented will be given in Chapter 5.)

Buildings

In buildings, structural flexibility comes into play and considerable differences between damped and undamped modes may occur. Consequently, the behavior of flexible structures is more complex and it is advantageous to examine the foundation damping separately from structural damping.

Foundation damping. Examples of the damping provided by flexible foundations are shown for five- and ten-storey shear buildings in Figures 3.8 to 3.12. (Some of the properties of the building are given in Table 3.1.)

The columns of the building presented in Figure 3.8 rest on three separate block foundations of plan dimensions $2 \times 2 \text{ m}^2$ ($6.56 \times 6.56 \text{ ft}^2$). The foundation (soil) damping of the first four modes is plotted for varying soil stiffness characterized by shear wave velocity $V_s = \sqrt{G/\rho}$ in which G is the shear modulus of soil and ρ is the mass density. The stiffness and damping constants of the foundations are established from the formulae given in subchapter 2.3 with $\nu = 0.25$ and embedment neglected. The structure is analyzed using equation 2.23. The results are shown for both methods of analysis. The damping obtained by the building from the foundation, D_j , increases monotonically as soil stiffness decreases. The magnitude of this damping ranges from about 1 to 8 percent for soils

of average stiffness such as clays or sands (V_s ranging from 400 to 700 ft/s, i.e. 122 to 213 m/s). Both approaches give almost the same results for the first mode and very close results for the higher modes. In this case, the damping is nonproportional but small.

Figure 3.9 shows the soil damping for the same building as used in Figure 3.8, except for the foundation which is, in this case, a large mat supporting all columns. For this foundation, the soil damping of the building can reach much higher values for the higher modes than in the previous case. This is so because the damping constants of the foundation grow with the radius squared for c_{uu} and radius to the power of four for $c_{\psi\psi}$. The variation of damping with soil stiffness is monotonic only in the first vibration mode (D_1), for which both approaches give almost identical results, and for the second mode evaluated using the energy method. For the higher modes, the soil damping ratios display marked peaks in which very high damping ratios are reached. The agreement between the two approaches becomes worse as the value of damping increases and considerable discrepancies of up to 50 percent or even more may occur in the higher modes. The first mode damping, most important for practical applications, is modest and predicted satisfactorily using either of the two approaches.

The complex eigenvalue approach yields not only larger peak values of the damping for the higher modes but indicates abrupt variations in the damping and a limiting envelope. To find out to which degree these features are affected by the very high damping of the higher modes the analysis was repeated with the damping matrix reduced to one fifth of that yielding Figure 3.9. (Such a reduction of damping can occur if the soil deposit resembles a stratum of limited thickness rather than a halfspace, a frequently occurring situation with large buildings.) The results are plotted in Figure 3.10. In this case, the modal damping due to soil is greatly reduced, particularly for the higher modes, and the agreement between the two approaches is far better. The peaks are not truncated but smooth and the abrupt change occurs only in the fourth mode damping obtained from the complex eigenvalues.

The damping derived from soil was also examined for a ten-storey shear building which differed from the one used in Figure 3.9 only by the addition of five more storeys. The results are plotted in Figure 3.11. The energy approach and the complex eigenvalue approach give almost identical results for the first mode, but considerable differences again occur for the higher, heavily damped modes. However, the damping values in excess of

50 percent, for which the truncated peaks appear in Figures 3.9 and 3.11, are not very meaningful because at this level of damping free motion just about ceases to be oscillatory and the eigenvalue analysis becomes spurious. (The gaps between the truncated peaks tend to close as indicated by dotted lines if the increment in V_s is refined.)

The ten-storey building is re-examined with the foundation damping matrix reduced to one half of the full value valid for an elastic halfspace (Figure 3.12). The plots are limited to the first three modes for which the damping is not excessive and the modes are well separated. The results are similar to those observed in the previous cases.

The variation of natural frequencies with soil stiffness is also of interest. Examples are shown in Figure 3.13 and 3.14. Figure 3.13 shows the undamped natural frequencies and the frequencies $\bar{\omega}_j = |\mu|$ for the five-storey building of Figure 3.9. For the full value of foundation damping, the damped natural frequencies as well as frequencies $\bar{\omega}_j$ lead to frequency curves which overlap or may even cross and this makes the shape of the damping curves dependent on the interpretation of the order of the modes. The ordering by ascending values of $\bar{\omega}_j$ was used for the figures shown because the frequencies $\bar{\omega}_j$ are

directly related to damping ratios. The ordering of the modes by ω_j^d would yield somewhat different shapes for the very high damping ratios. For the reduced foundation damping matrix the natural frequencies of the five-storey building are shown in Figure 3.14. These frequencies correspond to Figure 3.10: They are well separated and because the damping is smaller $\omega_j^d \approx \bar{\omega}_j$. Figure 3.14 also demonstrates that in the case of soil damping the damped natural frequencies of buildings may exceed the undamped natural frequencies, as is shown for the silo in Figure 3.5.

The differences in damping values obtained by the two approaches appear understandable because with a large mat foundation, the damping is high and concentrated at the base of the structure, consequently, the damped vibration modes differ significantly from the undamped modes. This difference can be seen from Figure 3.15 in which both the undamped and damped modes are plotted for the building shown in Figure 3.9. For the damped modes, the absolute value of the displacement $|\Phi|$ and the phase shift ϕ are defined by equations 3.26, and shown in Figure 3.15, as

$$|\Phi| = \sqrt{\phi_1^2 + \phi_2^2} \quad (3.26a)$$

and

$$\phi = \arctan \frac{\phi_2}{\phi_1} \quad (3.26b)$$

where ϕ_1 and ϕ_2 are the real and imaginary parts of the mode shape.

Figure 3.16 shows the free vibration at different instances of time. The shifting of nodal points due to damping can be noticed. The free vibration was evaluated using equation 3.18.

Effect of foundation flexibility on structural damping.

Foundation flexibility changes the natural frequencies of the structure and also its curvature. The latter effect changes the amount of energy dissipated in the structure itself due to internal damping. The examples of the effect of foundation flexibility on the original structural damping are shown in Figure 3.17 and Figure 3.18. The damping matrix of the structure was chosen as proportional to the stiffness matrix and the viscous damping constant so adjusted as to give the first mode damping equal to 1 percent for the case of a rigid foundation. For the higher modes the calculated damping ratios were normalized to give 1 percent for rigid foundations also. This was done to indicate the trends rather than real values of damping. Both the energy approach, equation 3.6, and the complex eigenvalue analysis, equation 3.25, give identical results for the examples shown. The reason for this agreement is the proportionality of the damping and stiffness matrices,

except for the foundation where the damping is absent, and low level of damping; consequently, the damped and undamped modes are almost identical.

In the example buildings, structural damping is always reduced by foundation flexibility. For the first mode, structural damping decreases monotonically with decreasing soil stiffness. This decrease is in good agreement with the approximate formula, derived for one-storey buildings by Veletsos and Meek (62) and Bielak (71), according to which

$$D_1^S = \bar{D}_1^S \left(\frac{\omega_1}{\bar{\omega}_1} \right)^3 \quad (3.27)$$

where the bar indicates the damping and first natural frequency the structure would have in the case of a rigid foundation; D_1^S and ω_1 are the structural damping and the first natural frequency of the structure on a flexible foundation.

For the higher modes, structural damping varies with soil stiffness in a more complicated manner and the damping reduction can be smaller or greater than that observed in the first mode, as Figures 3.17 and 3.18 indicate.

For heavy values of structural damping often used in aseismic design the reduction of damping due to foundation flexibility may be significant. This reduction is likely

to occur in strong earthquakes in which the soil shear modulus may be considerably reduced due to high strain.

Figure 3.19 shows the first circular natural frequencies and the total damping ratios of the ten-storey shear building, shown in Figure 3.11, for three types of foundations, depicted as cases (a), (b) and (c) in Figure 3.21. The data are again plotted for different values of soil shear wave velocity, and also assuming a structural damping ratio of 1 percent for the basic case of a rigid foundation. The pile foundation consists of fifteen floating reinforced concrete piles per bay. The pile diameter is 0.75 ft (0.23 m) and the pile length to diameter ratio is 40. In this example and previous ones, the building density is 10 lb/ft^3 (158 kg/m^3). Figure 3.19 indicates that the pile foundation provides the highest natural frequency but lowest damping. The three separate mats yield lower frequency and, for stiffer soils, higher damping than one large mat. The differences in the damping ratios and natural frequencies are associated with the differences in the shape of the first vibration mode shown in Figure 3.20. The higher the shear wave velocity, the stiffer the foundation and the closer the mode shape to the one observed with the fixed base.

The effect of soil-structure interaction is also

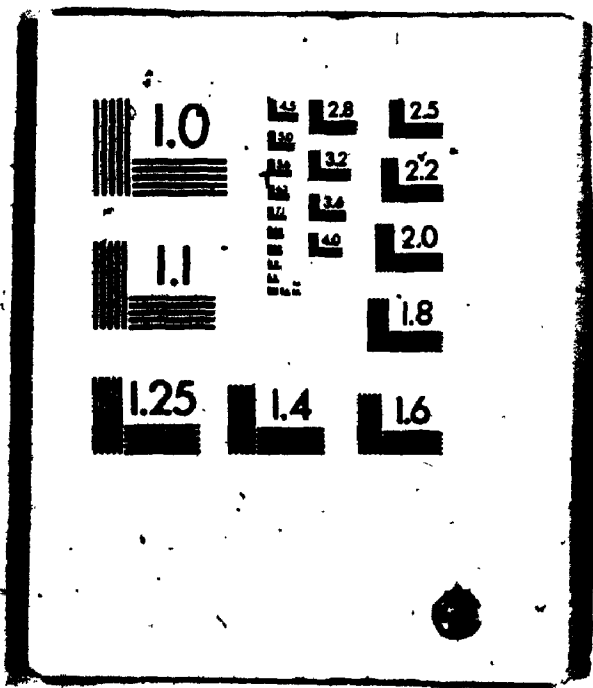
important for towers and tower-like structures such as chimneys because of their small structural damping and great sensitivity to dynamic excitation, especially to wind. An example of the variation of soil damping for a chimney is given in Chapter 7. Other examples of tower-like structures are available in Reference (72).

3.5 CONCLUSIONS

The effects of soil-structure interaction on natural frequencies, modal damping and mode shapes of structures are examined in detail in this chapter. The following conclusions emerge:

- The undamped natural frequencies are always reduced by soil flexibility.
- The damped natural frequencies of structures on flexible foundations may be lower or higher than the undamped natural frequencies.
- The modal shapes are those associated with the structural modes, and two additional ones, arising from the introduction of rocking and translation of the base.
- The softer the soil, the more the base translation and rotation, and the magnitude of the relative modal displacement.

2

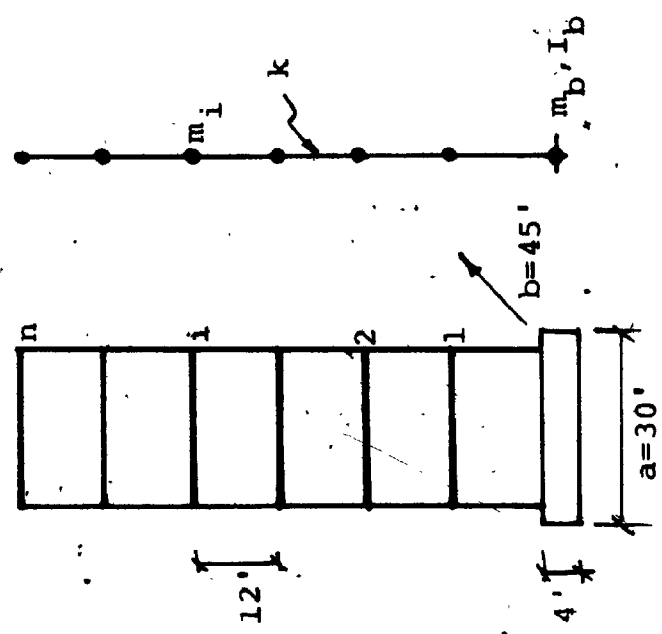


- The damped modes differ significantly from undamped modes.
- Foundation flexibility affects the total damping of a structure in two ways: (1) it provides damping due to energy dissipation in soil, and (2) modifies the original structural damping, reducing it for most structures.
- The possible loss of structural damping is usually more than replaced by the damping from the foundation but this need not be the case for strong earthquakes.
- The effects of the foundation on the damping of structures can be evaluated using an energy consideration, an approximate method, or the complex eigenvalue approach, an accurate method.
- For internal (structural) damping, both methods yield identical results because the undamped and damped modes do not differ very much.
- For foundation damping, which is nonproportional, both methods give almost the same results for the first mode but may give considerably different results for higher vibration modes.
- The error of the energy approach increases as the foundation damping increases and may reach 50 percent or even more for the higher vibration modes, depending on foundation conditions.

- Frequency dependent foundation impedance functions complicate the analysis. In such a case, modal damping can be evaluated by means of an iterative procedure or established from transfer functions of the system.
- The damping generated by the foundation can be exploited to reduce structural response to wind, earthquakes and other dynamic loads.
- The response of the complex soil-structure interaction system to dynamic loads can be analyzed accurately using superposition of damped modes since the equations of motion can be uncoupled using nonclassical modes.

TABLE 3.1 Building Properties (n floors)

m_i	4472.05 slugs	=	65376.00 kg
m_b	25155.28 slugs	=	367740.00 kg
I_b	1920180.40 slugs.ft ²	=	2607856.30 kgm ²
k	17.36 lb/ft ²	=	253.66 N/m
$R_o = \sqrt{ab/\pi}$	20.73 ft	=	6.32 m



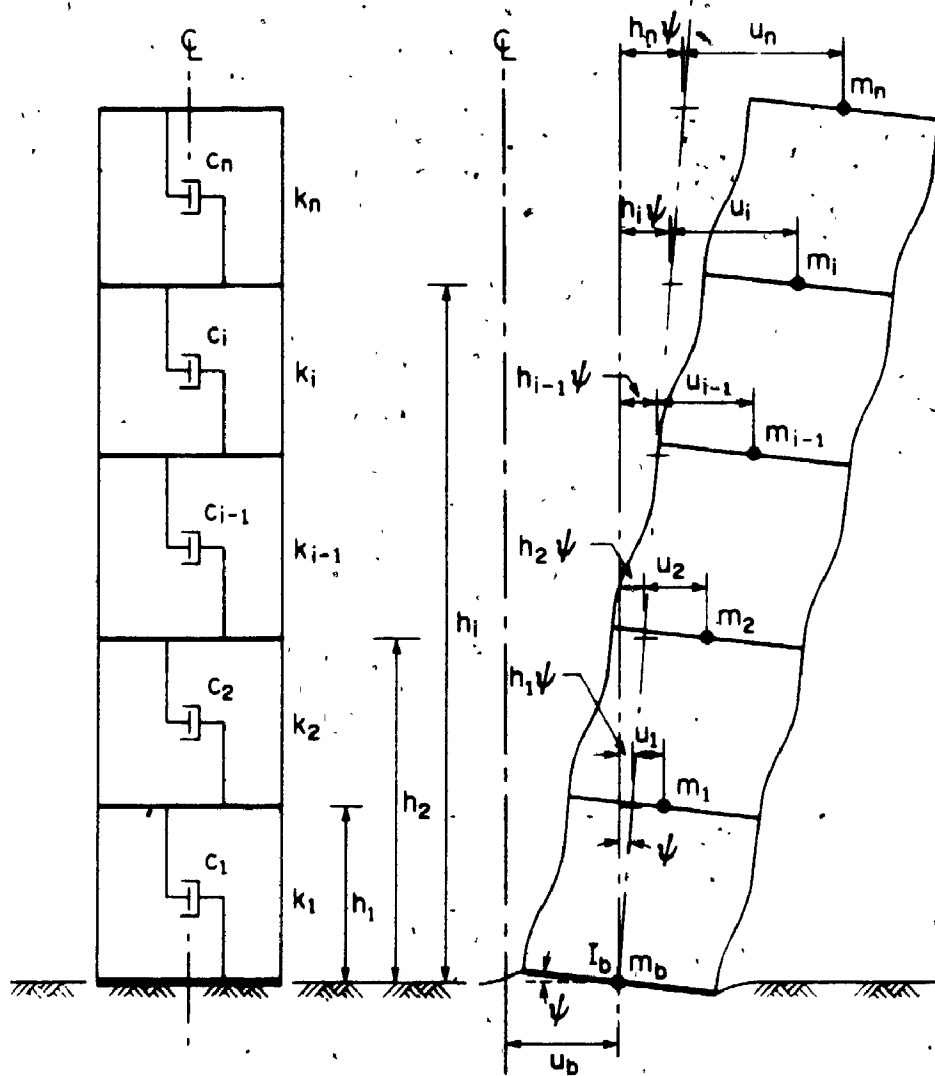


FIGURE 3.1 Vibrating Shear Building

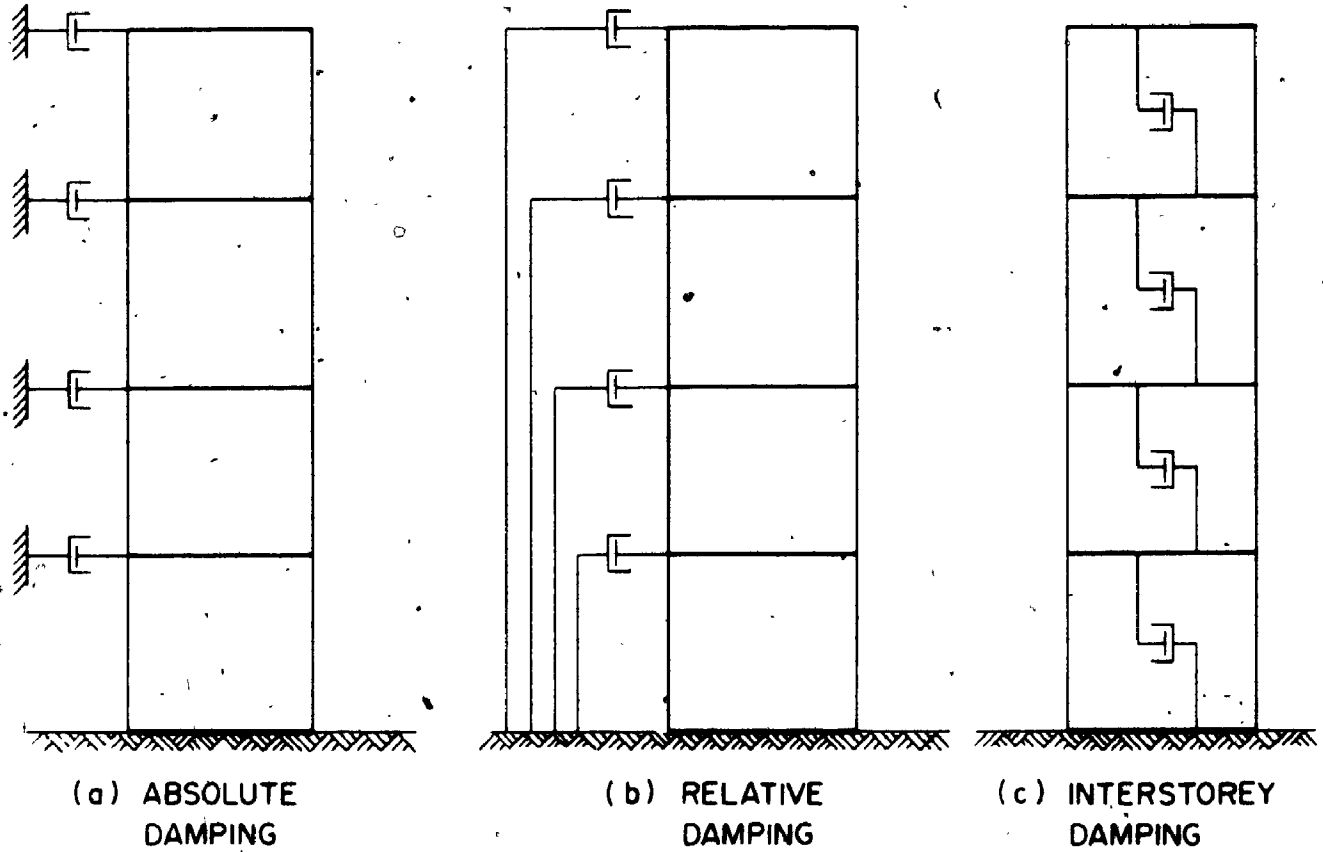


FIGURE 3.2 Basic Types of Models for Structural Damping

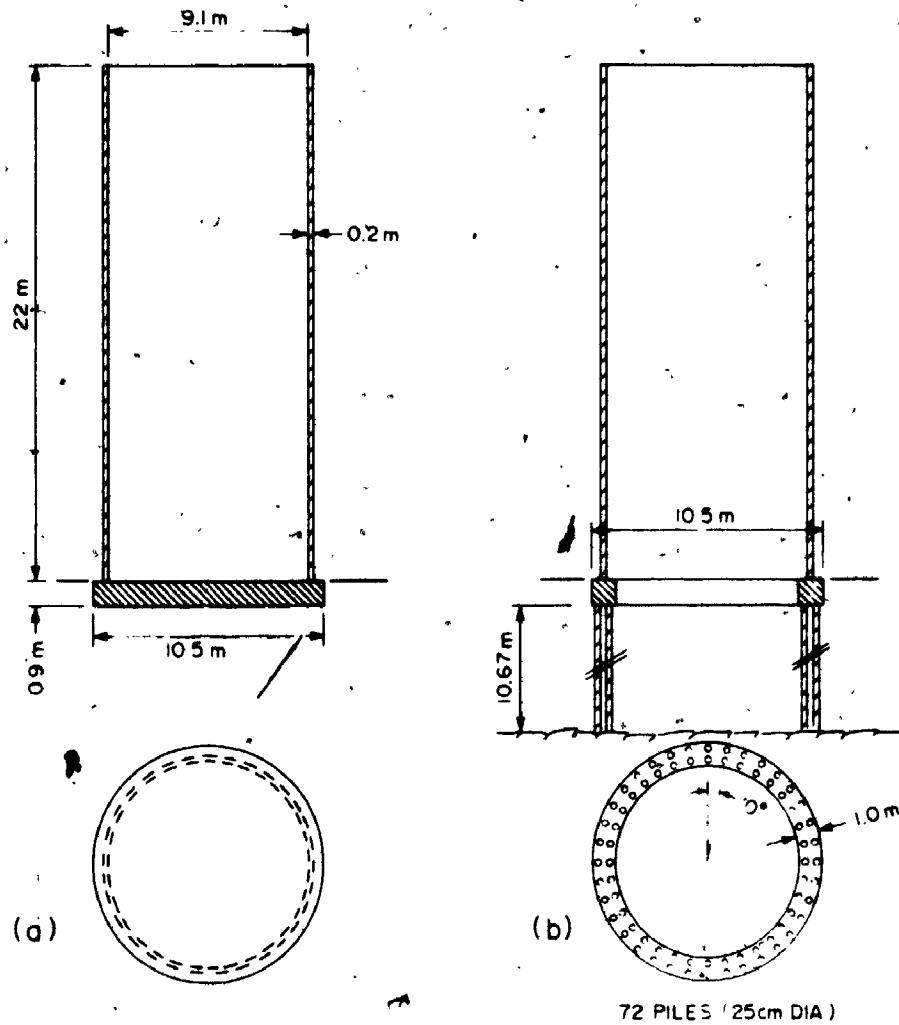


FIGURE 3.3 Silo Supported by (a) Mat Foundation and
(b) Pile Foundation. (1 m = 3.281 ft)

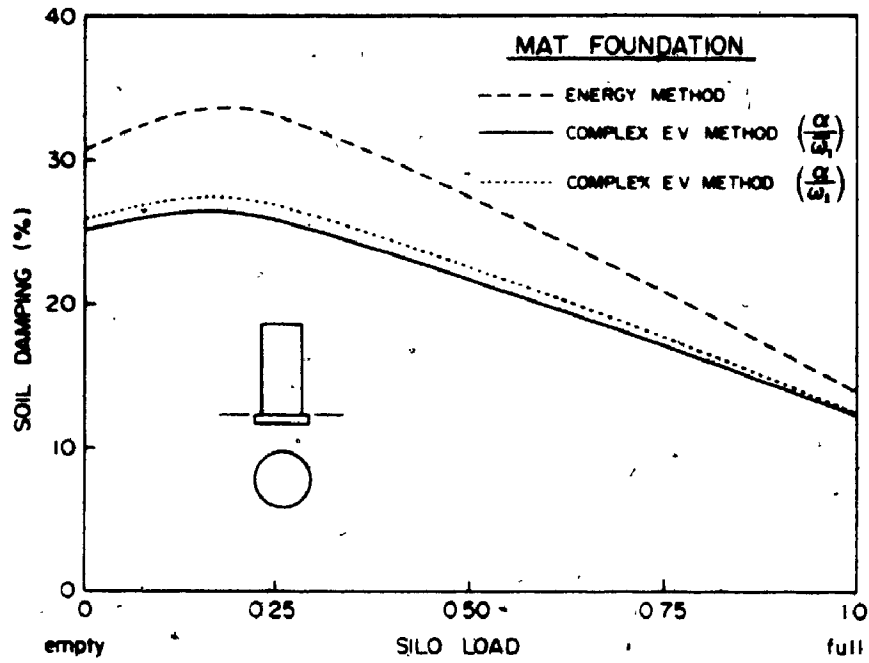


FIGURE 3.4 First Mode Damping Ratio of Mat Supported Silo for Various Silo Loadings

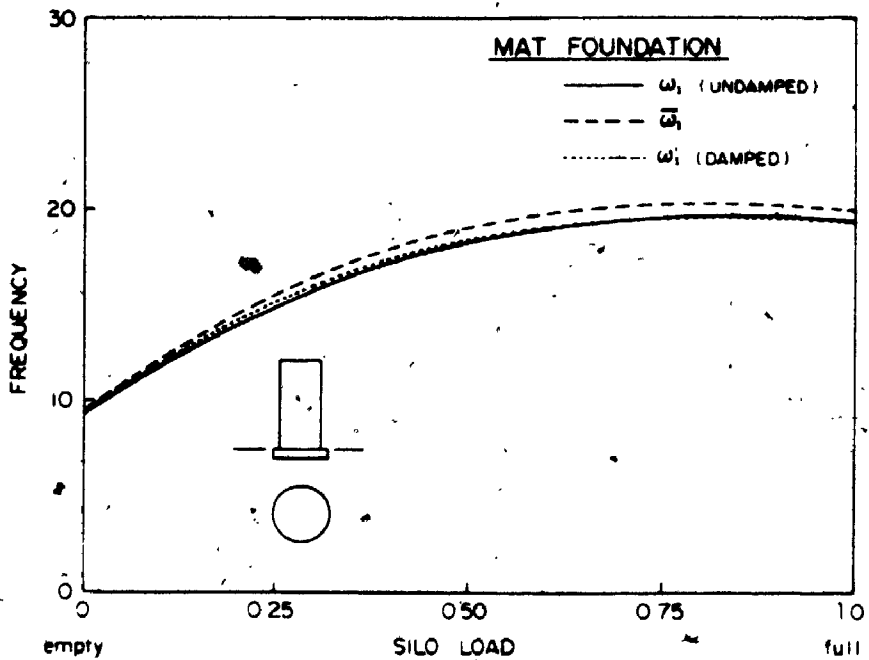


FIGURE 3.5 First Mode Frequencies of the Mat Supported Silo for Varying Silo Loading

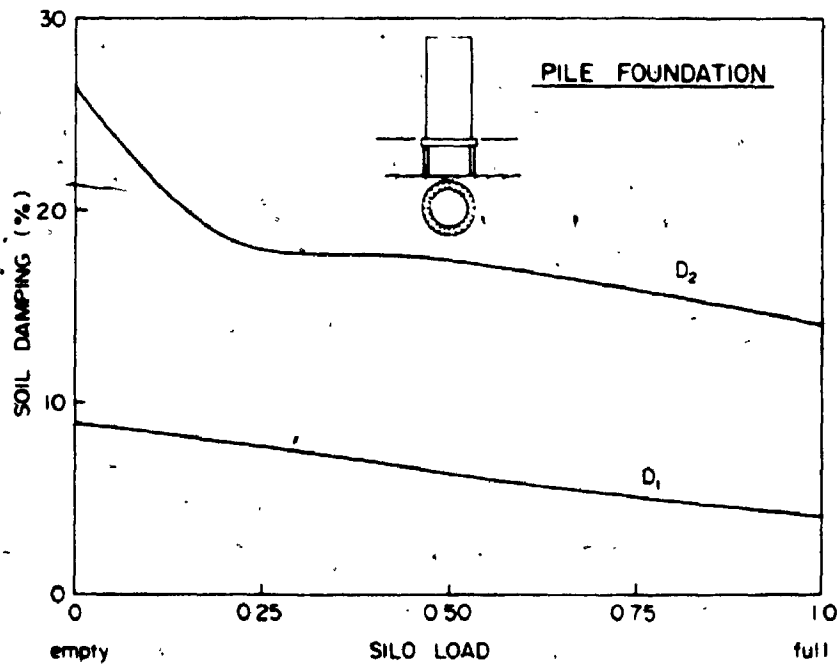


FIGURE 3.6 Modal Damping Ratios of Pile Supported Silo for Varying Silo Loading

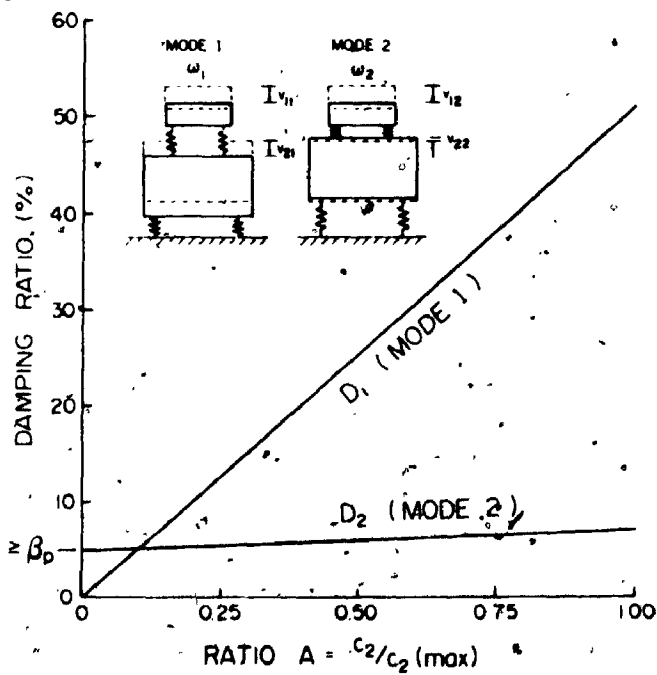


FIGURE 3.7 Modal Damping Ratios of Hammer Foundation for Variable Constant of Soil Damping

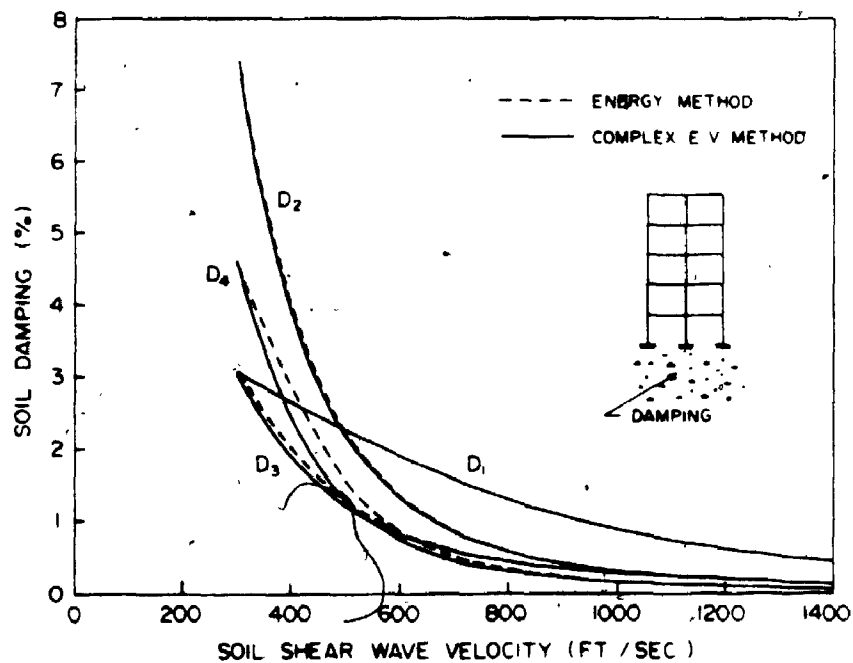


FIGURE 3.8 Modal Damping of Five-Storey Shear Building With Separate Foundations Derived From Soil of Varying Stiffness (1 ft/s = 0.3048 m/s)

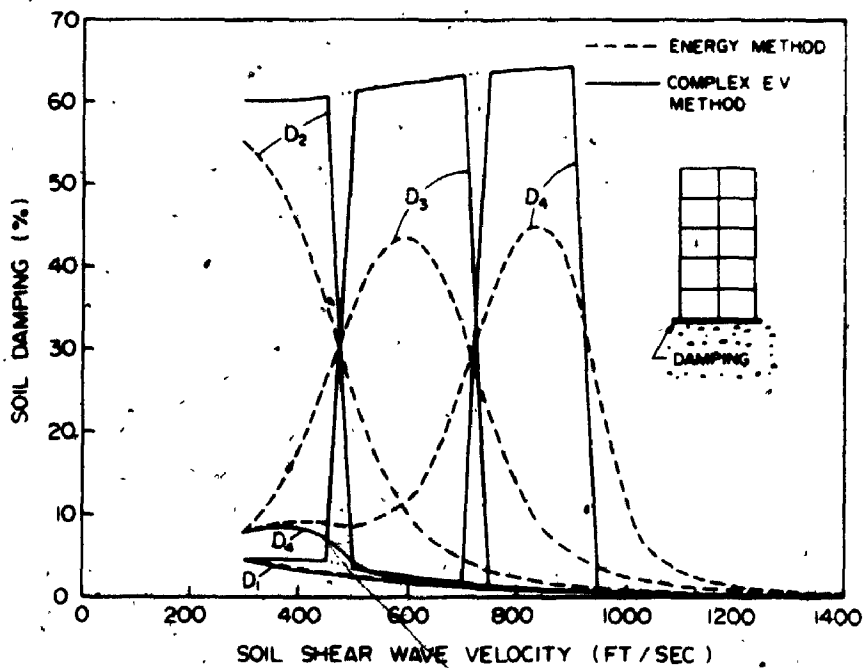


FIGURE 3.9 Modal Damping of Five-Storey Shear Building With Large Mat Foundation Derived From Soil of Varying Stiffness (1 ft/s = 0.3048 m/s)

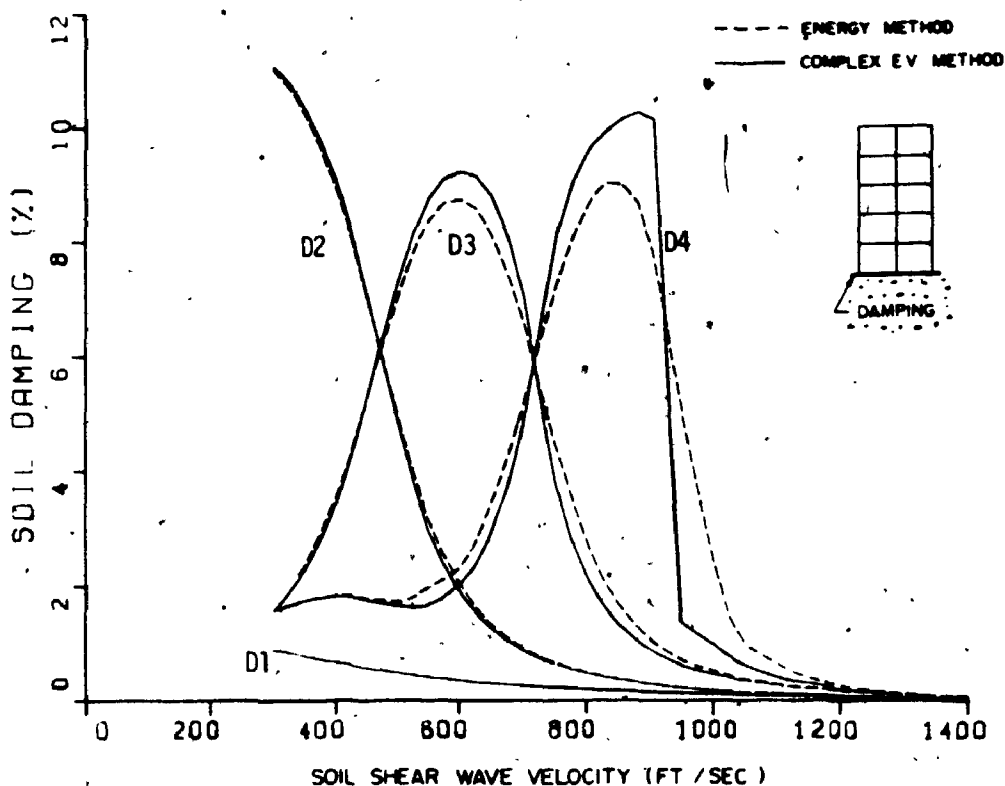


FIGURE 3.10 Damping of Five-Storey Shear Building With Mat Foundation Derived from Soil of Varying Stiffness and Foundation Damping Equal to One-Fifth of That Used in Figure 3.9 for Halfspace (1 ft = 0.3048 m)

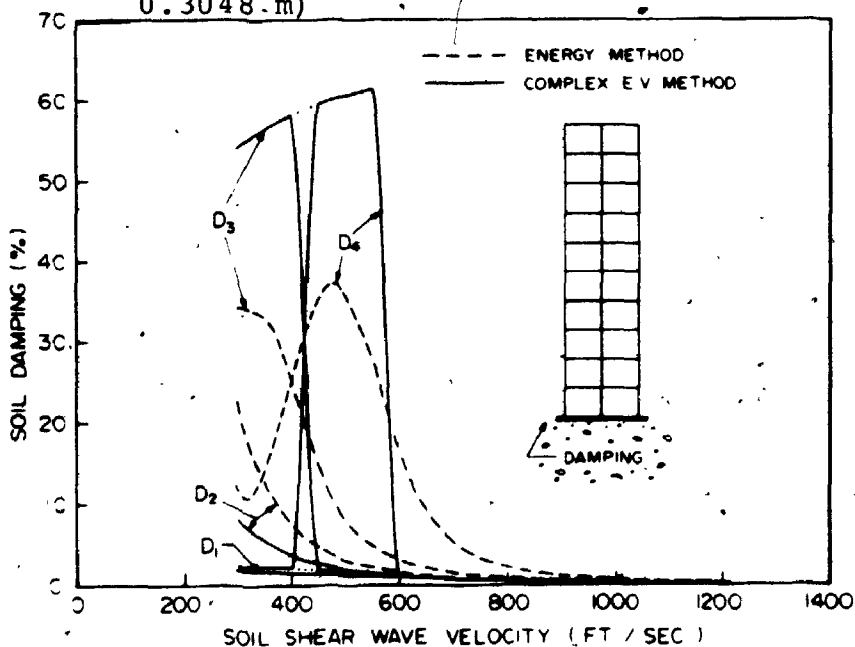


FIGURE 3.11 Modal Damping of Ten-Storey Shear Building With Large Mat Foundation Derived From Soil of Varying Stiffness (1 ft = 0.3048 m)

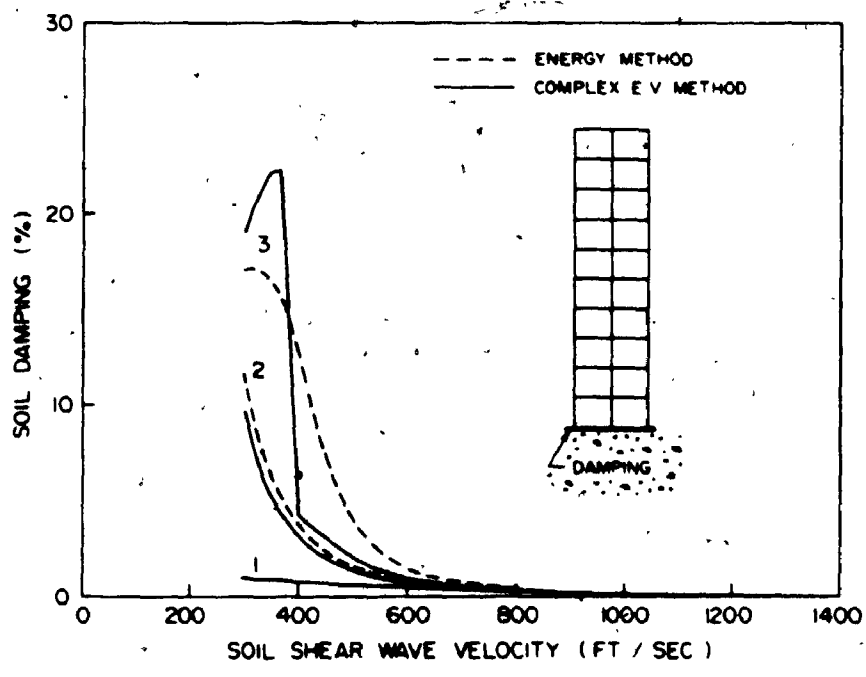


FIGURE 3.12 Modal Damping of Ten-Storey Shear Building Due to Reduced Damping in the Foundation

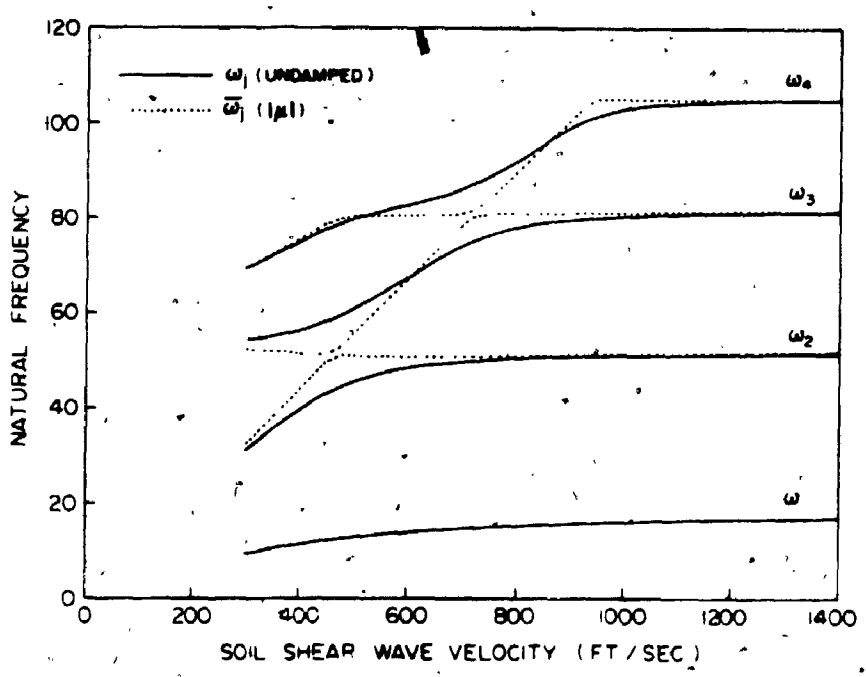


FIGURE 3.13 Undamped Natural Frequencies and Frequencies $\omega_j = |\mu_j|$ of Five-Storey Shear Building for Varying Soil Stiffness (1 ft = 0.3048 m)

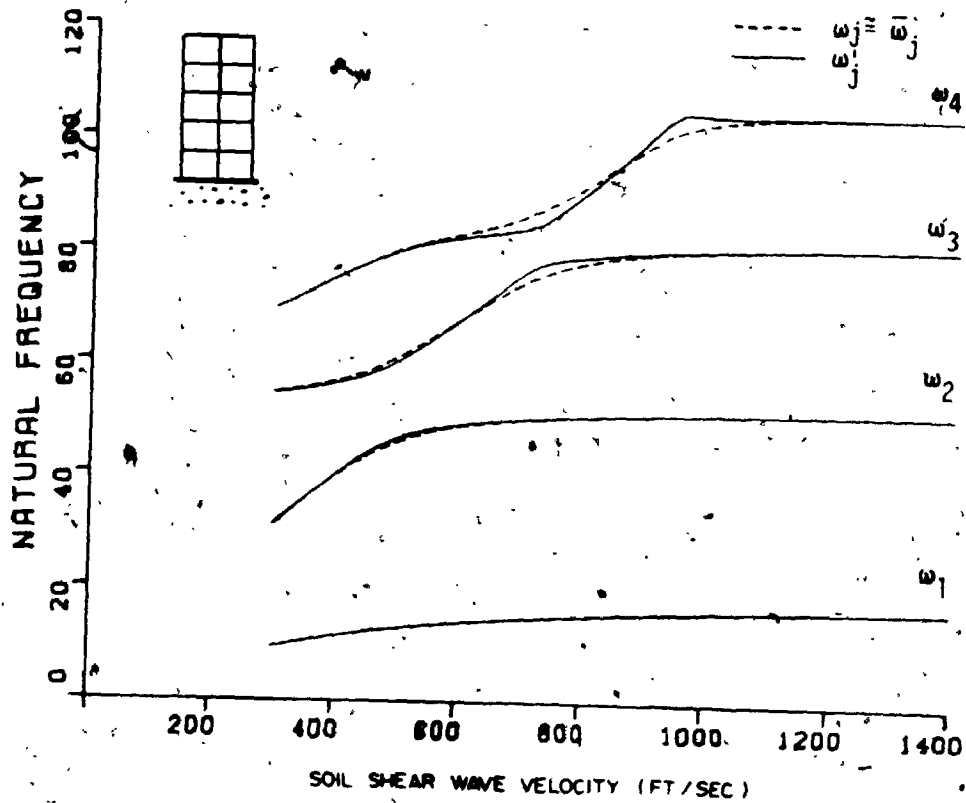


FIGURE 3.14 Undamped and Damped Natural Frequencies of Five-Storey Shear Building With Damping Matrix Reduced to One-Fifth of the Value for Halfspace

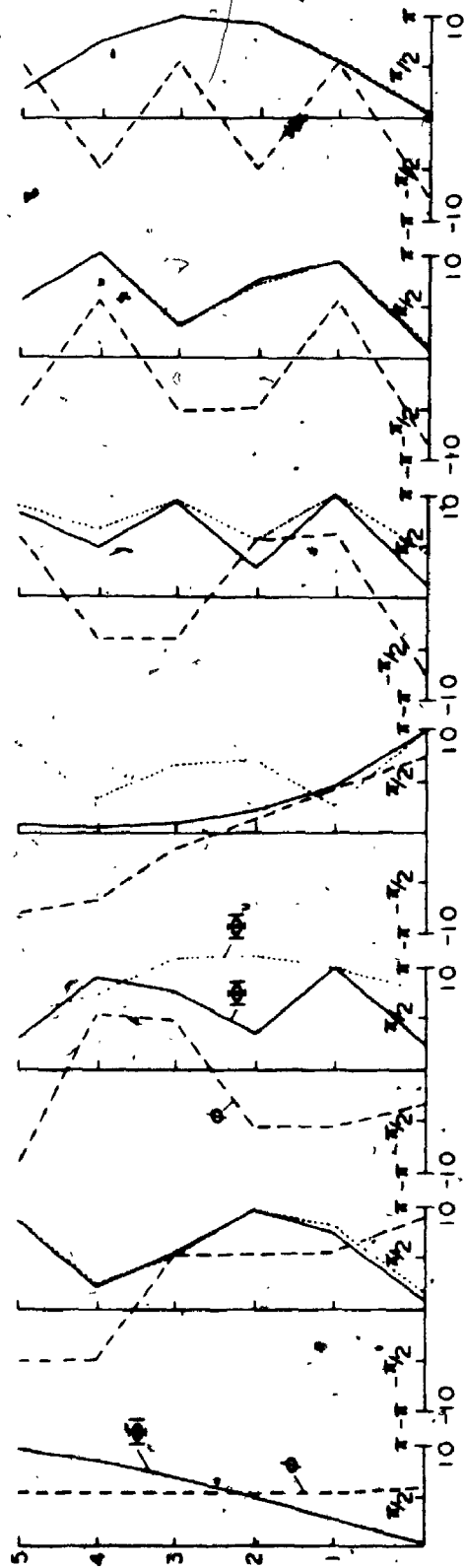


FIGURE 3.15 Undamped and Damped Vibration Modes of Five-Storey Building With Mat Foundation ($|\phi|$ -Absolute Displacement, ϕ Phase Shift, $|\phi|_u$ -Absolute Displacement of Undamped Mode; $V_s = 660$ ft/s = 201 m/s)

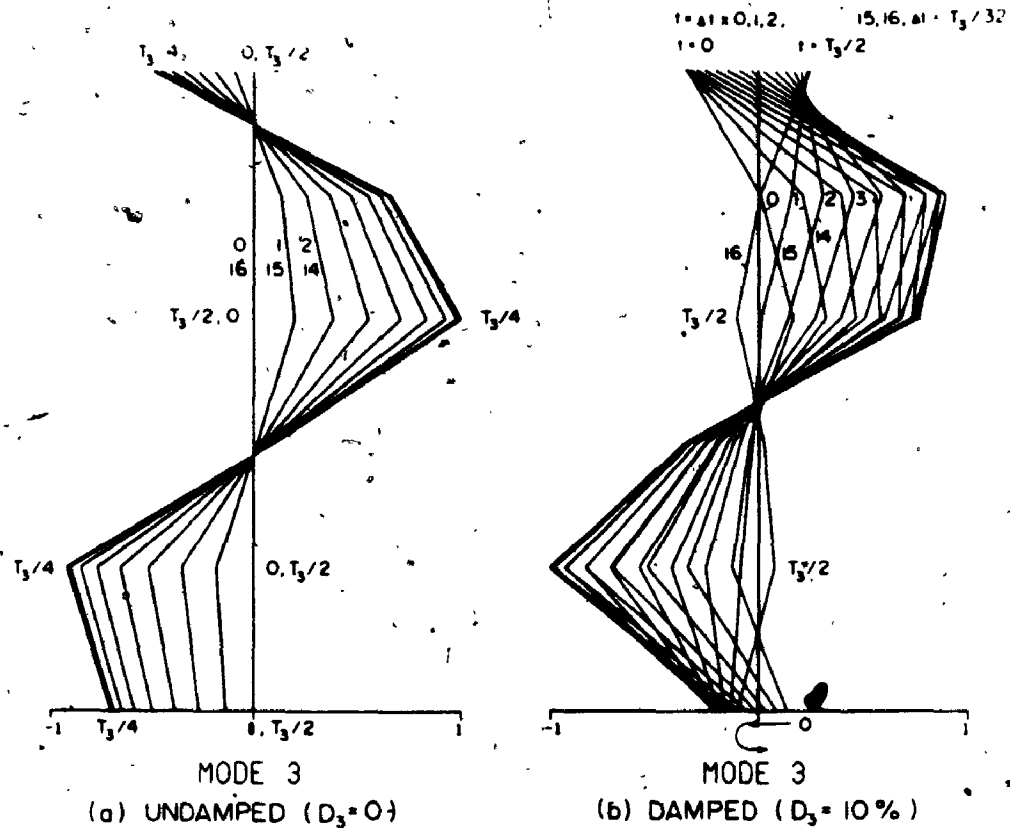


FIGURE 3.16. Comparison of Undamped Vibration in Classical Mode With Damped Vibration in Nonclassical Mode for Five-Storey Building With Mat Foundation. (Third mode with damping due to energy dissipation in soil; displacement shown at times ranging from $t=0$ to half of natural period $T_3/2$)

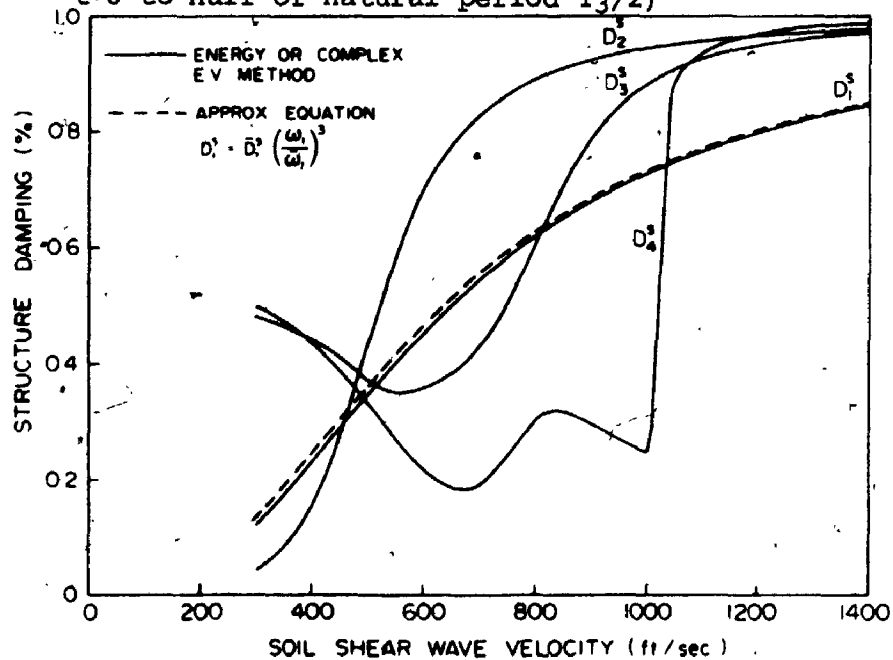


FIGURE 3.17 Structural Damping of Five-Storey Shear Building on Mat Foundation for Varying Soil Stiffness (1 ft = 0.3048 m; Both Methods Give Almost the Same Results)

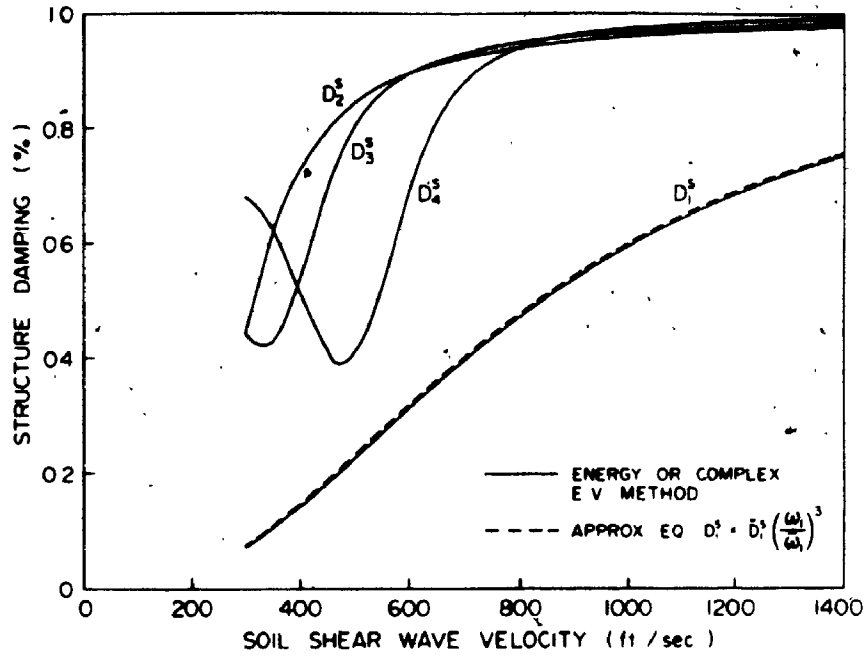


FIGURE 3.18 Structural Damping of Ten-Storey Shear Building on Mat Foundation For Varying Soil Stiffness (1 ft = 0.3048 m; Both Methods Give Almost the Same Results)

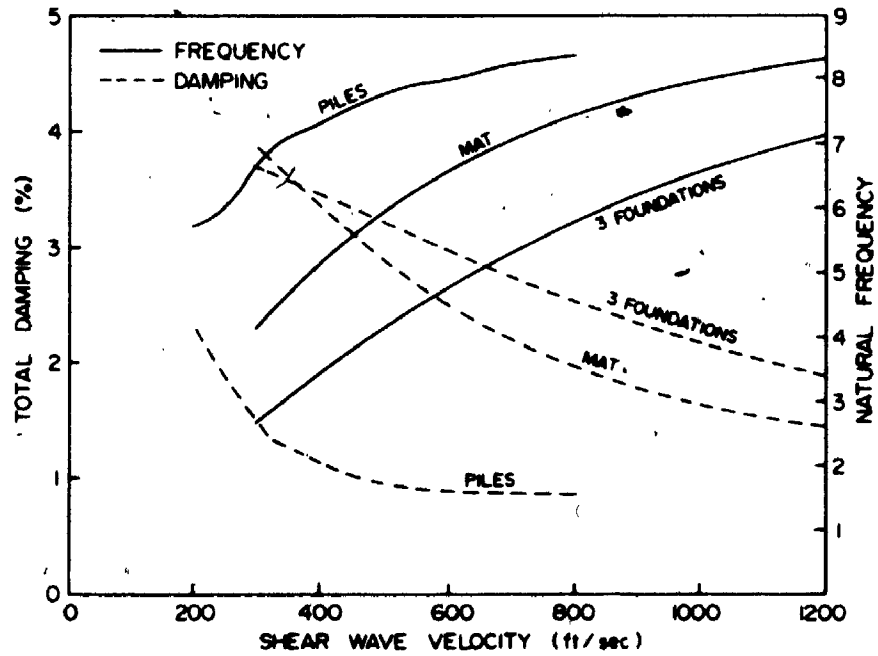


FIGURE 3.19 First Natural Frequency and Damping Ratio For Ten-Storey Building (1 ft = 0.3048 m)

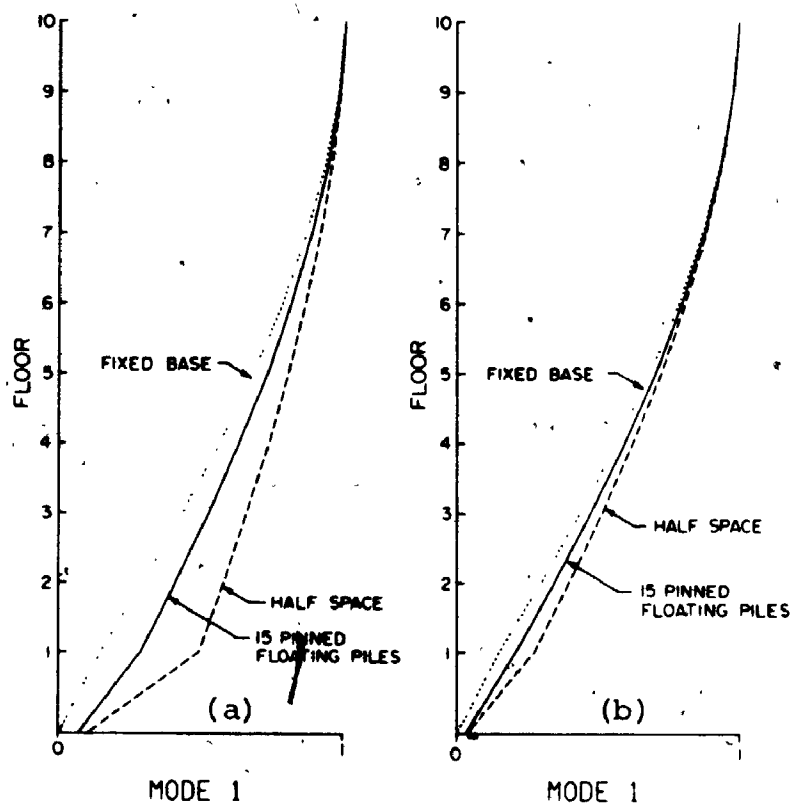


FIGURE 3.20 First Vibration Mode of Building On Different Foundations (a) - $V_s = 300$ ft/sec, (b) - $V_s = 600$ ft/sec, $1 \text{ ft/sec} = .3048 \text{ m/sec}$

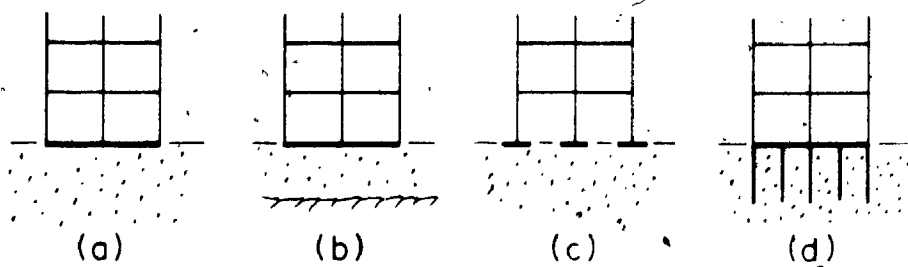


FIGURE 3.21 Types of Foundations

CHAPTER 4

RESPONSE TO DYNAMIC LOADS

4.1 INTRODUCTION

Once the input forces and the base impedances are known, the equations of motion of the soil-structure interaction system, given by equation 2.22, can be solved in many different ways. The solution can be carried out in the time domain or in the frequency domain. Both methods are discussed in this chapter. The frequency domain solution allows a probabilistic type analysis and the consideration of frequency dependent impedance functions. A time domain solution facilitates nonlinear analysis and in the form of linear modal analysis offers a simple physical interpretation of the results. Though, the foundation impedance coefficients are functions of frequency, therefore they should be selected by an iterative approach for the time domain analysis. These iterations can be made either automatically in the computer program used for the solution or each solution's results may be evaluated to determine if the assumed values of impedance coefficients are within acceptable limits. Also, this iteration can be circumvented using the procedure suggested by Chopra et al. (73).

When the equations of motion are not diagonalizable by a coordinate transformation using undamped modes, an exact normal mode analysis cannot be performed. However, very good approximations to the response can be obtained by the use of equivalent modal damping values and classical modal analysis (15, 28, 30). The other alternative is to use the nonclassical modal analysis which is particularly well suited for the solution of the equation of motion of the soil-structure interaction systems. A direct integration of equation 2.22 is of course possible (74, 75, 76). However, a common problem of all direct integration methods is that the time increment must be chosen small to ensure accuracy and stability of the solution.

A brief description and a discussion of the different methods are given below because these are used to analyze some basic cases of dynamic loading in the following chapters.

4.2 CLASSICAL MODAL ANALYSIS

Modal analysis is a general method for analyzing the response of linear multi-degree-of-freedom systems. It is particularly suitable for systems whose properties are frequency independent. The method describes the response

in terms of the modes of free undamped vibration whose orthogonality facilitates the solution.

This method neglects damping in the first stage of the computations and proceeds to solve the eigenvalue problem

$$([k] - \omega^2 [m])\{\phi\} = \{0\} \quad (4.1)$$

This leads to a set of corresponding natural frequencies $\omega_1 < \omega_2 < \dots < \omega_n$ and mode shapes $\{\phi\}_j$, $j = 1, \dots, n$, where n is the dimension of $\{u\}$; and $[k]$, $[m]$, $\{u\}$ are defined for the soil-structure system by equation 2.23. The method then expresses the actual displacements $\{u\}$ in terms of modal displacements

$$\{u\} = [\phi]\{\eta\} \quad (4.2)$$

where $[\phi]$ is an $n \times n$ matrix which contains the mode shapes $\{\phi\}$ in its columns and $\{\eta\}$ is the vector of generalized coordinates. Substitution of equation 4.2 into equation 2.22 and premultiply by the transpose of $[\phi]$ which is $[\phi]^T$

$$\begin{aligned} & [\phi]^T [m] [\phi] \{\ddot{\eta}\} + [\phi]^T [c] [\phi] \{\dot{\eta}\} + [\phi]^T [k] [\phi] \{\eta\} \\ & = [\phi]^T \{P\} \end{aligned} \quad (4.3)$$

Equation 4.3 considerably simplifies due to the generalized orthogonality conditions, according to which

$$[\phi]^T [m] [\phi] = [M] \quad (4.4a)$$

$$[\phi]^T [k] [\phi] = [K] = [\omega_j^2] [M] \quad (4.4b)$$

The matrices $[M]$ and $[K]$ are diagonal and contain the generalized masses M_j and generalized stiffnesses K_j respectively.

Clearly, it would be most desirable if the triple product

$$[\phi]^T [c] [\phi] \quad (4.5)$$

containing the damping constants of the system, resulted in a diagonal matrix. In such a case, equation 4.3 represents a set of n independent equations for η_j , $j = 1, 2, \dots, n$, that are "uncoupled".

Since $[\phi]^T$ and $[\phi]$, two multipliers, are the same in equation 4.5 and equation 4.4, the triple matrix product, equation 4.5, can result in a diagonal matrix only when the damping matrix, $[c]$, is proportional to either the mass matrix $[m]$ or the stiffness matrix $[k]$ or is a polynomial combination of them. In this case, equation 4.3 yields a set of n uncoupled equations. Each of them has the form

$$\ddot{\eta}_j + 2D_j \omega_j \dot{\eta}_j + \omega_j^2 \eta_j = \frac{P_j(t)}{M_j}, \quad j = 1, 2, \dots, n \quad (4.6)$$

in which

$$P_j(t) = \{\phi_j\}^T \{P(t)\} \quad (4.6a)$$

and D_j = modal damping ratio = $\{\phi_j\}^T [c] \{\phi_j\} / 2M_j \omega_j$ if the damping is proportional.

However, for soil-structure interaction, the damping is nonproportional. In such a case, the damping matrix $[c]$ is not diagonalized by the triple product, equation 4.5. Nevertheless, modal damping ratios D_j can be calculated using approximate methods, for example the energy approach outlined in the previous chapter.

Then, the simple differential equation 4.5 can be solved for the generalized coordinates $n_j(t)$. The solution of equation 4.5 takes the form

$$n_j(t) = e^{-D_j \omega_j t} \left[n_j(0) \cos \omega_j^! t + \frac{\dot{n}_j(0) + D_j \omega_j n_j(0)}{\omega_j^!} \sin \omega_j^! t \right] + \frac{1}{\omega_j^! M_j} \int_0^t P_j(\tau) e^{-D_j \omega_j (t-\tau)} \sin \omega_j^! (t-\tau) d\tau \quad (4.6b)$$

where $n_j(0)$ and $\dot{n}_j(0)$ can be determined from the initial conditions of the system and $\omega_j^!$ is the damped frequency of mode j equal to $\omega_j \sqrt{1-D_j^2}$, and τ is the integration variable. The first term of equation 4.6b represents the free vibration due to initial conditions. The second term represents forced vibration.

The actual displacements $\{u\}$ follow from the linear

transformation equation 4.2.

The success of the modal analysis method is due to the fact that for a majority of practical problems it is not necessary to determine and consider all of the eigenvalues and mode shapes.

This can obviously lead to considerable savings of computational effort. However, the results of the classical modal analysis may be inaccurate for cases of nonproportional damping because of the manner in which damping is introduced.

4.3 NONCLASSICAL MODAL ANALYSIS

To uncouple the equations of motion of the soil-structure system using modal analysis, equation 2.22 is transformed into the reduced equation 3.12 with the number of degrees of freedom doubled. The general solution of the reduced equation 3.12 can be obtained via the linear transformation

$$\{z(t)\} = [Z]\{q(t)\} \quad (4.7)$$

where $[Z]$ is the matrix containing $2n$ complex eigenvectors and $q(t)$ are the generalized coordinates for the damped system. Substituting this transformation into equation 3.12 yields:

$$[A][Z]\{\dot{q}(t)\} + [B][Z]\{q(t)\} = \{F(t)\} \quad (4.8)$$

Premultiplying this equation by $[Z]^T$ one obtains

$$[Z]^T[A][Z]\{\dot{q}(t)\} + [Z]^T[B][Z]\{q(t)\} = [Z]^T\{F(t)\} \quad (4.9)$$

Since $[Z]^T[A][Z] = \lceil A_j \rceil$ and $[Z]^T[B][Z] = \lceil B_j \rceil$, as stated by equation 3.19, equation 4.9 reduces to

$$\lceil A_j \rceil \{\dot{q}(t)\} + \lceil B_j \rceil \{q(t)\} = [Z]^T\{F(t)\} = \{f(t)\} \quad (4.10)$$

Because $\lceil A_j \rceil$ and $\lceil B_j \rceil$ are diagonal matrices, equation 4.10 results in the uncoupled inhomogeneous set of equations

$$\dot{q}_j(t) + \mu_j q_j(t) = f_j(t)/A_j, \quad j = 1, 2, \dots, 2n \quad (4.11)$$

in which μ_j is the complex eigenvalue defined by equations 3.16 and 3.19c. The solution of equations 4.11 has the form

$$q_j(t) = q_j(0) \exp(\mu_j t) + \frac{1}{A_j} \int_0^t \exp[\mu_j(t-\tau)] f_j(\tau) d\tau \quad (4.12)$$

$j = 1, 2, \dots, 2n$

where τ is the variable of integration.

The magnitude of $q_j(0)$ can be determined from the initial

conditions for $z(t)$ at $t = 0$ as

$$\{q(0)\} = [Z]^{-1} \{z(0)\} \quad (4.13)$$

When the quantities $q_j(0)$ are substituted into equation 4.12, $q_j(t)$ is determined and the solution $\{z(t)\}$ is obtained by superposition of the complex modal responses through the use of equation 4.7.

In equation 4.12, the first term provides the free vibration with prescribed initial conditions and the second term provides the response to time dependent forces.

The advantages of the nonclassical modal analysis are the insight it provides into the dynamic characteristics of the interaction system and the mathematical accuracy obtained even with nonproportional soil damping.

4.4 COMPLEX RESPONSE ANALYSIS

The equations of motion of the soil-structure interaction system, equation 2.22, can be solved in the frequency domain using Fourier transform method (complex response method). For this purpose, each input force $P(t)$ is assumed to be given for an even number, N , of equidistant points in the time domain as

$$P_k = P(k \cdot \Delta t) \quad , \quad k = 1, 2, \dots, N \quad (4.14a)$$

and is expanded into a continuous function by the trigonometric interpolation formula

$$P(t) = \operatorname{Re} \sum_{s=0}^{N/2} p_s e^{i\omega_s t} \quad (4.14b)$$

where the frequencies ω_s are

$$\omega_s = \frac{2\pi s}{N \Delta t}, \quad s = 0, 1, \dots, \frac{N}{2} \quad (4.15)$$

and p_s , $s = 0, 1, \dots, \frac{N}{2}$ are complex amplitudes in the frequency domain. These amplitudes can be computed from the P_k values by the very efficient Fast Fourier transform method (77).

Then, each of the terms of equation 4.14b is considered as an input to equation 2.22, i.e.

$$[m]\{\ddot{u}\}_s + [c]\{\dot{u}\}_s + [k]\{u\}_s = \{p_s\} e^{i\omega_s t} \quad (4.16)$$

Assuming the steady state solution

$$\{u\}_s = \{\bar{u}\}_s e^{i\omega_s t} \quad (4.17)$$

equation 4.16 reduces to

$$([k] + i\omega_s [c] - \omega_s^2 [m])\{\bar{u}\}_s = p_s \quad (4.18)$$

Equation 4.18 constitutes a set of linear equations which can be solved for the complex displacement amplitudes $\{\bar{u}\}_s$. Then, $\{u\}_s$ follows from equation 4.17. The

complete response in the time domain follows by superposition, remembering that the real part of the output corresponds to the real part of the input. Hence,

$$\{u\} = \operatorname{Re} \sum_{s=0}^{N/2} \{u\}_s = \operatorname{Re} \sum_{s=0}^{N/2} \{\bar{u}\}_s e^{i\omega_s t} \quad (4.19)$$

Thus, the displacement $\{u\}$ in the time domain can be obtained by performing an inverse Fast Fourier transform on each of the terms of $\{\bar{u}\}_s$.

In summary, the time history response can be computed through the use of Fourier transforms by (1) finding the direct transform of the excitation forces, (2) multiplying it by the transfer function

$$H(\omega) = ([k] + i\omega_s [c] - \omega_s^2 [m])^{-1} \quad (4.19a)$$

and (3) obtaining the inverse transformation of the product.

For problems of free vibration due to initial displacements and velocities, equation 4.18 can be rewritten as (65)

$$([k] + i\omega_s [c] - \omega_s^2 [m]) \{\bar{u}\}_s = (\omega_s [m] + [c]) \{\bar{u}_0\} + [m] \{\dot{\bar{u}}_0\} \quad (4.20)$$

where \bar{u}_0 , $\dot{\bar{u}}_0$ are, respectively, the initial displacement and velocity of the system. Again, equations 4.20 can be solved for $\{\bar{u}\}_s$ at each frequency ω_s and the time response

to initial conditions can be obtained from equation 4.19.

A frequency solution has some inherent advantages:

(1) frequency dependent impedance functions can be readily incorporated, (2) it allows control of the accuracy of the solution within different ranges of frequencies and, (3) once the transfer functions have been computed, it permits change of the excitation force, or its location, without having to repeat the complete procedure.

Also, the frequency domain solution allows a probabilistic type analysis (for nondeterministic excitation forces or random excitations). This is so because the spectral densities of the random forces and response are directly related through the transfer functions. The spectral solution can be carried out directly or via modal analysis. The latter type of solution is outlined in Chapter 7 where it is applied to the problem of structural response to randomly fluctuating gusting wind. The direct spectral approach is outlined in the next subchapter.

4.5 DIRECT SPECTRAL ANALYSIS

The random vibration theory was used to analyze problems involving soil-structure interaction by many authors including Vanmarcke (78). It is a powerful tool but not well understood by most civil engineers.

Efficient use of the random vibration theory relies on a function of frequency, ω , called the power spectral density, $S(\omega)$. The power spectral density, $S(\omega)$, describes how the energy of a random process, such as earthquake acceleration, is distributed with regard to frequency. The Fourier transform of a particular digitized process can be used to obtain the corresponding $S(\omega)$. Ideally, $S(\omega)$ should be computed from a number of measured samples. However, this is seldom possible for earthquake problems because of a lack of data. Thus, it is most often assumed that the excitation forces are stationary and ergodic. Stationarity implies that the ensemble averages are independent of time. Ergodicity means that the integration or time averaging of one (long) sample yields the same results as the integration or averaging among many samples of one ensemble.

The power spectral densities of a process can be obtained analytically or numerically. For example, for earthquake problems Tajimi (79) proposed an empirical analytical expression for power spectral density of earthquake ground acceleration. On the other hand, the $S(\omega)$ of a specific ground motion can be obtained by means of Fast Fourier transform of the given time history.

Once the power spectral density of the excitation force, $S_p(\omega)$, has been established, the spectral density of

the stationary response $S_u(\omega)$ is

$$S_u(\omega) = |H(\omega)|^2 S_p(\omega) \quad (4.21)$$

in which $H(\omega)$ is the transfer function between the input and output. This function is obtainable directly by means of the complex analysis outlined in the previous subchapter, as follows:

$$\begin{aligned} \{F_u(\omega)\} &= [[k] - \omega^2 [m] + i\omega [c]]^{-1} \{F_p(\omega)\} \\ &= [H(\omega)] \{F_p(\omega)\} \end{aligned} \quad (4.22)$$

where F_u and F_p are the Fast Fourier transform of the output and input respectively. Multiplying each row of equation 4.22 by its conjugate yields the spectral densities of displacements

$$\{S_{uu}(\omega)\} = |H(\omega)|^2 \{S_p(\omega)\} \quad (4.23a)$$

or

$$S_{uu_i}(\omega) = \text{Real} \left(\sum_{k=1}^n \sum_{j=1}^n H_{ik}(\omega) H_{ij}^*(\omega) S_{P_{kj}}(\omega) \right) \quad (4.23b)$$

in which i corresponds to the degree of freedom in direction i , the asterisk denotes complex conjugate and $S_{P_{kj}}$ are the cross spectral densities between forces in directions k and j . Cross spectral densities between output coordinates can be obtained in a similar way.

It can be seen from equation 4.23 that the direct

spectral approach is particularly suitable for rigid bodies on soil where the number of degrees of freedom is not more than six and the impedance functions are frequency dependent.

For buildings with many degrees of freedom, the problem is more conveniently treated in terms of orthogonal modes. The random response is evaluated at each significant mode and the final response is obtained by superposition of individual modes. This latter approach is particularly advantageous when the structure response is dominated by the first mode of vibration as will be shown in more detail in Chapter 7.

Mean Peak Response

The spectral densities of the response obtained from equation 4.23 are used to compute the mean peak response for a chosen level of probability. The maximum value of the response that will not be exceeded within a certain probability, α , can be computed using the approach due to Davenport (80) or Vanmarcke (81). The mean value of the peak response can be expressed using the peak factor g_α :

$$\bar{u} = g_\alpha \sigma_u \quad (4.24)$$

in which σ_u is the standard deviation of the stationary response found from

$$\sigma_u^2 = \int_0^{\infty} S_{uu}(\omega) d\omega \quad (4.25)$$

and g_α can be calculated using the approximate formula given by Davenport (80) as

$$g_\alpha = \sqrt{2 \ln v T} + \frac{0.5772}{\sqrt{2 \ln v T}} \quad (4.26)$$

In equation 4.26, v is the apparent frequency obtained from the formula due to Rice (82)

$$v \cong \frac{1}{2\pi} \sqrt{\frac{\int_0^{\infty} \omega^2 S_{uu}(\omega) d\omega}{\int_0^{\infty} S_{uu}(\omega) d\omega}} \quad (4.27)$$

and T is the period of the observation. Vanmarcke (81) describes a procedure to find the significant duration for a particular event.

It is also important to recognize that the response may not be stationary, but builds up with time until a stationary value of σ_u is reached. If the process is non-stationary, i.e. ensemble averages are time dependent, a correction for the response can be made in two ways. The first approach is to multiply the force record $P(t)$ by a suitable deterministic intensity function such as the box-car, trapezoidal or exponential functions shown in Figure 4.1.

In the second approach, the spectral density of the

response is described by an evolutionary spectral density function $S_{uu}(\omega, t)$ (78). Then the time dependent variance of the response can be obtained by integration over all frequencies,

$$\sigma_u^2(t) = \int_0^\infty S_{uu}(\omega, t) d\omega \quad (4.28)$$

The function $S_{uu}(\omega, t)$ depends on the input spectral densities and the system properties. Equation 4.28 yields approximately (78)

$$\sigma_u^2(t) = \sigma_u^2 (1 - e^{-2D\omega_n t}) \quad (4.29)$$

in which σ_u is the standard deviation of the stationary response, ω_n and D are the natural frequency and damping ratio respectively. Equation 4.29 indicates that the stationary variance is achieved when $D\omega_n t$ increases and $e^{-D\omega_n t}$ approaches zero. For rigid bodies on soil, the damping ratio D is high, often of the order of 20 to 30 percent as shown in Chapter 3. This indicates the very rapid rate at which the response approaches its steady-state condition.

In conclusion, the random vibration approach provides an efficient way to compute the response of a linear system to any irregular excitations. The response can be associated with a desired probability of occurrence. One limitation of the approach is that it usually requires a linear system even though soils may not be linear. The iterative

linear approximation to nonlinear properties can be used, and the errors in doing so are probably no worse than those of a deterministic solution. In this case, the analysis requires that the nonlinear response be sensitive to a narrow band of frequencies, as is the linear response, and that the equivalent linear properties are constant in time or vary slowly with time.

4.6 DIRECT INTEGRATION METHOD

In this method, solution is carried out in the time domain in which the system of differential equations 2.22 is solved through a step-by-step integration with respect to time. This is done by making assumptions about the variation of the displacement or accelerations during small time intervals; e.g., it may be assumed that during a small time interval the displacement is a cubic function of time or the acceleration varies linearly or is constant. With such assumptions the set of n second order differential equations 2.22 is replaced, in general, by h simultaneous algebraic equations. Their solution gives the displacement at the end of the short time step for the known conditions at the beginning. Successive application of this procedure gives the response.

Many methods exist; they include the Newmark β -method (76), Wilson θ -method (75) and α -method (83). To obtain a

comparable accuracy, the chosen numerical method should possess the following attributes (83):

- (1) Unconditional stability when applied to linear problems. The size of the time step in the case of an unconditionally stable method is determined only by the accuracy required. Conditionally stable algorithms require a time step which is less than a constant (usually 0.1) times the shortest period of the structure; otherwise, the method gives a divergent solution. This restriction is a stringent one and entails using a time step which is much smaller than that needed for accuracy.
- (2) Second-order accuracy. The error, ϵ , involved in a numerical procedure must be of the same order as $(\Delta t)^2$ where Δt is the time step. According to Dahlquist (84), there is no unconditionally stable linear multi-step method accurate up to the third order.
- (3) No more than one set of implicit equations should be solved at each time step.
- (4) Self-starting. Self-starting algorithms do not require data from more than two time steps to advance the solution.
- (5) Controllable algorithmic dissipation in the higher modes. Considering the response to comprise contribution from a number of normal modes, the approximations in

the direct integration methods usually cause artificial attenuation (numerical dissipation) of the response and some error in the period of the mode predicted by the numerical solution. These two effects increase as $\Delta t/T_n$ increases, where T_n is the period of the mode whose contribution is being concerned. For the Newmark β -method the error in the predicted modal period is higher than that of the other methods for the same value of Δt . Unlike other methods, the Newmark average acceleration method does not cause any artificial attenuation of the modal contributions to response. However, this is not necessarily the best algorithm, as the period errors cause the contribution to be combined with incorrect relative phase angles, and thus the maximum response may be in error. This leads to the recommendation (75, 83) that an algorithm should possess some artificial attenuation or numerical dissipation in order that the spurious response from higher modes is damped out. For ordinary structures, where only lower modes are of interest, this property is considered useful.

The predominant opinion is that only two numerical methods possess the five above-mentioned attributes: Wilson's θ -method and the α -method (other opinions also occurred in the literature (85)). The only difference between the two methods is in attribute no. 5. The α -method, as demonstrated by Hilber and Hughes (83), is more accurate in the lower modes than the Wilson- θ method but is more

strongly dissipative in the higher modes. This property makes the α -method superior over the Wilson- θ method when analyzing ordinary structures. However, the comprehensive study of Hilber and Hughes is based on matrix equation 2.22 without the damping term $[c]\{\dot{u}\}$. Therefore the Wilson- θ method was chosen to calculate the soil-structure system response to seismic forces in Chapter 6. It is also worth mentioning here that the numerical damping added to the system is of the order of 1% of the critical damping which is not significant when compared to the damping of the soil-structure system.

Wilson- θ Method

The Wilson- θ method is a modification of the Newmark linear acceleration method. This modification is based on the assumption that the acceleration varies linearly over an extended computation interval $\tau = \theta\Delta t$ as indicated in Figure 4.2. This integration method is unconditionally stable provided $\theta \geq 1.37$.

The procedure of step-by-step algorithm for linear structural system is summarized as follows:

1. Form an effective stiffness matrix $[\tilde{k}]$,

$$[\tilde{k}] = [k] + \frac{6}{\tau} [m] + \frac{3}{\tau} [c] \quad (4.30)$$

2. Initialize $\{u(0)\}$, $\{\dot{u}(0)\}$ and $\{\ddot{u}(0)\}$.

3. For each time step:

(i) Form an effective load vector $\{\Delta\tilde{P}\}$,

$$\begin{aligned} \{\Delta\tilde{P}\} &= \{P(t)\} + \theta\{P(t+\Delta t) - P(t)\} \\ &+ [m]\left(\frac{6}{\tau^2}\{u(t)\} + \frac{6}{\tau}\{\dot{u}(t)\} + 2\{\ddot{u}(t)\}\right) \\ &+ [c]\left(\frac{3}{\tau}\{u(t)\} + 2\{\dot{u}(t)\} + \frac{\tau}{2}\{\ddot{u}(t)\}\right) \end{aligned} \quad (4.31)$$

(ii) Solve for the effective displacement vector,

$\{u(t+\tau)\}$, using the relation

$$[\tilde{k}]\{u(t+\tau)\} = \{\Delta\tilde{P}\} \quad (4.32)$$

(iii) Calculate new acceleration, velocity and displacement vectors,

$$\begin{aligned} \{\ddot{u}(t+\Delta t)\} &= \left(1 - \frac{3}{\theta}\right)\{\ddot{u}(t)\} + \frac{6}{\theta\tau^2}(\{u(t+\tau)\} - \{u(t)\}) \\ &\quad - \frac{6}{\theta\tau}\{\dot{u}(t)\} \end{aligned}$$

$$\{\dot{u}(t+\Delta t)\} = \{\dot{u}(t)\} + \frac{\Delta t}{2}(\{\ddot{u}(t)\} + \{\ddot{u}(t+\Delta t)\})$$

$$\begin{aligned} \{u(t+\Delta t)\} &= \{u(t)\} + \Delta t\{\dot{u}(t)\} + \frac{\Delta t^2}{6}(\{\ddot{u}(t+\Delta t)\} \\ &\quad + 2\{\ddot{u}(t)\}) \end{aligned} \quad (4.33)$$

(iv) Calculate forces, moments and stresses of interest.

Step no. 3 is repeated for the next time step and so on until the whole time history of the response is obtained.

The above method can be used for nonlinear structural systems, but the algorithm will be quite different depending on the type of nonlinearity. Wilson (86) presented a general step-by-step solution technique for the evaluation of the dynamic response of structural systems with physical and geometrical nonlinearities.

4.7 CONCLUDING REMARKS

A brief review of some methods of determination of response of soil-structure systems to dynamic loads is presented in this chapter. The excitation may be simulated deterministically or stochastically.

For deterministic analysis, the choice of the solution method depends on the following factors: problem size, the nature of the excitation, frequency dependency or independency of foundation impedance coefficients, and nonlinear behavior of some parts of the soil-structure system.

The practical use of the stochastic approach to interaction problems is relatively limited because the technique is less understood by earthquake engineers. Application of the direct random approach to the response of rigid bodies to earthquake excitation is given in Chapter 6.

The random approach, using modal analysis, is more commonly used to study the effects of wind forces on a building. The application of the stochastic or probabilistic methods to the soil-structure interaction problem for the along-wind excitation is given in Chapter 7. The state-of-the-art of the stochastic approach has been surveyed recently by Christian (87).

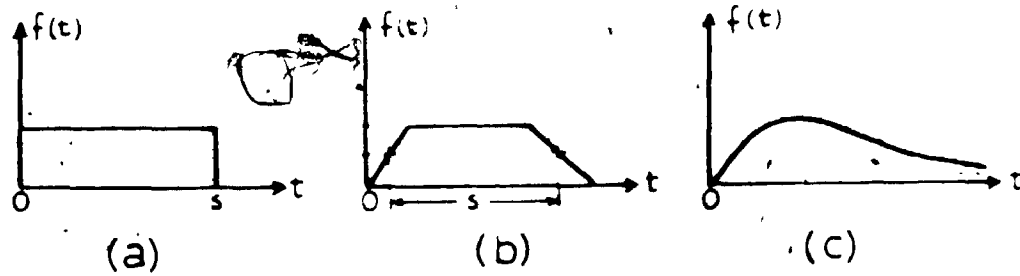


FIGURE 4.1 Intensity Envelope Functions: (a) Boxcar; (b) Trapezoidal, (c) Exponential

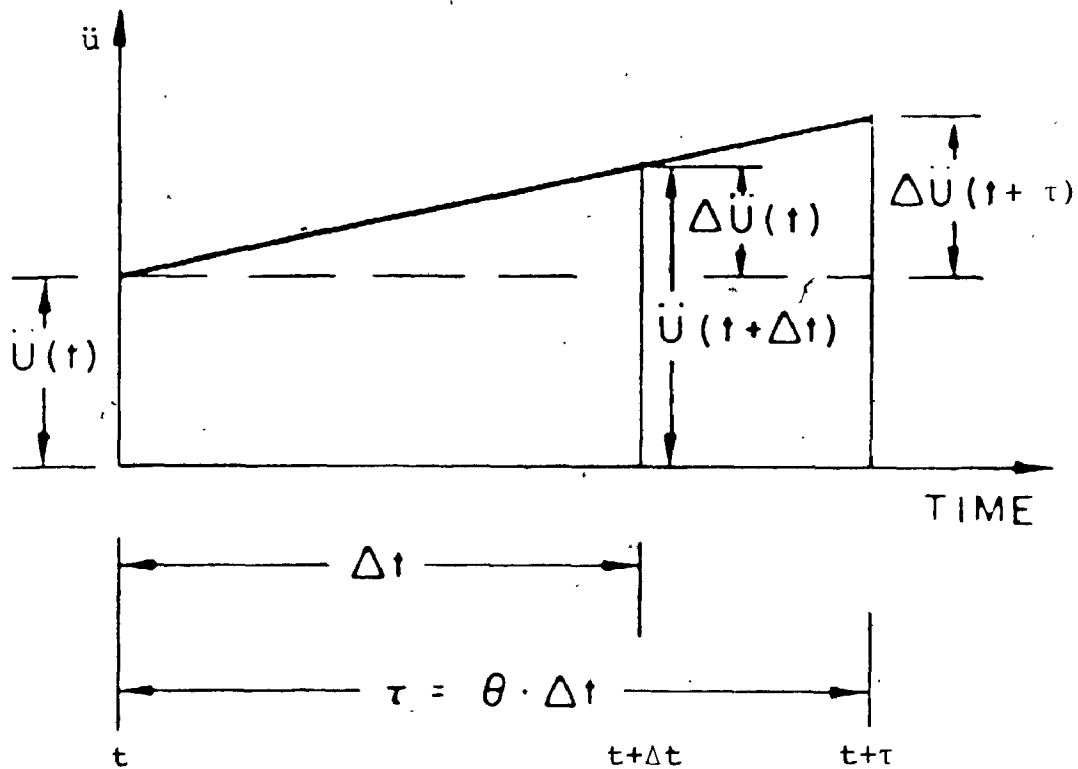


FIGURE 4.2 Linear Acceleration; Normal and Extended Time Steps for Wilson- θ Method

CHAPTER 5

STRUCTURAL RESPONSE TO SHOCK LOADING

5.1 INTRODUCTION

Many types of structures are subjected to transient dynamic forces that are quite short in duration and can be characterized as pulses or shocks. Typical examples of such loading involve forging hammers, collisions of aeroplanes with towers or a nuclear reactor building and impact of icebergs with offshore structures or oil drilling rigs (Figure 5.1). The forces generated in such structures are often very powerful and can result in many undesirable effects such as cracking or local crushing of the structure, large settlement of the foundations and unacceptable shaking of the vicinity. The objective of the structural design is to alleviate these hazards and secure optimum operation of the facility.

Hammers are most typical of the shock-producing machines and therefore this chapter is limited to them. This is not a serious limitation, however, because the analysis of the other structures subjected to shock loading would follow the same pattern and result in criteria that are in many respects similar to those applied to hammers.

The basic approaches to the analysis of foundations for shock producing machines were formulated by Rausch (90), Barkan (91) and a few others but apart from a few contributions, e.g. (29, 93), the area has been rather neglected in recent years. The methods of analysis of hammer foundations are well developed but suffer from inconsistent description of soil properties and particularly from the omission or arbitrary definition of damping.

This chapter presents two methods of analysis in which damping is accounted for in a rigorous way: in the first method, the analysis of the response of hammer foundations to the blows of the falling head (tup) is based on the assumption that the duration of the collision between the head and the anvil is much shorter than the natural periods of the foundation. Then the response can be treated as one resulting from the initial velocity of the anvil. This approach is acceptable in most situations but may not be quite justified in some cases of stiffly supported foundations such as pile foundations or rigidly supported anvils.

The second approach removes this limitation and is suitable for those cases in which the duration of the collision is not much shorter than the natural periods of the foundation; hence, the response is better dealt with

in terms of pulse loading.

With the aid of the computer, both approaches are suitable for any number of degrees of freedom; this is an advantage particularly for multi-mass systems and eccentric blows. The solutions are based on the notion of the complex eigenvalues outlined in Chapter 4. Both methods are presented in this chapter in full detail and examples as well as comparisons between the two approaches are given.

The theory is linear, separation (uplift) of the anvil from the anvil pad is not considered and all stiffness and damping constants are assumed to be independent of frequency; however, the damping matrix does not have to be proportional to stiffness or mass matrices.

5.2 HAMMER FOUNDATION SYSTEMS

There are many types of hammers. The description of the most common types can be found in (91, 94, 90, 95). The basic elements of a typical hammer-foundation system are the frame, head (tup), anvil and the foundation block embedded in soil (Figure 5.1c). When vibration transmission is of particular concern, springs and dampers are used to support the foundation block and/or the anvil and in some more recent designs, the foundation (inertial)

block is deleted. In these cases, a reinforced concrete trough is needed to protect the isolation elements from the environment.

The forging action of hammers is generated by the impact of the falling head against the anvil. To reduce the stress in the concrete and shock transmission into the frame, viscoelastic mounting of the anvil is usually provided. This may have the form of a pad of hard industrial felt, a layer of hardwood or, with very powerful hammers, a set of springs and dampers.

The foundation block or the protective trough are either cast on soil or supported by piles. The main foundation types are described in Chapter 2. The various types of hammer foundations can be modeled by lumped mass systems shown in Figure 5.2. The one mass model (a) can be used for a foundation with no elastic pad under the anvil; it is also adequate for a foundation with no inertial foundation block in which the anvil rests on springs and dashpots and the protective trough is rigidly supported. In the two mass model (b), the mass m_1 represents the elastically mounted anvil and m_2 the foundation block supported by soil or piles. With the directly sprung anvil, mass m_1 represents the anvil and m_2 the protective trough founded on soil or piles. Model (c) comprises the mass

of the anvil, m_1 , mass of the block, m_2 and mass of the trough, m_3 , all elastically supported.

If the blows are centric and the foundation arrangement is symmetrical, only vertical vibrations occur and the foundations have one, two or three degrees of freedom as indicated. With eccentric blows and/or asymmetrical arrangement of the system, horizontal translations and rotations of all masses occur and the number of degrees of freedom grows to three, six or nine for the three models shown in Figure 5.2.

5.3 STIFFNESS AND DAMPING CONSTANTS OF THE SYSTEM

The prediction of the response of the hammer foundation requires the description of the stiffness and damping of the foundation and the pad under the anvil.

Foundation

Stiffness and damping of foundations supported on soil or by piles are readily established as discussed in Chapter 2. Dynamic properties of soil needed in the approaches given in Chapter 2 can be established by experiments or estimated using published data, e.g. (21, 96).

Pads and Absorbers

When the foundation block or the anvil rests on a pad of viscoelastic material, the vertical stiffness constant of the pad is

$$k_p = E_p A_p / h \quad (5.1)$$

in which E_p = Young's modulus of the pad, A_p = area of the pad and h = its thickness. The damping constant can be calculated in terms of the complex Young's modulus and is,

$$c_p = 2\beta_p k_p / \omega \quad (5.2)$$

where β_p = the damping ratio of the pad material and ω = the frequency of the block or anvil vibration.

The stiffness in shear is analogously $G_p A_p / h$ where G_p = shear modulus of the pad. Rocking stiffness is

$$k_{p,\psi} = E_p I / h \quad (5.3)$$

in which I = second moment of pad area. Damping constants for shear and rocking are obtained as a fraction of stiffness, just as in equation 5.2.

It is obvious from equation 5.2 that frequency independent (hysteretic) material damping results in frequency dependent constants of equivalent viscous damping, c . If

material damping is assumed to be viscous, the constant β can be replaced by $\beta'\omega$, in which β' is the constant of viscous damping and the resultant damping constant becomes frequency independent and equal to $2\beta'_p k_p$.

5.4 EQUATIONS OF MOTION

A schematic of a typical hammer foundation is shown in Figure 5.3. The foundation comprises the block supporting the frame and the elastically mounted anvil. For the sake of generality, it is assumed that the anvil is mounted eccentrically and that the blows of the tup may act with eccentricity relative to the center of gravity of the anvil whose mass is m_1 . Choosing the center of gravity of the anvil and of the foundation block as reference points, the governing equation of motion can be written as

$$[m]\{\ddot{u}\} + [c]\{\dot{u}\} + [k]\{u\} = \{P(t)\} \quad (5.4)$$

in which, in the case of one vertical plane of symmetry as indicated in Figure 5.3, the displacement vector is

$$\{u\} = [u_1 \ v_1 \ \psi_1 \ u_2 \ v_2 \ \psi_2 \ \dots]^T \quad (5.5)$$

where $u = u(t)$ = horizontal translation, $v = v(t)$ = vertical translation, $\psi = \psi(t)$ = rotation in the vertical plane (rocking) and the subscript 1 pertains to the anvil and 2

to the foundation block. If there is a protective trough under the block, three additional displacements are needed to describe the motion of the trough and the total number of degrees of freedom, n , becomes 9. In the absence of the trough, the system has six degrees of freedom. The mass matrix $[m]$ is diagonal with the diagonal elements being

$$m_1 \quad m_1 \quad I_1 \quad m_2 \quad m_2 \quad I_2$$

where m_1 = mass of the anvil, m_2 = mass of the foundation block and I_1, I_2 = mass moments of inertia of the anvil and foundation, respectively. (The frame is usually included in m_2 and I_2 .)

The stiffness matrix $[k]$ can be assembled as follows:

$$[k] = \begin{bmatrix} k_{ul} & 0 & -k_{ul}y_1 & -k_{ul} & 0 & -k_{ul}y_2 \\ & k_{v1} & 0 & 0 & -k_{v1} & -k_{v1}r_2 \\ & & k_{\psi 1} + k_{ul}y_1^2 & k_{ul}y_1 & 0 & -k_{\psi 1} + k_{ul}y_1y_2 \\ & & & k_{ul} + k_{u2} & 0 & k_{u\psi} + k_{ul}y_2 \\ \text{symmetrical} & & & & k_{v1} + k_{v2} & k_{v1}r_2 + k_{v2}r_2 \\ & & & & & k_{\psi 2} + k_{\psi 1} + k_{v1}r_2^2 + k_{v2}r_1^2 + k_{ul}y_2^2 \end{bmatrix}$$

(5.6)

In these expressions (see Figure 5.4)

$$y_1 = d - e_2 - h$$

$$r_1 = a/2 - c$$

$$y_2 = e_2 - f$$

$$r_2 = b - c$$

and the constants k_{v1} , k_{u1} and $k_{\psi1}$ are the stiffness constants of the anvil. They follow from equations 5.1 to 5.3 as

$$k_{v1} = E_p A_p / h, \quad k_{u1} = G_p A_p / h, \quad k_{\psi1} = E_p I / h$$

Constants k_{u2} , k_{v2} , $k_{\psi2}$ and k_u describe the stiffness of the foundation block. For embedded foundations and pile supported foundations, these constants are evaluated using the approaches referred to in Chapter 2.

The damping matrix has the same form as the stiffness matrix and its elements c_{ij} are calculated in the same way as k_{ij} except that the constants k_u , k_v and k_{ψ} are replaced by c_u , c_v and c_{ψ} . For the anvil, these damping constants follow as a fraction of stiffness from equation 5.2. The frequency to use is the dominant frequency for the anvil. The force vector $\{P(t)\}$ describes the impulse, if the response is to be analyzed for a given time history of the load. For a pulse acting with eccentricity e relative to mass m_1 , the force vector is

$$\{P(t)\} = [0 \quad P(t) \quad eP(t) \quad 0 \quad 0 \quad \dots]^T$$

If the response is treated as free vibration triggered by initial velocity $\{P(t)\} = \{0\}$. Both approaches are considered. Using the complex eigenvectors introduced in

Chapter 4, the complete solution to equation 5.4 can be sought in the form

$$\{z(t)\} = [Z]\{q(t)\} \quad (5.7a)$$

where

$$\{z(t)\} = \begin{Bmatrix} \dot{u}(t) \\ u(t) \end{Bmatrix} \quad (5.7b)$$

Here, $[Z]$ is the matrix containing $2n$ complex eigenvectors; $\{z(t)\}$ is the vector containing displacements $\{u(t)\}$ and velocities $\{\dot{u}(t)\}$; and $\{q(t)\}$ are generalized coordinates given by equation 4.12 as

$$q_j(t) = q_j(0) \exp(\mu_j t) + \frac{1}{A_j} \int_0^t \exp[\mu_j(t-\tau)] f_j(\tau) d\tau$$

$$j = 1, 2, \dots, 2n \quad (5.7c)$$

in which μ_j are the complex eigenvalues and $f_j(\tau)$ is (according to equation 4.10)

$$f_j(t) = [Z]^T \{F(t)\} \quad (5.7d)$$

where

$$\{F(t)\} = \begin{Bmatrix} \{0\} \\ \{P(t)\} \end{Bmatrix} \quad (5.7e)$$

Other terms of equation 5.7c are defined in Chapter 4.

The first term of equation 5.7c can be used to describe the response of the hammer foundation to initial velocities caused by the impact of the head; the second

term can be used to evaluate the response to the pulse given by its time history.

5.5 INITIAL VELOCITY APPROACH

The duration of the pulse of hammers is quite short, in the order of 0.01 to 0.02 s. For the most severe impact, which occurs with the blank absent, the pulse duration may be even shorter, about 0.001 or 0.002 s. Thus, it appears possible to predict the response using the assumption of an infinitely short pulse which is tantamount to the assumption that the response is caused by an initial velocity imparted by the impact. For pulses of longer duration, this assumption is conservative because the response decreases with increasing duration of the pulse.

For the application of the initial conditions only the initial velocities of the anvil are nonzero giving

$$\{\dot{u}(0)\} = \langle 0 \quad \dot{v}_1 \quad \dot{\psi}_1 \quad 0 \quad 0 \quad \dots \rangle^T$$

and $\{u(0)\} = \{0\}$. These initial conditions determine the initial values of $\{z(t)\}$ by equation 5.7b and then, the initial values of $q_j(0)$ follow from equation 5.7a. The initial velocity \dot{v}_1 follows from the basic formula for collision as

$$\dot{v}_1 = (1 + k_r) \frac{m_o}{m_o + m_1 + e^2/i_1^2} c_o \quad (5.8)$$

The initial angular velocity follows from the well known expression

$$\dot{\psi}_1 = (1 + k_r) \frac{e}{i_1^2 (1 + m_1/m_o) + e^2} c_o \quad (5.9)$$

where m_o , c_o are the mass and impact velocity of the hammer head respectively and k_r is the coefficient of restitution, usually taken as 0.5 or so; e is the blow eccentricity relative to mass m_1 , and $i_1^2 = I_1/m_1$ is the square of the radius of gyration. The mass m_1 is the mass of the anvil in multi-mass systems or the total mass in one mass systems.

With q_j established from equation 5.7c $\{z(t)\}$ follows from equation 5.7a and this determines the displacements $\{u\}$ by equation 5.7b.

5.6 RESPONSE TO PULSE LOADING

When considering the pulse given by its time history, the second part of equation 5.7c describes the response during the duration of the pulse; the first part, i.e., the homogeneous solution, describes the response for time exceeding the duration of the pulse. The integral in equation 5.7c has to be evaluated for a specific time

history $P(t)$ and hence $f_j(t)$ given by equation 5.7d.

For simple shapes of the pulse, such as those shown in Figure 5.5, the integral can be evaluated in closed form. (For one mass systems analytical and numerical solutions of the response are available in the literature, e.g. 93, 97 and 98). For more complicated pulses and multidegree of freedom systems, numerical integration of the integral in equation 5.7c can provide the solution. However, the exact time history of the pulse is rarely known and in hot forging may change from blow to blow. Thus it may be adequate to concentrate on the principal characteristics of the pulse which are its total power and the duration of the dominant (strong) part, T_p . Then the true pulse may be replaced by a suitable simpler time history $P'(t)$ (Figure 5.6), amenable to closed form integration, such that

$$\int_0^{T_p} P(t) dt = \int_0^{t_p} P'(t) dt \quad (5.10)$$

in which t_p is the duration of the replacement pulse.

One simple time history which seems to be suitable is a half-sine wave shown in Figure 5.5b. Dropping the prime, this time history is

$$P(t) = P_0 \sin \omega_p t \quad (5.11)$$

where frequency $\omega_p = \pi/t_p$ and P_0 is force amplitude. For this sine pulse, equation 5.7e yields the loading vector

$$\{F(t)\} = \begin{Bmatrix} \{0\} \\ \{P(t)\} \end{Bmatrix} \quad (5.12)$$

in which, limiting the symbolics for $\{0\}$ and $\{P(t)\}$ to six degrees of freedom each, as it would correspond to the foundation shown in Figure 5.3,

$$\{P(t)\} = [0 \ P_0 \sin\omega t \ eP_0 \sin\omega t \ 0 \ 0 \ 0]^T \quad (5.13)$$

Substituting into equation 5.7d,

$$f_j(t) = P_0 (Z_{j,8} + Z_{j,9}e) \sin\omega_p t \quad (5.14)$$

in which $Z_{j,8}$ and $Z_{j,9}$ are the eighth and ninth modal coordinates of mode j . Then, the second term of equation 5.7c is

$$q_j(t) = \frac{1}{A_j} P_0 (Z_{j,8} + eZ_{j,9}) \exp(\mu_j t) \int_0^t \exp(-\mu_j \tau) \sin\omega_p (t-\tau) d\tau \quad (5.15)$$

Performing the integration, the (generalized) coordinates $q_j(t)$ determining the motion for $t \leq t_p$ through the vector $\{q(t)\}$ in equation 5.7a become

$$q_j(t) = \frac{1}{A_j} P_0 (Z_{j,8} + eZ_{j,9}) \frac{-\mu_j \sin\omega_p t + \omega_p [\exp(\mu_j t) - \cos\omega_p t]}{\mu_j^2 + \omega_p^2} \quad (5.16)$$

for $j = 1, 2, \dots, 2n$, with $2n = 12$ for the foundation considered.

For $t > t_p$, the coordinates $q_j(t)$ are described by the first term in equation 5.7c in which the constant $q_j(0)$ is given by the initial condition

$$q_j(0) \exp(\mu_j t_p) = q_j(t_p)$$

Thus,

$$q_j(0) = q_j(t_p) \exp(-\mu_j t_p)$$

and the coordinates $q_j(t)$ are

$$q_j(t) = q_j(t_p) \exp \mu_j (t - t_p) \quad \text{for } t > t_p \quad (5.17)$$

and $j = 1, 2, \dots, 2n$.

With $q_j(t)$ established respectively from equations 5.16 and 5.17, the vector $\{z(t)\}$ follows from equation 5.7a and the vector of true displacements $\{u\}$ from equation 5.7b. The i th displacement component u_i of the vector $\{u\}$ is equal to the $(6+i)$ th element of the vector $\{z\}$, i.e.

$$u_i(t) = z_{6+i}(t) \quad (5.18)$$

For other types of pulses the calculations of hammer response follows the same pattern and differs only in the form of equation 5.16 for $q_j(t)$. The coordinates $q_j(t)$

can be written in a general form as

$$q_j(t) = \frac{P_0}{A_j} (z_{j,8} + e^{z_{j,9}}) \bar{q}_j(t) \quad (5.19)$$

For the four types of pulses shown in Figure 5.5 the functions $\bar{q}_j(t)$ are given in Table 5.1.

The principal advantages of the complex eigenvalue approach are that the effect of damping is incorporated in a rigorous way, the equations for generalized coordinates uncouple for any type of damping and the integrals involved are somewhat simpler than the Duhamel integral used in standard modal analysis. The analysis was efficiently programmed and included in a general code for analysis of machine foundations (97).

5.7 EXAMPLES

The above theory can be used to analyze any foundation for the effect of a given pulse $P(t)$ or initial velocity $\dot{v}_1(0)$.

In the examples shown here, the character of the response and the effect of pulse duration will be demonstrated.

First, the complex eigenvalue method was used to analyze the response of symmetrical two mass hammer foundations with two degrees of freedom. The foundation analyzed

is described in detail in Ref. (92) and differs from the one shown in Figure 5.3 only by symmetrical arrangement and absence of any eccentricity ($e=e_1=0$). In order to facilitate a comparison with the initial velocity approach and to indicate the effect of pulse duration the pulse is taken as equal to the momentum of the anvil after the collision, i.e.,

$$\int_0^{t_p} P(t) dt = m_1 \hat{c} \quad (5.20)$$

in which $\hat{c} = \dot{v}_1(0)$ is the initial velocity of the anvil calculated by means of Newton's formula for collision (equation 5.8 with $e=0$). The last column of Table 5.1 gives the values of the force amplitudes P_0 that satisfy equation 5.20 for the four basic types of pulses.

The response histories shown in Figures 5.7 and 5.8 were calculated for sine pulses (Figure 5.5b) having different durations, t_p , but the same power $\int_0^{t_p} P(t) dt = \text{const.}$ The duration of the pulse is expressed as t_p/T_1 where T_1 is the fundamental natural period of the system, $T_1 = 2\pi/\omega_1$. The curves with $t_p/T_1 = 0$ represent the initial velocity approach results. For the response shown in Figure 5.7, full value of damping was considered as it was obtained from the elastic halfspace theory for soil and a viscoelastic anvil pad of hard felt 6 in (0.15 m) thick. The response shown in Figure 5.8 was calculated with the

soil damping reduced to one fourth as it may be appropriate for a shallow soil layer and the anvil pad thickness reduced to 1.5 in (0.04 m). The peak displacements of both the anvil and foundation are shown vs the ratio t_p/T_1 for the two cases in Figures 5.9 and 5.10. They are normalized by the peak displacements for $t_p = 0.0$. It can be seen that the peak response decreases as the pulse duration increases and the decrease of the anvil response is much more than that of the foundation block for ratios of t_p/T_1 higher than about .05. Thus the initial velocity approach (infinitely short pulse) overestimates the real response and its assumption is, therefore, conservative. It can also be seen from Figures 5.7 to 5.10 that damping due to both the anvil pad and soil has a profound effect on the time histories of the vibration, modal damping ratios and the peak values of the response.

In another example, the complex eigenvalue method was used to analyze the response of the hammer foundation with eccentrically mounted anvil shown in Figure 5.3 but with $e = 0.0$. The basic dimensions of the foundation are shown in the figure. The foundation differs from that used in the preceding example only by the eccentric position of the anvil and consequently, by the eccentricity of the hammer blow relative to the foundation block. The system has six degrees of freedom as indicated in Figure 5.4.

Full value of soil and anvil pad damping was assumed. The damped response calculated for sine pulse of varying duration and constant power is shown in Figure 5.11. (The response curves for $t_p/T_1 = 0.0$ are again those of the initial velocity approach.) The vertical response shown in Figure 5.11 can be compared with the damped vertical response shown in Figure 5.7. While the level of the vertical displacements is changed only slightly by the eccentricity of the blows (notice the difference in scales), horizontal response and rocking are obtained for both the anvil and the block of the asymmetrical foundation. The rocking, although not very large, translates into vertical and horizontal displacements comparable with the others and for the anvil does not decay very fast.

The variation in the peak response with pulse duration can be seen from Figure 5.11 or in more detail from Figure 5.12. Figures 5.11 and 5.12 show that the response decreases with the increase in pulse duration but the decrease need not be monotonic. For ratio $t_p/T_1 = 0.5$, the peak vertical and rocking response values of the anvil are about 50 percent of those calculated assuming infinitely short pulse; for the foundation, the peak vertical response is decreased by 20 to 30 percent but the reduction of the peak horizontal displacement is much less. Figure 5.13 shows the undamped and damped vibration modes of the

foundation from Figure 5.3. The foundation block movement dominates the first three modes which explains the high values of modal damping in these modes.

Figure 5.13b shows absolute values of the complex damped modal displacements but does not indicate the phase shift between the anvil and the foundation block. The inphase and antiphase motions of the two masses of the system can be seen most clearly in the undamped modes (Figure 5.13a).

In the last example shown in Figure 5.14, the response of a symmetrical two mass hammer foundation ($e=e_1=0$) is plotted for loading by a rectangular pulse and by a sine pulse with both pulses satisfying equation 5.20. The peak values of the response differ only slightly but the anvil response to rectangular pulse indicates a more significant contribution from the second vibration mode. This is to be expected because a Fourier description of the rectangular pulse would contain higher harmonic components which are absent from the sine pulse.

5.8 CONCLUSIONS

Two approaches are presented that make it possible to predict the damped response of hammer foundations to the blows of the head either as caused by initial velocity,

imparted to the anvil or as a pulse. These approaches are based on complex eigenvalues and damped vibration modes and incorporate damping in a rigorous way. With the aid of a computer, the approach can be applied to complicated hammer foundations and particularly to those in which asymmetry of the arrangement and/or eccentricity of the blows call for the consideration of more degrees of freedom. A few examples were analyzed for initial velocity of the anvil, sine pulse loading of constant power but different duration and for a rectangular pulse. This analysis suggests the following conclusions:

- The complex eigenvalue method is an efficient and accurate method for the analysis of hammer foundation response to either initial velocity or pulse loading.
- The initial velocity approach overestimates the response to pulse loading and is, therefore, conservative.
- Depending on the duration of the pulse the simpler initial velocity approach may overestimate the true response by up to about 100 percent for the anvil and less than that for the foundation.
- With asymmetric hammers, significant horizontal vibration as well as rocking may be generated.
- The reduction of the peak response with the increase of pulse duration is more in the vertical and rocking vibration than in the horizontal vibration.


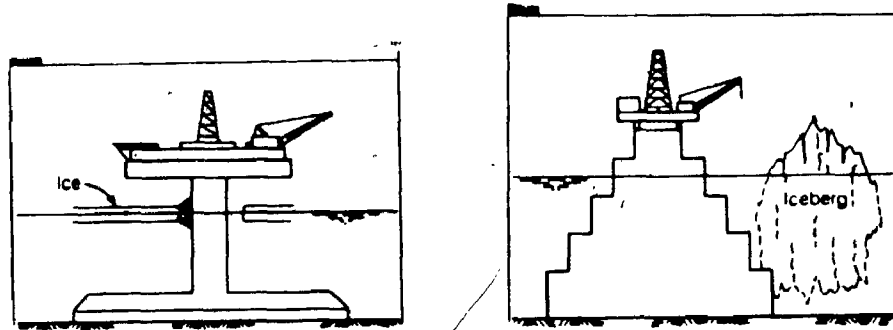
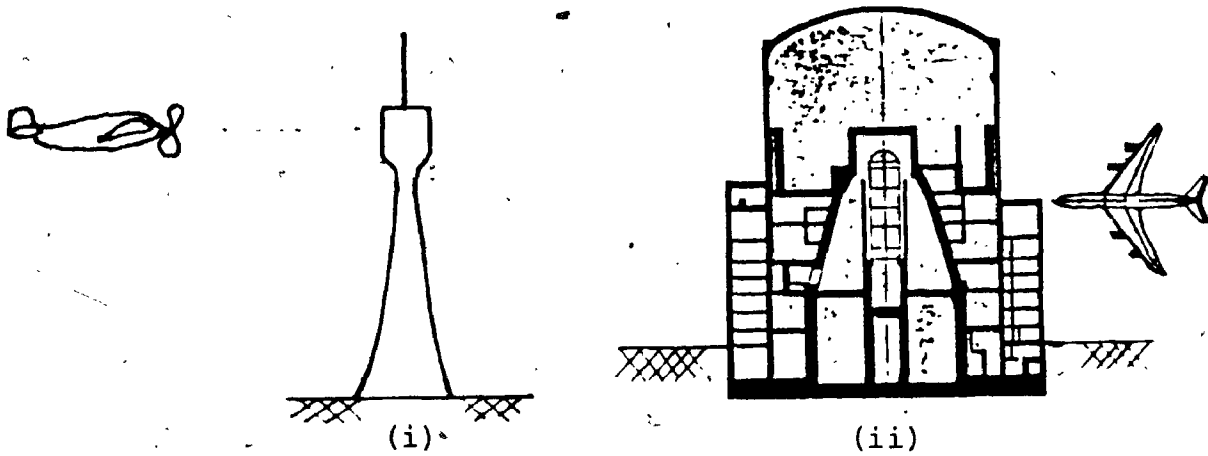
- The exact shape of pulse loading affects the time history of the response, particularly for the anvil, but has little effect on the peak value of the response.
 - The complex eigenvalue approach is a very suitable method for the solution of collision problems in which large damping due to soil-structure interaction is anticipated.
- 

TABLE 5.1 Functions $\bar{q}_j(t)$ for Main Types of Pulses

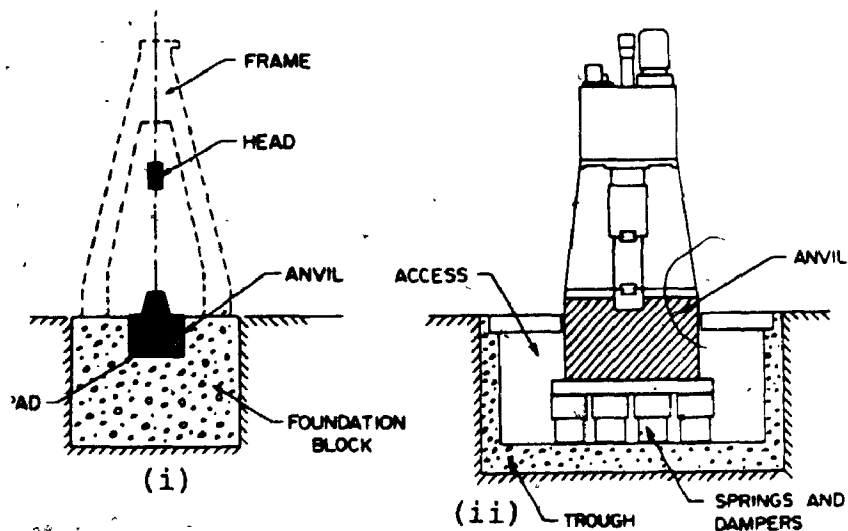
Type of Pulse	P(t)	$\bar{q}_j(t)$	P ₀
Rectangle (Figure 5.5a)	P ₀	$\frac{\mu_j t}{\mu_j - 1}$	$m_1 \hat{c}/t_p$
Sine (Figure 5.5b)	$P_0 \sin \omega_p t, [\omega_p = \frac{\pi}{t_p}]$	$\frac{-\mu_j' \sin \omega_p t + \omega_p (e^{\mu_j t} - \cos \omega_p t)}{\mu_j^2 + \omega_p^2}$	$\frac{\pi}{2} m_1 \hat{c}/t_p$
Versed sine (Figure 5.5c)	$\frac{P_0}{2} (1 - \cos 2\omega_p t), [\omega_p = \frac{\pi}{t_p}]$	$\frac{\mu_j^2 (\cos 2\omega_p t - 1) + 4\omega_p^2 (e^{\mu_j t} - 1) - 2\omega_p \mu_j \sin 2\omega_p t}{2\mu_j (\mu_j^2 + 4\omega_p^2)}$	$2 m_1 \hat{c}/t_p$
Damped sine (Figure 5.5d)	$P_0 e^{-\alpha t} \sin \omega_p t, [\omega_p = \frac{n\pi}{t_p}]$ $\alpha = \beta \omega_p, n = \text{number of waveforms}$ $\beta = \text{damping ratio}$	$\frac{-(\mu_j + \alpha) e^{-\alpha t} \sin \omega_p t + \omega_p (e^{\mu_j t} - e^{-\alpha t} \cos \omega_p t)}{(\mu_j + \alpha)^2 + \omega_p^2}$	$\frac{\omega_p + \alpha^2}{\omega_p (1 + e^{-\alpha t_p})} m_1 \hat{c}$



(a) Impact of Ice or Iceberg With Offshore Structures



(b) Collision of Airplane With (i) Tower, (ii) Nuclear Reactor Building



(c) Schematic of Forging Hammer and Its Foundation (i) Most Common Arrangement; (ii) Directly Sprung Hammer

FIGURE 5.1 Examples of Structures Exposed to Pulse Loading

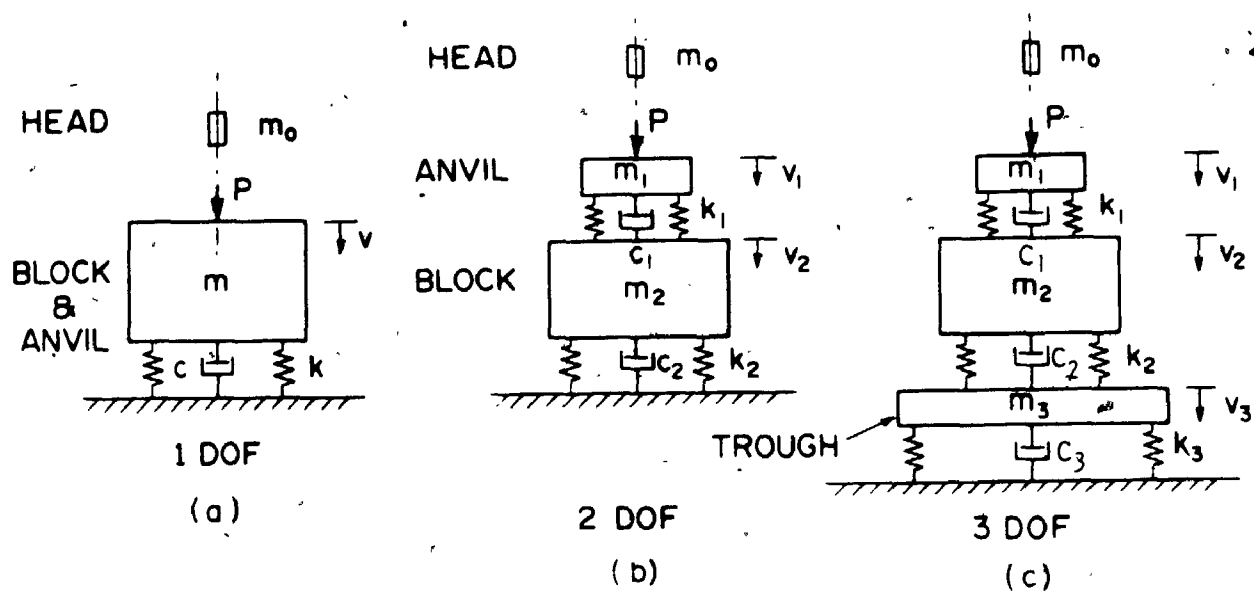


FIGURE 5.2 Basic Mathematical Models for Hammer Foundations

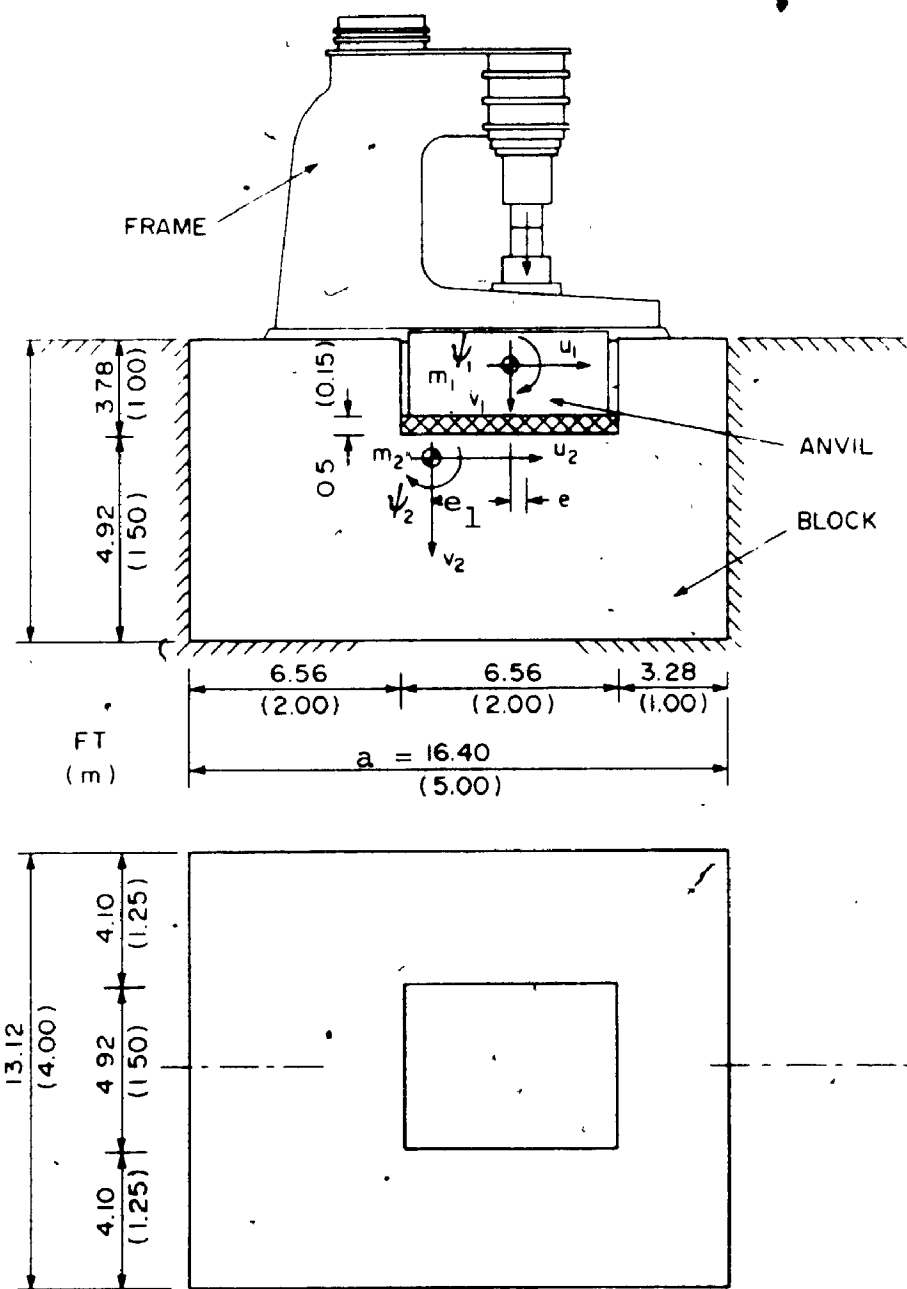


FIGURE 5.3 Schematic of Hammer Foundation

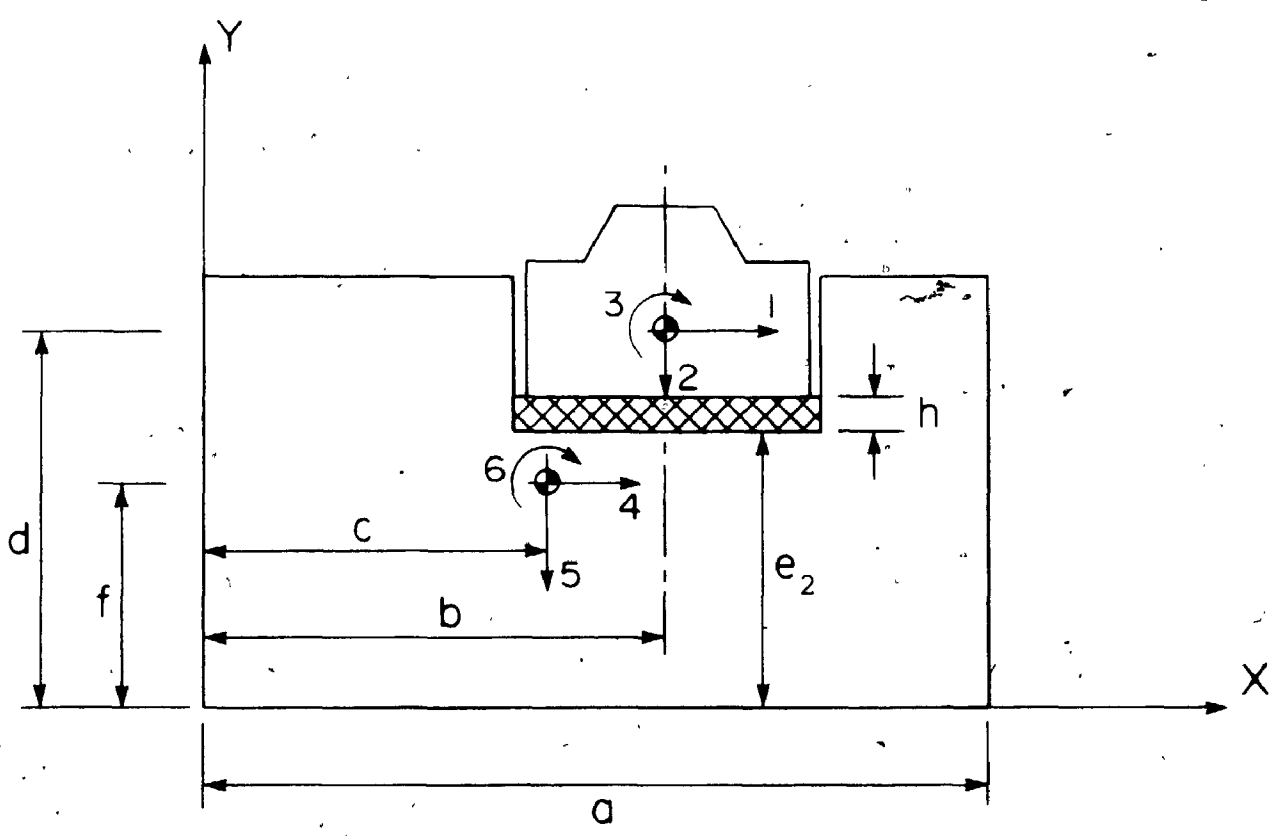
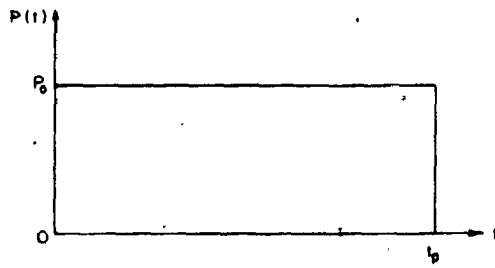
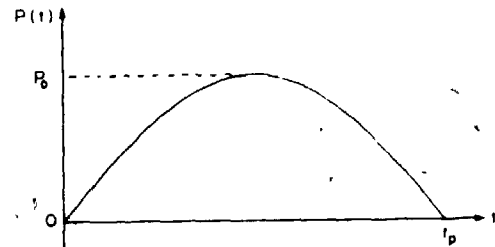


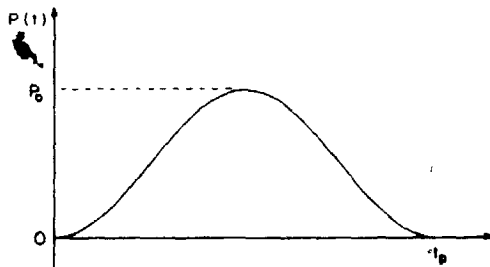
FIGURE 5.4 Notations for Asymmetrical Hammer Foundation With Six Degrees of Freedom



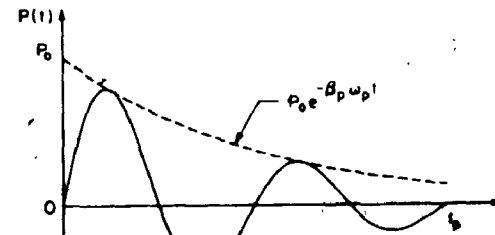
(a) RECTANGULAR PULSE



(b) HALF-SINE PULSE



(c) VERSED SINE



(d) DAMPED SINE

FIGURE 5.5 Basic Types of Pulses

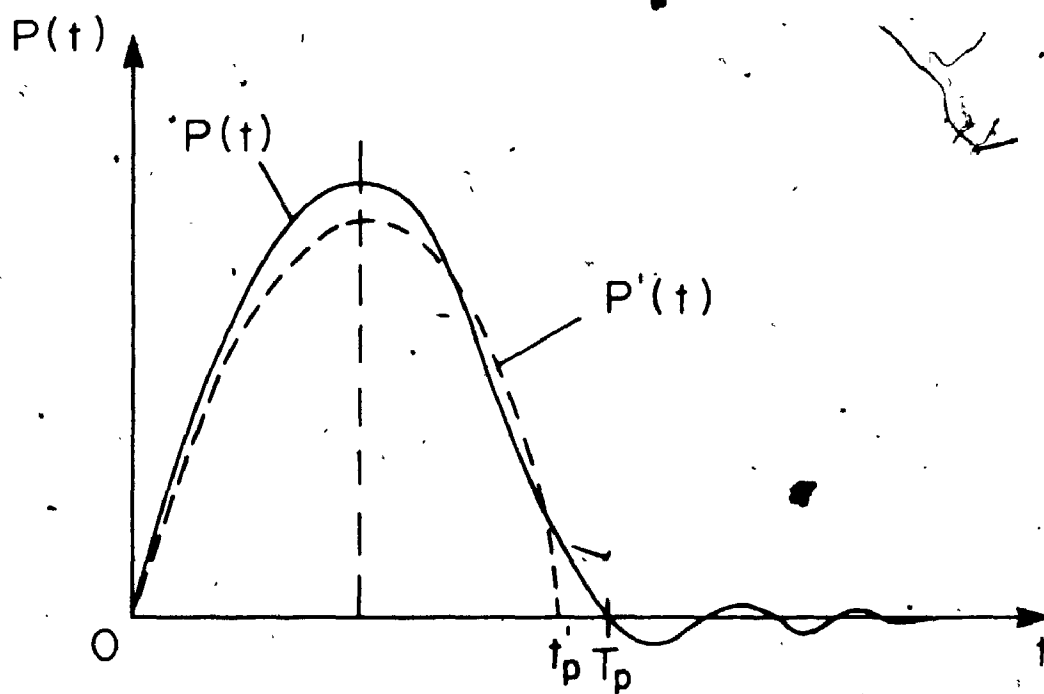


FIGURE 5.6 Replacement of Pulse History By Simple Shape

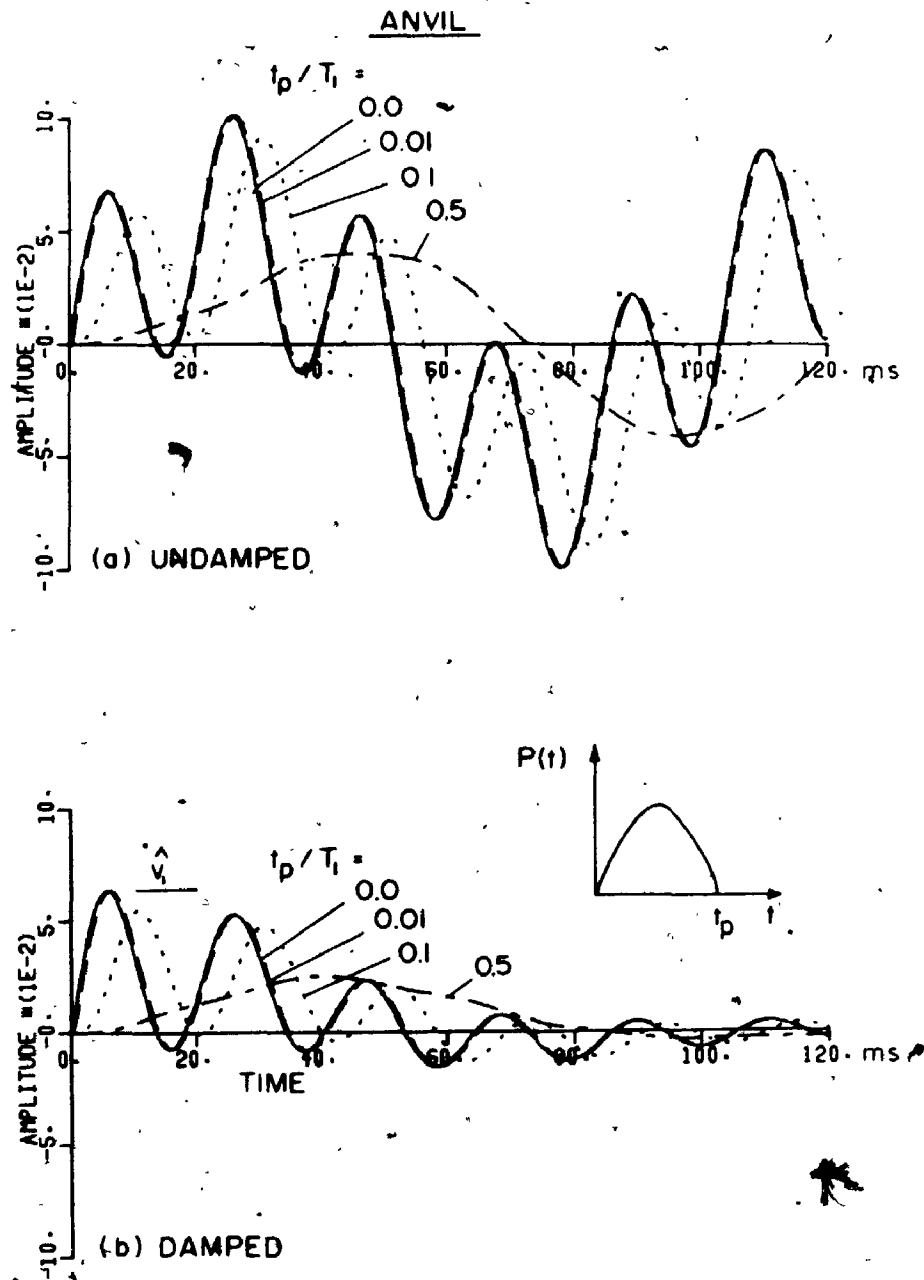


FIGURE 5.7a Undamped and Damped Response of Two Mass Hammer Foundation to Sine Pulse of Varying Duration and Constant Power; Embedded Footing, Anvil Pad 6 in (0.15 m) Thick ($D_1=51\%$, $D_2=7.4\%$, Displacements in in., 1 in = 2.54 cm, Time in Milliseconds):
 (a) Anvil

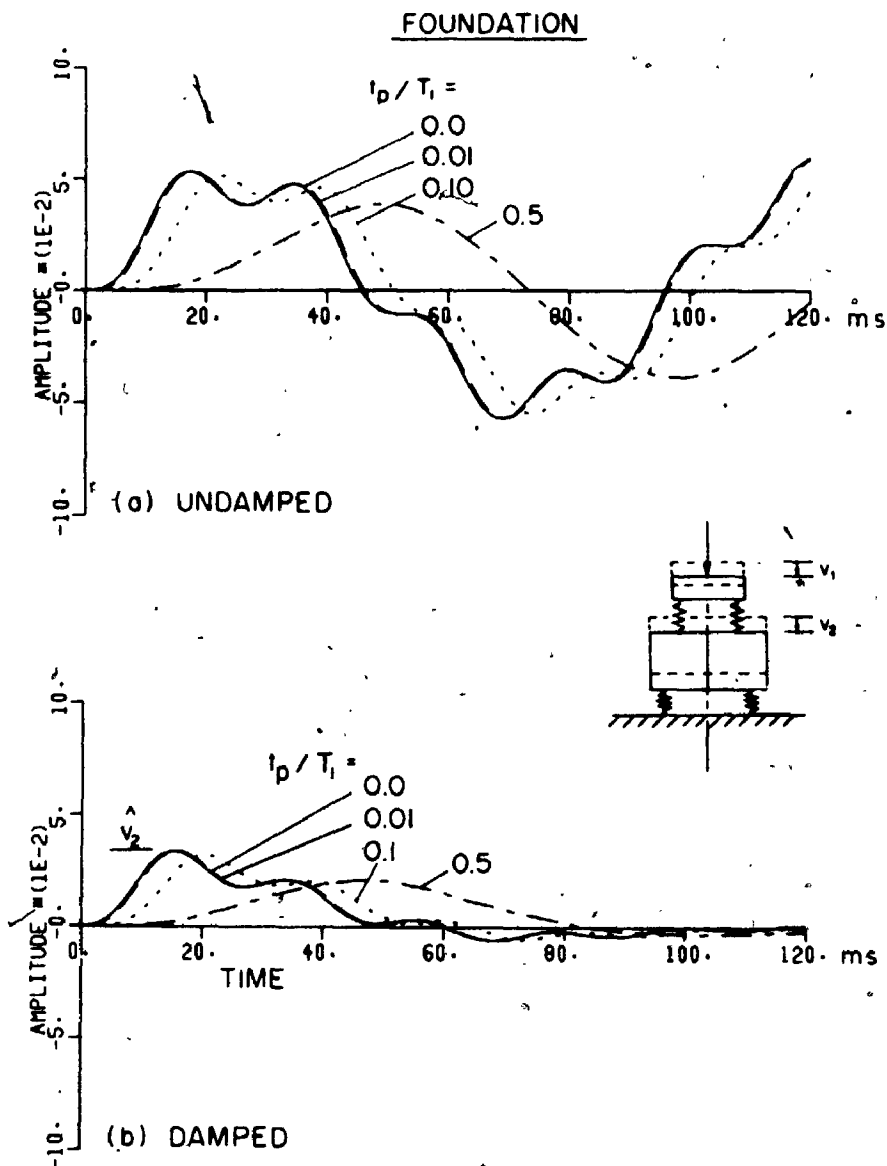


FIGURE 5.7b Undamped and Damped Response of Two Mass Hammer Foundation to Sine Pulse of Varying Duration and Constant Power; Embedded Footing, Anvil Pad 6 in (0.15 m) Thick ($D_1=51\%$, $D_2=7.4\%$, Displacements in in., 1 in = 2.54 cm, Time in Milliseconds): (b) Foundation Block

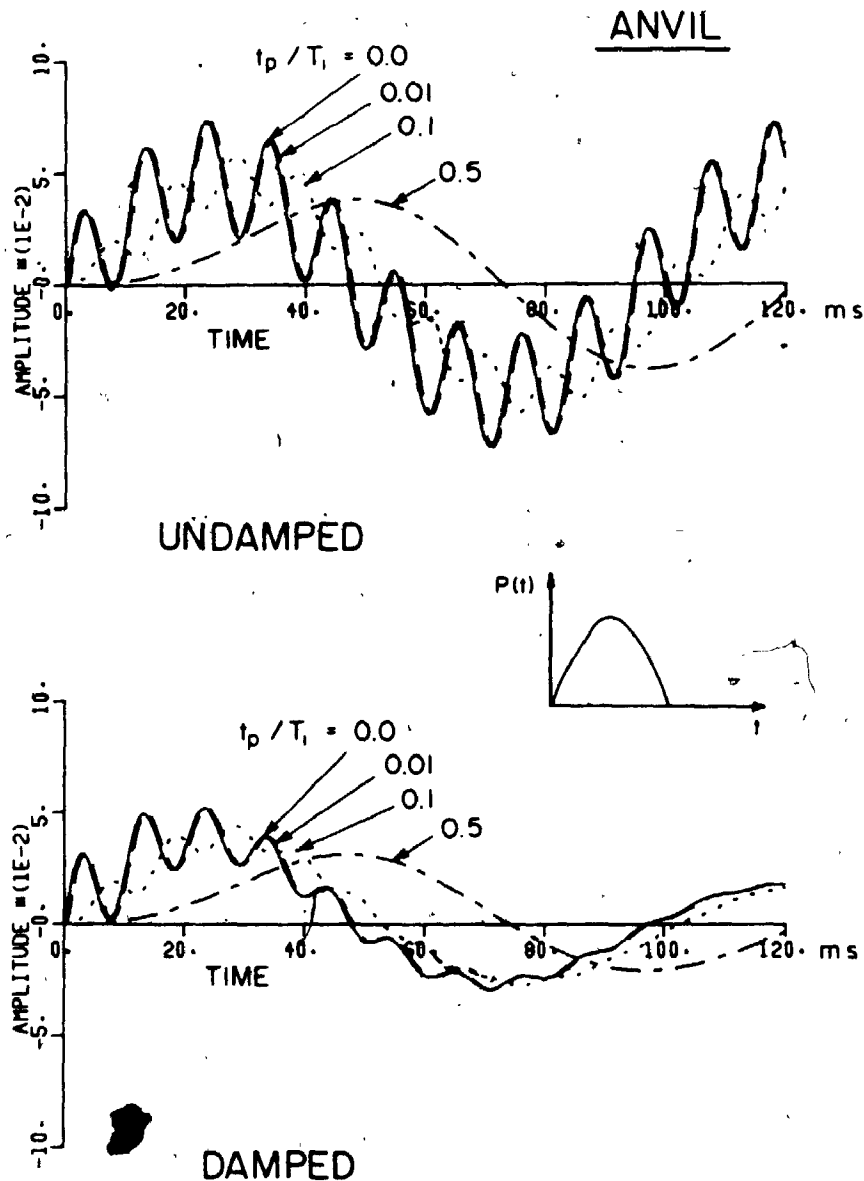


FIGURE 5.8a Undamped and Damped Response of Two Mass Hammer Foundation to Sine Pulse of Varying Duration and Constant Power; Embedded Footing, Anvil Pad 1.5 in (0.04 m) Thick, Damping of Soil Reduced to 1/4 ($D_1=12.9\%$, $D_2=5.3\%$, Displacements in in., 1 in = 2.54 cm): (a) Anvil

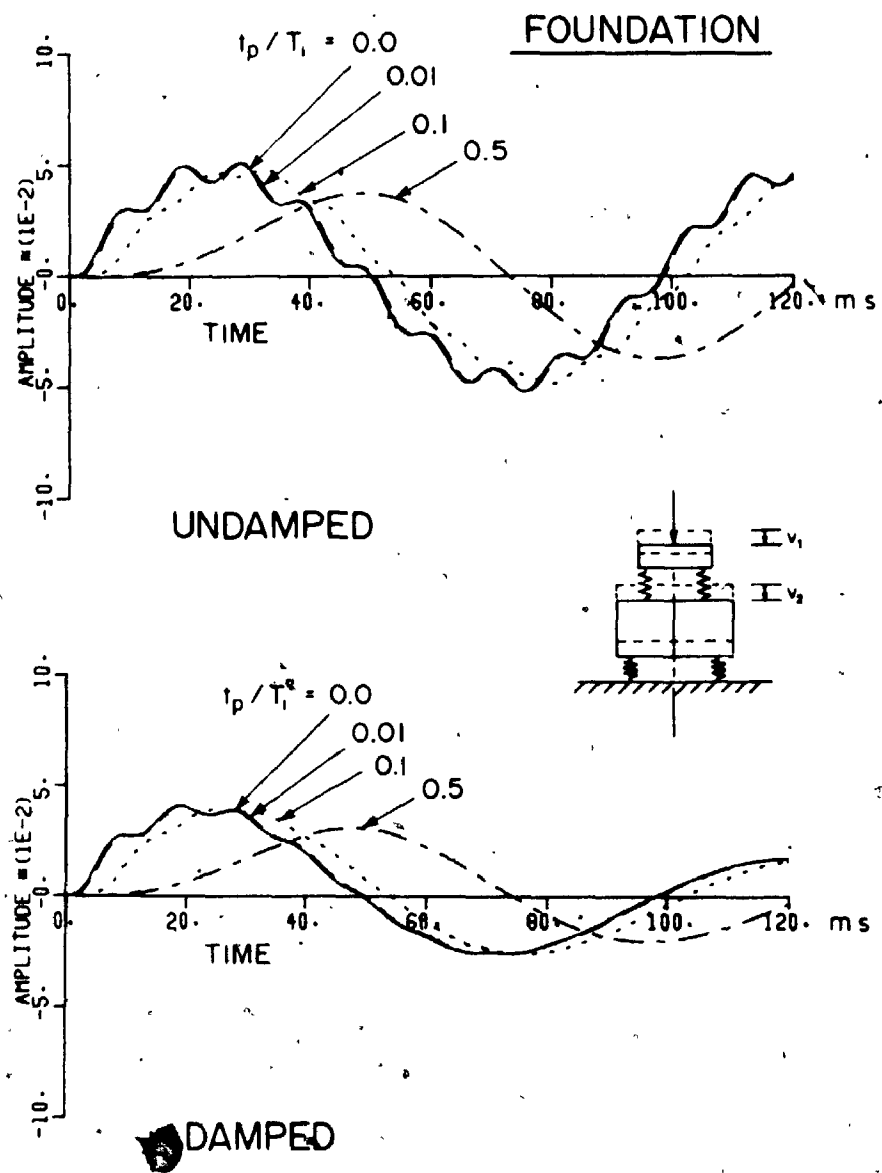


FIGURE 5. 8b Undamped and Damped Response of Two Mass Hammer Foundation to Sine Pulse of Varying Duration and Constant Power; Embedded Footing, Anvil Pad 1.5 in (0.04 m) Thick, Damping of soil Reduced to 1/4 ($D_1=12.9\%$; $D_2=5.3\%$, Displacements in in., 1 in = 2.54 cm):
 (b) Foundation Block

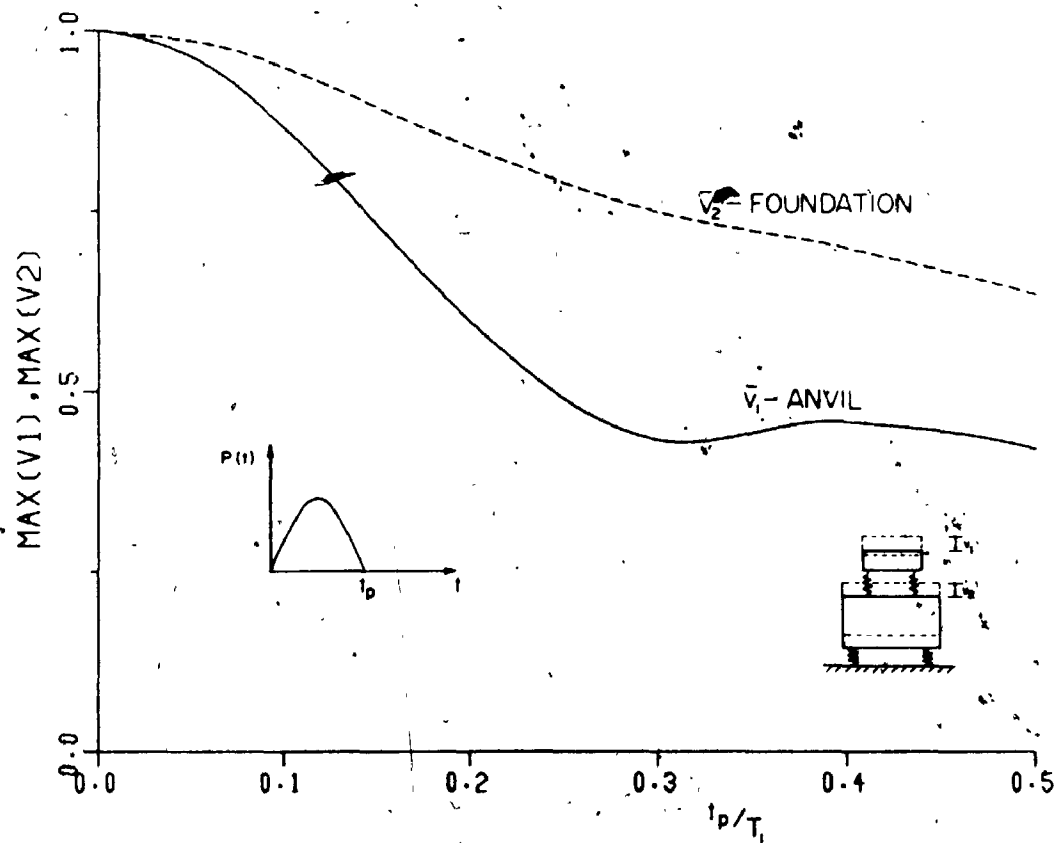


FIGURE 5.9 Peak Values of Damped Vertical Response of Two Mass Hammer Foundation to Sine Pulse of Varying Duration and Constant Power for Full Value of Damping as in Figure 5.7

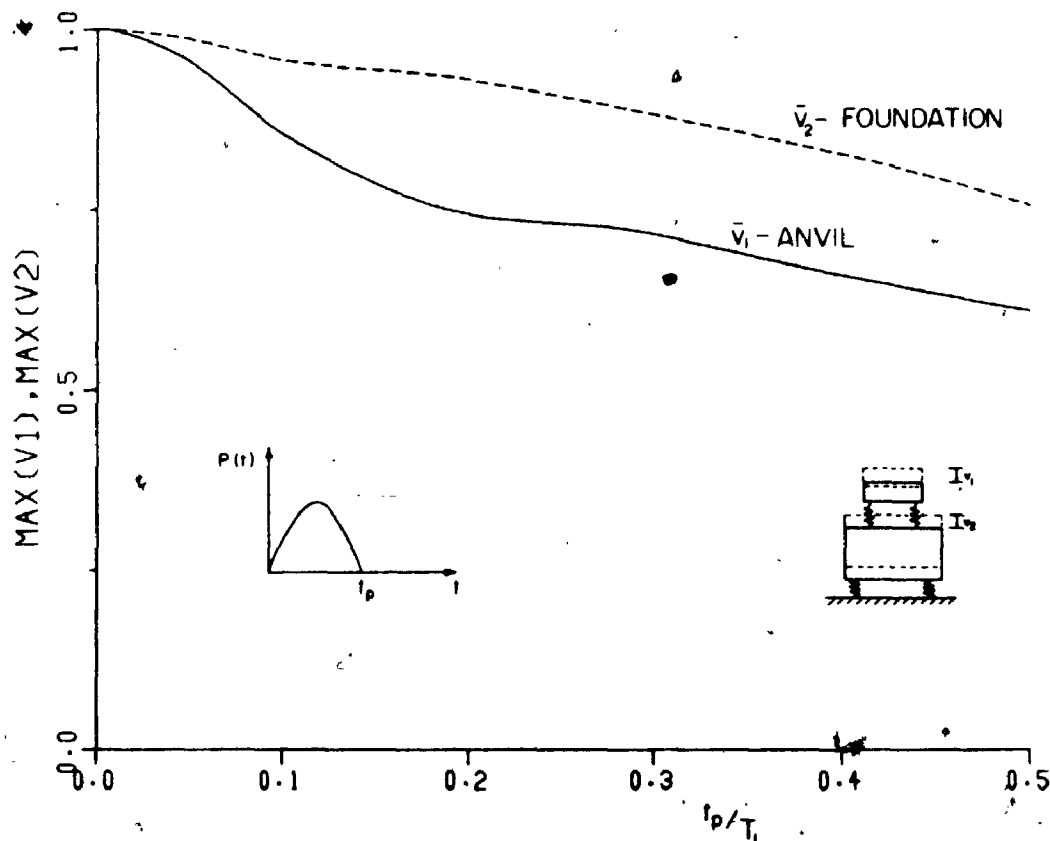


FIGURE 5.10 Peak Values of Damped Vertical Response of Two Mass Hammer Foundation to Sine Pulse of Varying Duration and Constant Power for Damping Reduced to 1/4 as in Figure 5.8

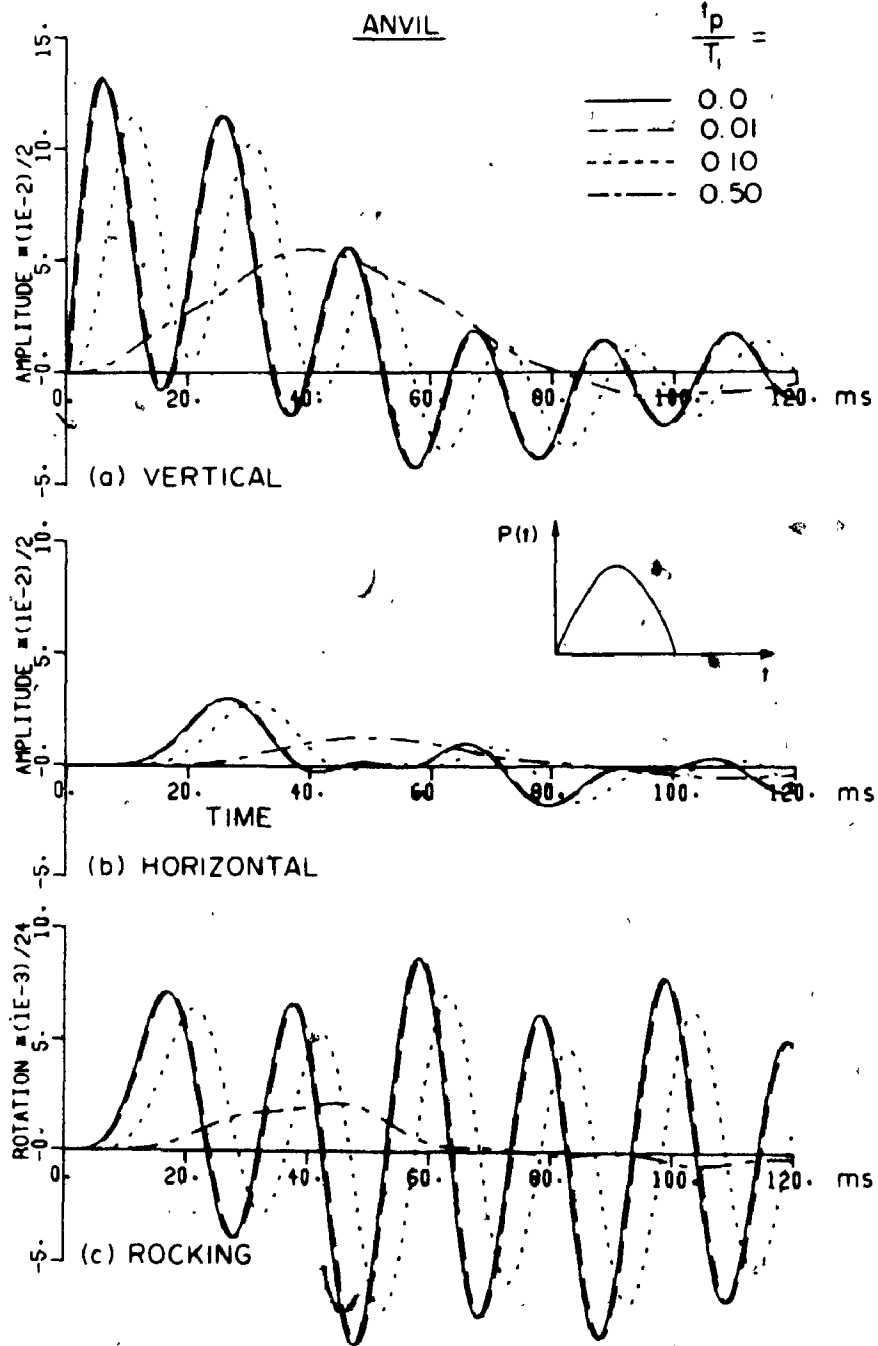


FIGURE 5.11a Vertical, Horizontal and Rocking Response of the Asymmetrical Hammer Foundation Shown in Figure 5.3 for Sine Pulse Loading of Different Duration and Constant Power ($e=0$, $e_1=2.0$ ft = 0.61 m; Response in in. and Radians, 1 in. = 2.54 cm; $D_1=30.6\%$, $D_2=44.6\%$, $D_3=47.3\%$: (a) Anvil

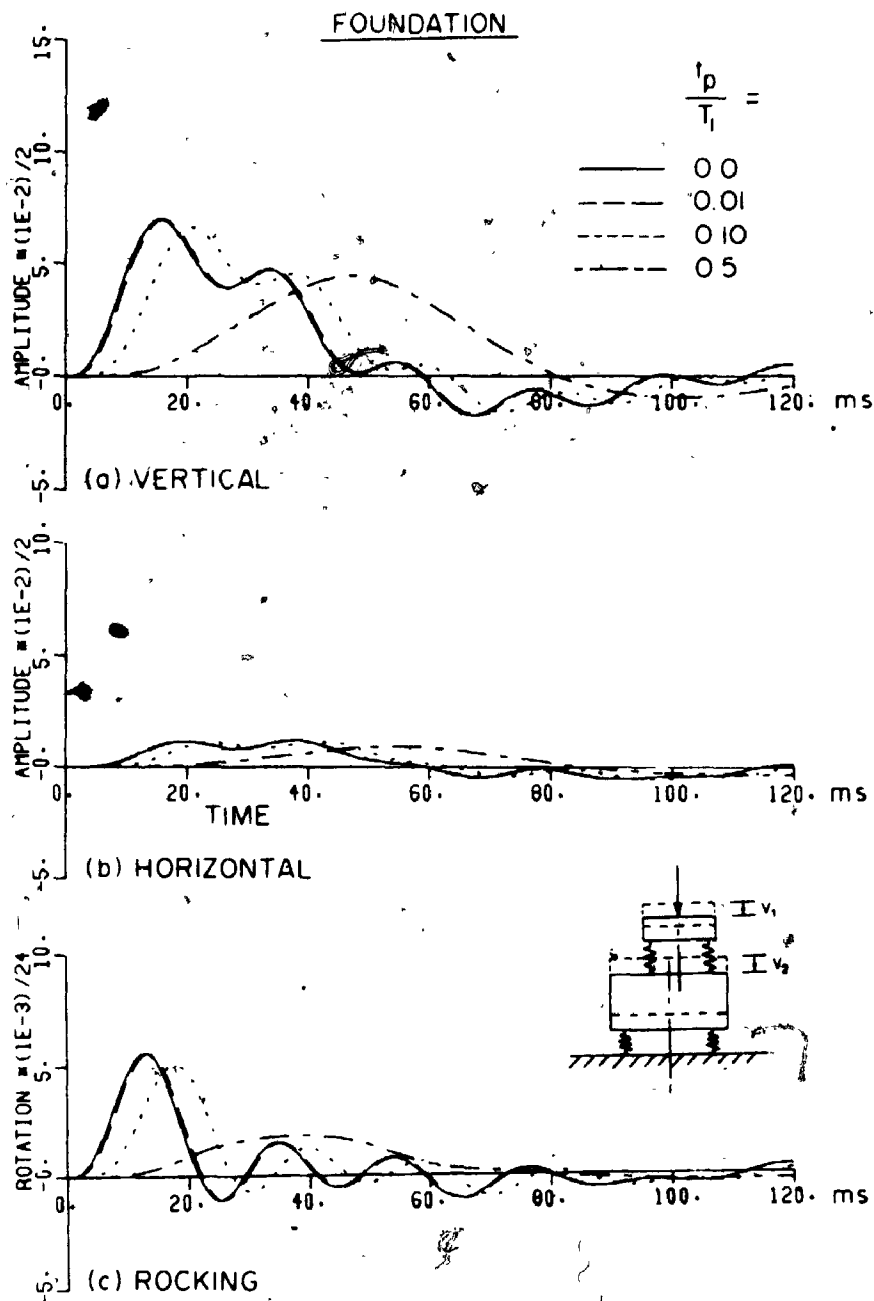


FIGURE 5.11b Vertical, Horizontal and Rocking Response of the Asymmetrical Hammer Foundation Shown in Figure 5.3 for Sine Pulse Loading of Different Duration and Constant Power ($e=0$, $e_1=2.0$ ft = 0.61 m; Response in in. and Radians, 1 in = 2.54 cm; $D_1=30.6\%$, $D_2=44.6\%$, $D_3=47.3\%$, $D_4=3.2\%$, $D_5=4.4\%$, $D_6=5.0\%$;
(b) Foundation

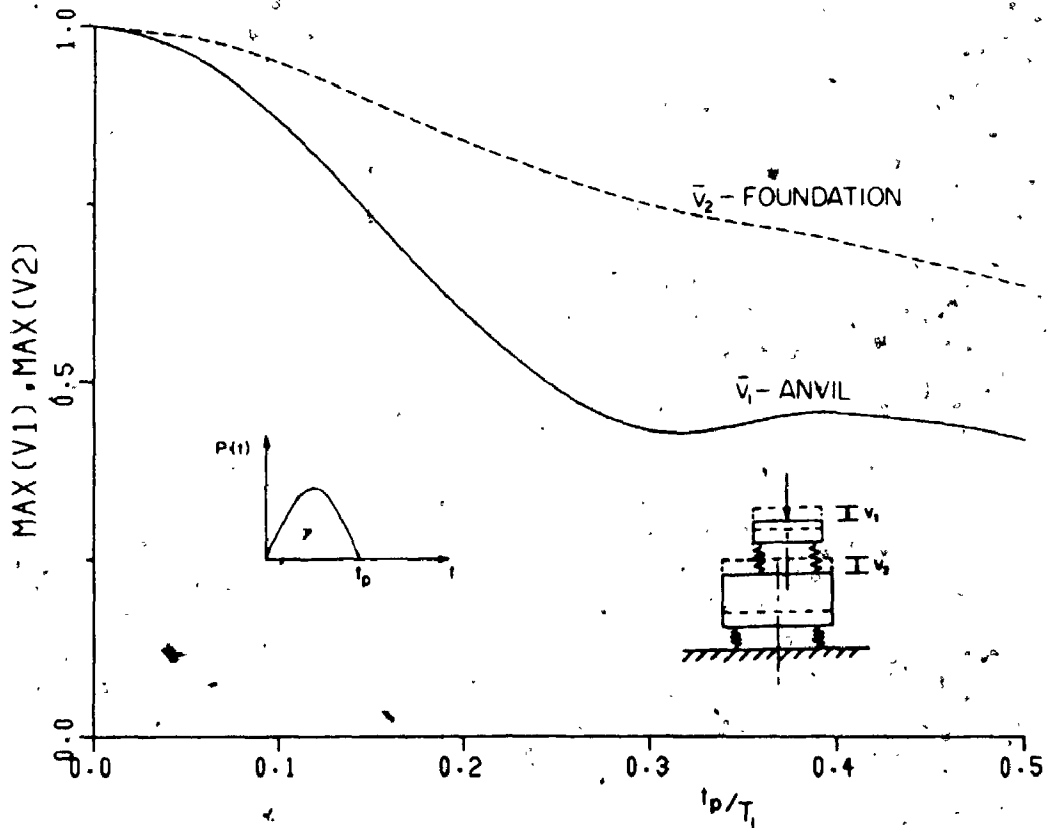
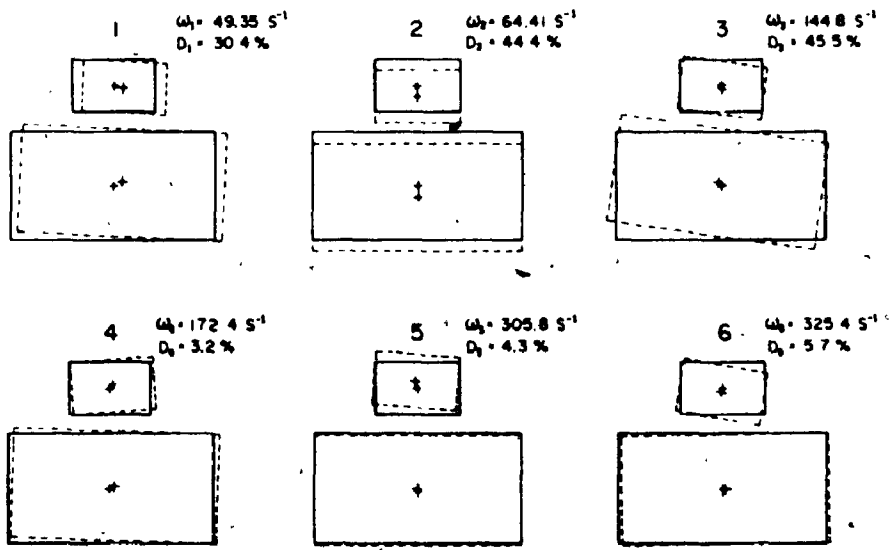
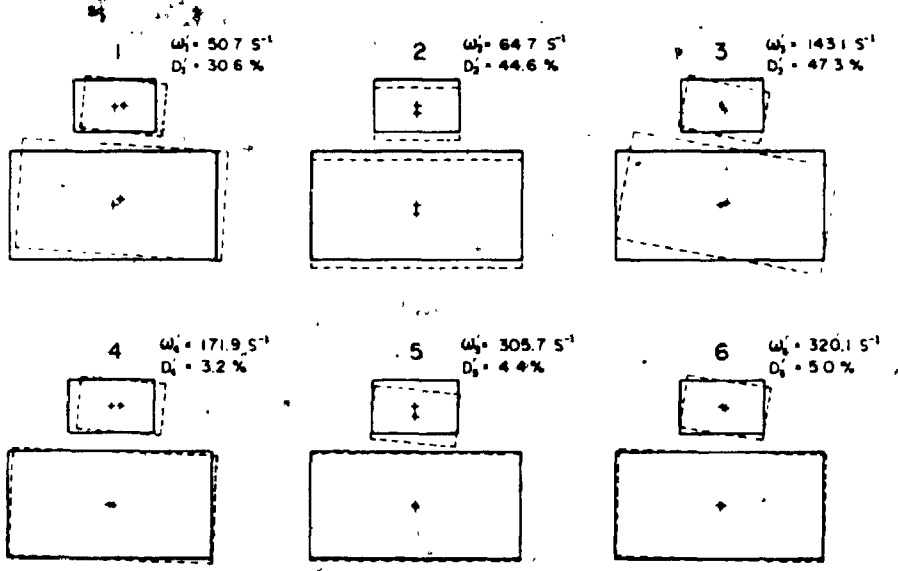


FIGURE 5.12 Variation in Normalized Peak Values of Vertical Response of the Asymmetrical Foundation From Figure 5.3 With Duration of Sine Pulse Loading (Six Degrees of Freedom)



(a) UNDAMPED MODES



(b) DAMPED MODES

FIGURE 5.13. Undamped and Damped Vibration Modes of Hammer Foundation From Figure 5.3 (Damping for undamped modes is evaluated using the energy approach)

ANVIL

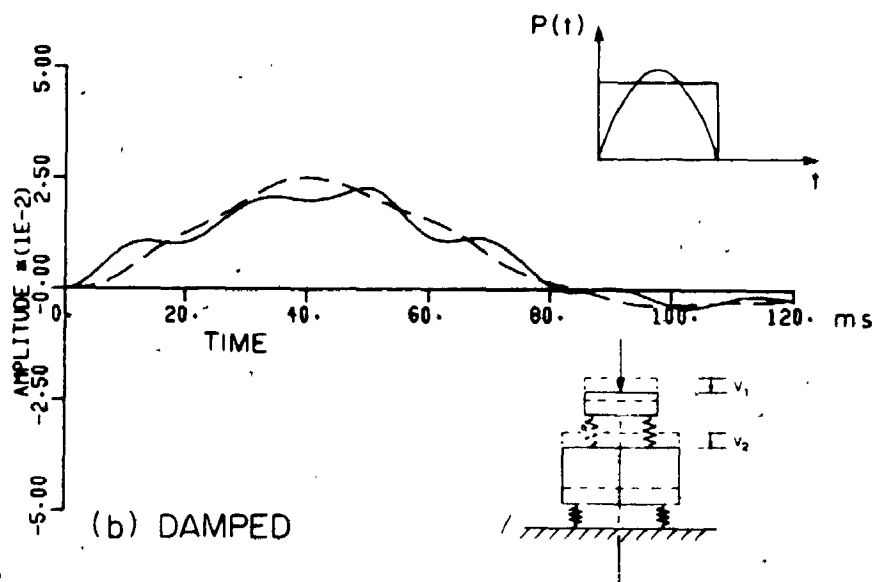
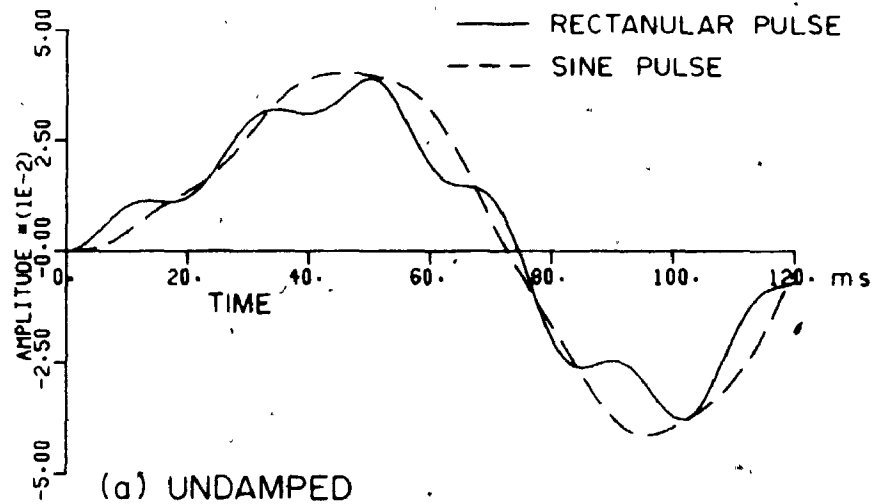


FIGURE 5.14a. Undamped and Damped Vertical Response of Two Mass Hammer Foundation for (a) Rectangular Pulse and (b) Sine Pulse ($e=e_1=0$, $t_p/T_1=0.5$) - Anvil

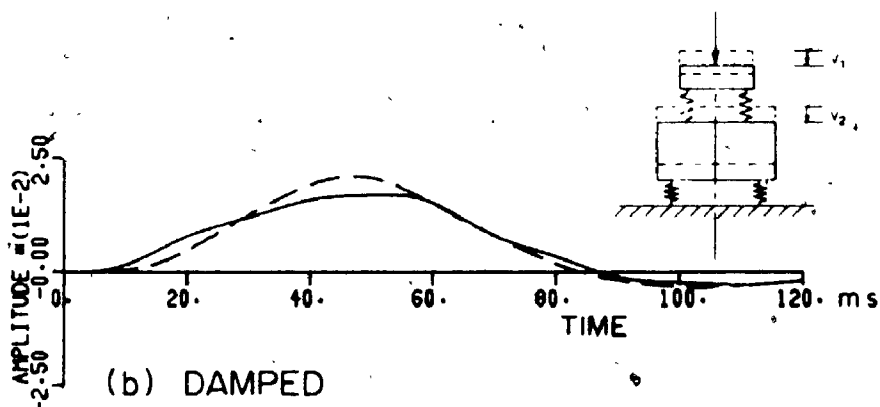
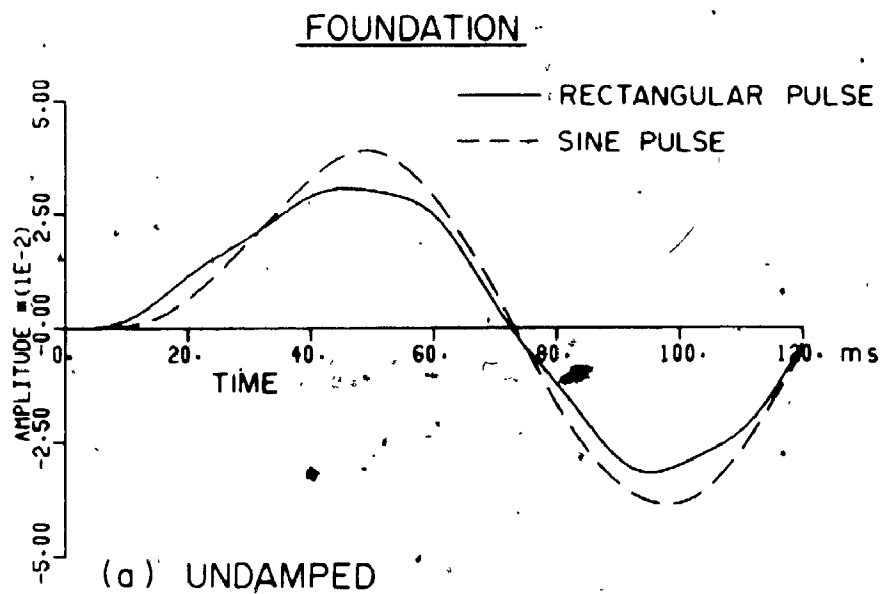


FIGURE 5.14b Undamped and Damped Vertical Response of Two Mass Hammer Foundation for (a) Rectangular Pulse and (b) Sine Pulse ($e=e_1=0$, $t_p/T_1=0.5$) - Foundation

CHAPTER 6

SOIL-STRUCTURE INTERACTION UNDER SEISMIC LOADING

6.1 INTRODUCTION

Flexibility of the foundation medium affects the modal properties of structures and may affect the free-field ground motion in the vicinity of the footing. The net effect of these two factors on seismic loads and response of the structure depends on the properties of the structure relative to the foundation, intensity of seismic excitation and the type of foundation. Numerous analytical studies have been conducted to investigate the influence of the flexibility of the foundation on the seismic response of structures. It was observed (17, 30) that shallow flexible foundations may produce an increase or a decrease in the flexural response and base shear of the structure, as compared to the response of the same building on a rigid base. Nevertheless, the predominant opinion is that for shallow foundations soil-structure interaction is a favorable factor which usually reduces base shear. This opinion was adopted even in the well known document ATC (14), based largely on the studies due to Veletsos (13, 62), which allows a reduction of base

shear of up to 30 percent on account of soil-structure interaction.

Little information is available concerning pile supported structures. Bielak and Palencia (98) used a single storey building having a base mass supported on piles and subjected to harmonic excitation to study these effects. They concluded that the peak response decreases as a result of interaction and that actual reduction is strongly dependent upon the system parameters.

This chapter examines and compares the seismic response of rigid structures as well as multi-storey buildings supported by various types of flexible foundations. Mat foundations are supported by a deep deposit or a stratum of limited thickness. Piles are considered in different configurations; pull-out stiffness and damping differ from push-in values and uplift of the cap is prevented or allowed. In all cases, the response is calculated for the San Fernando Valley earthquake of 1971; component S90W with peak acceleration of 0.11 g. It is assumed that the excitation at the base of the structure is the same as the free-field surface motion, i.e., the effects of kinematic interaction are neglected. This is equivalent to saying that the design ground motion is some sort of average free-field motion in the immediate

vicinity of the foundation site under consideration (99). Other authors justify the omission of kinematic interaction by assuming that the ground motion results from upward propagating shear waves.

6.2 MODELING THE BUILDING AND ITS FOUNDATION.

The mathematical model chosen is shown in Figure 3.1 which represents a multistorey shear building supported by either a shallow foundation or piles. This system has $N+2$ degrees of freedom, horizontal translation u_i of floor mass m_i , horizontal translation u_b and rocking in the vertical plane ψ of the base mass m_b . The mass of the floors is assumed to be equal and the interstorey damping coefficients c_{ij} , where $i = 1, 2, \dots, N$, are assumed to be proportional to the flexural stiffness k_{ij} of storey i . The proportionality factor is evaluated on the basis of one percent of critical damping in the first mode of vibration of the structure supported on a rigid foundation. Five and ten storeys are analyzed. Three rows of columns are assumed to facilitate the choice of various foundations.

The types of foundations considered are schematically depicted in Figure 3.21. For shallow foundations, two types of mats are chosen; one large mat supporting all

columns and three separate mats supporting individual columns. The soil is either a deep deposit modeled by a homogeneous viscoelastic halfspace or a shallow layer modeled as a homogeneous viscoelastic stratum of limited thickness.

The pile foundations comprise groups of floating or endbearing piles whose number and configuration vary. Each pile is treated as an endbearing pile as long as there is a downward end force produced by the pile tip. When this force vanishes or starts tending upwards due to pull-out forces, the pile is treated as floating. This distinction implies overall nonlinearity but is necessary because friction piles provide less stiffness but more damping than endbearing piles. Pile heads are either connected to the cap in a tension resistant way or are allowed to separate from the cap when the pile force is tending upwards in which case uplift and nonlinearity occur as indicated in Figure 6.1. The figure shows the two models considered in the analysis, i.e. a) the tension resistant connection; b) connection with no resistance in tension. The dynamic vertical force per pile, F_D , is calculated as the pile vertical displacement, v , times its vertical stiffness, k_v , (Figure 6.2),

$$F_D = vk_v$$

$$= x_r \psi k_v$$

(6.1)

in which ψ is the rocking of the base in the vertical plane and x_r is the horizontal distance between the pile and the center of the base. Then the average total load per pile, F_t , is calculated as the sum of the static and dynamic loads.

$$F_t = F_D + (m_b + \sum_{i=1}^N m_i) g_0 / n \quad (6.2)$$

where g_0 is the gravity acceleration and n is the number of piles.

Using the impedance function approach and limiting the analysis to the consideration of inertial interaction, both shallow and deep foundations can be treated in the same way.

Impedance Functions of Foundations

The impedance functions are described in terms of the true stiffness k and constants of equivalent viscous damping c . Then, the relationship between the applied force P_x and moment M_b and the horizontal translation of the base u_b and its rotation in the vertical plane ψ are written in the standard form (equation 2.18).

The constants k and c are given by equations 2.2 to 2.4 and 2.7 for halfspace and 2.9 to 2.12 for a stratum. Material damping of soil is assumed to be hysteretic which

results in frequency dependent constants k and c (equation 2.7). Therefore, the constants are calculated for the first natural frequency of the system and then considered as frequency independent.

For pile foundations, impedance functions of single piles are obtained from equations 2.13 and Figures 2.8 to 2.10. Pile-soil-pile interaction is neglected and the group impedance functions are evaluated using equations 2.14 to 2.17.

Finally, nonlinearity of soil behavior is always of concern particularly with piles. Here it is assumed to be accounted for approximately by adjusting soil shear modulus and material damping to the expected level of strain.

6.3 GOVERNING EQUATIONS AND THEIR SOLUTION

The governing equations of the building motion are given by equation 2.22,

$$[m]\{\ddot{u}\} + [c]\{\dot{u}\} + [k]\{u\} = \{P\} \quad (6.3)$$

in which $[m]$, $[c]$, $[k]$, $\{u\}$ and $\{P\}$ are defined by equation 2.23. With ground acceleration \ddot{u}_g , the loading vector $\{P\}$ becomes

$$\{P\} = - \langle \{m_i\} \mid m_b + \sum_1^N m_i \sum m_i h_i \rangle^T \ddot{u}_g \quad (6.4)$$

in which h_i is the height of floor i .

With the structure and foundation stiffness, damping and mass matrices defined, the equation of motion, 6.3, is solved by the numerical integration technique, the Wilson- θ method, described in Chapter 4. In this method, displacement, velocity and acceleration of each floor and the foundation are calculated at each time step. The floor equivalent earthquake forces $P_i(t)$, the base shear, $Q_b(t)$, and overturning moment $M_b(t)$ are calculated at each time step as

$$P_i(t) = m_i (\ddot{u}_i(t) + \ddot{u}_b(t)) + m_i h_i \ddot{\psi}(t) \quad (6.5)$$

$$Q_b(t) = \sum_{i=1}^N m_i \ddot{u}_i(t) + (m_b + \sum_{i=1}^N m_i) \ddot{u}_b(t) + \sum_{i=1}^N m_i h_i \ddot{\psi}(t) \quad (6.6)$$

$$M_b(t) = \sum_{i=1}^N m_i h_i (\ddot{u}_i(t) + \ddot{u}_b(t)) + (I_t + \sum_{i=1}^N m_i h_i^2) \ddot{\psi}(t) \quad (6.7)$$

in which I_t is the sum of mass moments of inertia of all masses including the foundation. The storey drift, $\Delta_i(t)$, defined as the relative displacement between consecutive floors, is

$$\Delta_i(t) = (u_i(t) - u_{i-1}(t)) + (h_i - h_{i-1})\psi(t) \quad (6.8)$$

6.4 EXAMPLES

The different types of flexible foundations depicted in Figure 3.21 may have a profound effect on the response of buildings to seismic excitation, the resultant storey shear and the base shear. Examples of these effects are presented for a ten-storey building in Figures 6.3 and 6.4. The earthquake signal used is shown in Figure 6.5. The soil layer indicated as case (b) in Figure 3.21 is of two different depths, yielding the first natural frequency of the layer equal to either $2\omega_1$ or $4\omega_1$ where ω_1 is the fundamental natural frequency of the building on the elastic halfspace. The response of the structure on a fixed base was obtained from the N equations of motion given by equation 2.23 with u_D and ψ identically equal to zero.

For both the halfspace and shallow layer, Figures 6.3 and 6.4 show an appreciable decrease of the base shear with decreasing shear wave velocity, V_s , i.e., as the foundation medium becomes more flexible. This pattern of behavior is not observed for the case of pile foundation. In this case as the shear wave velocity of the foundation medium increased from 300 ft/sec (≈ 91 m/sec) to 600 ft/sec (≈ 183 m/sec), there is a decrease in the base shear.

Generally, the effect of piles depends on the number and type of piles as is shown in the next section.

Figures 6.3 and 6.4 also show that the limited depth of the layer results in larger displacements and storey shears than those obtained from halfspace. Therefore, the procedure assuming a halfspace may not be conservative if small material damping is assumed. As soil-material damping, characterized here by the damping ratio β increased from 0.025 to 0.05, the storey displacement, shear and base shear decreased for the case of the layer. Thus the loss of geometric damping is replaced by the effect of material damping. For the case of halfspace, the effect of soil-material damping is not pronounced. The two depths considered for the soil layer yield almost the same result.

For all foundations, the maximum storey shears are reduced and the maximum storey displacements and drift are increased by foundation flexibility.

Pile Cap Uplift

It is a common design practice, sometimes required by codes, to attach the piles to the cap in a tension resisting way (anchorage) and if it appears necessary, to design the piles for tension. The aim of these often

costly measures is to prevent cap uplift and, supposedly, to secure a greater measure of safety. According to the National Building Code of Canada (100), "anchorage is required if the effect of the loads tends to cause uplift, overturning or sliding." Therefore, it is of interest to examine how the response, overturning moments and seismic loading change if rigid connection of the pile with the cap is not provided. The problem which is non-linear is solved as a stepwise linear problem in the time domain. Any time a pile is excluded due to cap uplift or tip uplifts, the stiffness and damping matrices change. Examples of these are shown in Figures 6.6 to 6.12.

Figure 6.6 shows pile forces and storey drift for a ten-storey building supported by 15, 21 or 27 piles installed in three rows and differing in the tip condition. Variation with ground motion intensity is also shown. It can be seen that with pile cap uplift allowed (no connection), the vertical pile loading may increase by 30 to 50 percent and the storey drift may increase by 10 to 30 percent. Tension, denoted by a minus sign, is more likely to occur in floating piles. For high intensity of ground shaking, pile forces may even be doubled if the rigid connection is not provided. However, with rigid connection and high earthquake intensity, the tensile force per pile is quite high. The dramatic increase

7

in pile compression caused by the elimination of even a small tensile force is caused by the substantial decrease of group stiffness in rocking due to the elimination of piles in tension.

However, the rigid connection of piles to the cap may reduce or increase the overturning moment and base shear depending on the number and type of piles. This is depicted in Figure 6.7 which also shows that for low intensity of ground shaking, there is no significant difference between the two arrangements (presence of rigid connection or not) as far as base shears and overturning moments are concerned. The difference increases with increasing intensity of ground shaking.

Figure 6.8 shows the maximum storey displacement for the same building supported by 15 pinned piles. It can be seen from the figure that, for both floating and end-bearing piles, the rigid connection of the pile to the cap reduces the maximum displacement by no more than 10 percent. The same trend is observed for endbearing piles under high intensity of ground shaking. For floating piles, the response is more than doubled when the cap uplift is allowed and the ground acceleration increased from .11g to .44g.

In smaller buildings, pile tension is likely to occur

only at high ground acceleration. This is indicated in Figure 6.9 which shows the pile forces and storey drift for a five-storey building. In this case, the increase of compression force per pile due to the absence of the tensile connection is less than that for the case of the high building. Figure 6.10a indicates that, for this small building exposed to strong ground motion, the base shear and overturning moment are increased when the rigid connection is provided for endbearing piles. For floating piles (Figure 6.10b), the seismic forces may increase or decrease if the cap uplift is allowed. For ground acceleration of the order of .11g or .22g, there is no significant difference between the two arrangements.

Another important aspect to examine is the effect of pile configuration or arrangement on the pile forces. This is shown in Figure 6.11a which represents the same ten-storey building supported by 27 piles with different tip conditions and three different pile arrangements depicted as cases a, b and c in Figure 6.12. The magnitude of the pile force can be seen to decrease when the piles are concentrated at the extreme part of the foundation. The same trend is observed from Figure 6.11b for the same ten-storey building on 21 piles.

Rigid Structures

Under seismic forces, rigid structures such as nuclear containment vessels, silos or machine foundations, usually have just two degrees of freedom, i.e. horizontal translation u and rotation in the vertical plane ψ . Consequently, the use of the direct spectral approach to solve for the response is best suited for these types of structures. The silo shown in Figure 3.3a resting on a mat foundation and full of slag is analyzed for the same earthquake signal given in Figure 6.5. Dimensions of the silo and its footing, and soil properties are given in Chapter 3. The response referred to the C.G. of the silo-foundation system is calculated using the direct spectral approach and the Wilson- θ method of numerical integration.

Random vibration approach. The power spectral density of the ground acceleration, $S_{\ddot{u}_g}(\omega)$, is calculated as the Fourier transform of $\ddot{u}_g(t)$, $F_{\ddot{u}_g}(\omega)$, times its conjugate, $F_{\ddot{u}_g}^*(\omega)$

$$S_{\ddot{u}_g}(\omega) = F_{\ddot{u}_g}(\omega)F_{\ddot{u}_g}^*(\omega) = |F_{\ddot{u}_g}|^2 \quad (6.9)$$

where ω is the frequency in rad/sec. Figure 6.13 shows the normalized spectrum of the ground acceleration, $S_{\ddot{u}_g}^n(\omega)$,

where

$$\int_0^{\infty} S_{\ddot{u}_g}^n(\omega) d\omega = 1 \quad (6.10)$$

and

$$S_{\ddot{u}_g}(\omega) = \sigma_{\ddot{u}_g}^2 S_{\ddot{u}_g}^n(\omega)$$

in which $\sigma_{\ddot{u}_g}$ is the root mean square of the ground acceleration. This spectrum is compared with the empirical normalized spectrum, obtained from analysis of strong motion records by Tajimi (79), as

$$S_{\ddot{u}_g}^n(\omega) = \frac{[1 + 4\epsilon_g^2 (\frac{\omega}{\omega_g})^2]}{[1 - (\frac{\omega}{\omega_g})^2]^2 + 4\epsilon_g^2 (\frac{\omega}{\omega_g})^2} \cdot \frac{4\epsilon_g}{\pi\omega_g (1 + 4\epsilon_g^2)} \quad (6.11)$$

in which ω_g is a characteristic ground frequency and ϵ_g is a characteristic damping ratio of ground. This comparison of the local spectrum of the San Fernando earthquake and the empirical form is made to verify the suitability of theoretical spectrum and to establish its parameters. Optimization yields the following values of ω_g and ϵ_g

$$\omega_g = 7.259 \quad \epsilon_g = .933 \quad (6.11a)$$

Tajimi's spectrum (equation 6.11) is calculated using these values and is shown in Figure 6.13.

The spectral density of the response is calculated using equation 4.23 which for the two degrees of freedom takes on the following form:

$$\begin{aligned}
S_{uu}(\omega) &= H_{uu}(\omega)H_{uu}^*(\omega)S_{p_{uu}}(\omega) + H_{uu}(\omega)H_{u\psi}^*(\omega)S_{p_{u\psi}}(\omega) \\
&\quad + H_{u\psi}(\omega)H_{uu}^*(\omega)S_{p_{\psi u}}(\omega) + H_{u\psi}(\omega)H_{u\psi}^*(\omega)S_{p_{\psi\psi}}(\omega)
\end{aligned}
\tag{6.12a}$$

$$\begin{aligned}
S_{\psi\psi}(\omega) &= H_{\psi u}(\omega)H_{\psi u}^*(\omega)S_{p_{uu}}(\omega) + H_{\psi u}(\omega)H_{\psi\psi}^*(\omega)S_{p_{u\psi}}(\omega) \\
&\quad + H_{\psi\psi}(\omega)H_{\psi u}^*(\omega)S_{p_{\psi u}}(\omega) + H_{\psi\psi}(\omega)H_{\psi\psi}^*(\omega)S_{p_{\psi\psi}}(\omega)
\end{aligned}
\tag{6.12b}$$

In equations 6.12, $S_{uu}(\omega)$ and $S_{\psi\psi}(\omega)$ are the spectral densities of displacement u and rocking in the vertical plane ψ ; $H_{ij}(\omega)$ the elements of the transfer matrix

$$[H(\omega)] = [[k] - \omega^2 [m] + i\omega [c]]^{-1} \tag{6.13}$$

The asterisk represents complex conjugate and $S_{p_{ij}}(\omega)$ are the cross spectral densities of the excitation forces.

For the case of earthquake shaking, only the force in the horizontal direction, $S_{p_{uu}}(\omega)$, exists and is equal to

$$\begin{aligned}
S_{p_{uu}}(\omega) &= m^2 \cdot S_{\ddot{u}_g}(\omega) \\
&= m^2 \cdot \sigma_{\ddot{u}_g}^2 S_{\ddot{u}_g}^n(\omega)
\end{aligned}
\tag{6.14}$$

In such a case, equations 6.12 reduce to

$$S_{uu}(\omega) = m^2 \sigma_{\ddot{u}_g}^2 H_{uu}(\omega)H_{uu}^*(\omega) S_{\ddot{u}_g}^n(\omega) \tag{6.15a}$$

and

$$S_{\psi\psi}(\omega) = m^2 \sigma_{\ddot{u}_g}^2 H_{\psi u}(\omega) H_{\psi u}^*(\omega) S_{\ddot{u}_g}^n(\omega) \quad (6.15b)$$

The mean peak response is evaluated using equations 4.24 to 4.27 and compared with the values obtained using the numerical integration of the equations of motion in Table 6.1. It can be seen that the agreement between the two approaches is fairly good. The time histories of the response displacement u and rocking ψ are shown in Figure 6.14.

Table 6.1 Comparison of Peak Responses of a Silo Obtained by Time History Analysis and Random Vibration Approach

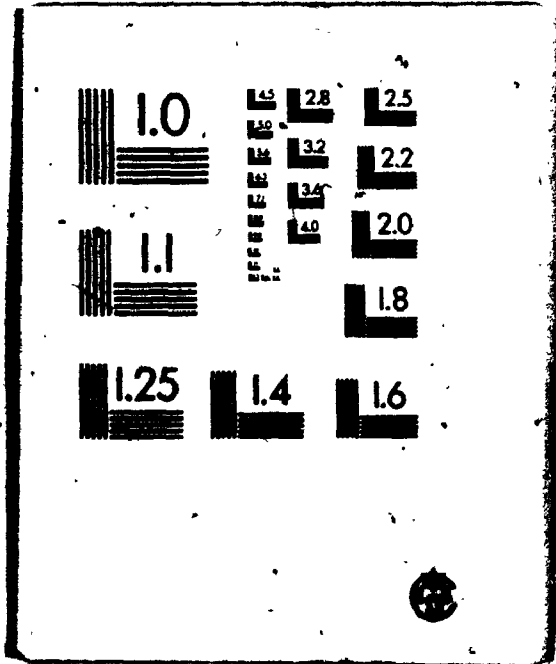
	Maximum Displacement u (cm)	Maximum Rocking ψ
Time History Response	2.010	.0016
Random Vibration Approach	2.098	.0017

CONCLUSIONS

The examination of dynamic response of buildings and rigid structures supported by different foundations suggests the following conclusions:

Seismic response and loading of buildings depend on the flexibility of the foundation and its type. For

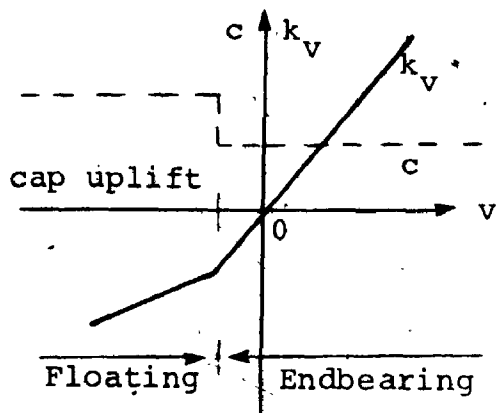
3 3
OF / DE



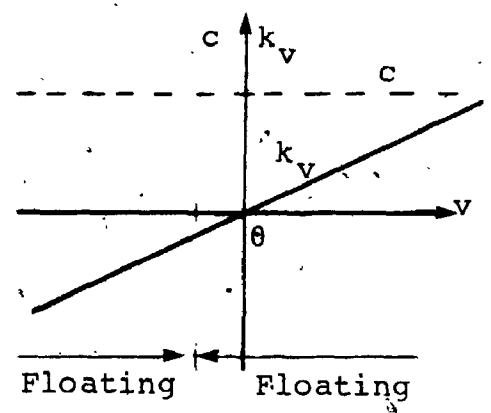
shallow foundations, the response increases and the seismic forces decrease as the soil medium becomes more flexible. These effects are due to the rocking motion of the foundation and the reduction in natural frequency due to soil flexibility.

- The limited depth of the stratum results in insignificant increase in both displacement and storey shears compared to those obtained with the halfspace when moderate material damping is assumed.
- Soil material damping decreases both response and base shear for the case of a layer of limited depth. With a halfspace, these effects are insignificant.
- The effect of piles depends on the number and type of piles, their arrangement and, as with the other foundations, soil stiffness and the kind of seismic excitation.
- Rigid connection of piles with the cap may not always be necessary particularly for small buildings and/or low intensity earthquakes.
- The direct spectral approach is a very effective method of analysis of dynamic response of rigid structures on soil.
- In this analysis, the San Fernando Valley earthquake signal is used. For other types of earthquakes and for other structural systems, somewhat different

results might be obtained. Nevertheless, the general trend described here can be expected to occur.

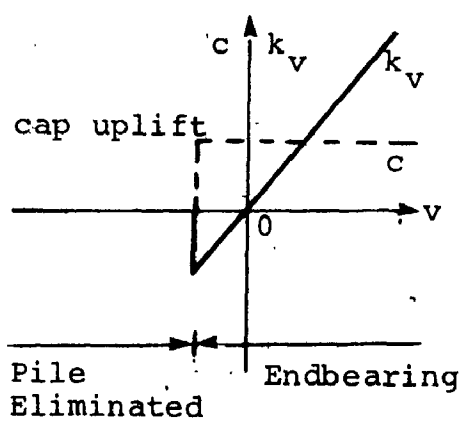


(i) Endbearing Pile

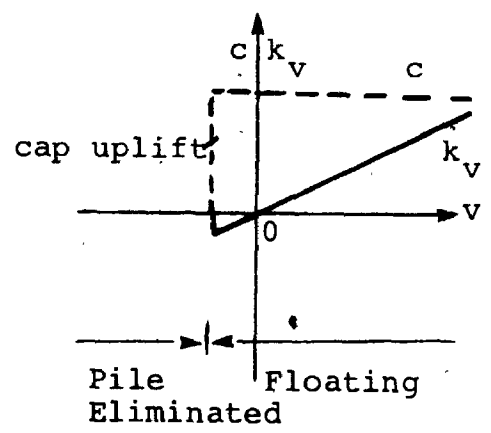


(ii) Floating Pile

(a) Tensile Resisting Connection



(i) Endbearing Pile



(ii) Floating Pile

(b) Without Tensile Resisting Connection

FIGURE 6.1 Pile Restoring Force k_v and Damping Coefficient c vs. Vertical Displacement v .

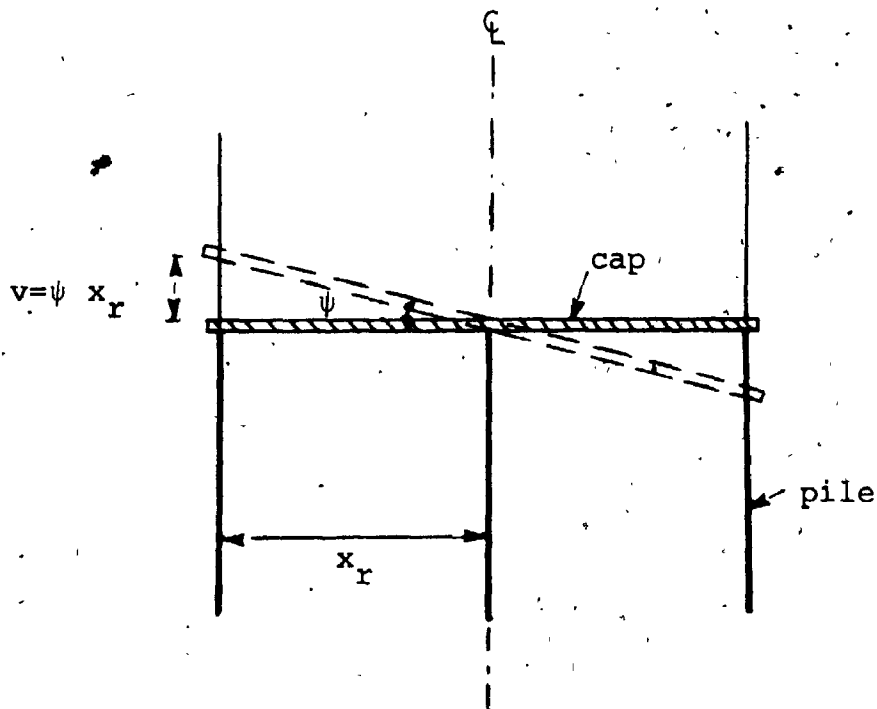


FIGURE 6.2 Pile Vertical Displacement v As a Result of Cap Rocking in the Vertical Plane ψ

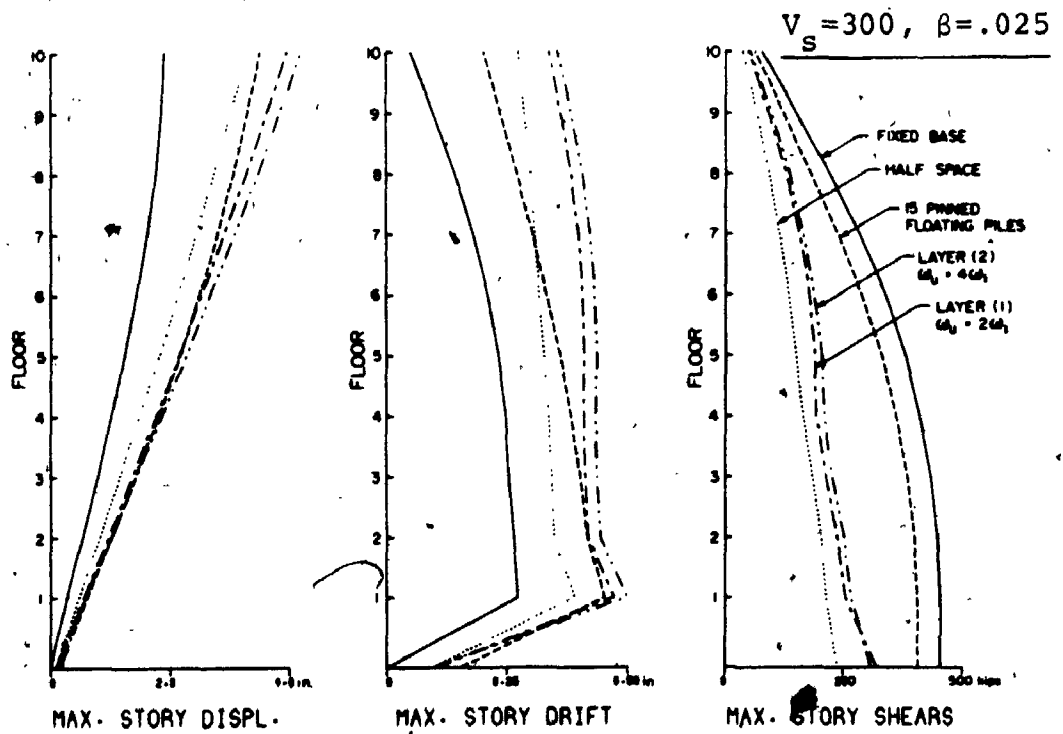
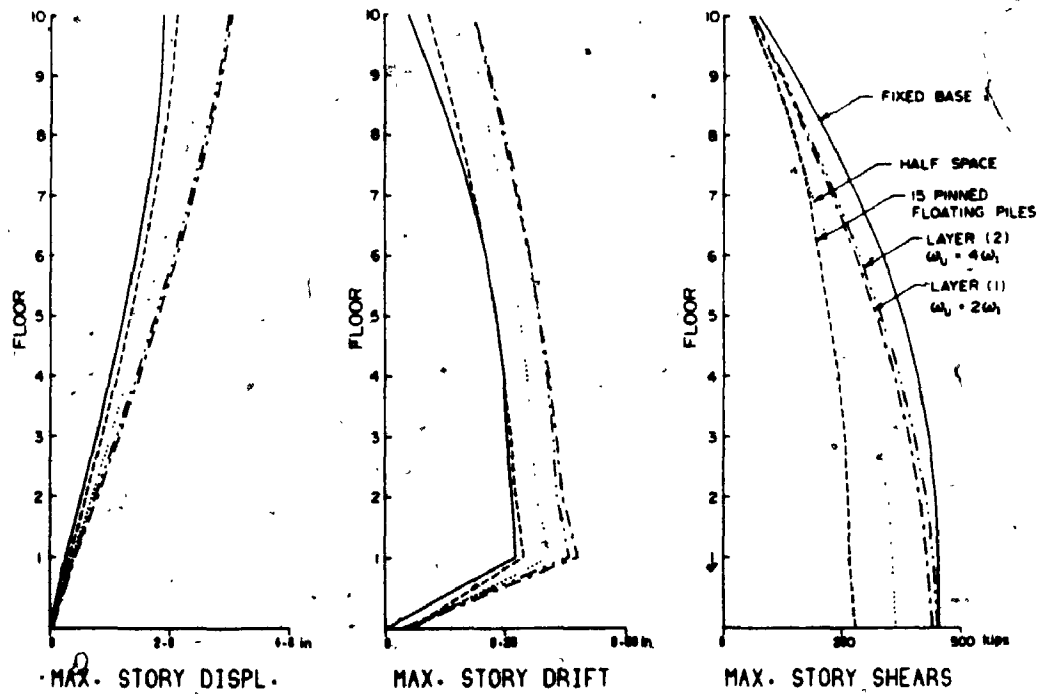


FIGURE 6.3 Maximum Storey Displacements, Drifts, and Shears for Ten-Storey Building on Different Foundations, for Two Soil Shear Wave Velocities and Soil Material Damping $\beta = .025$ (1 in = 2.54 cm, 1 kip = 4.45 kN)

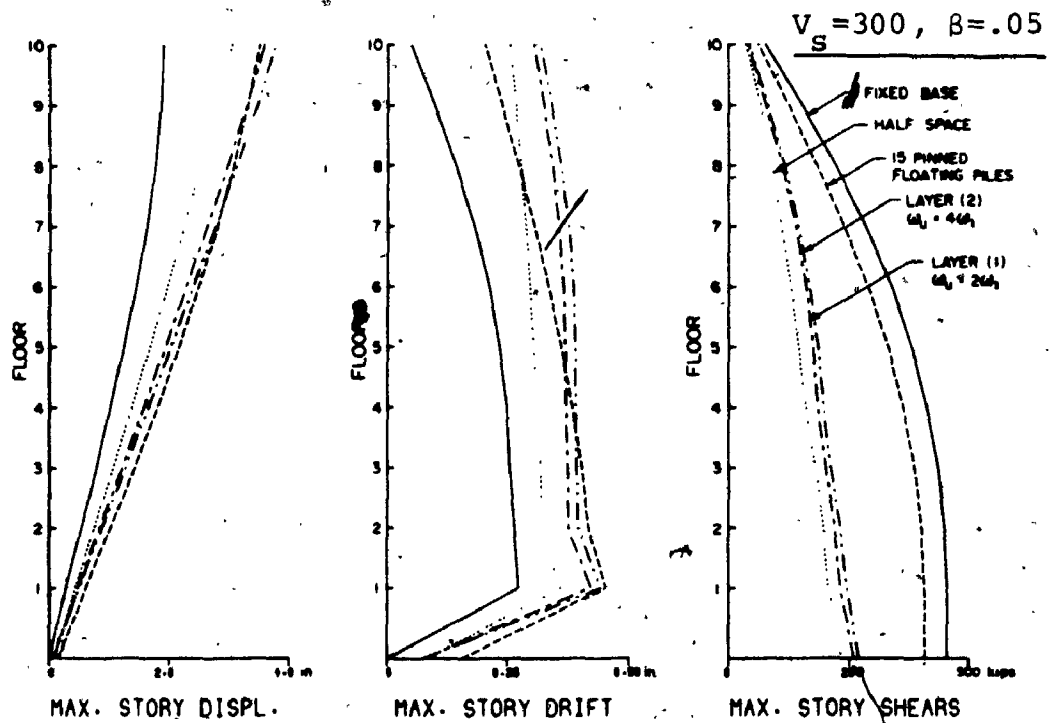
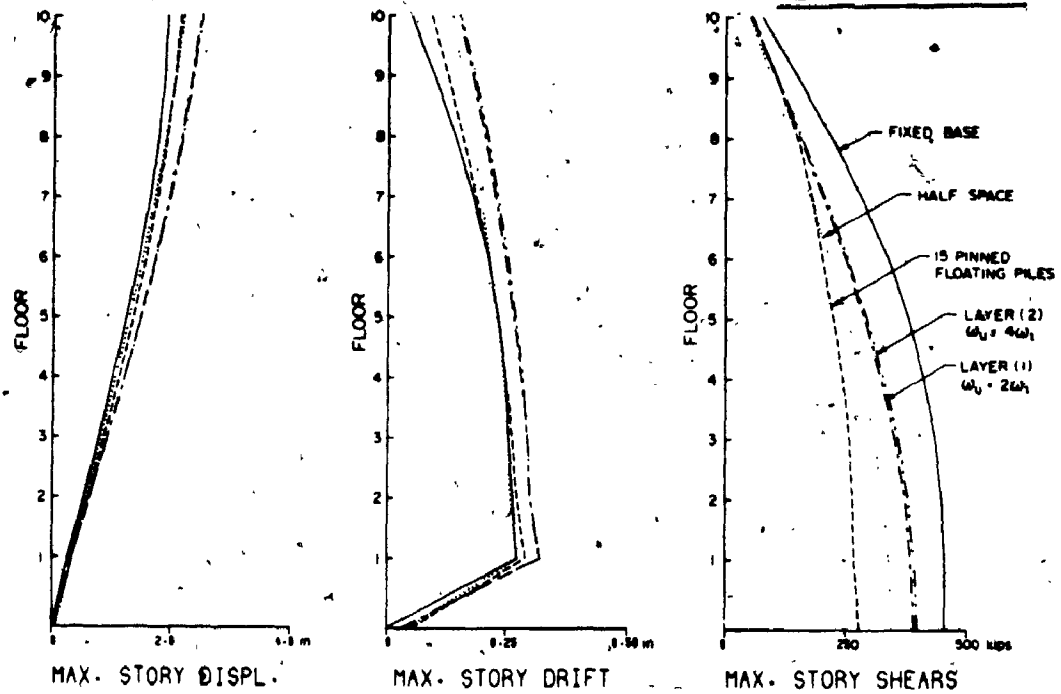


FIGURE 6.4 Maximum Storey Displacements, Drifts and Shears for Ten-Storey Building on Different Foundations, for Two Soil Shear Wave Velocities and Soil Material Damping $\beta = .05$ (1 in. = 2.54 cm, 1 kip = 4.45 kN)

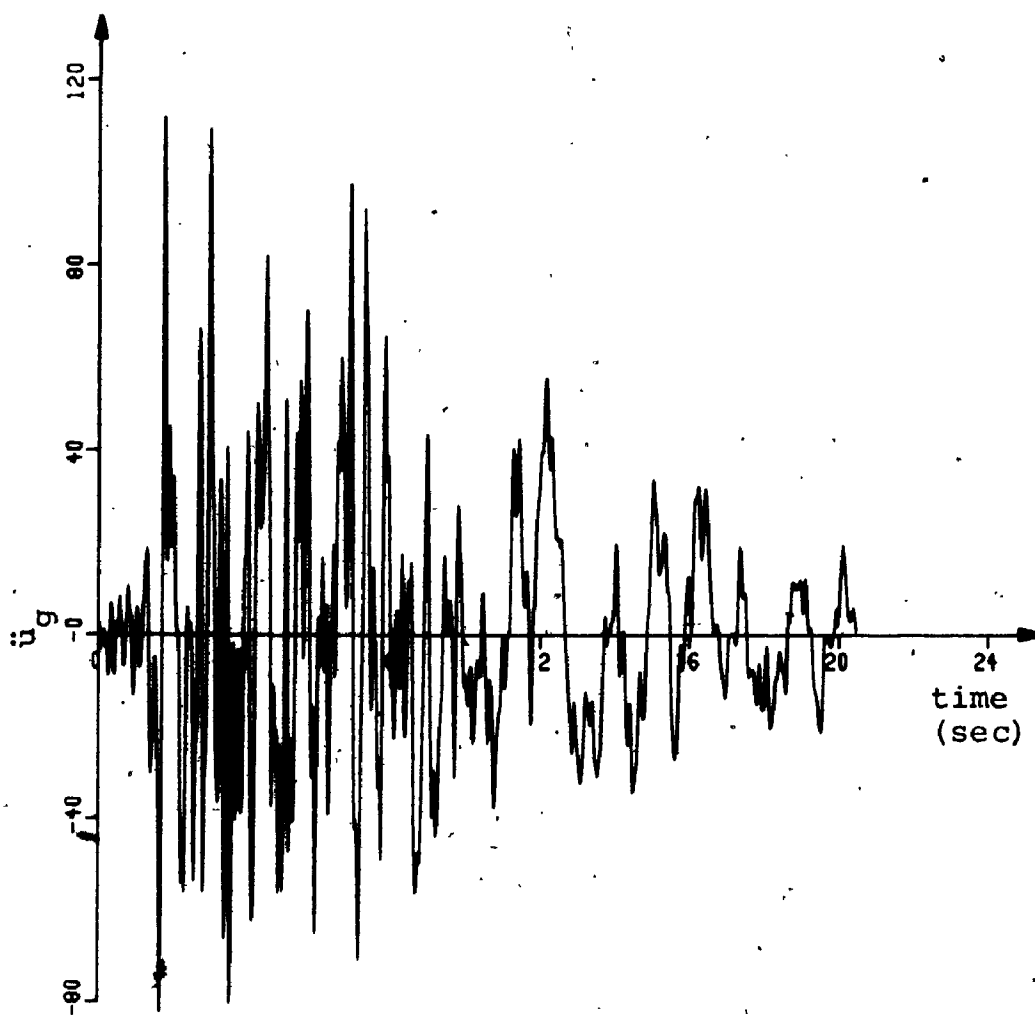


Figure 6.5 San Fernando Earthquake Record

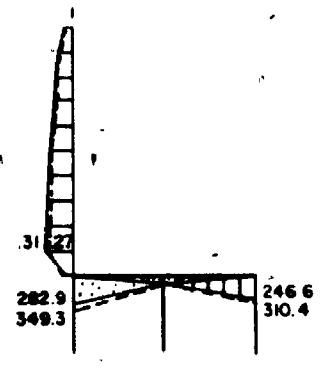
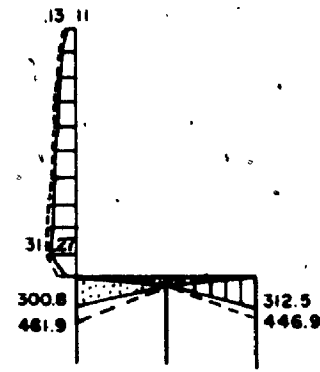
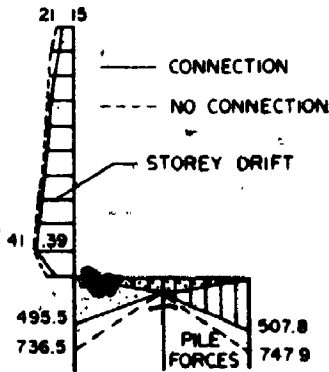
PINNED END BEARING PILES

15 PILES

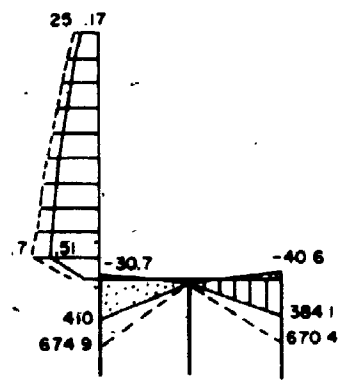
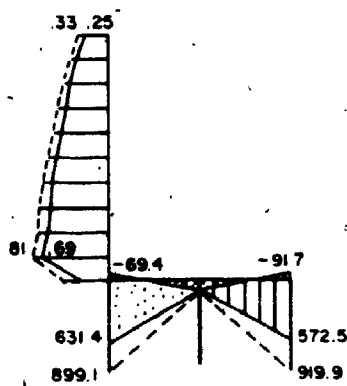
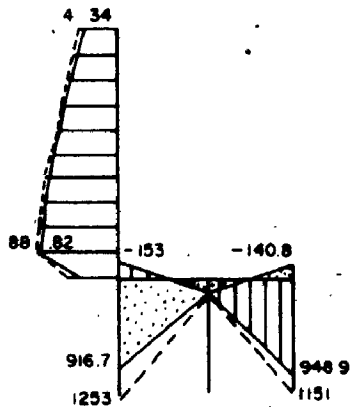
21 PILES

27 PILES

(a) $\hat{\delta} = 0.11g$



(b) $\hat{\delta} = 0.22g$



(c) $\hat{\delta} = 0.44g$

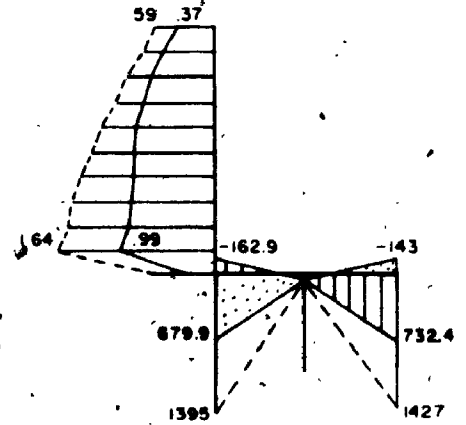
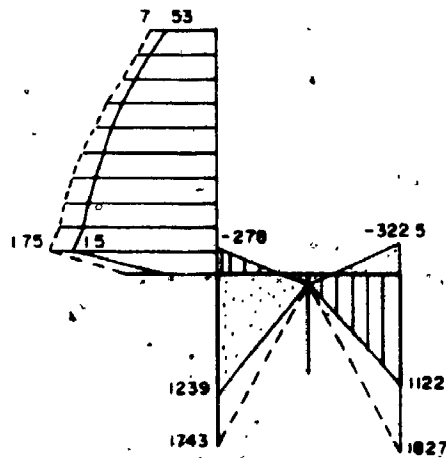
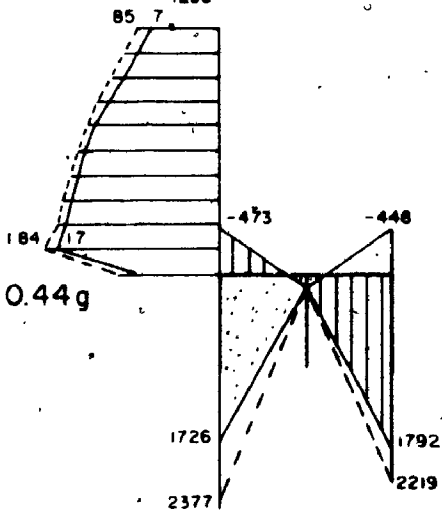


FIGURE 6.6a Pile Forces (kips) and Storey Drift (in) for Ten-Storey Building Supported by 15, 21 and 27 Piles For Different Earthquake Intensity (Pinned Endbearing Piles).

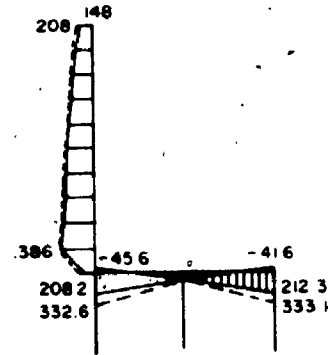
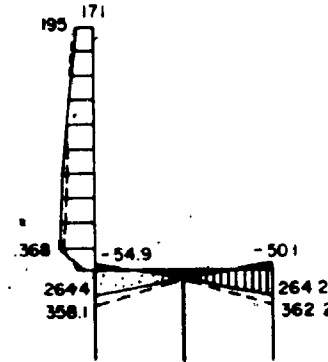
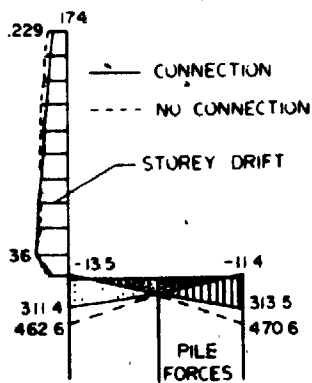
PINNED FLOATING PILES

15 PILES

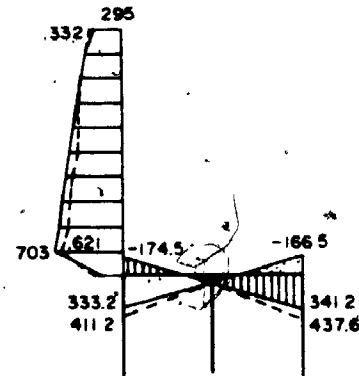
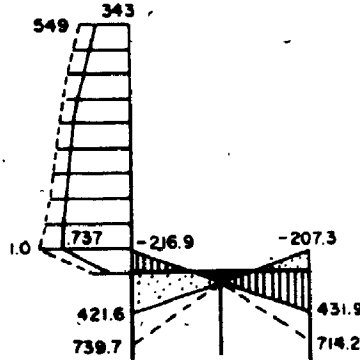
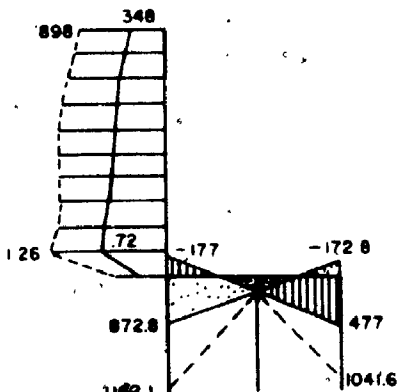
21 PILES

27 PILES

(a) $\hat{\delta} = 0.11g$



(b) $\hat{\delta} = 0.22g$



(c) $\hat{\delta} = 0.44g$

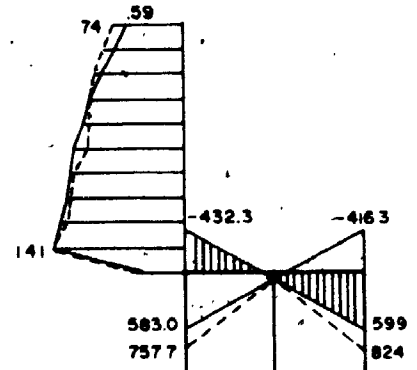
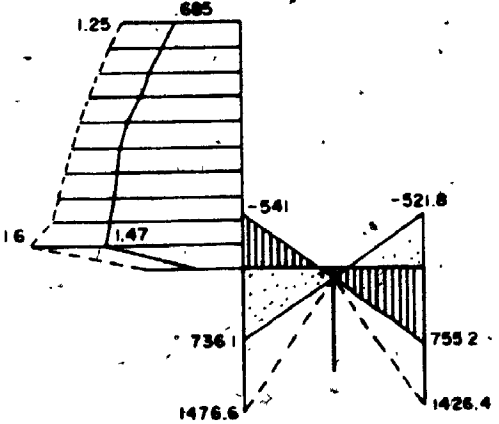
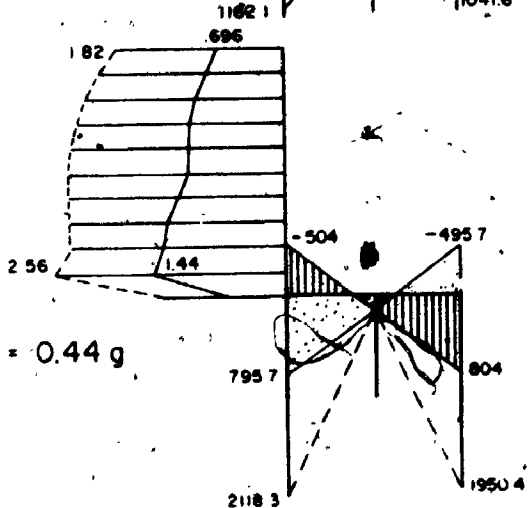


FIGURE 6.6b Pile Forces (kips) and Storey Drift (in) for Ten-Storey Building Supported by 15, 21 and 27 Piles For Different Earthquake Intensity. (Pinned Floating Piles)

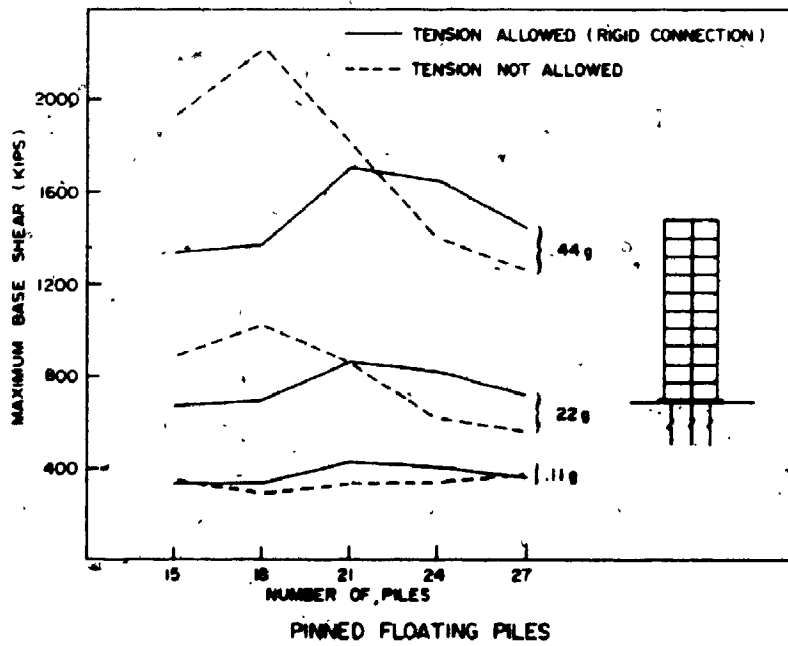
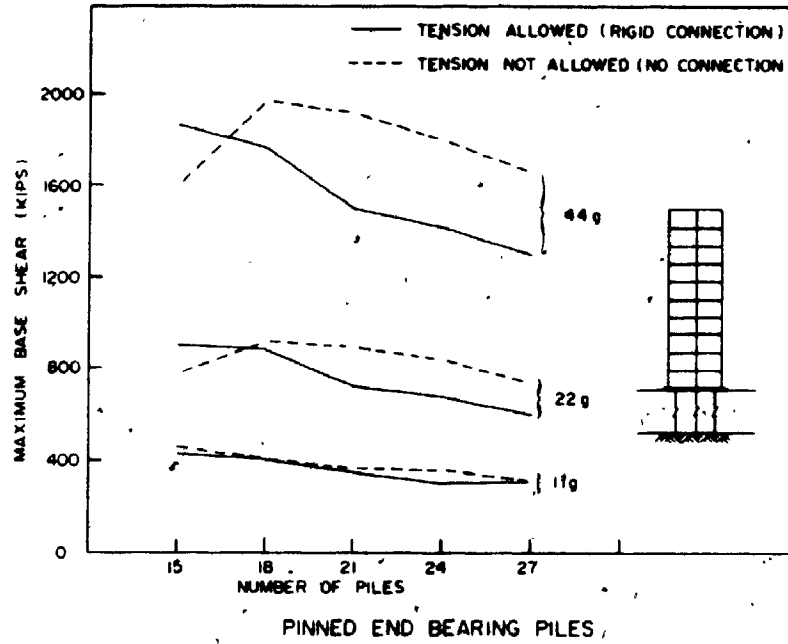


FIGURE 6.7a Base Shear of Ten-Storey Building vs. Number and Type of Piles and Intensity of Ground Shaking (1 kip = 4.45 kN)

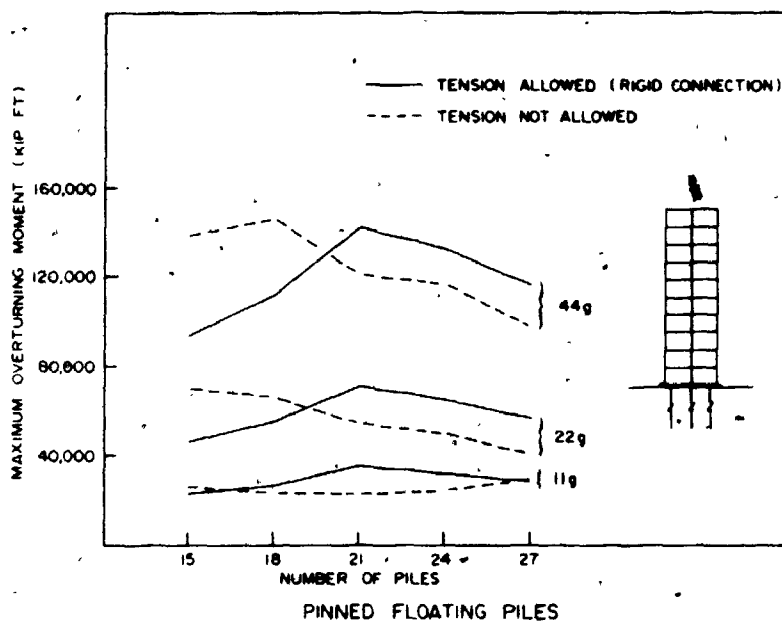
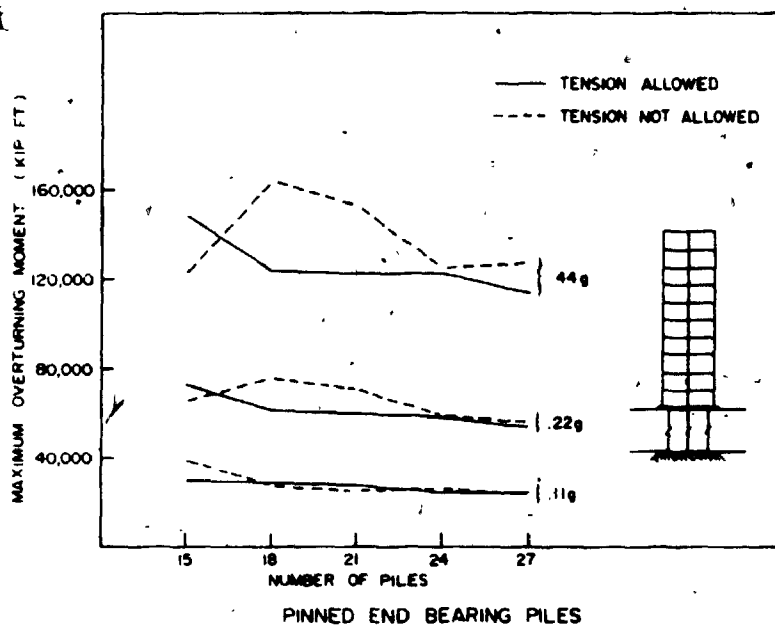


FIGURE 6.7b Overturning Moment of 10-Storey Building vs. Number and Type of Piles and Intensity of Ground Shaking (1 kip.ft = 1.36 kN.m)

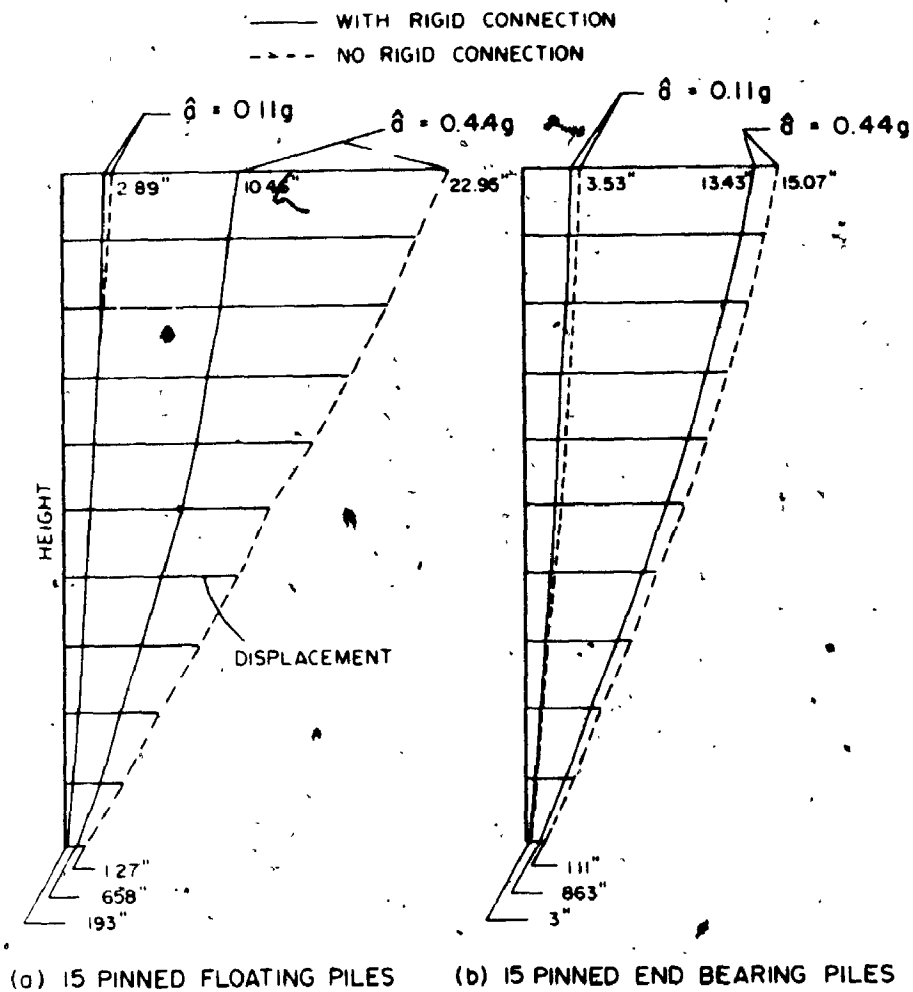


FIGURE 6.8 Maximum Storey Displacement of Ten-Storey Building Supported by 15 Piles For Different Tip Conditions and Intensity of Ground Shaking (1 in = 2.54 cm)

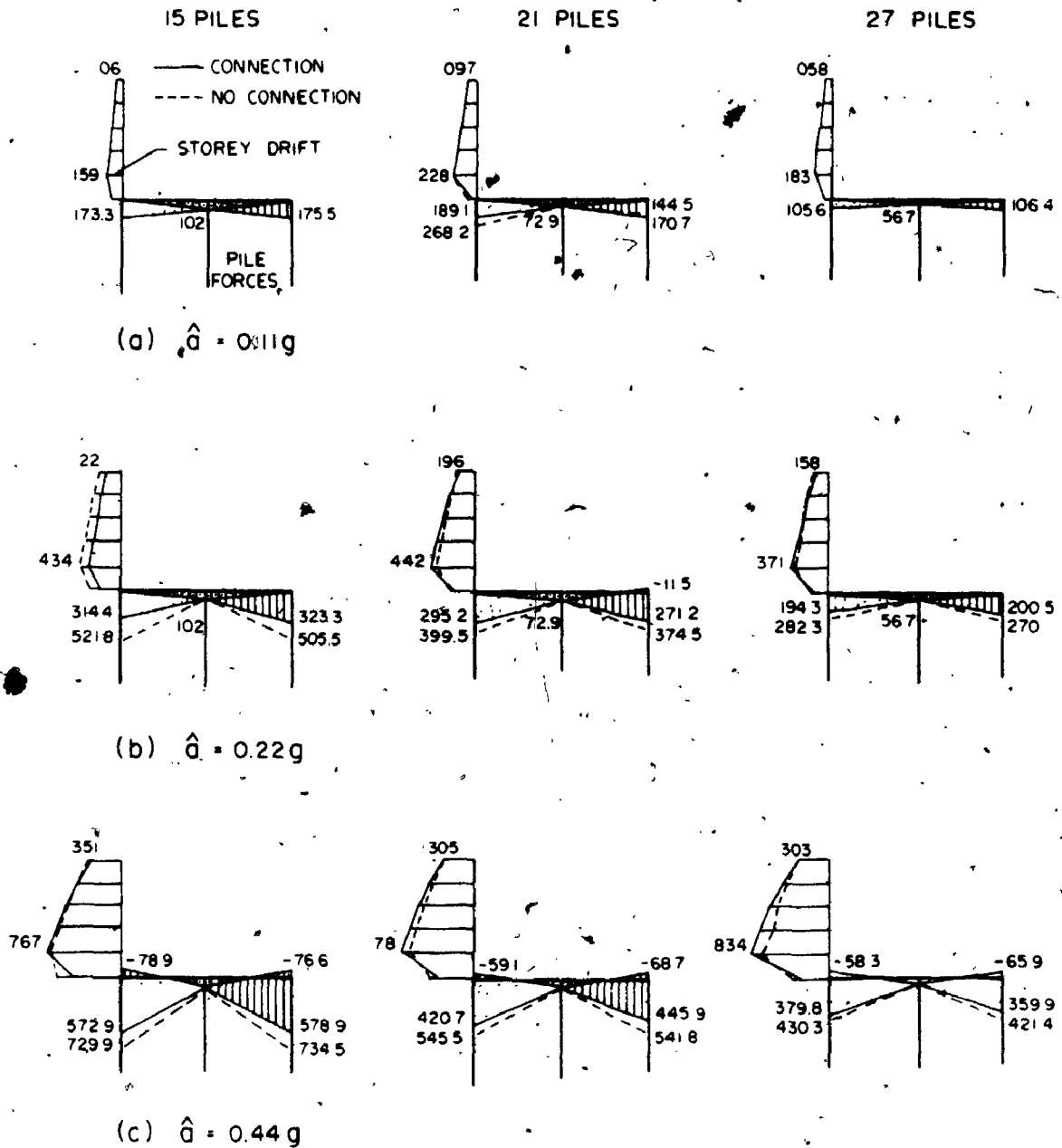


FIGURE 6.9a Pile Forces (kips) and Storey Drift (in) for Five-Storey Building Supported by 15, 21 and 27 Piles For Different Earthquake Intensity (Pinned Endbearing Piles)

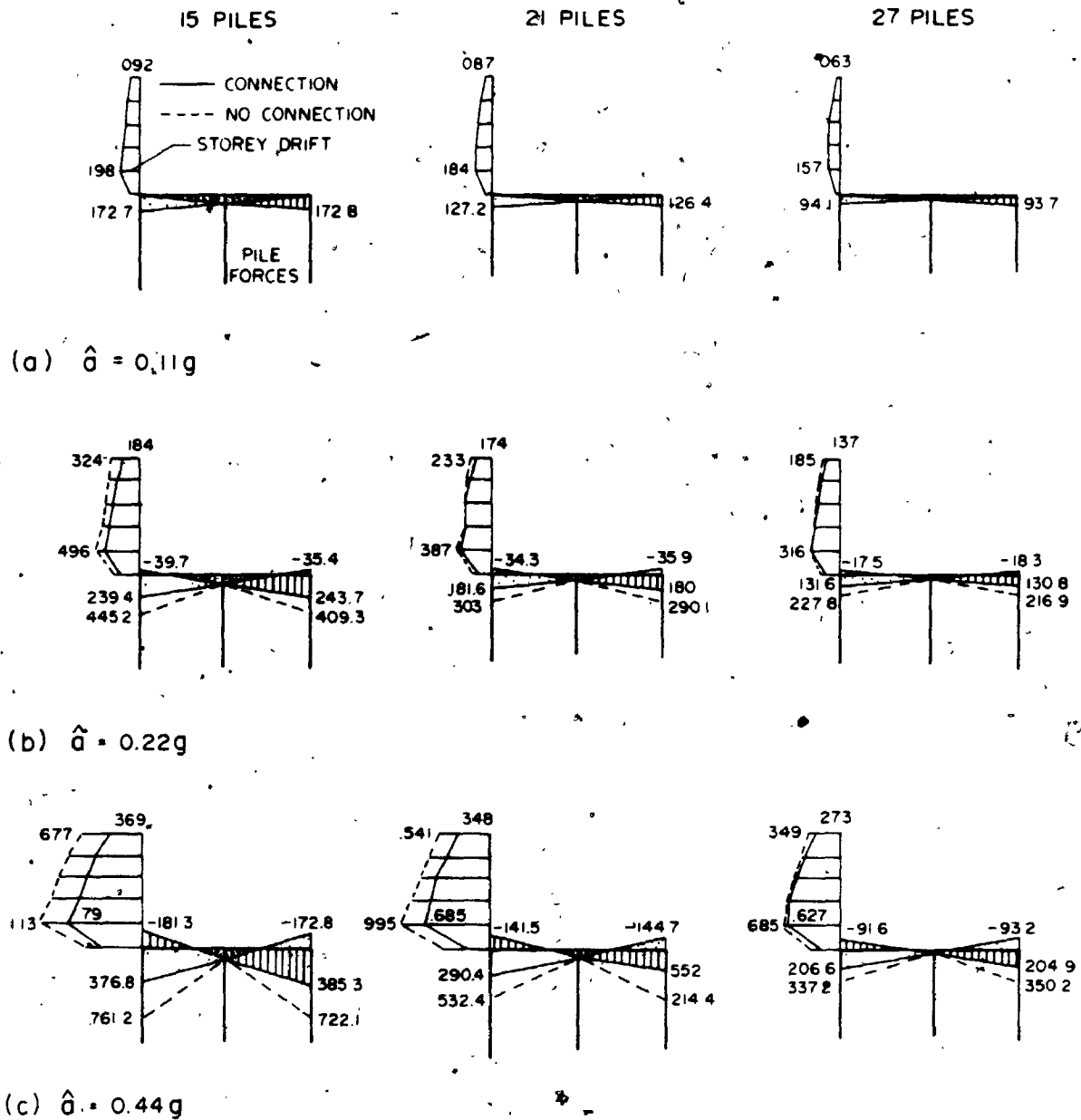


FIGURE 6.9b Pile Forces (kips) and Storey Drift (in) for Five-Storey Building Supported by 15, 21 and 27 Piles For Different Earthquake Intensity (Pinned Floating Piles)

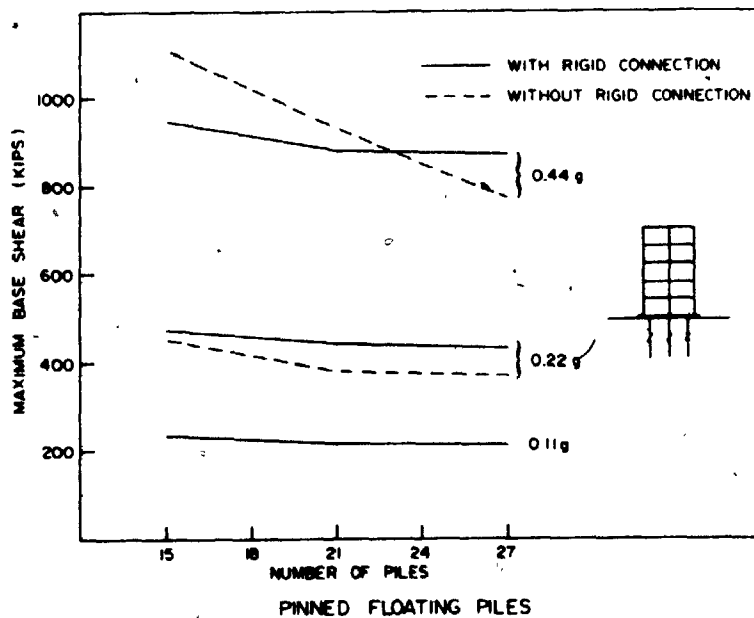
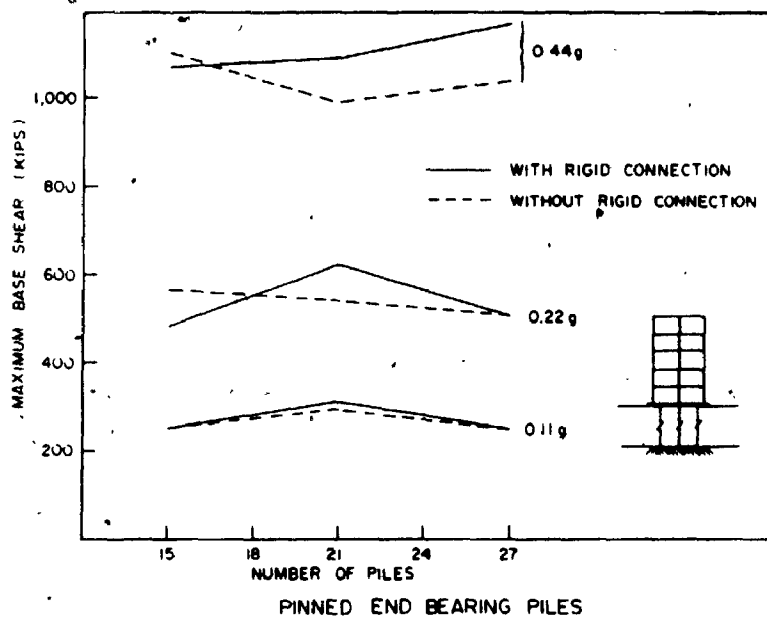


FIGURE 6.10a Base Shear of 5-Storey Building vs. Number and Type of Piles and Intensity of Ground Shaking (1 kip = 4.45 kN)

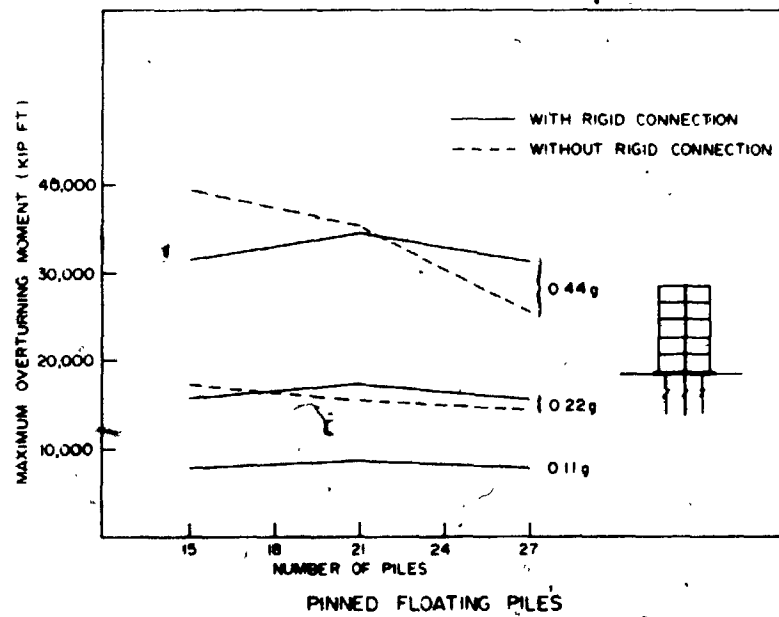
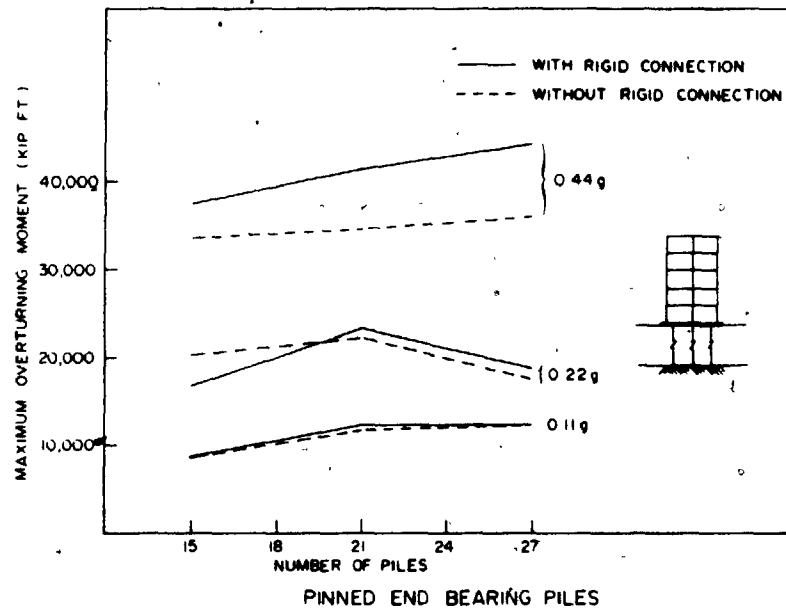


FIGURE 6.10b Overturning moment of 5-Storey Building vs. Number and Type of Piles and Intensity of Ground Shaking (1 kip.ft = 1.36 kN.m)

27 PINNED END BEARING PILES

27 PINNED FLOATING PILES

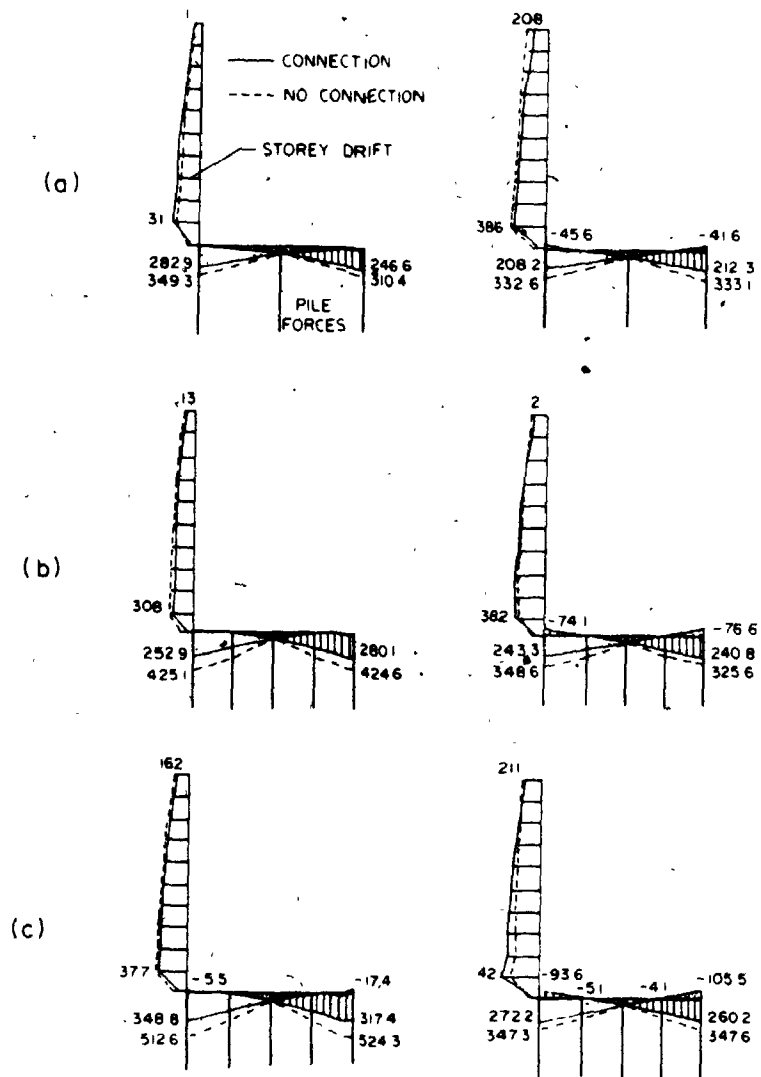


FIGURE 6.11a Pile Forces (kips) and Storey Drift (in) For Ten-Storey Building Supported by 27 Piles Arranged in Three or Five Rows ($\hat{a} = 0.11g$)

21 PINNED END BEARING PILES

21 PINNED FLOATING PILES

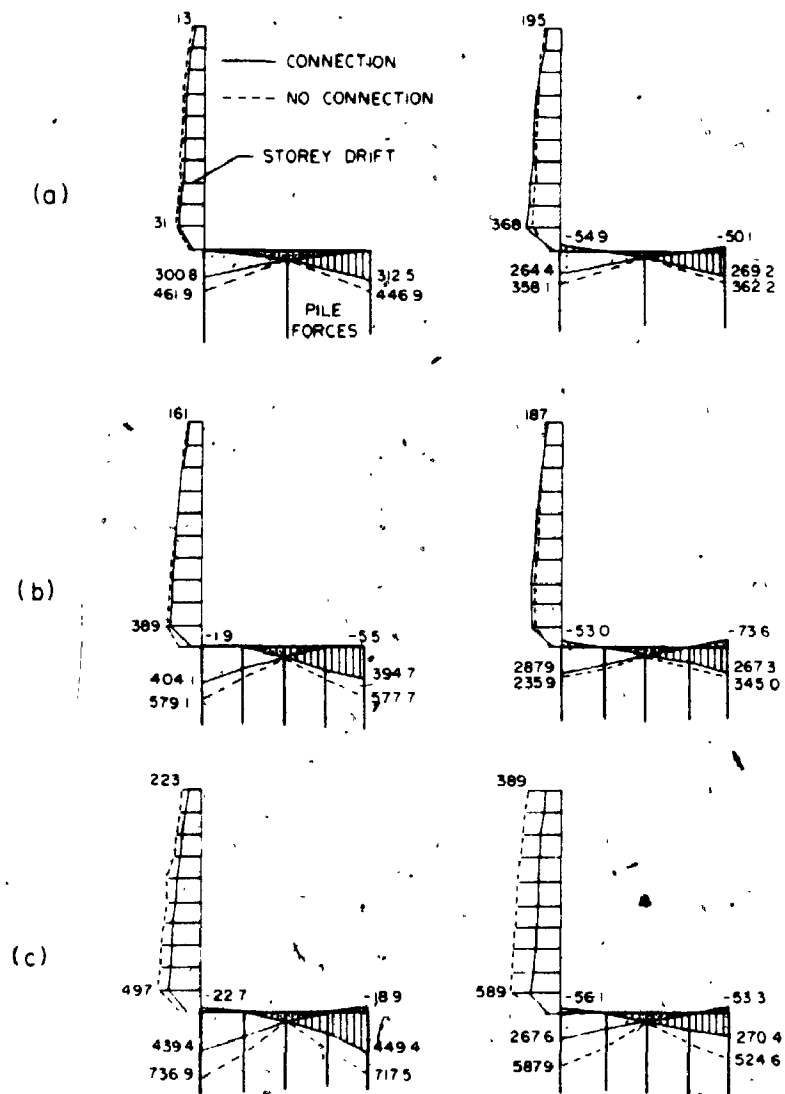
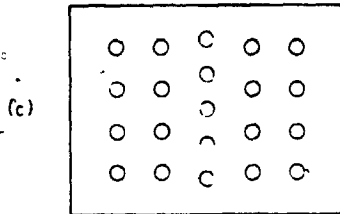
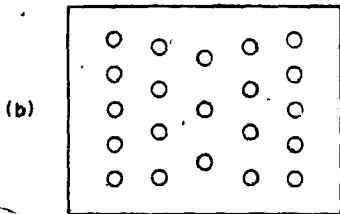
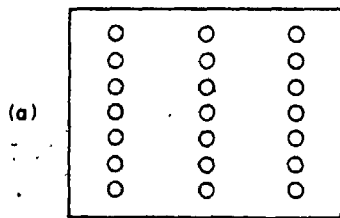
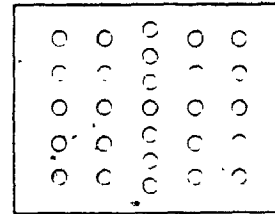
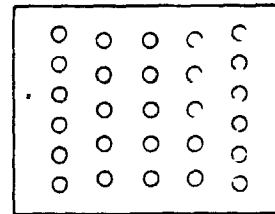
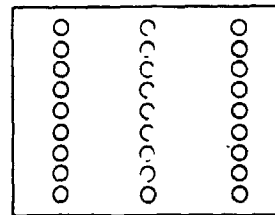


FIGURE 6.11b Pile Forces (kips) and Storey Drift (in) For Ten-Storey Building Supported by 21 Piles Arranged in Three or Five Rows ($\hat{a} = 0.11g$)



i) 21 piles



ii) 27 piles

FIGURE 6.12 Pile Configurations

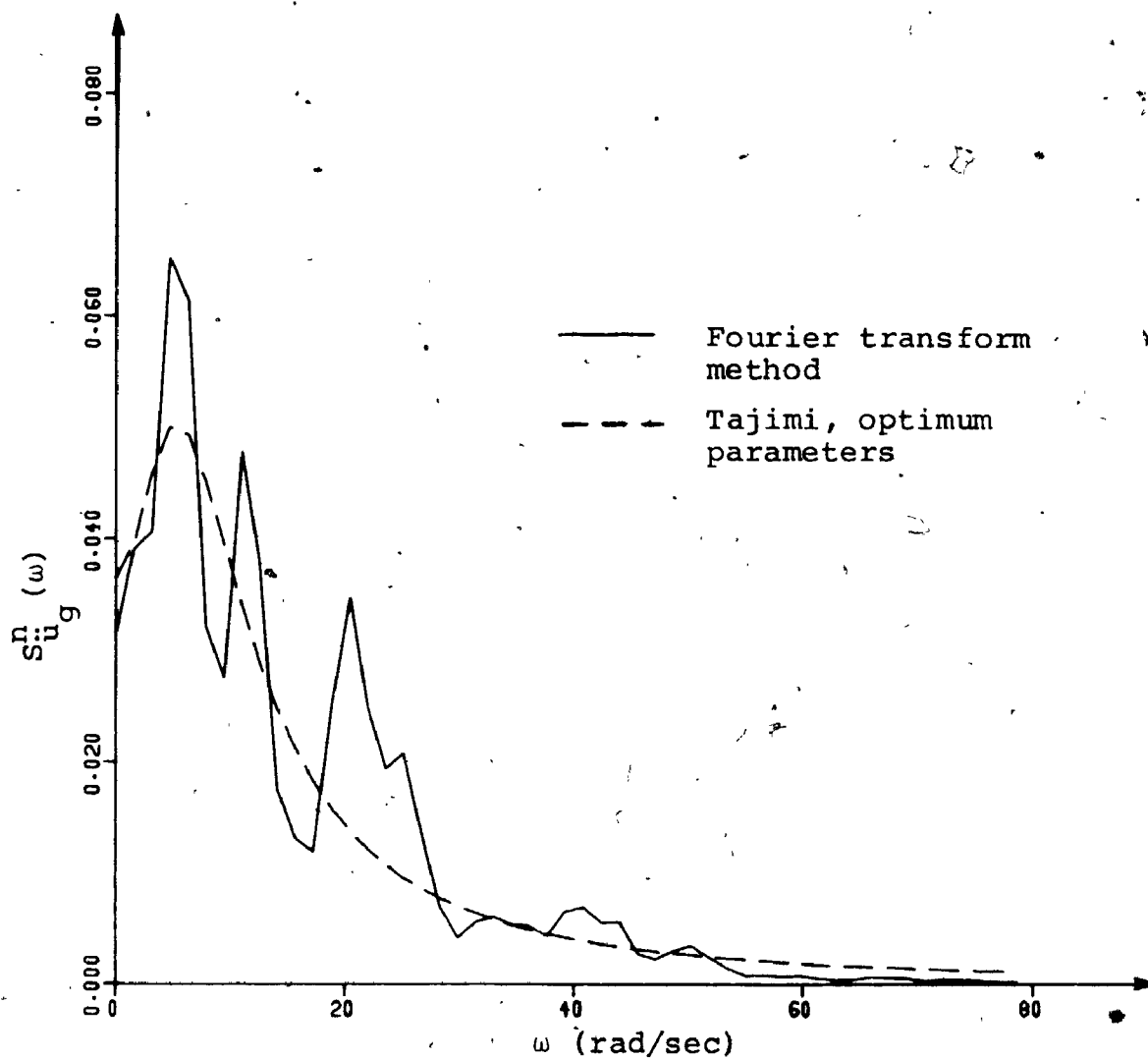


FIGURE 6.13 Power Spectrum for San Fernando Earthquake Acceleration

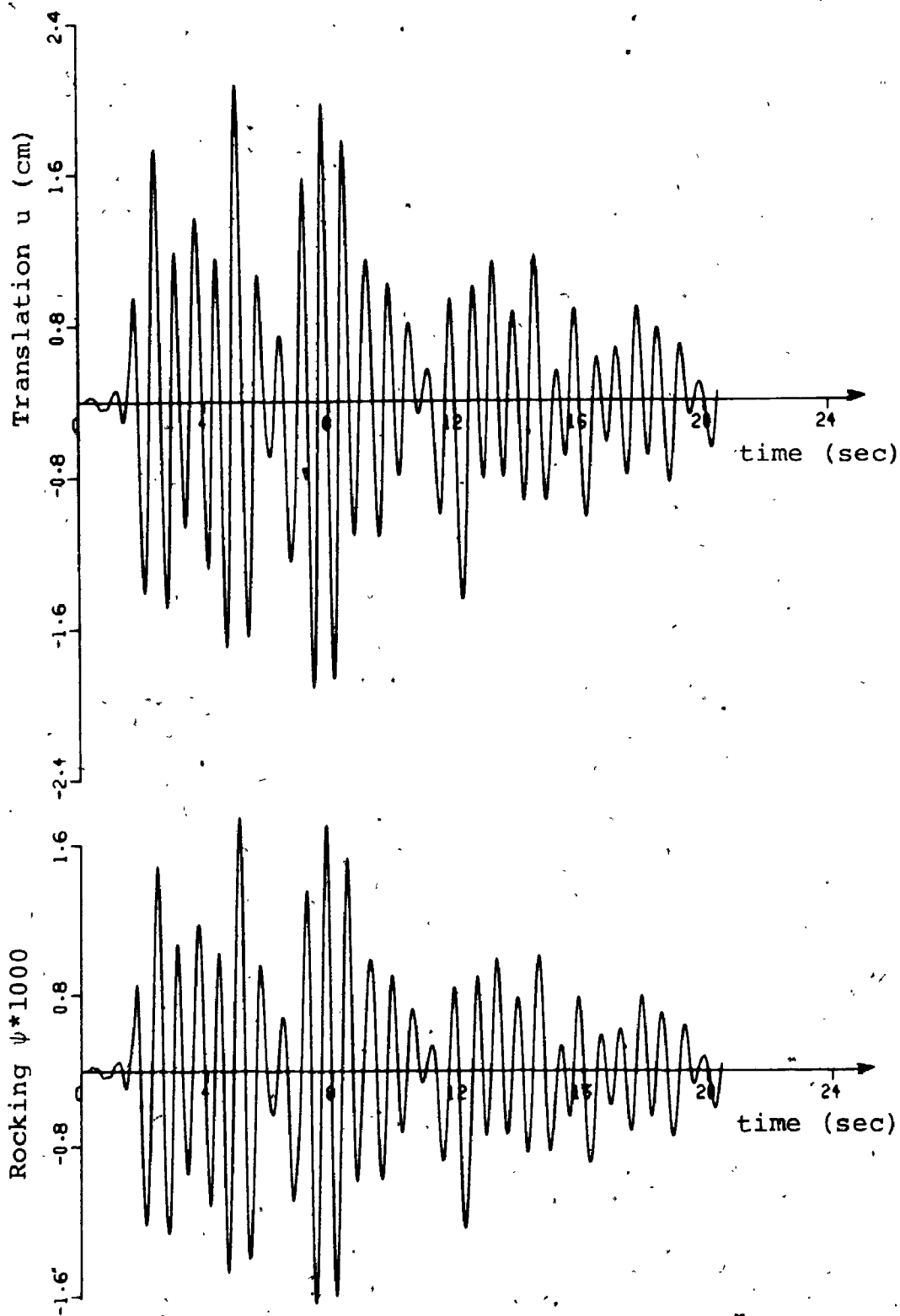


FIGURE 6.14 Response of Mat Supported Full Silo to Seismic Excitation: (a) Sliding in Horizontal Direction, u ; (b) Rocking in the Vertical Plane, ψ

CHAPTER 7

SOIL-STRUCTURE INTERACTION UNDER WIND LOADING

7.1 INTRODUCTION

The effect of the foundation flexibility on the structural response to dynamic loads has received much attention in machine foundations, e.g. (21) and earthquake engineering, e.g. (10). In wind engineering, soil-structure interaction is mostly either ignored or limited to the inclusion of soil flexibility into the calculation of natural frequencies and modes. Studies done by Novak (30, 102) support the contention that the effect of foundation on the structural response to wind may also be important.

For any form of aerodynamic excitation, the response can be analyzed either directly using Fourier analysis and other methods (103, 104, 105) or in terms of modal analysis (102, 105, 107). The latter approach offers great simplicity, since the structural response is quite often dominated by one modal component with the contribution of other modes being negligible.

In this chapter, the direct method is briefly reviewed

and then the effect of foundation flexibility on along-wind response is explored in detail using the more practical approach based on modal analysis and the concept of the gust factor.

7.2 TYPES OF AERODYNAMIC EXCITATION

The effect of soil-structure interaction on the response of a structure to dynamic loads depends not only on the properties of the structure foundation system but also on the type of excitation.

There are three main types of wind-induced oscillations experienced by structures (106):

1. Turbulence-induced oscillations. This type is due to turbulence in the oncoming flow. These oscillations may be described as gust induced oscillations. The gusts may cause longitudinal, transverse or torsional oscillations of the structure which monotonically increase with wind velocity. In this case, the excitation forces have the nature of a broad band random process.
2. Wake-induced oscillations. When the wind blows across a slender prismatic or cylindrical body, vortices are shed alternately from one side and then the other

giving rise to fluctuating forces acting at right angles to the wind direction along the length of the body. The resultant motion is known as vortex-induced oscillation. The excitation forces have the nature of a narrow band random process. A structure may be considered slender in this context if the ratio of height to diameter exceeds about 5. (108)

3. Galloping and flutter mechanisms. The final mechanism for excitation is associated with the movement of the structure itself. As the structure moves relative to the flow in response to the exciting forces, it changes the flow regime surrounding it and these changes are coupled with the motion.

A pressure change coupled with the velocity may be termed aerodynamic damping. It may either be positive or negative. If positive, it adds to the mechanical damping and leads to higher effective damping and a reduced tendency to vibrate; if negative, it can lead to instability and large amplitudes of motion. This type of excitation occurs with a wide variety of rectangular building shapes as well as bridge cross-sections and common structural shapes such as angles and I-sections.

In other instances, the coupling may be with either the displacement or acceleration, in which case its effects

are described as either aerodynamic stiffness or mass terms. The effect of this is to modify the stiffness or mass in the equation of motion. If the aerodynamic stiffness is negative, it may lead to a form of instability known as divergence. All types of instability feature a sudden start at a critical wind velocity and a rapid increase of violent displacements with wind velocity.

Typical variations of vibration amplitudes with wind velocity are shown for the three types of responses in Figure 7.1. The mechanism of excitation is different for each of the types shown and consequently, the foundation conditions affect the response to different degrees.

Since response of most structures can be attributed almost exclusively to turbulence in the oncoming wind, the gust-induced oscillation is considered as the basic type for design. The treatment of the transverse or torsional oscillations of the structure due to gusts is somewhat tentative but it could be guided through wind tunnel experiments. On the other hand, the longitudinal response of the structure due to turbulent gusty wind could be analyzed analytically by making use of the general methodology of random vibration (109, 103, 104).

The present work attempts to integrate the various aspects of the problem of along-wind response of structures on flexible foundation into three comprehensive approaches.

The first two approaches are rather complex and only the basic theoretical steps are outlined. The third approach, which is the design procedure known as the gust factor approach, is given in more detail and is applied to 10- and 20-storey buildings on mat foundations. Because the oscillations depend on the properties of wind, some basic wind characteristics are discussed first.

7.3 BASIC WIND CHARACTERISTICS

Wind is caused by differences in atmospheric pressure. At great altitude, the air motion is independent of the roughness of the ground surface and is called gradient or geostrophic wind. Its velocity, \bar{V}_G , is reached at the gradient height z_G which lies between 1,000 and 2,000 ft (≈ 305 to 610 m). Below the gradient height, the flow is affected by surface friction and the wind kinetic energy dissipates due to turbulence and air viscosity. The longitudinal component of the wind velocity below the gradient height consists of mean velocity, \bar{V}_z , plus an irregular turbulent component, $v(t)$. Hence, the longitudinal wind velocity at height z can be expressed as

$$V_z(t) = \bar{V}_z + v(t) \quad (7.1)$$

It was suggested by Davenport (110) that for most occasions of high wind, the mean wind speed \bar{V}_z at height z

(below z_G) can be described by the power law of the type:

$$\bar{V}_z = \bar{V}_G \left(\frac{z}{z_G}\right)^\alpha \quad (7/2)$$

where z_G and α are functions of the ground roughness which can be characterized by the surface drag coefficient κ . Suggested values of these quantities for three types of terrain are given in Figure 7.2. Another often used law is the theoretically substantiated logarithmic law. McNamara (111) found in his extensive investigation that the wind profiles are actually random.

The mean wind profiles are useful when predicting the wind speed at a particular site. To that end, the gradient wind speed is estimated using the wind profile and the wind speed registered by the nearest meteorological stations at the standard height, which is usually 33 ft (\approx 10 meters).

The mean wind velocity generally depends on the period over which the wind speed is averaged. Periods from 10 to 60 minutes appear adequate for engineering considerations and usually yield reasonably steady mean values. The same duration is suitable to define the fluctuating wind component. The fluctuating components of the wind change with height less than the mean wind and are random both in time and space. The random nature of the wind requires the application of statistical concepts.

The basic statistical characteristics of turbulent wind are the intensity of turbulence, σ_v/\bar{V}_z , where $\sigma_v = \sqrt{\overline{v^2}(t)}$ is the root-mean square velocity fluctuation in the longitudinal direction, the power spectral density $S_v(f)$, (f = frequency), the spatial correlation between velocities at different points $\gamma_{12}(f)$, and the probability distribution.

The spectrum of horizontal gustiness in strong wind is largely independent of height above the ground, and is proportional to both surface drag coefficient κ and the square of the mean velocity at the standard height of 10 meters, \bar{V}_{10} . Davenport (109) suggested to represent the spectrum, with some approximations, as

$$S_v(f) = \frac{4\kappa\bar{V}_{10}^2}{f} \frac{x^2}{(1+x^2)^{4/3}} \quad (7.3)$$

in which f = frequency, in Hz; κ is given in Figure 7.2.

and $x = \frac{Lf}{\bar{V}_{10}}$ where L = scale length \approx 4000 ft. (1220 meters).

This spectrum is shown in Figure 7.3. Other forms of spectrum have been proposed as well, e.g., by Harris (112), Simiu (113) etc., but they do not result in a significantly different response prediction.

The variance of the velocity fluctuation is

$$\sigma_v^2 = \int_0^{\infty} S_v(f) df \quad (7.4)$$

which for the spectrum represented by equation 7.3 yields

$$\sigma_v^2 = 6.0025 \kappa \bar{v}_{10}^2 \quad (7.5)$$

The spatial correlation of wind speed at two different stations 1 and 2 is described by the coherence function

$$\gamma_{12}^2(f) = \frac{|S_{12}(f)|^2}{S_1(f)S_2(f)} \leq 1 \quad (7.6)$$

where $S_{12}(f)$ = cross spectrum (generally complex) between stations 1 and 2; $S_1(f)$ and $S_2(f)$ are power spectra at the two stations. The coherence function depends primarily on the parameter $\Delta z f / \bar{v}$, where Δz = separation = $|z_1 - z_2|$ and $\bar{v} = \frac{1}{2}(\bar{v}_1 + \bar{v}_2)$ is the average wind speed. A simple empirical formula, often used to describe the coherence function, is

$$\sqrt{\text{coherence}} = e^{-c(\Delta z f / \bar{v})} \quad (7.7)$$

where c is a constant having a value of approximately 7 for vertical separation and approximately 15 for horizontal separation. Coherence is decreased with both frequency and separation.

For homogeneous flows, $S_1(f) = S_2(f) = S_v(f)$, and substituting equation 7.7 into equation 7.6 yields:

$$S_{12}(f) = S_v(f) e^{-c(\Delta z f / \bar{v})}$$

or

$$S_{12}(z_1, z_2, f) = S_v(f) e^{-\frac{cf}{\bar{v}} |z_1 - z_2|} \quad (7.8)$$

The probability density function of velocity fluctuations in turbulence can be considered approximately as Gaussian and defined as (Figure 7.4):

$$p(v) = \frac{1}{\sqrt{2\pi} \sigma_v} e^{-\frac{(v-\bar{v})^2}{2\sigma_v^2}} \quad (7.9)$$

Also shown in Figure 7.4 are the distribution for peak gust speeds in periods T defined by $\mu T = 100, 1000$ and $10,000$. The parameter μ is the effective cycling rate of the process which is given by the formula due to Rice (82):

$$\mu = \frac{\int_0^{\infty} f^2 S_v(f) df}{\int_0^{\infty} S_v(f) df} \quad (7.10)$$

A more detailed discussion of the wind characteristics is given in references (106, 110 and 112).

7.4 AERODYNAMIC FORCES DUE TO TURBULENCE

The relative motion between air particles and a building generates both drag and lift forces. The drag forces are responsible for the along-wind motion of the

building. If the face area, A , of the structure is small relative to the significant turbulent eddies, the so-called quasi-steady theory for turbulence can be used to estimate aerodynamic forces. Drag force in the along-wind direction is

$$\begin{aligned} F(t) &= \frac{1}{2} \rho c_D A v^2(t) \\ &= \frac{1}{2} \rho c_D A \bar{v}^2 \left[1 + 2 \frac{v(t)}{\bar{v}} + \frac{v^2(t)}{\bar{v}^2} \right] \end{aligned} \quad (7.11a)$$

where ρ = air density (normally equal to .0024 slugs/ft³ = 1.24 kg/m³), and c_D = drag coefficient. As $v(t) \ll \bar{v}$, the squared term may be ignored and equation 7.11a is written as

$$F(t) = \bar{F} \left[1 + 2 \frac{v(t)}{\bar{v}} \right] \quad (7.11b)$$

where \bar{F} is the mean drag (static component of the drag),

$$\bar{F} = \frac{1}{2} \rho c_D A \bar{v}^2 \quad (7.12)$$

The spectra of the fluctuating drag and velocity are then related as

$$S_F(f) = 4 \frac{\bar{F}^2}{\bar{v}^2} S_v(f) \quad (7.13)$$

With the information on the power spectrum, cross-correlation between different points and the probability distribution of the drag forces available, the response of structures on elastic foundations can be analyzed.

7.5 DIRECT SOLUTION

This method of solution dispenses the intermediate step of computing the normal modes and deals directly with both displacement and force types of structural response. The approach by Lin (103, 105) allows the analyzing of the along-wind induced vibrations of a multi-storey building by making use of the concept of transfer matrices (114). This method is especially suitable for tall buildings with every storey in the building identically constructed.

7.5.1 Formulation

The structural model used for this analysis is shown in Figure 7.5a. The following assumptions are made to simplify the analysis: (1) The structure is composed of N identical units typified by the one shown in Figure 7.5b; (2) the superstructure is linearly elastic; (3) wind excitations are applied at discrete floor levels; (4) damping is linear and viscous; (5) the soil behavior is characterized by the impedance matrix which is frequency dependent; and (6) the response of the structure to external excitation can be described by displacements and forces variable at each construction unit.

Let u_j and Q_{j-1} be, respectively, the displacement

at the floor and the shear force in the column of the j th unit (Figure 7.5c). It can be seen that

$$Q_j = Q_{j+1} + m(\ddot{u}_j + \ddot{u}_b + jh\ddot{\psi}) + c(\dot{u}_j + \dot{u}_b + jh\dot{\psi}) - F_j \quad (7.14)$$

$$Q_{j-1} = k(u_j^* - u_{j-1}) \quad (7.15)$$

in which m = the mass of the j th floor, c = aerodynamic damping coefficient related to absolute vibration velocity, and k = the stiffness which is complex-valued if the structural interstorey damping is taken into account.

The motion of the footing is governed by the following equations:

$$Q_b^- = m \sum_{j=1}^N \ddot{u}_j + (m_b + mN)\ddot{u}_b + mh\ddot{\psi} \sum_{j=1}^N j \quad (7.16a)$$

$$Q_b^+ = m \sum_{j=1}^N \ddot{u}_j + mN\ddot{u}_b + mh\ddot{\psi} \sum_{j=1}^N j \quad (7.16b)$$

for the horizontal direction and

$$\begin{aligned} mh \sum_{j=1}^N j \ddot{u}_j + mh\ddot{u}_b \sum_{j=1}^N j + (mh^2 \sum_{j=1}^N j^2 + I_t)\ddot{\psi} \\ + M_b = h \sum_{j=1}^N jF_j \end{aligned} \quad (7.17)$$

for the rocking direction. In these equations, m_b = mass of the footing, $I_t = \sum_{j=0}^N I_j$ with I_j being the inertia of the j th floor about its own centroidal axis; Q_b and M_b

respectively are reactive horizontal traction and base moment from the soil. Equations 7.16 and 7.17 can be re-written as

$$\dot{Q}_b^- - Q_b^+ = m_b \ddot{u}_b \quad (7.18)$$

$$M_b = h \sum_{j=1}^N j F_j - mh \sum_{j=1}^N j \ddot{u}_j - \frac{N(N+1)}{2} mh \ddot{u}_b - \left[\frac{N(N+1)(2N+1)}{6} mh^2 + I_t \right] \ddot{\psi} \quad (7.19)$$

Q_b^- and M_b are related to u_b and ψ as:

$$\begin{Bmatrix} Q_b^- \\ M_b \end{Bmatrix} = \begin{bmatrix} k_{xx} & k_{x\psi} \\ k_{\psi x} & k_{\psi\psi} \end{bmatrix} \begin{Bmatrix} u_b \\ \psi \end{Bmatrix} \quad (7.20)$$

where the k-matrix may be frequency dependent. Taking the Fourier transform and rearranging the terms, equations 7.14, 7.15 and 7.18, 7.19 may be written in a matrix form as follows:

$$\begin{Bmatrix} \bar{u}_j \\ \bar{Q}_j \end{Bmatrix} = \begin{bmatrix} 1 & 1/k \\ (-m\omega^2 + ic\omega) & 1 + \frac{1}{k}(-m\omega^2 + ic\omega) \end{bmatrix} \begin{Bmatrix} \bar{u}_{j-1} \\ \bar{Q}_{j-1} \end{Bmatrix} + (-m\omega^2 + ic\omega) \begin{Bmatrix} 0 \\ \bar{u}_b + jh\bar{\psi} \end{Bmatrix} - \begin{Bmatrix} 0 \\ \bar{F}_j \end{Bmatrix} \quad (7.21)$$

$$\begin{Bmatrix} \bar{Q}_b \\ \bar{M}_b \end{Bmatrix} = \begin{bmatrix} 0 & -m\omega^2 & 0 \\ mh\omega^2 & \frac{N(N+1)}{2} m\omega^2 h & [I_t + \frac{N(N+1)(2N+1)}{6} mh^2] \omega^2 \end{bmatrix} \begin{Bmatrix} \sum_{j=1}^N j \bar{u}_j \\ \bar{u}_b \\ \bar{\psi} \end{Bmatrix} \\
 + \begin{bmatrix} 1 & 0 \\ 0 & h \end{bmatrix} \begin{Bmatrix} \bar{Q}_b^+ \\ N \\ \sum_{j=1}^N j \bar{F}_j \end{Bmatrix} \quad (7.22)$$

where $i = \sqrt{-1}$; and an overbar denotes the Fourier transform. Equation 7.21 may be written more concisely as:

$$\{z\}_j = [T]\{z\}_{j-1} + (-\omega^2 m + i\omega c) \begin{Bmatrix} 0 \\ \bar{u}_b + jh\bar{\psi} \end{Bmatrix} - \begin{Bmatrix} 0 \\ \bar{F}_j \end{Bmatrix} \quad (7.23)$$

in which $\{z\}_j = \langle \bar{u}_j, \bar{Q}_j \rangle$ = a state vector; and $[T]$ is known as the transfer matrix. The matrix $[T]$ represents the transfer mechanism of a construction unit.

Equation 7.23 can be applied repeatedly to obtain a relation between $\{z\}_0$ and $\{z\}_N$; namely:

$$\{z\}_N = [T]^N \{z\}_0 + (-m\omega^2 + i\omega c) \sum_{j=1}^N [T]^{N-j} \begin{Bmatrix} 0 \\ \bar{u}_b + jh\bar{\psi} \end{Bmatrix} \\
 - \sum_{j=1}^N [T]^{N-j} \begin{Bmatrix} 0 \\ \bar{F}_j \end{Bmatrix} \quad (7.24)$$

With the boundary conditions $u_0 = u_b$, and $Q_N^+ = 0$, the vectors $\{z\}_N$ and $\{z\}_0$ at the base and at the top floor of the building dictate that

$$\{z\}_0 = \begin{Bmatrix} \bar{u}_b \\ \bar{Q}_b^- \end{Bmatrix} ; \quad \{z\}_N = \begin{Bmatrix} \bar{u}_N \\ 0 \end{Bmatrix} \quad (7.25)$$

Substituting equation 7.25 into equation 7.24 and making use of equation 7.20 which relates u_b and ψ to Q_b^- and M_b , the solution can be obtained in the frequency domain in which the \bar{F}_j ($j = 1, 2, \dots, N$) are the inputs and $\{z\}_\ell$ the outputs at the ℓ th floor. $\{z\}_\ell$ can be obtained from equation 7.24 by replacing N by ℓ .

The solution can be put in a closed form by making use of the fact that the eigenvalues of the matrix $[T]$ in equation 7.23 are reciprocal (115) and can be put in the form, $\exp(\pm i\theta)$, where

$$\cos\theta = 1 + \frac{-m\omega^2 + ic\omega}{2k} \quad (7.26)$$

7.5.2 Spectral Relationship

When the wind loads on a building are modeled as stochastic process, the inputs \bar{F}_j ($j = 1, 2, \dots, N$) in equation 7.24 are Fourier transform of stochastic process. If the wind loads $F(t)$ are assumed to be statistically stationary in time (may be assumed to have commenced at

$t = -\infty$ and must be presumed to continue until $t = \infty$) then their Fourier transforms do not exist. There is no difficulty, however, in determining the Fourier transform of a signal $F'(t)$ which is defined to be identical with $F(t)$ over the interval $-\frac{T}{2} < t < \frac{T}{2}$ and to be zero at all other times. In this case, equation 7.24 can still be used conveniently to construct spectral relationship between the inputs and outputs. For example, the spectral density of the random displacement u_j at the j th floor, denoted by $S_{u_j u_j}(\omega)$, can be obtained by multiplying the first row in equation 7.24 by its conjugate. This equation results in a very lengthy formula given in (104). The cross-spectral density $S_{F_r F_q}(\omega)$ of the wind loads $F_r(t)$ and $F_q(t)$ at stations r and q is given by equations 7.11 and 7.13 as

$$S_{F_r F_q}(\omega) = \bar{F}_r \bar{F}_q [\delta(\omega) + 4 S_{v_r v_q}(\omega)] \quad (7.27)$$

in which $\delta(\) =$ Dirac delta function and $S_{v_r v_q}(\omega) =$ cross-spectral density of the nondimensional random processes $v_r(t)$ and $v_q(t)$ obtained from equations 7.3 and 7.8 as

$$S_{v_r v_q}(\omega) = \frac{4k \bar{V}_{10}^2}{\bar{V}_r(t) \bar{V}_q(t) |\omega|} \frac{\left(\frac{610\omega}{\pi \bar{V}_{10}}\right)^2}{\left[1 + \left(\frac{610\omega}{\pi \bar{V}_{10}}\right)^2\right]^{4/3}} \exp\left(-\frac{c |\omega| \cdot |r-q|h}{2\pi \bar{V}_{10}}\right) \quad (7.28)$$

in which \bar{V}_r , \bar{V}_q , \bar{V}_{10} are in m/sec. Having equations 7.28 and 7.27 and the spectral expression for $S_{u_j u_j}$, one can obtain the frequency spectra of floor displacements and shear forces.

In this way, a closed form solution for the displacement and shear force at each storey unit in the structure is made possible by making use of the transfer matrices. However, despite the fact that each matrix [T] is only 2 x 2, the response equations are very complicated and may only be evaluated using the computer.

Lin (103, 104) gives these reasons for adopting this direct solution: (1) the calculation of normal modes for complicated structures is extremely difficult and time consuming; and (2) the magnitude of damping in each mode must be assumed and is rather arbitrary. However, these arguments do not seem to be completely justified. As outlined in Chapter 3, the normal mode prediction is straightforward and the damping associated with each vibration mode can be calculated accurately. Also, for a complicated structure, the shear building model is not applicable. Finally, the structural response to wind loading is dominated by only the first few modes. This is particularly so with flexible foundations which provide heavy damping in the higher modes.

The direct solution is presented here for completeness but it is far more advantageous to use normal modes to express the structural response to fluctuating wind as will be outlined in the next two subchapters.

7.6 PREDICTION OF FLUCTUATING RESPONSE USING MODAL ANALYSIS

This approach is preferred by researchers and practising engineers (106, 109, 110). It enables the peak stresses, accelerations, deflections, etc., to be expressed in terms of the mean wind velocity (equation 7.2), the spectrum of the gustiness (equations 7.3 and 7.8), and the mechanical and aerodynamic properties of the structure. In this case of the wind treated as a random input, the resultant spectrum of the wind force must be evaluated with regard to spatial correlation of wind velocity. This effect can be described in terms of another transfer function called the 'aerodynamic admittance function', $|X_{\text{aero}}(f)|^2$. This function describes how the turbulence in the wind is modified by its encounter with the building. Then the modified drag spectrum (equation 7.13) is

$$S_F(f) = 4 \frac{\bar{F}^2}{\bar{V}^2} |X_{\text{aero}}(f)|^2 S_V(f) \quad (7.29)$$

7.6.1 Response of a Single Degree of Freedom System

If the forces defined by equation 7.29 act on a structure modeled as an elastic spring-mass-damper system, the response, u , has the spectrum

$$\begin{aligned} S_u(f) &= \bar{u}^2 |X_{\text{aero}}|^2 |X_{\text{mech}}|^2 \frac{4S_v(f)}{\bar{V}^2} \\ &= \frac{4\bar{F}^2}{\bar{V}^2} |X_{\text{aero}}|^2 |X_{\text{mech}}|^2 \frac{1}{k^2} S_v(f) \end{aligned} \quad (7.30)$$

where static deflection $\bar{u} = \bar{F}/k$, $k =$ stiffness constant, and the mechanical admittance function

$$|X_{\text{mech}}|^2 = \frac{1}{[1 - (f/f_0)^2]^2 + 4D(f/f_0)^2} \quad (7.31)$$

where $D =$ critical damping ratio, and $f_0 =$ natural frequency of the system.

The transition from the spectrum of the wind-velocity fluctuation to the spectrum of the response defined by equation 7.30 is shown diagrammatically in Figure 7.6. The variance of the response σ_u^2 is obtained from the spectrum of the response,

$$\sigma_u^2 = \int_0^{\infty} S_u(f) df \quad (7.31)$$

The above relationships describe the mean \bar{u} and the variance σ_u^2 of the response. For engineering purposes, it is also useful to define the extreme values. It is

usually satisfactory to assume the process in question is Gaussian with probability density function given by

$$p(u) = \frac{1}{\sqrt{2\pi} \sigma_u} e^{-\frac{(u-\bar{u})^2}{2\sigma_u^2}} \quad (7.32)$$

This distribution is fully described by the mean and the variance. The expected peak value of the response during a period, T , can be written as

$$u_{\max} = \bar{u} + g \sigma_u \quad (7.33)$$

where g = peak factor given by the relation (80,109)

$$g = \sqrt{2 \ln \mu T} + \frac{0.5772}{\sqrt{2 \ln \mu T}} \quad (7.34)$$

where μT is defined earlier in Figure 7.4 as the average number of times the mean value of the displacement (or load) is crossed during the averaging time T . μ (apparent frequency) depends on the spectrum and is obtained from equation 7.10. As can be seen from Figure 7.4, when the period T or the frequency μ increases, the expected peak displacement also increases. The factor g usually ranges between 3 and 5.

7.6.2 Response of Multi Degree of Freedom Systems

For multi degree of freedom systems the concept includes the cross-correlation of the wind loads at different

stations (e.g., heights), the properties of the vibration mode, and the nonuniformity of the mean flow. These factors can be conveniently included into the solution formulated in terms of modal analysis.

With a prismatic one dimensional structure, the response may be expressed in the form

$$u(z,t) = \sum_{j=1}^{\infty} n_j(t) \phi_j(z) \quad (7.35)$$

where $n_j(t)$ = the generalized coordinate and $\phi_j(t)$ = the natural vibration mode chosen to an arbitrary scale. The generalized coordinates are given by

$$M_j \ddot{n}_j + 4\pi D_j f_j M_j \dot{n}_j + k_j n_j = p_j(t) \quad (7.36)$$

where $M_j = \int_0^H m(z) \phi_j^2(z) dz$, $k_j = 4\pi^2 f_j^2 M_j$, D_j = modal damping ratio, f_j = j th natural frequency, $m(z)$ = mass of structure per unit length and $p_j(t)$ = generalized force

$$p_j(t) = \int_0^H p_j(z,t) \phi_j(z) dz \quad (7.37)$$

in which $p(z,t)$ is the load per unit length and H = height of the structure.

Squaring and averaging equation 7.35 gives the mean-square displacement (the variance) as

$$\overline{u^2(z,t)} = \sum_{i=1}^{\infty} \sum_{j=1}^{\infty} \overline{n_i n_j} \phi_i(z) \phi_j(z) \quad (7.38a)$$

However, in slightly damped systems with well separated frequencies, the cross-correlation terms are insignificant and can be neglected. Then the double series in equation 7.38a reduces to a simple series,

$$\overline{u^2(z,t)} = \sum_{j=1}^{\infty} \overline{n_j^2} \phi_j^2(z) \quad (7.38b)$$

The variance of the generalized coordinate $\overline{n_j^2}$ is determined from equation 7.36 if the power spectrum of the generalized force $p_j(t)$ is known. When the lateral dimension of the structure is small, only cross-correlation in direction z needs to be considered. Then the power spectrum of the generalized force is

$$S_{p_j}(f) = \int_0^H \int_0^H S_{12}(z_1, z_2, f) \phi_j(z_1) \phi_j(z_2) dz_1 dz_2 \quad (7.39)$$

where $S_{12}(z_1, z_2, f)$ = cross spectrum of the wind loads at heights z_1 and z_2 . With respect to equations 7.8 and 7.13, the cross spectrum of the wind loads can be expressed in terms of the cross spectrum of the wind speed as

$$S_{12}(z_1, z_2, f) = \frac{\bar{F}^2}{\bar{V}^2} S_v(f) e^{-\frac{cf}{\bar{V}} |z_1 - z_2|} \quad (7.40)$$

where $S_v(f)$ = power spectrum of the wind speed defined by equation 7.3 and \bar{F} and \bar{V} are taken as independent of height.

Then the spectrum of the generalized force is

$$S_{p_j}(f) = 4 \frac{\bar{F}_j^2}{\bar{V}^2} S_V(f) \int_0^H \int_0^H e^{-\frac{cf}{\bar{V}} |z_2 - z_1|} \phi_j(z_1) \phi_j(z_2) dz_1 dz_2 \quad (7.41)$$

The spectrum of the generalized coordinate n_j is as in a single degree of freedom system with $k_j = (2\pi f_j)^2 M_j$,

$$\begin{aligned} S_{n_j}(f) &= \frac{1}{k_j^2} |x_{\text{mech}_j}(f)|^2 S_{p_j}(f) \\ &= \frac{S_{p_j}(f)}{(2\pi f_j)^4 M_j^2 \{ [1 - (\frac{f}{f_j})^2]^2 + 4D_j^2 (\frac{f}{f_j})^2 \}} \end{aligned} \quad (7.42)$$

Then the variance of n_j is

$$\begin{aligned} \overline{n_j^2} &= \int_0^\infty \frac{1}{k_j^2} \frac{1}{[1 - (f/f_j)^2]^2 + 4D_j^2 (f/f_j)^2} S_{p_j}(f) df \\ &= \frac{1}{k_j^2} \frac{\pi}{4} \frac{f_j}{D_j} S_{p_j}(f_j) + \frac{1}{k_j^2} \int_0^{f_j} S_{p_j}(f) df \end{aligned} \quad (7.43)$$

The approximate integration of equation 7.43 yields the response composed of two parts, the resonance effect (the first term) and the background turbulence effect (the second term) (Figure 7.7). The response variance follows from equation 7.38b, and its standard deviation (rms dynamic displacement) is

$$\sigma_u(z) = \sqrt{\overline{u^2}(z,t)} \quad (7.44)$$

The peak response is established from equation 7.33 by means of peak factor g (equation 7.34). The mean deflection $\bar{u}(z)$ is the static deflection due to the mean wind speed \bar{V}_z .

In application to buildings and free-standing towers, the analysis can usually be limited to the first modal component in equation 7.38b.

For structures which are not very slender, the cross-correlation of the wind pressures in the horizontal direction also has to be accounted for as the pressure on an area $A = H \times b$ is $p(z, x, t)$. The spectrum of the total load $P(t)$ may be written as

$$S_p(f) = \int_0^H \int_0^H \int_0^b \int_0^b S_{p_1 p_2}(z_1, z_2, x_1, x_2, f) dz_1 dz_2 dx_1 dx_2 \quad (7.45)$$

in which $S_{p_1 p_2}(z_1, z_2, x_1, x_2, f)$ is the cross-spectrum of the load per unit length at positions (z_1, x_1) and (z_2, x_2) . Davenport (116) derived an approximate expression for generalized drag forces acting on buildings and structures with significant lateral dimensions. Davenport (106, 116) also gave a complete solution established by means of simplifying assumptions and numerical integration. This simplified solution is known as the gust factor approach and is outlined below.

7.7 GUST FACTOR APPROACH

The gust factor approach is a design procedure derived on the basis of the above theory by means of a few simplifying assumptions (108, 117, 118). It considers only the response in the first vibration mode which is assumed to be linear. These assumptions are particularly suitable for buildings. The method yields all the data needed in design: the maximum response, the equivalent static wind load that would produce the same maximum response, and the maximum acceleration needed for the evaluation of the physiological effects of strong winds (human comfort).

The gust factor G is, as defined by Davenport (118), the ratio of the expected peak displacement (load) in a period T to the mean displacement (load) \bar{u} . Hence, maximum expected response

$$u_{\max} = G \bar{u} = \left(1 + g \frac{\sigma_u}{\bar{u}}\right) \bar{u} \quad (7.46)$$

Similar approaches have been proposed by others but these can all be reduced to the same form of equation 7.46. The Canadian National Building Code (108) has adopted this approach and gives the gust factor G as

$$G = 1 + g \sqrt{\frac{\kappa}{c_e} \left(B + \frac{SF}{D^t}\right)} \quad (7.47)$$

where g = peak factor, κ = roughness factor, c_e = exposure factor, B = the background turbulence effect and $\frac{SF}{D^t}$ = the resonance effect, in which F = gust energy ratio, S = size reduction factor, and D^t = total modal damping of the structure. For a flexible foundation the total damping of the structure can be evaluated as shown in Chapter 3. An explanation of these factors follows (109).

1. The peak factor, g , (Figure 7.8) is a function of the average fluctuation rate, μ , and the averaging period, T , which typically is a period between 5 minutes and 1 hour. The average fluctuation rate follows from equations 7.3 and 7.10 as,

$$\mu = f_o \sqrt{\frac{SF/D^t}{B+SF/D^t}} \quad (7.48)$$

where f_o = the natural frequency.

2. The roughness factor, κ , is equal to
 - 0.08 for open terrain (Zone A)
 - 0.10 for suburban, or wooded terrain (Zone B)
 - 0.14 for concentrations of tall buildings (Zone C).
3. Exposure factor, c_e , is based on the mean speed profile (Figure 7.2) and thus on surface roughness. For the three zones, the exposure factor is obtained from Figure 7.9 for the height of the building H . c_e relates to wind pressure rather than speed. Hence,

the mean wind speed at the top of the building is given by

$$\bar{V}_H = \bar{V}_{10} \sqrt{c_e} \quad (7.49)$$

where \bar{V}_{10} = reference wind speed at the standard height of 10 meters; \bar{V}_{10} can be obtained from meteorological stations.

Factor κ/c_e can be thought of as scaling the result for the appropriate input turbulence level.

4. The background turbulence factor, B , is obtained from Figure 7.10 as a function of height, H , and width, W , of the windward face of the structure.
5. The size reduction factor, S , (Figure 7.11) depends on the reduced frequency $f_o H/\bar{V}_H$ and the width to the height ratio W/H .
6. The gust energy factor, F , (Figure 7.12) is a function of the wave number at resonance, f_o/\bar{V}_H . Factor F represents the spectrum of the wind speed given in equation 7.3.
7. The total damping ratio, D^t , depends on the structural damping D^s , damping due to energy dissipation in soil, D , and aerodynamic damping, D^a . Typical values for structural damping for structures on rigid

foundations are:

concrete structures: $D^S = 0.01 - 0.02$

steel structures: $D^S = 0.005 - 0.01$

Soil damping, D , can be calculated from equation 3.4. Aerodynamic damping can be obtained from the approximate formula given by Davenport (119) for the case of building:

$$D^a = \frac{3 \rho c_D \bar{V}_H}{4\pi(3+\alpha) f_o \rho_b b} \quad (7.50)$$

in which

ρ_b = equivalent density of building

= total mass/total volume

b = depth of building (direction of wind)

α = exponent of velocity profile appearing
in Figure 7.9

f_o = fundamental frequency of the structure on
flexible foundation

and ρ and c_D were defined earlier.

7.7.1 Design Wind Pressure

The parameters given above yield the design wind pressure p , which produces displacement u_{\max} if applied as a static load. This design pressure is

$$p = q c_e G c_p \quad (7.51)$$

where $q = 1/2 \rho \bar{v}_{10}^2$ is the reference mean velocity pressure, and c_p = average pressure coefficient, which depends on the shape of the structure and the flow pattern around it. For a typical building with a flat roof and a height greater than twice the width, the coefficients are given for the windward and leeward faces in Figure 7.13 together with the pressure distribution. Exposure factor, c_e , varies continuously with elevation according to Figure 7.9 for pressures acting on the windward face of the structure; for the leeward face, c_e is constant and is evaluated at one-half the height of the building.

7.7.2 Wind Induced Building Motion

While it is generally found that the maximum wind loading and deflection are in the direction of the wind (the along-wind direction), the maximum acceleration of motion or even discomfort may occur in the direction perpendicular to wind (across-wind direction). While the theory for the along-wind response is well developed, the across-wind response can only be predicted much less reliably and is best treated experimentally or empirically.

It has been found that the across-wind accelerations are likely to exceed along-wind acceleration if the building is slender about both axes, that is if \sqrt{Wb}/H is less than 1/3, where W and b are the across-wind and along-wind

plan dimensions. The peak across-wind acceleration, a_w , at the top of the building can be found from the following formula, based on a wide range of turbulent boundary layer wind tunnel studies (108, 120)

$$a_w = f_o^2 g \sqrt{wb} \left(\frac{a_r}{\rho_b g_o \sqrt{D^t}} \right) \quad (7.52)$$

where $a_r = 78.5 \times 10^{-6} [\bar{V}_H / (f_o \sqrt{wb})]^{3.3}$, kN/m^3 , ρ_b is in kg/m^3 , D^t is the total damping ratio pertinent to the first vibration mode, and $g_o = \text{acceleration due to gravity} = 9.81 \text{ m/s}^2$.

For less slender structures or for lower wind speeds, the maximum acceleration may be in the along-wind direction, a_D , and can be found from the expression for the gust effect factor assuming approximately that acceleration equals the frequency squared times the peak displacement due to turbulence with the background effect ignored. Thus, (106, 108)

$$a_D = (4\pi^2 f_o^2) \left(\frac{u_{\max}}{G} \right) \left(g \sqrt{\frac{\kappa S F^2}{c_e D^t}} \right) \quad (7.53)$$

where u_{\max} = maximum top deflection under the design pressure p . The other parameters are equal to those used in equation 7.47.

When the maximum acceleration exceeds one percent of gravity or even less, the motion is usually perceptible

(120).

7.8 SOIL-STRUCTURE INTERACTION UNDER GUSTING WIND

In this work, the gust factor approach, outlined above, is used to examine the effect of soil-structure interaction on response to gusting wind. This is of interest because the gust factor approach is widely used and experimental work done at The University of Western Ontario and elsewhere verified the results of this method both on full scale structures in the natural wind and on models. Also, the gust factor approach is adopted in the National Building Code of Canada and in only a slightly different form in a few other codes.

As was shown in Chapter 3, flexibility of the foundation affects the natural frequencies and modal damping ratios. An examination of equation 7.47 reveals that foundation flexibility affects the factors g , S , F and D^t . As the soil stiffness decreases the natural frequency, f_o , decreases and the total damping D^t increases. The reduction in natural frequency for a certain building due to soil flexibility results in a few effects: increase in the size reduction factor S (Figure 7.11), decrease in the peak factor g (Figure 7.8), and increase or decrease in the gust energy factor F (Figure 7.12). Consequently, the net result

is to reduce or enhance the gust factor G and hence the loading and the response of the building. This trend of the soil-structure interaction effects depends on all the factors involved, i.e. soil, footing, structure, and the wind characteristics.

7.8.1 Design Wind Loads and Maximum Response

The design wind pressure p given by equation 7.51 is used to produce the equivalent static wind forces F_i at each floor i (Figure 7.14) as

$$F_i = p_i \cdot W \cdot \ell_i \quad i = 0, 1, 2, \dots, N \quad (7.54)$$

where ℓ_i is the tributary height of floor i and W is the width of the building. The base shear and overturning moment are given by

$$Q_b = \sum_{i=0}^N F_i \quad (7.55)$$

$$M_b = \sum_{i=0}^N F_i \cdot h_i$$

These forces, applied to the structure on flexible foundation, yield the total maximum displacements. These are given by the relative displacements, u_i , and the base displacements u_b, ψ for which the equilibrium conditions can be written as

$$\{u\} = [k]^{-1} \{P\} \quad (7.56)$$

in which

$$\{u\} = \langle u_1 \ u_2 \ u_3 \ \dots \ u_N \mid u_b \ \psi_b \rangle^T \quad (7.57a)$$

$$\{P\} = \langle F_1 \ F_2 \ F_3 \ \dots \ F_N \mid Q_b \ M_b \rangle^T \quad (7.57b)$$

and

$$[k] = \begin{bmatrix} [k] & \{0\} & \{0\} \\ \langle 0 \rangle & k_{xx} & k_{x\psi} \\ \langle 0 \rangle & k_{\psi x} & k_{\psi\psi} \end{bmatrix} \quad (7.57c)$$

in which $[k]$ is the condensed structural stiffness matrix (matrix expressing stiffness in translation with rotation eliminated) and k_{xx} , $k_{x\psi} = k_{\psi x}$ and $k_{\psi\psi}$ are stiffness constants of the foundation. The absolute maximum top displacement is, then,

$$\Delta_{\max} = u_N + u_b + h_N \psi_b \quad (7.58)$$

The maximum top accelerations in both across- and along-wind directions are obtained from equations 7.52 and 7.53.

7.8.2 Numerical Examples

With impedance functions available for footing on soil, the effect of soil-structure interaction on structural response to gusting wind can be evaluated. The consequence of the soil flexibility is best illustrated using some typical examples. A few 10- and 20-storey buildings are examined, and the results are compared with an earlier study of a tall reinforced concrete chimney (102). Constant stiffness and damping parameters are considered, as it is quite adequate when analyzing just the first mode response.

Buildings

For a 10-storey building resting on a large mat supporting all columns, Figures 7.15 to 7.17 show the effect of foundation flexibility on damping, frequency and wind response. The data on the building and the foundation for which these figures are obtained are given in Chapter 3. Figure 7.15 shows the variation of structural damping D^S , soil damping D and total damping $D^t = D^S + D$ of the first mode with varying soil stiffness. The structural damping decreases monotonically as soil stiffness decreases, while the damping obtained by the building from the foundation increases. The net result is an increase of the total damping with the soil flexibility. The magnitude of this

damping ranges from about 2 to 3 percent for soils with shear wave velocity varying from 400 to 700 ft/s (\approx 122 to 213 m/s). For structural damping, the value of one percent was assumed for the structure on rigid foundation.

Figure 7.16 shows the effect of soil flexibility on gust effect factor G , mean top displacement, Δ_{st} , and maximum top displacement, Δ , for the same building on mat foundation. These values are normalized by the corresponding values for the building with a fixed base. Exposure A is used to obtain this figure with assumed design wind speed of 27.2 m/sec.

It can be seen that the gust effect factor is not affected by soil flexibility for this specific problem. This is so because the resonant term in equation 7.47 (SF/D^t) is increased due to the reduction of soil flexibility while the peak factor g is decreased. The net result is to keep the gust factor G almost independent of soil flexibility. On the other hand, both mean and maximum displacements, at the top of the building, increased by up to 50 percent when the shear wave velocity decreases from about 800 to 300 ft/s (\approx 244 to 91 m/s). This is so because the loads P appearing in equation 7.56 are not sensitive to soil flexibility while the stiffness parameters pertinent to the foundation decrease, with soil flexibility,

as they are proportional to the square of soil shear wave velocity.

For the same building, Figure 7.17 shows the variations of the natural frequency f_0 and the along-wind acceleration with soil flexibility. The across-wind acceleration, calculated from the empirical formula (7.52), is also shown in Figure 7.17. The across-wind acceleration increases with decreasing stiffness of the soil while the along-wind acceleration decreases.

The effect of soil-structure interaction on modal properties of the structure and on the structural response to gusting wind is also examined for a twenty-storey shear building which differs from the one used in Figures 7.15 to 7.17 only by the addition of ten more storeys. The results are plotted in Figures 7.18 to 7.20. They are similar to those observed in the previous case.

Exposure C is also applied to the 10- and 20-storey buildings to examine the soil-structure interaction effects on response to more turbulent wind. The trend of the normalized results obtained for exposure C is quite similar to that shown in Figures 7.15 to 7.20 for exposure A. However, the gust factor, G , maximum top displacement and acceleration differ significantly. Comparisons between the results obtained for the two exposures are given in Tables

7.1 and 7.2. It can be observed from these tables that the gust factor for exposure C is higher than that for exposure A. This is mainly because (equation 7.47) of the higher value of the friction coefficient, κ , and of the lower value of the exposure factor, c_e , for exposure C. Tables 7.1 and 7.2 also indicate that the maximum displacements as well as along- and across-wind accelerations for exposure C are less than those for exposure A. This is so because the exposure factor, c_e , is lower for exposure C than for exposure A. For the same reason, the peak values of base shear for exposure C are less than one-half the values for exposure A as shown in Tables 7.1 and 7.2. Those tables also illustrate that the peak base shear values are not sensitive to variation of soil flexibility.

The above observations appear rather typical of buildings of moderate size. For very large structures, somewhat different effects of foundation flexibility may occur. This is shown using an example of a large chimney examined by Novak (102). The chimney is 1,000 ft (304.8 m) tall, the outer diameter is 44.7 ft (13.6 m) at the top and 84.7 ft (25.8 m) at the base. The foundation is a circular flat slab with a radius of 100 ft (30.5 m) and an embedment ratio $l/R = 0.25$. Horizontal translation and rotation in the vertical plane are taken into account.

The stiffness of soil is considered variable and is characterized by the shear wave velocity. Soil density ρ is considered constant and equal to 3.6 slug/ft³ (1861 kg/m³).

Figure 7.21 shows the first three natural frequencies and soil damping ratios, plotted vs shear wave velocity of the soil. All natural frequencies decrease with decreasing stiffness of the soil. The general trend for the damping is to increase with the order of the mode and with decreasing stiffness of the soil.

The gust effect factor obtained with different soil properties for the chimney is shown in Figure 7.22. Three exposures are considered. It can be seen that with decreasing stiffness of the soil the gust factor decreases. The dependence of the gust factor on the nature of the terrain is minor because the chimney considered is very tall and reaches very close to the level of the gradient wind where the effect of surface roughness on wind characteristics is not very significant.

Chimneys and other cylindrical structures are also sensitive to vortex shedding and their response to this type of excitation may be affected by soil-structure interaction very strongly. This is so because the vortices depend very much on damping (102).

7.9 CONCLUSIONS

The approaches in use for the prediction of structural response to gusting wind are examined. The fluctuating part of the response is treated as a stationary random process. The general conclusion is that the gust factor approach, available in the Canadian Building Code, is the most simple and practical approach. The approach considers just the first vibration mode which is well justified by experimental observations. However, all vibration modes can be taken into account together with some other refinements in the approaches by Vickery (121) and Simiu (113).

This study examines the effects of soil-structure interaction under the main type of loading due to turbulent wind. The effect of soil-structure interaction results from soil flexibility and enters the analysis through the modifications of the modal properties of the structure.

The gust effect factor may or may not be sensitive to soil flexibility depending on the shift of the natural frequency of the structure with regard to the region of the peak of the loading spectrum. Gust effect factor increases with the roughness of terrain.

The resultant vibration may be substantially modified due to soil flexibility. The along-wind acceleration is reduced when the soil structure interaction is accounted for, while the across-wind acceleration increases dramatically. However, this depends on the type of the structure and may not be quite generally true because the formula for the across-wind acceleration is an empirical one. Soil flexibility has a minor effect on peak values of base shear.

Response displacement, acceleration and base shear are smaller for large cities than for open exposures.

In the buildings studied, surface foundations were considered. For embedded foundations, the above observations may change. This is so because with embedded foundations soil damping increases but also stiffness increases.

Soil-structure interaction affects structural response to gusting wind and must, in general, be considered in design when the foundation is flexible.

Response to vortex shedding, critical for some cylindrical structures, can be affected by soil-structure interaction even more markedly.

TABLE 7.1 Comparison Between Exposures A and C Results for a Fixed-Base and Flexible Foundation
10-Storey Building

	Peak Displacement Δ (cm)	Peak Displacement Δ_{st} (cm)	Gust Factor G	Along-Wind Acceleration a_{along_2} (cm/s ²)	Across-Wind Acceleration a_{across} (cm/s ²)	Peak Base Shear Q_b (kN)
Exposure A	$V_s = \infty$ 1.384	0.6838	2.035	23.76	50.96	681
	$V_s = 122m/s$ 1.652	0.8311	1.997	11.09	52.13	688
	$V_s = \infty$ 0.604	0.1994	3.068	7.407	7.206	308
Exposure C	$V_s = 122m/s$ 0.719	0.2428	2.996	3.581	7.359	301

TABLE 7.2 Comparison Between Exposures A and C Results for a Fixed-Base and Flexible Foundation
20-Storey Building

	Peak Displacement Δ (cm)	Peak Displacement Δ_{st} (cm)	Gust Factor G	Along-Wind Acceleration a_{along_2} (cm/s ²)	Across-Wind Acceleration a_{across} (cm/s ²)	Peak Base Shear Q_b (kN)
Exposure A	$V_s = \infty$ 6.740	3.300	2.064	50.01	168.8	1620
	$V_s = 122m/s$ 9.257	4.379	2.135	21.73	240.77	1680
	$V_s = \infty$ 3.204	1.177	2.772	21.21	41.14	754
Exposure C	$V_s = 122m/s$ 4.371	1.562	2.856	9.769	59.25	775

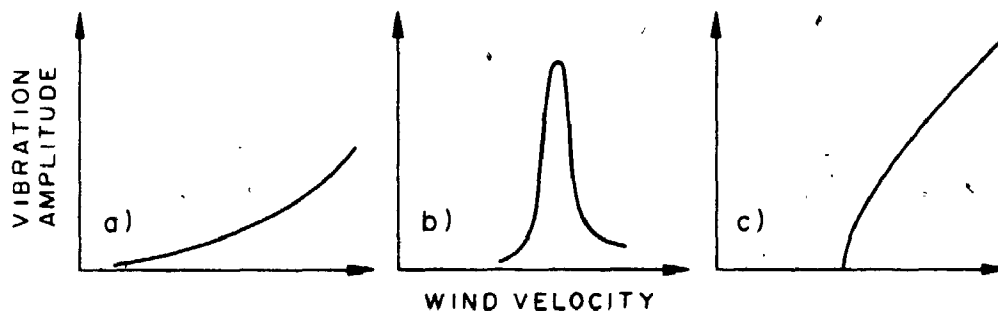


FIGURE 7.1 Main Types of Wind-Induced Oscillations:
 (a) Vibration Due to Turbulence, (b) Vibration Due to Vortex Shedding, and (c) Aerodynamic Instability

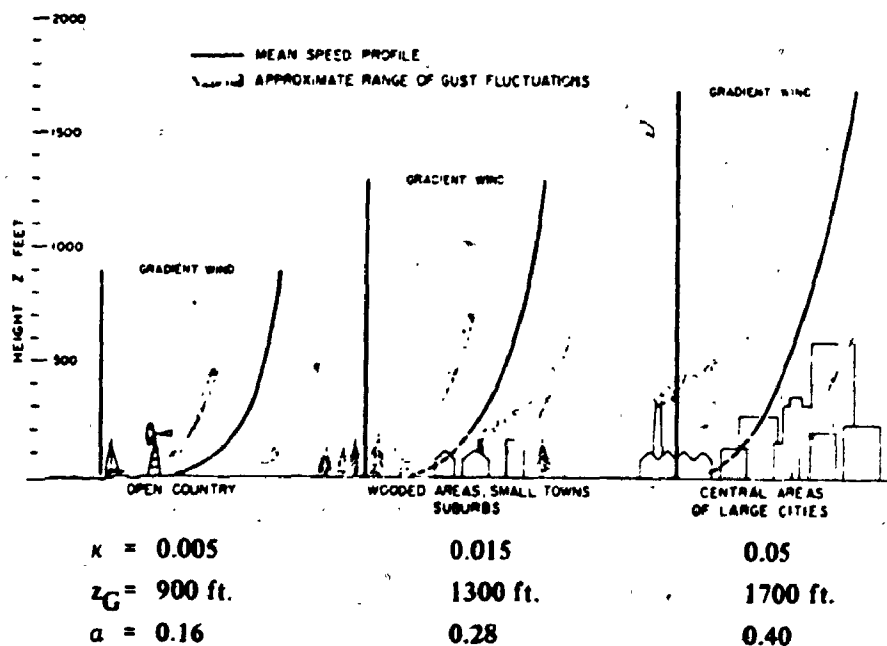


FIGURE 7.2 Vertical Profiles of Mean Wind Velocity for Three Typical Terrains (1 ft = .3048 m)

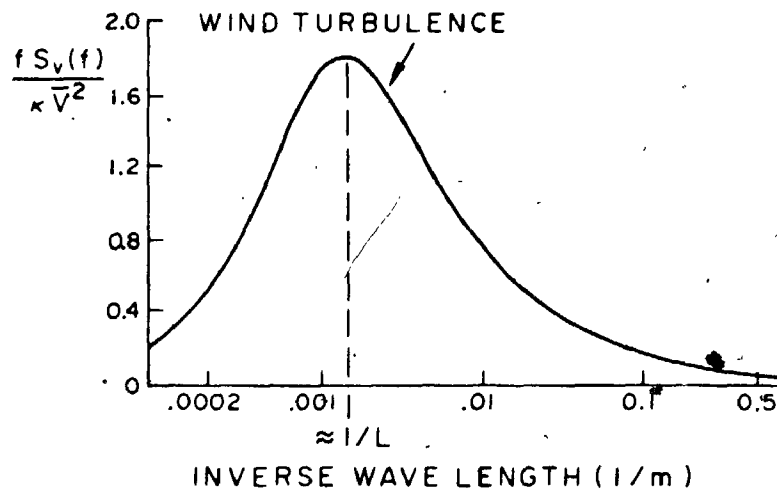


FIGURE 7.3 Universal Spectrum of Horizontal Gustiness in Strong Winds

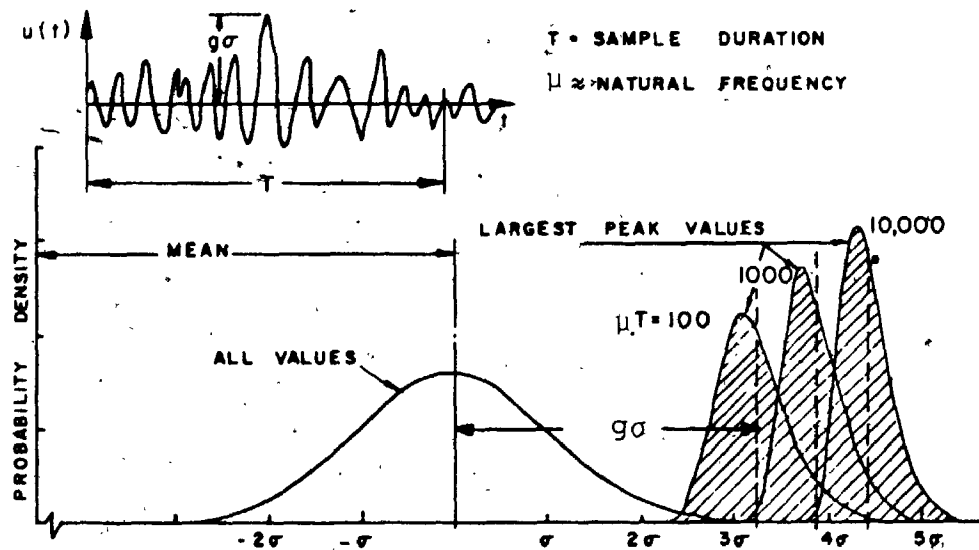


FIGURE 7.4 Relationship of Distribution of Largest Peak to Distribution of All Values (For a Stationary Random Process)

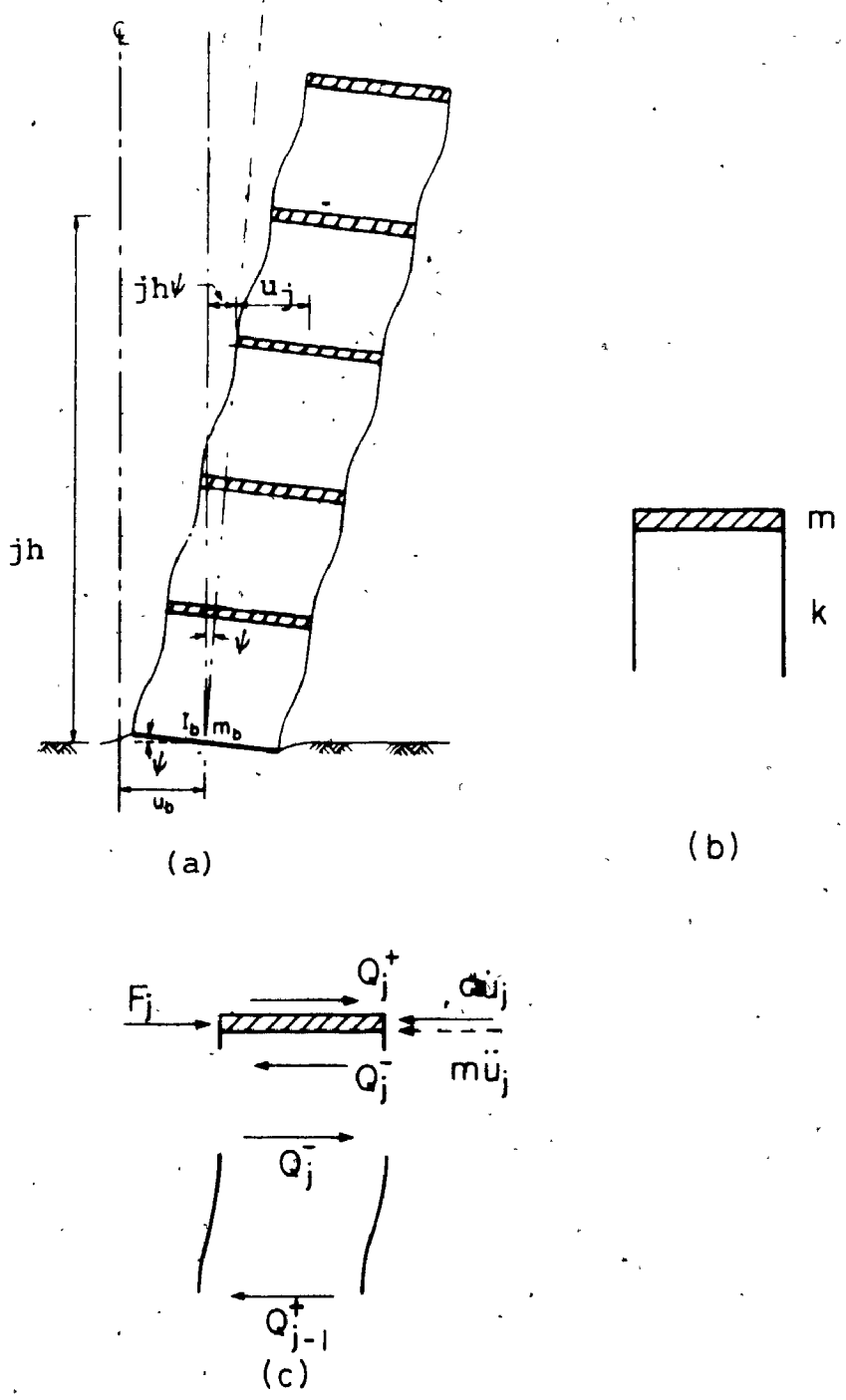


FIGURE 7.5 Structural Model: (a) N-Storey Building; (b) Storey Unit; (c) Forces on j th Storey Unit

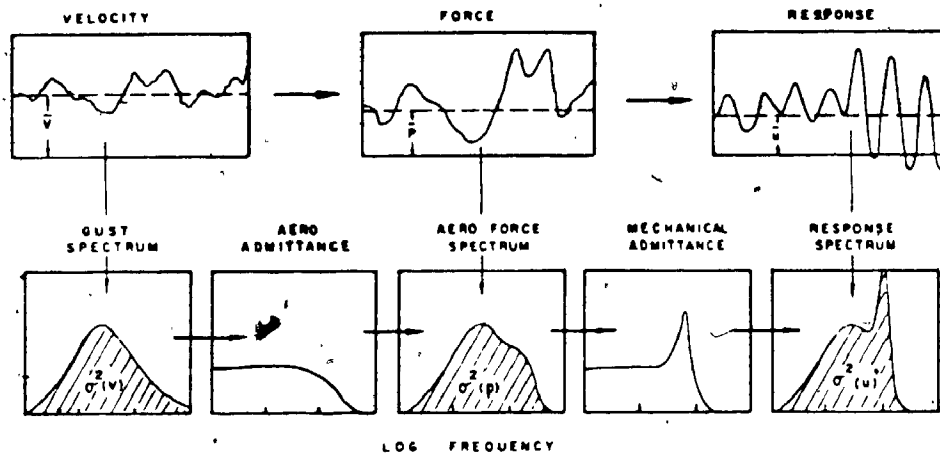


FIGURE 7.6 Transition From Gust Spectrum to Response Spectrum (Ref. 106)

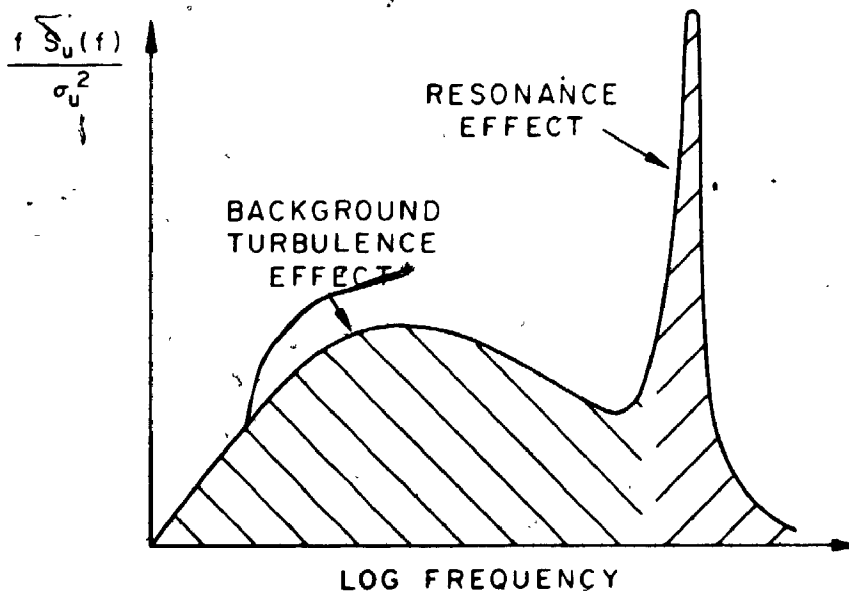


FIGURE 7.7 Spectrum of Structural Response With Indication of Resonance Effect and Background Turbulence Effect

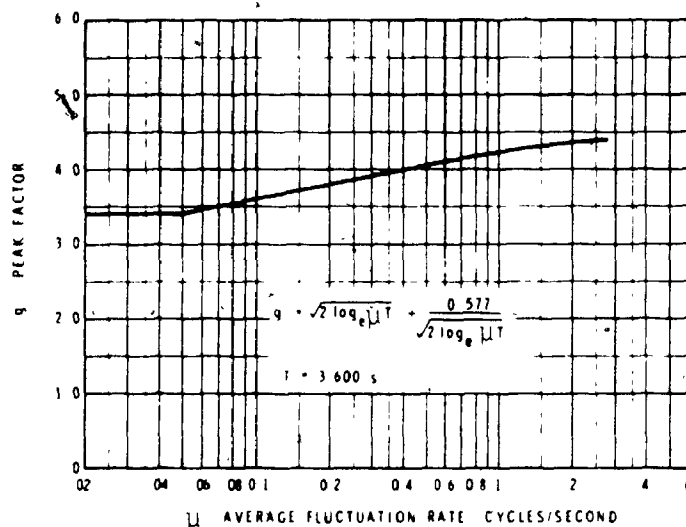


FIGURE 7.8 Peak Factor As a Function of Average Fluctuation Rate (Ref. 108)

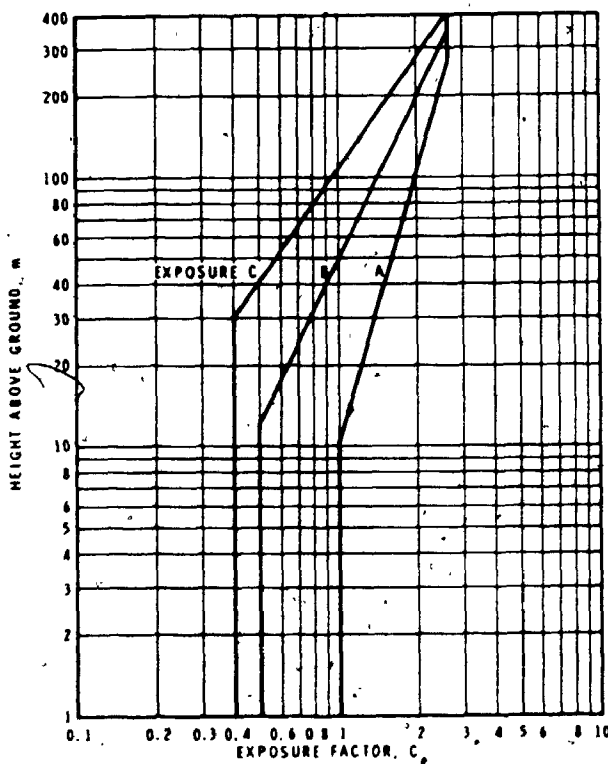


FIGURE 7.9 Exposure Factor As a Function of Terrain Roughness and Height Above Ground (Ref. 108)

$$C_e = (z/\bar{V}_{10})^{.28}, C_e \geq 1.0 \quad \text{Zone A}$$

$$C_e = 0.5(z/\bar{V}_{10})^{.5}, C_e \geq 0.5 \quad \text{Zone B}$$

$$C_e = 0.4(z/\bar{V}_{10})^{.72}, C_e \geq 0.5 \quad \text{Zone C}$$

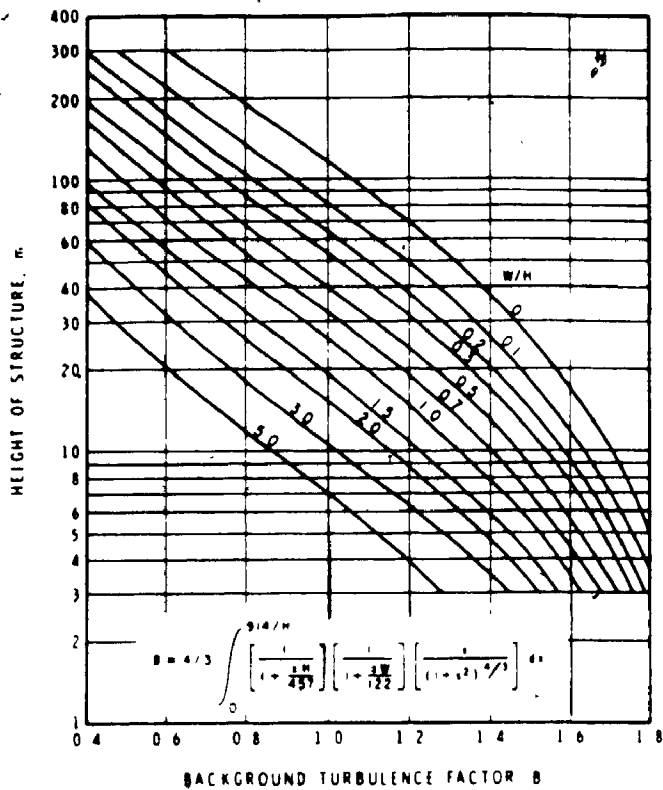


FIGURE 7.10 Background Turbulence Factor As a Function of Width and Height of Structure (Ref. 108)

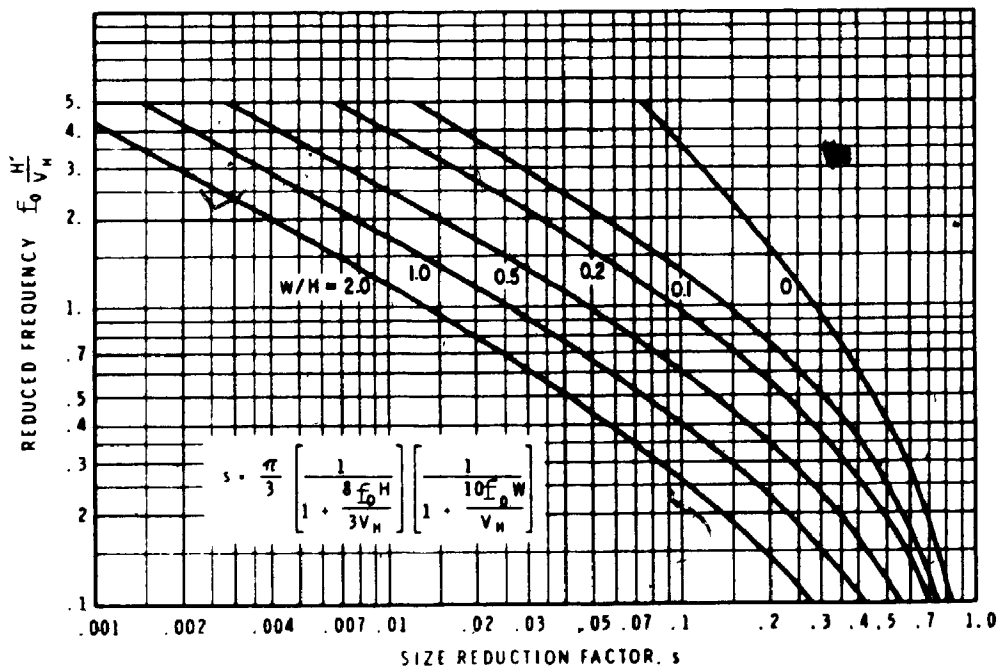


FIGURE 7.11 Size Reduction Factor As a Function of Width, Height and Reduced Frequency of Structure (Ref. 108)

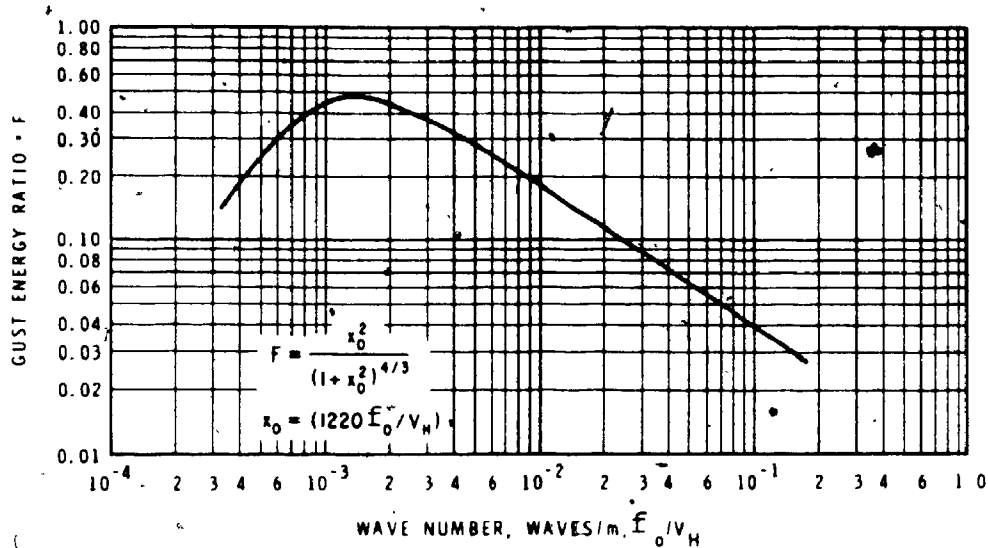


FIGURE 7.12 Gust Energy Ratio As a Function of Wave Number (Ref. 108)

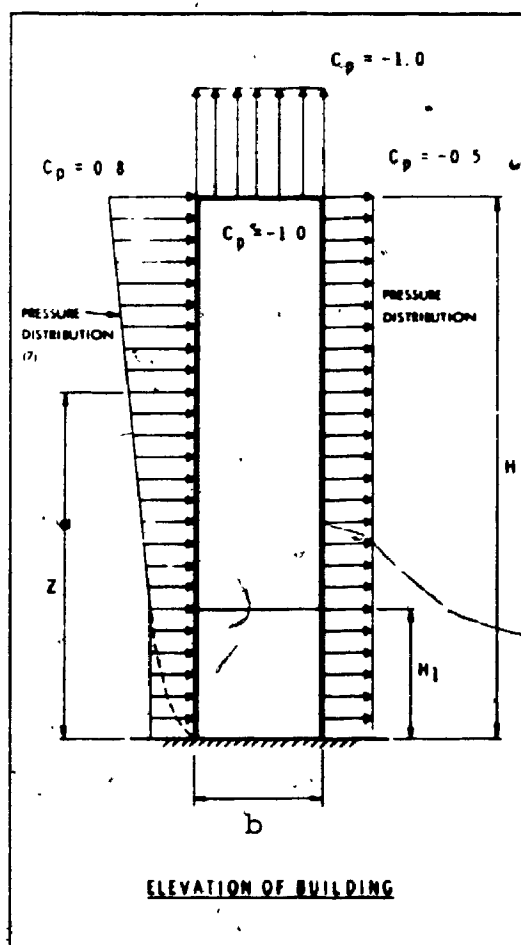


FIGURE 7.13 Flat Roof Buildings of Height Greater Than Twice the Width (Ref. 108)

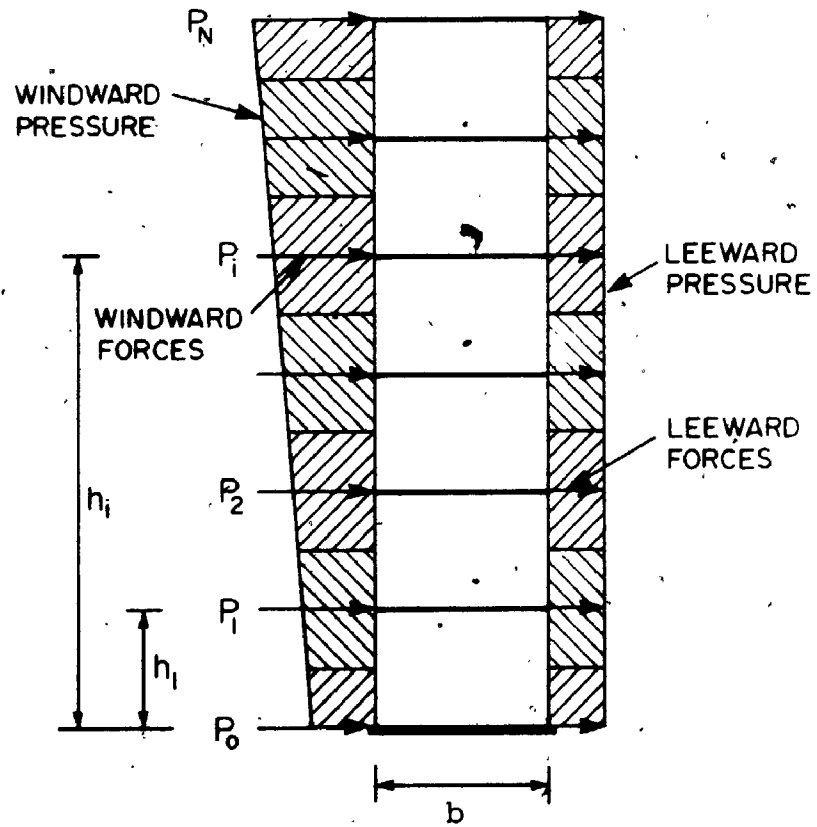


FIGURE 7.14 Windward and Leeward Forces Due to Wind Pressure

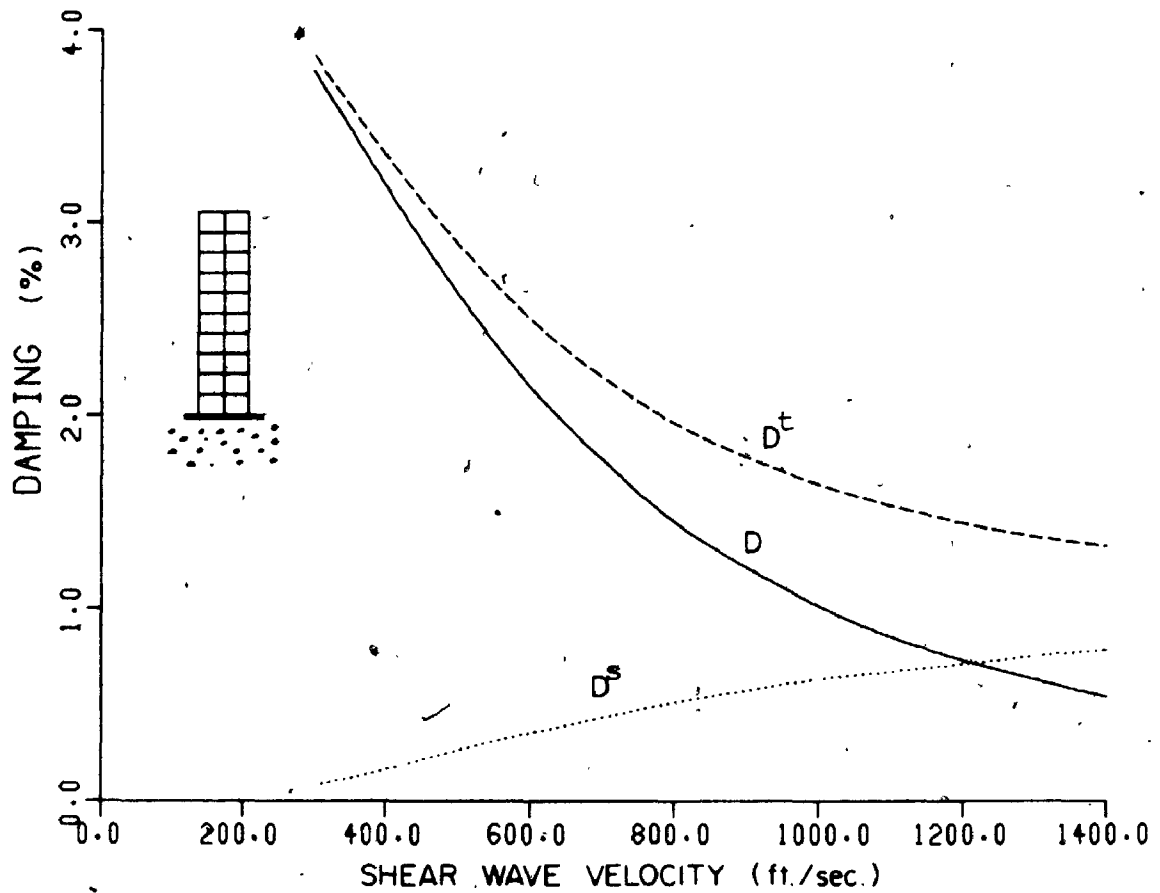


FIGURE 7.15 First Mode Damping Ratios of 10-Storey Building On Mat Foundation Computed With Various Shear Wave Velocities of Soil (1 ft. = .3048 m)

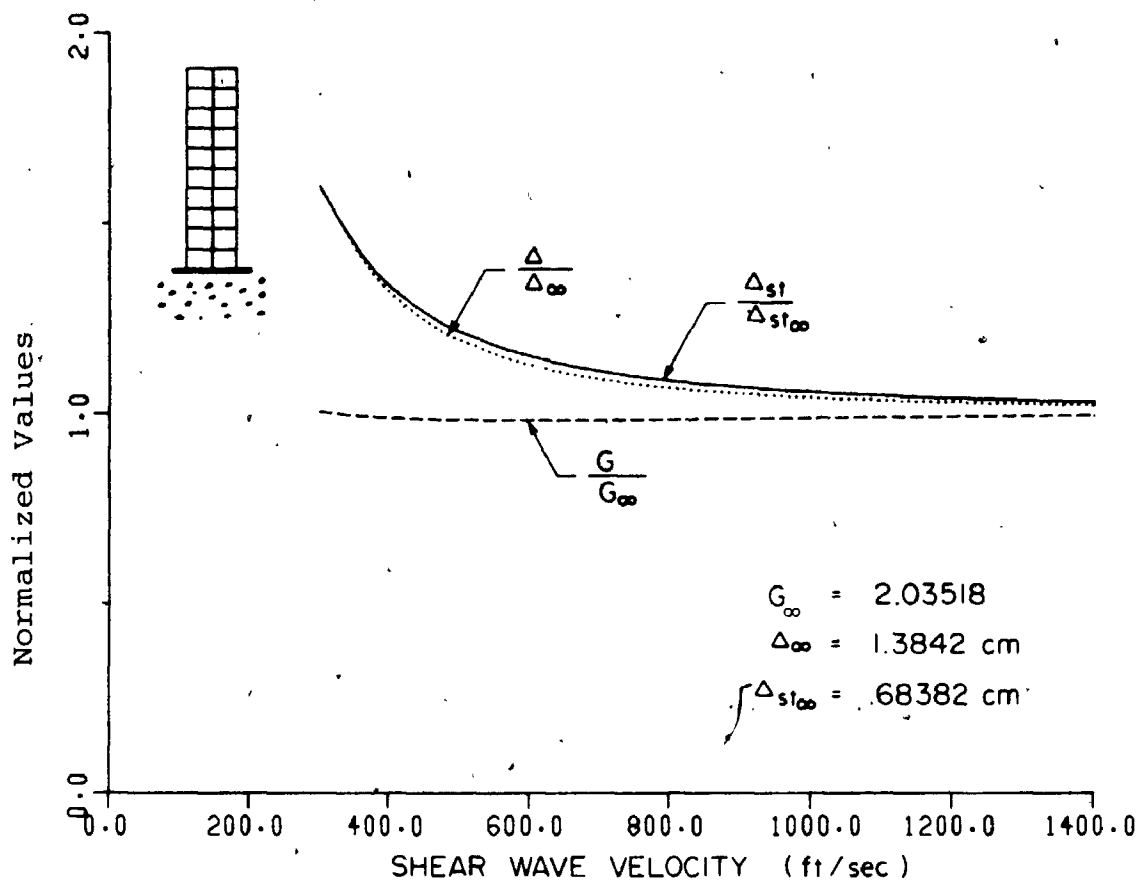


FIGURE 7.16 Variation of Gust Effect Factor, Maximum Top Total and Mean Displacements of 10-Storey Building on Mat Foundation With Wave Velocity of Soil (Exposure A; ∞ Indicated Fixed Base) (1 ft = .3048 m)

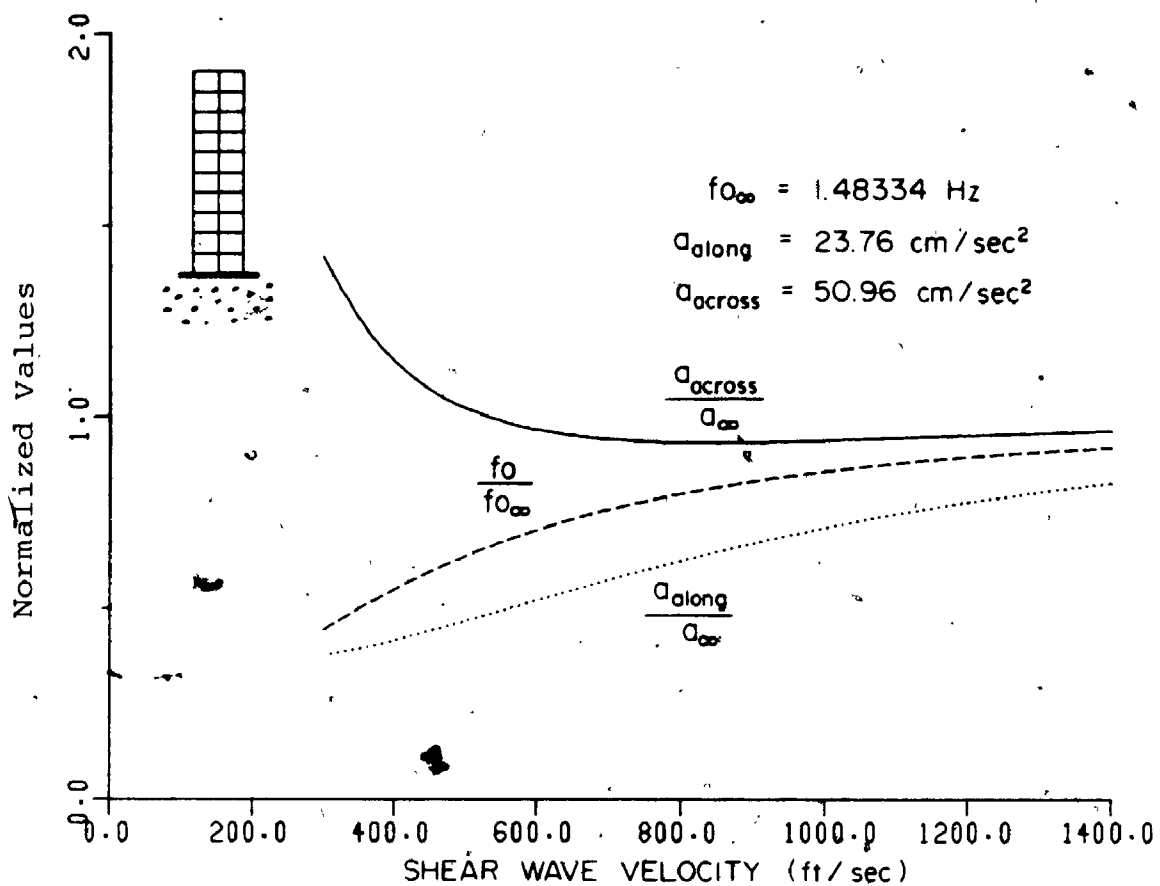


FIGURE 7.17 Natural Frequency and Along- and Across-Wind Acceleration of 10-Storey Building on Mat Foundation Computed With Various Shear Wave Velocities of Soil (Exposure A; ∞ Indicates Fixed Base) (1 ft = .3048 m)

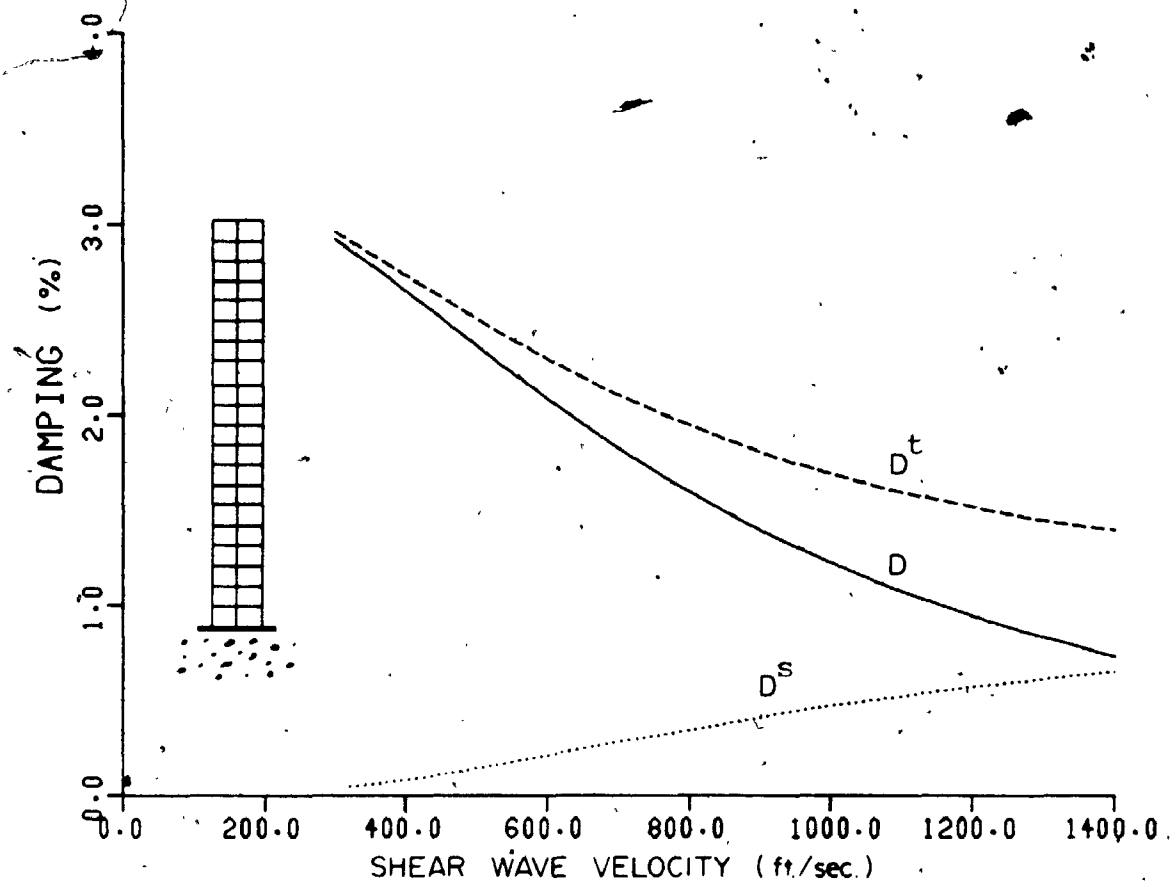


FIGURE 7.18 First Mode Damping Ratios of 20-Storey Building On Mat Foundation Computed With Various Shear Wave Velocities of Soil (1 ft = .3048 m)

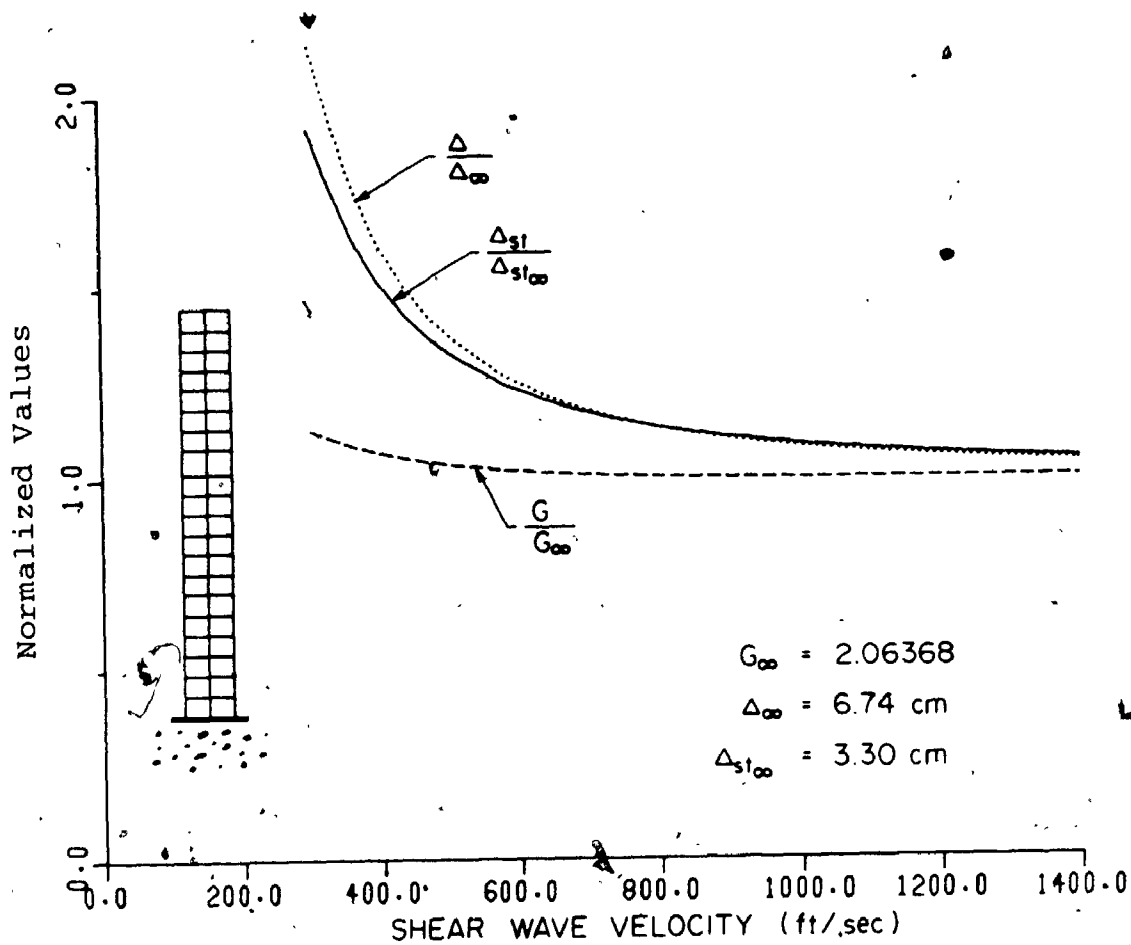


FIGURE 7.19 Variation of Gust Effect Factor, Maximum Top Total and Mean Displacements of 20-Storey Building on Mat Foundation With Wave Velocity of Soil (Exposure A; ∞ Indicates Fixed Base) (1 ft = .3048 m)

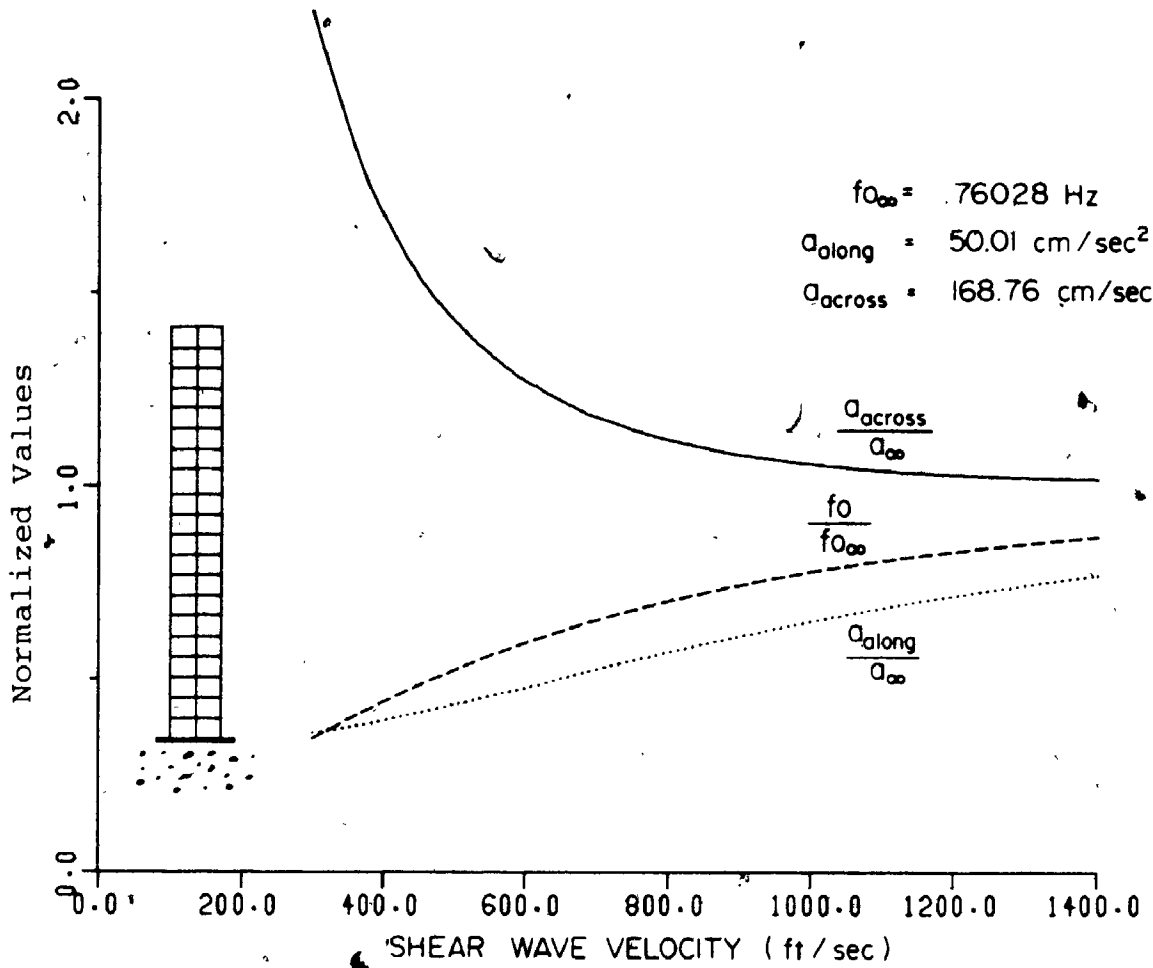


FIGURE 7.20 Natural Frequency and Along- and Across-Wind Acceleration of 20-Storey Building on Mat Foundation Computed With Various Shear Wave Velocity of Soil (Exposure A; ∞ Indicates Fixed Base) (1 ft = .3048 m)

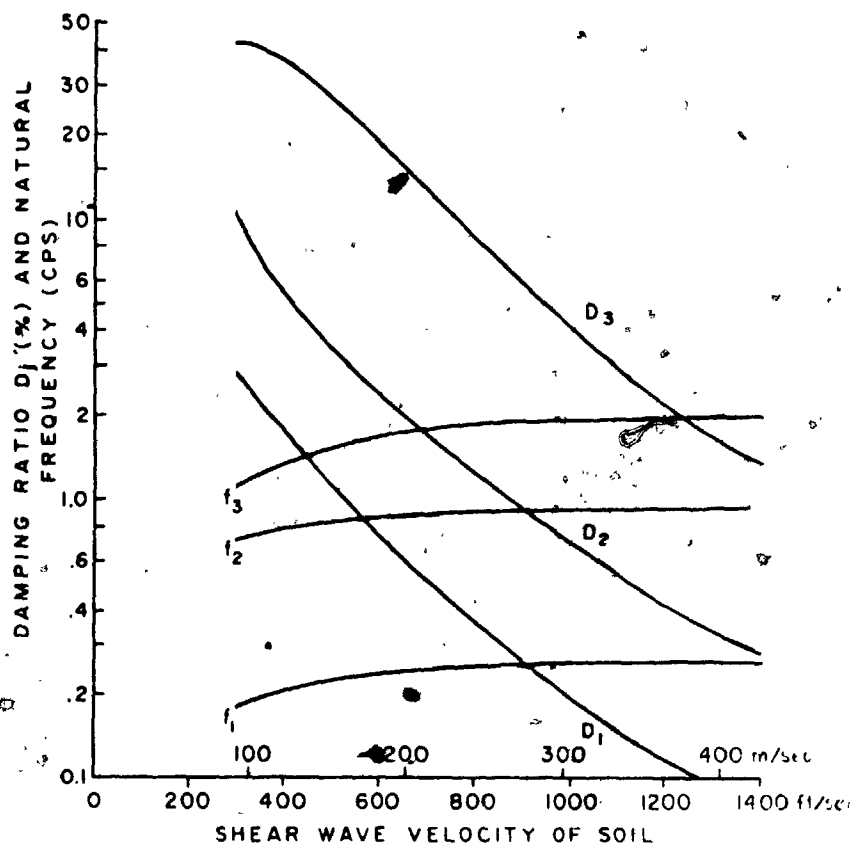


FIGURE 7.21 Natural Frequencies and Modal Damping Ratios of Chimney Computed With Various Shear Wave Velocities of Soil (Ref. 102) (1 ft = .3048 m)

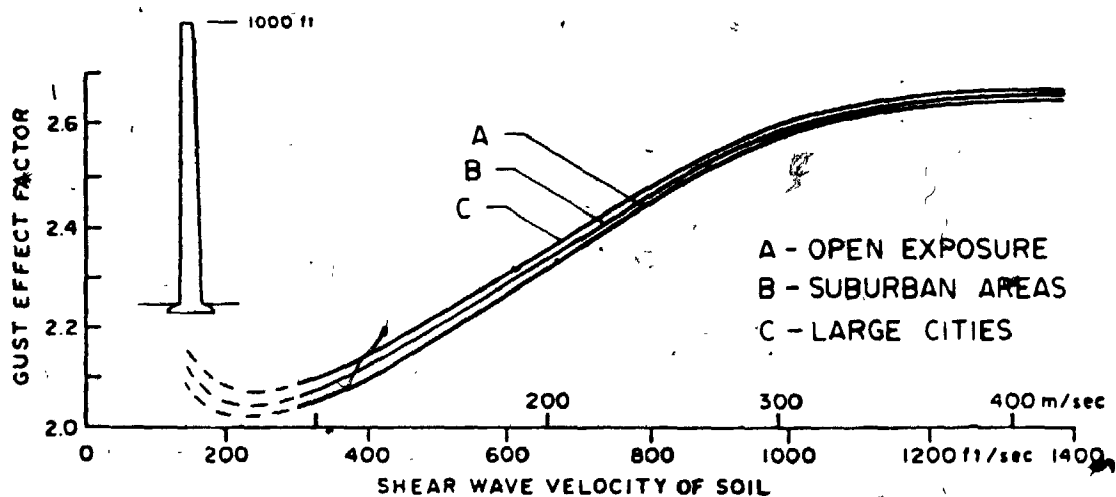


FIGURE 7.22 Variations of Gust Effect Factor for Chimney With Shear Wave Velocity of Soil (Three Exposures) (Ref. 102)

CHAPTER 8

SUMMARY AND CONCLUSIONS

The effect of soil flexibility on the dynamic behavior of structures is investigated theoretically using the impedance approach and the idea of substructuring. First, foundation impedance functions are established from static and dynamic continuum theories. Then, the response of the structure supported by flexible soils is analyzed. Free vibration and dynamic response to shock loading, earthquakes and wind are examined. The study suggests the following conclusions:

A. Free Vibration

1. Undamped natural frequencies are always reduced by soil flexibility.
2. Damped frequencies of structures on flexible foundations may be lower or higher than the undamped natural frequencies.
3. Damped modes may differ significantly from undamped modes.
4. Damping of structures resting on flexible foundations is affected by soil-structure interaction in two ways.
 - (1) The structure gains damping through energy dissipation in soil, and
 - (2) the damping the structure would have on a rigid foundation is reduced. These effects are calculated using an energy consideration, an approximate method, and the complex eigenvalue

analysis, an accurate method.

5. For internal (structural) damping, both methods yield almost identical results.
6. The foundation damping of the first mode is also the same from both methods. However, considerably different results are obtained for the higher vibration modes.

B. Response to Shock Loading

1. Hammers are used to exemplify the analysis of response to shock loading. However, the analysis of other structures would follow a similar pattern.
2. The complex eigenvalues and eigenvectors are used to predict the response of hammer foundations to the blows of the head either as caused by initial velocity of the anvil or as a pulse.
3. The initial velocity approach overestimates the response to pulse loading and is, therefore, conservative.
4. The exact shape of the pulse loading affects the time history of the response but has little effect on the peak value of the response.
5. The complex eigenvalue method is an efficient and accurate method for the analysis of collision problems in which large damping due to soil-structure interaction is expected.

C. Response to Seismic Loading

1. Seismic forces and response of a structure depend on the flexibility of the foundation and its type.
2. For shallow foundations, soil-structure interaction may reduce seismic forces and increase peak response.
3. The inclusion of soil material damping is shown to decrease the seismic responses and loads for the case of a layer of limited thickness. However, with a halfspace, these effects are not significant.
4. The limited depth of the stratum with moderate soil material damping results in insignificant decrease in base shear compared to that obtained with a fixed base. This implies that the ATC document allowance of reducing base shear by up to 30 percent to account for soil-structure interaction may not be valid for the case of a layer of limited depth.
5. For piles supported structures, the interaction effects depend on the number and type of piles, their arrangement and the tensile resistance of the connection of the piles to the cap.
6. A tension resistant connection of the piles may not always be necessary particularly for short structures and/or low intensity of seismic excitation.
7. The direct random vibration analysis is a very efficient and accurate method for the seismic analysis

of rigid structures on soil.

D. Response to Turbulent Wind

1. The gust factor approach, available in the Canadian Building Code, is the most simple and practical approach to the prediction of structural response to gusting wind.
2. The effect of soil-structure interaction on modal properties results in modifications of the gust effect factor and the along-wind response, pressure and acceleration.
3. The gust effect factor may increase or decrease with soil flexibility. This depends on the relationship between the natural frequency of the structure and the dominant frequency region of the design wind spectrum.
4. Lateral response of buildings to wind loading may be dramatically increased due to soil-structure interaction.
5. Soil flexibility has a minor effect on the design wind pressures.
6. The maximum acceleration of a building leading to possible human perception of motion is affected by soil flexibility in two different ways: (1) the along-wind acceleration decreases and (2) the across-wind acceleration increases.

7. Response of cylindrical structures to vortex shedding may be affected by soil-structure interaction very strongly.

E. Recommendations for Further Research

1. A complete solution of the seismic response of the pile supported buildings should allow for kinematic interaction, wave scattering between piles and pile-soil-pile interaction.
2. The complex eigenvalue approach employed for the analysis of the response of structures with nonproportional damping could be extended to analyze modern tall buildings provided with vibration control devices against wind loadings.
3. The complex eigenvalue analysis should be extended to accommodate frequency dependent foundation impedance functions. In such a case, modal properties could be evaluated by means of iterative procedure.
4. Experimental study is needed to verify the theoretical observations of the effects of the soil-structure interaction on structural response to wind loading.
5. Further research is required to study the phenomenon of nonlinear soil behavior, particularly with piles.
6. The coupling between foundation flexibility and the $P-\Delta$ effect should also be studied.

REFERENCES

1. Clough, R.W. "The Finite Element Method in Plane Stress Analysis," Proc. 2nd Conf. Electronic Computation, ASCE, Pittsburgh, 8-9, 1960.
2. Desai, C.S. and Abel, J.F. "Introduction to the Finite Element Method," Van Nostrand Reinhold Co., New York, pp. 16-17, 1972.
3. Lysmer, J. "Analytical Procedure in Soil Dynamics," Earthquake Engineering Research Center, Report No. EERC-78/29, U.C. Berkeley, CA., 1979.
4. Lysmer, J., Udaka, T., Tsai, C.F. and Seed, H.B. "Flush - A Computer Program for Approximate 3-D Analysis of Soil-Structure Interaction Problems," Earthquake Engineering Research Center, Report No. EERC-75/30, U.C. Berkeley, CA., 1975.
5. Gomez-Masso, A., Lysmer, J., Chen, J. and Seed, H.B. "Soil-Structure Interaction in Different Seismic Environments," Earthquake Engineering Research Center, Report No. EERC-79/18, U.C. Berkeley, CA., 1979.
6. Clough, R.W. and Penzien, J. "Dynamics of Structures," McGraw-Hill, Inc., New York, pp. 198-199, 226-230 and 578-594, 1975.
7. Luco, J.E. "Vibrations of a Rigid Disc on a Layered Viscoelastic Medium," Nuclear Engrg. and Design, Vol. 36, pp. 325-340, 1976.
8. Veletsos, A.S. and Wei, T.Y. "Lateral and Rocking Vibration of Footings," Proc. ASCE, J. Soil Mech. & Foundation Div., SM9, pp. 1227-1248, 1971.
9. Luco, J.E. and Westmann. "Dynamic Response of Circular Footings," Proc. ASCE, J. Engrg. Mech., Vol. 97, EM5, pp. 1381-1395, 1971.
10. Veletsos, A.S. and Verbic, B. "Vibrations of Viscoelastic Foundations," Int. J. Earthquake Engineering and Structural Dynamics, Vol. 2, No. 1, pp. 87-102, 1973.
11. Wong, H.L. "Dynamic Soil-Structure Interaction," Earthquake Engineering Research Laboratory, Report No. EERL 75-01, Cal. Tech., Pasadena, CA., 1975.

12. Kausel, E. and Ushijima, R. "Vertical and Torsional Stiffness of Cylindrical Footings," Research Report Pub. No. R79-6, Dept. of Civil Engrg., M.I.T., MA., 1979.
13. Veletsos, A.S. "Dynamic of Structure-Foundation System," in Structural and Geotechnical Mechanics, ed. by W.J. Hall, Prentice-Hall, Inc., Englewood Cliffs, N.J., pp. 333-361, 1977.
14. ATC-3 Code, "Tentative Provisions for the Development of Seismic Regulations for Buildings," Prepared by Applied Technology Council, ATC Pub. ATC 3-06, National Bureau of Standards Special Pub. 510, NSF Pub. 78-8, 1978.
15. Roesset, J.M., Whitman, R.V. and Dobry, R. "Modal Analysis of Structures With Foundation Interaction," Proc. ASCE, Struc. Div., ST3, pp. 399-416, 1973.
16. Foss, A.K. "Co-ordinate Which Uncouple the Equations of Motion of Damped Linear Dynamic System," J. Applied Mech., Vol. 25, pp. 361-364, 1958.
17. Parmelee, R.A., Perelman, D.S. and Lee, S.L. "Seismic Response of Multiplestory Structure on Flexible Foundations," Bulletin Seismological Society of America, 59, pp. 1061-1070, 1969.
18. Newmark, N.M. and Rosenblueth, E. "Fundamentals of Earthquake Engineering," Prentice-Hall, Inc., Englewood Cliffs, N.J., pp. 93-101 and 149-151, 1971.
19. Kausel, E., Roesset, J.M. and Waas, G. "Dynamic Analysis of Footings on Layered Media," Journal of the Engineering Mechanics Division, ASCE, October 1975a.
20. Kausel, E., Roesset, J.M. "Dynamic Stiffness of Circular Foundations," Journal of the Engineering Mechanics Division, ASCE, Vol. 101, No. EM6, pp. 771-785, December 1975b.
21. Richart, Jr., F.E., Hall, Jr., J.R. and Woods, R.D. "Vibrations of Soils and Foundations," Prentice-Hall, Inc., New Jersey, 1970.
22. Lugo, J.E. "Impedance Functions for a Rigid Foundation on a Layered Medium," Nuclear Engineering and Design, Vol. 31, No. 2, December 1974.

23. Beredugo, Y.O. and Novak, M. "Coupled Horizontal and Rocking Vibration of Embedded Footings," Canadian Geotechnical J., pp. 477-497, November 1972.
24. Johnson, G.R., Christians, P., Epstein, H.I. "Stiffness Coefficients for Embedded Footings," Journal of the Geotechnical Engineering Division, ASCE, Vol. 101, No. GT8, pp. 789-800, August 1975.
25. Novak, M. "Vibration of Embedded Footings and Structures," Proceedings of the ASCE National Structural Engineering Meeting, San Francisco, 1973.
26. Tsai, N.C., Neihoff, D., Swatta, M. and Hadjian, A.E. "The Use of Frequency Independent Soil-Structure Interaction Parameters," Nuclear Engineering and Design, Vol. 31, No. 2, December 1974.
27. Kobori, T., Minai, R. and Suzuki, T. "The Dynamical Ground Compliance of a Rectangular Foundation on a Viscoelastic Stratum," Bull. Disaster Prevention Research Institute, Kyoto University, Vol. 20, pp. 289-329, 1971.
28. Dominguez, J. "Dynamic Stiffness of Rectangular Foundations," Publication No. R78-20, Dept. of Civil Engrg., M.I.T., 1978.
29. Gazetas, G.C. "Dynamic Stiffness Functions of Strip and Rectangular Footings on Layered Soil," S.M. Thesis, Dept. of Civil Engrg., Mass. Inst. of Tech., Cambridge, Mass., 1975.
30. Novak, M. "Effect of Soil on Structural Response to Wind and Earthquake," Inter. J. Earthquake Engineering and Struct. Dyn., Vol. 3, No. 1, pp. 79-96, 1974.
31. Novak, M. and Beredugo, Y.O. "Vertical Vibration of Embedded Footings," J. Soil Mechanics and Foundations Division, ASCE, SM12, pp. 1291-1310, December 1972.
32. Roesset, J.M. "Stiffness and damping Coefficients of Foundation," Proceedings, Specialty Session, ASCE National Convention, Florida, pp. 1-30, 1980.
33. Novak, M. "Prediction of Footing Vibrations," J. of the Soil Mechanics and Foundations Division, Proceedings of the ASCE, Vol. 96, No. SM3, pp. 837-861, May 1970.

34. Novak, M. and Sheta, M. "Approximate Approach to Contact Problems of Piles," Proc. Geotech. Engrg. Div. ASCE National Convention "Dynamic Response of Pile Foundations: Analytical Aspects," pp. 53-79, October 1980.
35. Warburton, G.B. "Forced Vibration of a Body On An Elastic Stratum," J. Applied Mechanics, pp. 55-58, March 1957.
36. Bycroft, G.N. "Forced Vibrations of a Rigid Circular Plate on a Semi-Infinite Elastic Half Space and on an Elastic Stratum," Philosophical Transactions of the Roy. Soc., London, Series A, Vol. 248, No. 948, pp. 327-368, 1956.
37. Luco, J.E. "Impedance Functions for a Rigid Foundation on a Layered Medium," Nuclear Engineering and Design 31, pp. 204-217, 1974.
38. Nogami, T. and Novak, M. "Soil-Pile Interaction in Vertical Vibration," International Journal of Earthquake Engineering and Structural Dynamics, Vol. 4, No. 3, pp. 277-293, January-March 1976.
39. Elsabee, F. and Morray, J.P. "Dynamic Behavior of Embedded Foundations," Research Report R77-33, Civil Engineering Department, Massachusetts Institute of Technology, September 1977.
40. Kobori, T., Minai, R. and Baba, K. "Dynamic Behaviour of a Laterally Loaded Pile," 9th Int. Conf. Soil Mech., Tokyo, Session 10, 6, 1977.
41. Kuhlemeyer, R.L. "Static and Dynamic Laterally Loaded Piles," J. Geotech. Eng. Div., ASCE, Vol. 105, No. GT2, pp. 289-304, 1979.
42. Novak, M. "Dynamic Stiffness and Damping of Piles," Canadian Geotechnical Journal, Vol. II, pp. 574-598, 1974.
43. Novak, M. and Aboul-Ella, F. "Stiffness and Damping of Piles in Layered Media," Proc. Earthq. Engrg. and Soil Dyn., ASCE Specialty Conf., Pasadena, California, pp. 704-719, June 19-21, 1978b.
44. Novak, M. and Grigg, R.F. "Dynamic Experiments With Small Pile Foundations," Canadian Geotechnical Journal, Vol. 13, No. 4, pp. 372-385, November 1976.

45. Tajimi, H. "Dynamic Analysis of a Structure Embedded in an Elastic Stratum," Proc. 4th World Conf. Earthquake Engineering, Chile, 1969.
46. Kaynia, A.M. and Kausel, E. "Dynamic Behavior of Pile Groups," 2nd Int. Conf. on Numerical Methods in Offshore Piling, Austin, Texas, 1982.
47. Nogami, T. "Dynamic Stiffness and Damping of Pile Groups in Inhomogeneous Soil," Proc. of Session on Dynamic Response of Pile Foundations: Analytical Aspects, ASCE Nat. Conv., pp. 31-52, October 1980.
48. Sheta, M. and Novak, M. "Vertical Vibration of Pile Groups," Journal of the Geotechnical Engineering Div., ASCE, Vol. 108, No. GT4, pp. 570-590, April 1982.
49. Trbojevic, V.M., Marli, J., Danish, R. and Delinic, K. "Pile-Soil-Pile Interaction Analysis for Pile Groups," 6th SMIRT, Paris, 1981.
50. Waas, G. and Hartmann, H.G. "Pile Foundations Subjected to Dynamic Horizontal Loads," European Simulation Meeting "Modelling and Simulation of Large Scale Structural Systems," Capri, Italy, pp. 17, September, 1981 (also SMIRT, Paris).
51. Wolf, J.P. and von Arx, G.A. "Impedance Functions of a Group of Vertical Piles," Proc. ASCE Specialty Conf. on Earthquake Engrg. and Soil Dynamics, Pasadena, Calif., II, pp. 1024-1041, 1978.
52. Poulos, H.G. "Behaviour of Laterally Loaded Piles. II - Pile Groups," J. Soil Mech. Foundations Div., ASCE, 97 (SM5), pp. 733-751, 1971.
53. Poulos, H.G. "Group Factors for Pile-Deflection Estimation," J. Geotech. Engrg. Div., ASCE, GT12, pp. 1489-1509, 1979.
54. Poulos, H.G. and Davis, E.H. "Pile Foundations Analysis and Design," John Wiley and Sons, pp. 397, 1980.
55. Poulos, H.G. and Randolph, M.F. "A Study of Two Methods for Pile Group Analysis," J. Geot. Engrg. Div., ASCE (to appear).
56. Novak, M. and El Sharnouby, B. "Stiffness Constants of Single Piles," J. Geot. Engrg. Div., ASCE, Vol. 109, No. 7, pp. 961-974, July 1983.

69. Muto, K. and Kobayashi, T. "Experimental Vibration Analysis of RC Building Model," (in Japanese), Trans. Architect. Inst. Japan, No. 205, pp. 43-51, 1973.
70. Traill-Nash, R.W. "Modal Methods in the Dynamics of Systems With Non-Classical Damping," Earthquake Eng. Struct. Dyn., 9, pp. 153-169, 1981.
71. Bielak, J. "Dynamic Behavior of Structures With Embedded Foundations," Res. Report E8, Universidad Nacional Autonoma de Mexico, p. 36, April 1974.
72. Novak, M. and El Hifnawy, L. "Effect of Soil-Structure Interaction on Damping of Structures," Earthquake Engrg. and Structural Dynamics, Vol. 11, pp. 595-621, 1983.
73. Chopra, A.K. and Gutierrez, J.A. "Earthquake Response Analysis of Multistory Buildings Including Foundation Interaction," Int. J. Earthquake Engrg. Struct. Dyn., 3, pp. 65-77, 1974.
74. Argyris, J.H., Dunne, P.C. and Anelopoulos, T. "Dynamic Response by Large Step Integration," Computer Methods in Applied Mechanics and Engineering, Vol. 2, pp. 185-203, 1973.
75. Bathe, K.J. and Wilson, E.L. "Numerical Method in Finite Element Analysis," Prentice-Hall, Inc., Englewood Cliffs, N.J., pp. 494-506, 1976.
76. Newmark, N.M. "A Method of Computation for Structural Dynamics," J. Engrg. Mech. Div., ASCE, No. EM3, pp. 67-94, July 1959.
77. Cooley, J.W. and Tukey, J.W. "An Algorithm for the Machine Calculation of Complex Fourier Series," Mathematics of Computation, Vol. 19, No. 19, pp. 297-301, 1965.
78. Vanmarck, E.H. "Structural Response to Earthquakes," in Seismic Risk and Engineering Decisions, C. Lomnitz and E. Rosenblueth, Eds., Elsevier Publishing Co., Inc., Amsterdam, The Netherlands, pp. 425-446, 1976.
79. Tajimi, H. "A Structural Method of Determining the Maximum Response of a Building Structure During an Earthquake," Proceedings of the Second World Conference on Earthquake Engineering, Vol. 11, 1960.
80. Davenport, A.G. "The Distribution of Largest Values of a Random Function With Application to Gust Loading," Proceedings, Institution of Civil Engineers, London, Vol. 28, pp. 187-196, 1964.

81. Vanmarcke, H. "Random Vibration Approach to Soil Dynamics Problems," The Use of Probability in Earthquake Engineering, ASCE, pp. 143-176, 1977.
82. Rice, S.O. "Mathematical Analysis of Random Noise," Bell System Technical Journal, Vol. 24, pp. 40-116. 1945.
83. Hilber, H.M. and Hughes, T.J.R. "Collocation, Dissipation and 'Overshoot' for Time Integration Scheme in Structural Dynamics," Earthquake Engineering and Structural Dynamics, 6, pp. 99-117, 1978.
84. Dahlquist, G. "A Special Stability Problem for Linear Multistep Methods," BIT, 3, pp. 27-43, 1963.
85. Sharpe, R.D. "The Seismic Response of Inelastic Structures," Ph.D. Thesis, University of Canterbury, Christchurch, New Zealand, 1974.
86. Wilson, E.L., Farhoomand, I. and Bathe, K.J. "Non-linear Dynamic Analysis of Complex Structures," Earthquake Engineering and Structural Dynamics, Vol. 1, pp. 241-252, 1973.
87. Christian, J.T. "Probabilistic Soil Dynamics State-of-the-Art," Journal of the Geotechnical Division, ASCE, 106, pp. 385-397, 1980.
88. Rausch, E. "Maschinen Fundamente," VDI-Verlag, Dusseldorf (in German), Chapter 6, pp. 107-232, 1950.
89. Barkan, D.D. "Dynamics of Bases and Foundations," McGraw-Hill Book Co., Inc., Chapter 5, pp. 185-241, 1962.
90. Novak, M. "Foundations for Shock-Producing Machines," Canadian Geotechnical Journal, No. 1, 1983.
91. Rivin, E.I. "Design of Vibration Isolation Systems for Forging Hammers," Sound and Vibration, pp. 12-15, April 1978.
92. Major, A. "Vibration Analysis and Design of Foundations for Machines and Turbines," Collet's Holdings Limited, London, Chapters XII and XIII, pp. 221-269, 1962.

93. Srinivasulu, P. and Vaidyanathan, C.V. "Handbook of Machine Foundations," Tata McGraw-Hill Publ. Co. Ltd., New Delhi, Chapter 4, pp. 103-134, 1976.
94. Kim, T.C. and Novak, M. "Dynamic Properties of Some Cohesive Soils of Ontario," Canadian Geotechnical Journal, Vol. 18, No. 3, pp. 371-389, August 1981.
95. Harris, C.M. and Crede, C.E. "Shock and Vibration Handbook," McGraw-Hill, Chap. 8, 1976.
96. Lysmer, J. and Richart, F.E. "Dynamic Response of Footings to Vertical Loading," Journal of the Soil Mechanics and Foundations Division, ASCE, 92, pp. 65-91, 1966.
97. Novak, M., Sheta, M., El Sharnouby, B. and El Hifnawy, L. "DYNA, A/Computer Program for Calculation of Response of Rigid Foundations to Dynamic Loads," The Systems Analysis, Control and Design Activity (SACDA), The University of Western Ontario, London, Canada, May 1983.
98. Bielak, J. and Palencia, V.J. "Dynamic Behavior of Structures With Pile-Supported Foundation," Proc. 6th World Conference on Earthquake Engineering, New Delhi, Vol. 11, pp. 1576-1581, 1977.
99. Whitman, R.V. 2nd ASCE Specialty Conf. on Structural Design of Nuclear Plant Facilities, New Orleans, La., Vol. II, Session 6, Soil Structure Interaction, Pub. by ASCE, New York, pp. 257-268, 1975.
100. National Building Code of Canada, Issued by the Associate Committee on the National Building Code, National Research Council of Canada, Ottawa, 1980.
101. Structural Analysis and Design of Nuclear Plant Facilities, Supplement. "Analysis for Soil-Structure Interaction Effects for Nuclear Power Plants," Report by the Ad Hoc Group on Soil-Structure Interaction, Structural Division of ASCE, May 1976.
102. Novak, M. "Soil-Structure Interaction Under Wind Loading," Proceedings 14th Annual Meeting of the Society of Engineering Science, Inc., Bethlehem, Pa., pp. 1099-1110, November 14-16, 1977.
103. Yang, J.N. and Lin, Y.K. "Along-Wind Motion of Multy-story Building," J. Engrg. Mech. Div. ASCE, Vol. 107, No. EM2, Proc. Paper 16170, pp. 295-307, April 1981.

104. Lin, Y.K. and Wu, W.F. "Along-Wind Response of Tall Building on Compliant Soil," Fourth International Conference on Application of Statistics and Probability in Soil and Structural Engineering, Universita di Firenze, (Italy, Pitagora Editrice, 1983.
105. Vickery, B.J. "A Model for the Prediction of the Response of Chimneys to Vortex Shedding," International Chimney Design Symposium, Munich, pp. 25-26, October 1978.
106. Davenport, A.G. and Novak, M. "Vibration of Structures Induced by Wind," Chapter 29-11 in Shock and Vibration Handbook, Second Edn., edited by C.M. Harris and C.E. Crede, McGraw-Hill, 1976.
107. Vickery, B.J. and Clark, A.W. "Lift or Across-Wind Response of Tapered Stacks," Journal of Structural Division, ASCE, January 1972.
108. The Supplement to the National Building Code of Canada, Issued by the Associate Committee on the National Building Code, National Research Council of Canada, Ottawa, Commentary B, p. 149, 1980.
109. Davenport, A.G. "The Application of Statistical Concepts to the Wind Loading of Structures," Proceedings of the Institution of Civil Engineers, Vol. 19, pp. 449-472, August 1961.
110. Davenport, A.G. et al. "New Approaches to Design Against Wind Action," Research Report, Faculty of Engineering Science, University of Western Ontario.
111. McNamara, K. "Characteristics of the Mean Wind and Its Effects on Tall Towers," Ph.D. Thesis, University of Western Ontario.
112. Harris, R.I. "Seminar of Construction Industry Research and Information Association," Paper 3, Institution of Civil Engineers, 1970.
113. Simiu, E. "Wind Spectra and Dynamic Along Wind Response," Journal of the Structural Division, ASCE, Vol. 100, No. ST9, Proc. Paper 10815, pp. 1897-1910, September 1974.

114. Pestel, E.C. and Leckie, F.A. "Matrix Methods in Elasto-Mechanics," McGraw-Hill Book Co., Inc., New York, 1963.
115. Lin, Y.K. "Random Vibration of Periodic and Almost Periodic Structures," in Mechanics Today (Ed. S. Nemat-Nasser), Vol. 3, pp. 93-124, 1976.
116. Davenport, A.G. "Gust Loading Factors," J. Struct. Div., ASCE, 93, pp. 11-34, June 1967.
117. Davenport, A.G. "The Response of Slender Line-Like Structures to a Gusty Wind," Proceedings, Institution of Civil Engineering, London, Vol. 23, pp. 389-408, 1962.
118. Davenport, A.G. "The Distribution of Largest Values of a Random Function With Application to Gust Loading," Proceedings, Institution of Civil Engineers, London, Vol. 28, pp. 187-196, 1964.
119. Davenport, A.G. "The Prediction of the Response of Structures to Gusty Wind," International Research Seminar on Safety of Structures Under Dynamic Loading, Trondheim, June 1977, TAPIR, V. 1, pp. 257-284, 1978.
120. Hansen, R.J., Reed, J.W. and Van Marke, E.H. "Human Response to Wind-Induced Motion of Buildings," Journal of Structural Division, ASCE, Vol. 99, pp. 1587-1605, July 1973.
121. Vickery, B.J. and Kao, K.H. "Drag or Along-Wind Response of Slender Structures," J. Struct. Div., ASCE, Vol. 98, pp. 21-36, 1972.

END

1 1 H 0 9 1 8 4

FIN